ÇUKUROVA UNIVERSITY
INSTITUTE OF NATURAL AND APPLIED SCIENCES

PhD THESIS

Çağlar CONKER

COMMAND GENERATION TECHNIQUES FOR ELIMINATION OF RESIDUAL VIBRATIONS FOR ROBOTIC APPLICATIONS

DEPARTMENT OF MECHANICAL ENGINEERING

ADANA, 2016

ÇUKUROVA UNIVERSITY
INSTITUTE OF NATURAL AND APPLIED SCIENCES

COMMAND GENERATION TECHNIQUES FOR ELIMINATION OF RESIDUAL VIBRATIONS FOR ROBOTIC APPLICATIONS

Çağlar CONKER

PhD THESIS

DEPARTMENT OF MECHANICAL ENGINEERING

We certify that the thesis titled above was reviewed and approved for the award of degree of the Doctor of Philosophy by the board of jury on 14/01/2016.

……..	…….....	……...
Prof. Dr. Hakan YAVUZ	Assoc. Prof. Dr. Mehmet BİLGİLİ	Prof. Dr. Emel ORAL
SUPERVISOR	MEMBER	MEMBER

……...	……..
Prof. Dr. Sadettin KAPUCU	Assoc. Prof. Dr. Selçuk MISTIKOĞLU
MEMBER	MEMBER

This PhD Thesis is written at the Department of Institute of Natural And Applied Sciences of Çukurova University.
Registration Number:

Prof. Dr. Mustafa GÖK
Director
Institute of Natural and Applied Sciences

ABSTRACT

PhD THESIS

COMMAND GENERATION TECHNIQUES FOR ELIMINATION OF RESIDUAL VIBRATIONS FOR ROBOTIC APPLICATIONS

Çağlar CONKER

ÇUKUROVA UNIVERSITY
INSTITUTE OF NATURAL AND APPLIED SCIENCES
DEPARTMENT OF MECHANICAL ENGINEERING

Supervisor : Prof. Dr. Hakan YAVUZ
Year: 2016, Pages: 234
Jury : Prof. Dr. Hakan YAVUZ
: Prof. Dr. Kadir AYDIN
: Prof. Dr. Emel ORAL
: Prof. Dr. Sadettin KAPUCU
: Assoc. Prof. Dr. Selçuk MISTIKOĞLU

One method used to reduce or eliminate residual vibrations is to modify the input signal by using previously determined system parameters. In order to eliminate the residual vibration completely, these system parameters must be known very accurately. In real systems, achieving such accuracy may not always be possible. To address this problem and to provide a solution, a new residual vibration elimination method is introduced in this thesis. It has been proven to be useful especially in cases of uncertain system parameters that are estimated or predicted. It is shown that the technique is capable of handling high levels of uncertainty and is able to successfully eliminate or reduce residual vibrations in flexible robotic systems. In this approach, the desired position of the system is primarily divided into two or more equal parts for each of which a sectional input command is generated. In generation of each of the input signal, cycloid-plus-ramped and versine-plus-ramp functions are used. This reference input is composed of three key functions. Each part is travelled by each of the three functions within the same travel time. Provided that the specified move time and the total distance are unchanged, vibration can be eliminated by adjusting excursion distance of each function. The thesis presents theoretical and experimental results of the techniques applied to flexible robotic systems; a comparative study of robustness performance is also provided. The presented simulation and experimental results show that the residual vibrations are considerably decreased with a high degree of robustness in the presence of estimation related uncertainty regarding system parameters.

Keywords: Flexible Robotic Systems, Residual Vibration Elimination, Command Generation, Input Shaping, Parameter Estimation.

ÖZ

DOKTORA TEZİ

ROBOTİK UYGULAMALAR İÇİN ARTIK TİTREŞİMİN ELİMİNASYONUNDA KOMUT ÜRETİM TEKNİKLERİ

Çağlar CONKER

ÇUKUROVA ÜNİVERSİTESİ
FEN BİLİMLERİ ENSTİTÜSÜ
MAKİNA MÜHENDİSLİĞİ ANABİLİM DALI

Danışman : Prof. Dr. Hakan YAVUZ
Yıl: 2016, Sayfa: 234
Jüri : Prof. Dr. Hakan YAVUZ
: Prof. Dr. Kadir AYDIN
: Prof. Dr. Emel ORAL
: Prof. Dr. Sadettin KAPUCU
: Doç. Dr. Selçuk MISTIKOĞLU

Artık titreşimlerin azaltılması ya da ortadan kaldırılması için kullanılan yöntemlerden bir tanesi önceden belirlenen sistem parametrelerini kullanarak girdi sinyalinin düzenlenmesidir. Artık titreşimi tamamen ortadan kaldırmak için, bu sistem parametrelerinin tam olarak bilinmesi gerekmektedir. Gerçek sistemlerde, bu ölçüde bir doğruluk elde etmek her zaman mümkün olmayabilir. Bu probleme bir çözüm sağlamak için, tezde yeni bir artık titreşim eleme yöntemi tanıtılmıştır. Yeni metodun özellikle tahmin edilen sistem parametrelerinin belirsiz olduğu durumlarda yararlı olduğu kanıtlanmıştır. Bu teknikle, yüksek düzeyde belirsizlik içeren esnek robotik sistemlerde başarılı bir şekilde artık titreşimleri ortadan kaldırmanın veya azaltmanın mümkün olduğu gösterilmiştir. Bu yaklaşımda, sistemin istenen konumu esas olarak, iki veya daha fazla eşit parçaya ayrılır ve her bir parçayla bölgesel bir girdi komutu üretilir. Her bir girdi sinyalinin üretilmesinde sikloid rampalı versin ve rampa fonksiyonu kullanılmaktadır. Bu referans girişi, üç temel fonksiyondan oluşur. Her parça bu üç fonksiyonla aynı süre içerisinde yol almaktadır. Belirlenen seyahat süresi ve toplam mesafeyi değiştirmeden, her fonksiyonun genliği ve yer değişimi ayarlanarak titreşim elimine edilebilir. Tez esnek robotik sistemlere uygulanan metotların teorik ve deneysel sonuçlarını sunmakta ve gürbüzlük performanslarını karşılaştırmaktadır. Sunulan benzetim ve deney sonuçları sistem parametrelerinin tahmini ile ilgili belirsizlik varlığında, artık titreşimlerin yüksek derecede gürbüzlükle önemli ölçüde azaldığını göstermektedir.

Anahtar Kelimeler: Esnek Robotik Sistemler, Artık Titreşim Eleme, Komut Üretimi, Girdi Şekillendirme, Parametre Tahmini

ACKNOWLEDGEMENTS

There are many people who are associated with this thesis directly or indirectly whose help and timely suggestions have been highly appreciable for timely completion of this thesis. First of all, I am most grateful to my thesis supervisor and an excellent teacher, Prof. Dr. Hakan YAVUZ, for his expert guidance, superb insight and valuable professional advice that he has given me throughout my PhD study. He has been a great source of motivation, both personal and technical. I admire his knowledge, intelligence, and patience. I am blessed and honoured to be his student.

I wish to thank the dissertation committee members Prof. Dr. Kadir AYDIN, Prof. Dr. Emel ORAL, Prof. Dr. Sadettin KAPUCU, Assoc. Prof. Dr. Selçuk MISTIKOĞLU, for their time and efforts on my dissertation. It is an honour for me to have them as my committee members.

I would like to thank my friends, Hasan Hüseyin BİLGİÇ, Hürrem AKBIYIK, Alper BURGAÇ Kaan BALTACIOĞLU, Hüseyin Turan ARAT, Ali KILIÇ, who gave me necessary support and positive energy for my studies.

I owe special thanks to Cenap ATİLLA for his charitable, constant support and encouragement throughout my thesis.

My family has been a source of constant support. I would like to thank my wife, Ayşe CONKER for her encouragement and faith. Without her help and patience, this document would never be completed on time. And, of course my parents, Nuri CONKER and Nesrin CONKER have given me the most generous help that is beyond my imagination.

This thesis is dedicated to everyone who has helped me along the way.

CONTENTS **PAGE**

LIST OF TABLES **PAGE**

LIST OF FIGURES **PAGE**

LIST OF ABBREVIATIONS

2H-EI : Two hump extra insensitive input shaper

3H-EI : Three hump extra insensitive input shaper

A_j : Input shaper magnitudes

B_{eq} : Equivalent viscous damping coefficient

B_p : Viscous damping coefficient, as seen at the pendulum axis

CPRVPR : Cycloid plus ramped versine plus ramp function

EI : Extra insensitive input shaper

F_c : Driving force

g : Gravitational constant of earth

HIS : Hiybrid input shaper

J_{eq} : Equivalent moment of inertia

J_l : Flexible link moment of intertia

J_m : Rotor inertia

J_p : Pendulum moment of inertia

K_g : Total gear ratio

K_m : Motor back-EMF constant

K_s : Experimentally determined stiffness for flexible link

k_t : Motor torque constant

L_1 : Maximum excursion distance to be travelled by ramp motion profile

L_2 : Maximum excursion distance to be travelled by cycloid motion profile

L_3 : Maximum excursion distance to be travelled by ramped versine motion profile

L_l : Flexible link length

l_p : Pendulum length from pivot to center of gravity

M-CPRVPR : Modified cycloid plus ramped versine plus ramp function

MIS : Modified input shaping methdod

m_l : Flexible link mass

M_p : Pendulum mass

PS : Partial sum constraint

R_m : Motor armature resistance

r_{mp} : Motor pinion radius

t : Time

T_d : Period of vibration

UM : Unity magnitude constraint

V_m : DC input voltage

V_{tol} : Tolerable level of vibration

$V_{(w_n,z)}$: Single mode vibration amplitude

x_c : Cart position

ZV : Zero vibration input shaper

ZVD : Zero vibration derivative input shaper

ZVDD : Zero vibration derivative derivative input shaper

ZVDDD : Zero vibration derivative derivative derivative input shaper

a : Link angle / Tip deflection

q : Position of load angle

h_g : Gearbox efficiency

h_m : Motor efficiency

z : Damping ratio

w_n : Natural frequency

w_d : Damped frequency

t : Travelling time

1. INTRODUCTION

Today, the motion control studies have become one of the main subjects of robotics and other automation related research areas. In modern manufacturing industry, high speed and sensitive motion control is necessary for the high speed and high quality production. However, the high speed requirements of applications make the sensitive motion control difficult due to residual vibrations. Therefore, finding a balance between the speed of motion and the elimination (or at least reduction of) residual vibration becomes an important part of the motion control study and related practical applications.

Many researchers reported that most existing robotic manipulators are designed and built in a manner to maximize stiffness, in an attempt to minimize system vibration and achieve good positional accuracy (Dimo et al., 2001; Mohamed and Tokhi, 2004; Dwivedy and Eberhad, 2006; Jabbour et al., 2009; Boucetta and Abdelkrim, 2012; Khoiy et al., 2013; Singh and Krishna, 2014; Rana and Deepika, 2014) Stiffness in a robot manipulator is associated to the system's vibration and accuracy of positioning. In order to minimize the vibration in the system as well as to accomplish good positional accuracy, the stiffness of the manipulator is maximized. This high stiffness is achieved by using heavy material and a bulky design (Dwivedy and Eberhad, 2006; Jabbour et al., 2009; Khoiy et al., 2013; Singh and Krishna, 2014). As a consequence, such robots are usually heavier with respect to the operating payload. This, in turn, limits the operation speed of the robot manipulation, increases the actuator size, and boosts energy consumption and increase the overall cost. Moreover, the payload to robot weight ratio, under such situation, is low. In order to solve these problems, robotic systems are designed to be lightweight with some level of flexibility. Conversely, flexible robot manipulator exhibits many advantages over their rigid counterparts as they require less material, they are lighter in weight, have higher manipulation speeds, lower in power consumption levels, they require small actuators. They are also more manoeuvrable, transportable, safer to operate due to reduced inertia, have less overall cost and higher payload to robot

weight ratio (Book and Majette, 1983). Although lightweight manipulators offer several advantages over the rigid manipulators due to their flexibility, they are more difficult to control. Therefore, the control mechanism of the flexible robot becomes more challenging with complex mathematical computations than that of their rigid counterparts. An accurate control of flexible robotic systems is a complex technical problem and it has been an active area of robotic research for decades.

1.1. Vibration Control of Flexible Robotic Systems

The most common control strategies for flexible mechanical systems can be classified as feed-forward (open-loop) and feed-back (closed-loop) control schemes. The feed-back control strategies mainly use measurements and/or estimations of the system states to suppress vibrations. The feedback control systems can be expensive and difficult to implement, as they require the system to be equipped with sensors. Furthermore, they can require significant computing power and also raise the possibility of unstable system behaviour (Vaughan et al., 2008).

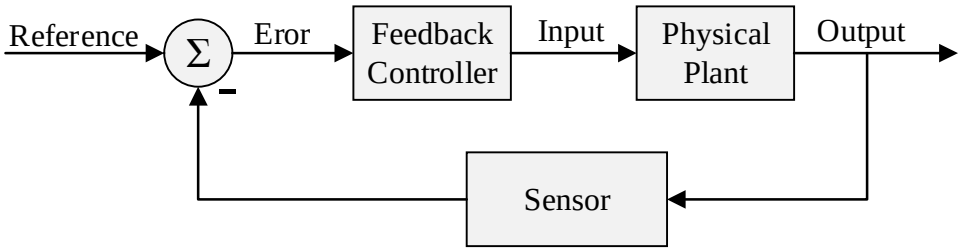

Figure 1.1. Block diagram of the feedback control configuration

Feed-forward techniques for vibration suppression involve developing the control input through consideration of the physical and vibrational properties of the system, so that amplitudes of the system vibrations at response modes are reduced. This method does not require any additional sensors or actuators and does not account for changes in the system once the input is developed.

Figure 1.2. Block diagram of the feed-forward control configuration

Figure 1.1 and Figure 1.2 shows, block diagram of feedback and feed forward control configurations respectively. For clarity, the following nomenclature will be used here.

- The physical plant is a piece of equipment the purpose of which is to perform a particular operation. (Ogata, 2003)

  In feedback systems:
- The feedback control block compares the reference command signals from the command generation block with measurements of the system states and determines a force (torque, voltage, etc.) vector to act on the plant.

  In feed-forward systems:
- The command generation block transforms the desired system performance objective into sets of reference command signals designed to direct the system to achieve the specified motion objective.
- The feed-forward control block employs an internal model of the system to transform the reference commands from the command generation block into a force vector to act on the plant in addition to the force vector from the feedback control block. In the absence of a feedback control loop, the command generation and feed forward control blocks can be combined into a single block.

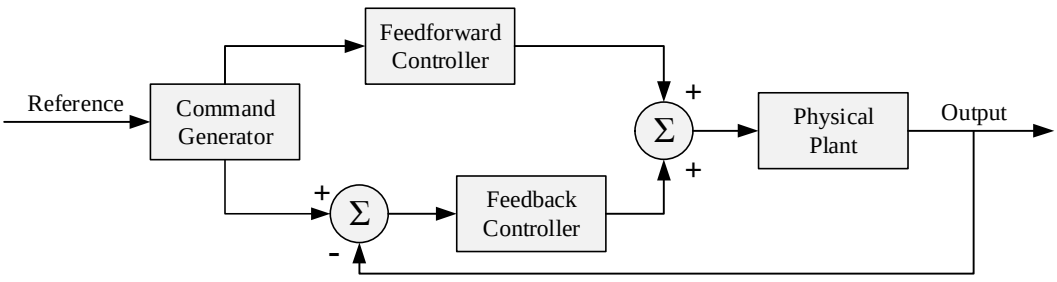

Figure 1.3. Block diagram of the generic system

The command shaping method is a feed forward control technique for improving the settling time and positioning accuracy, while minimizing residual vibrations. The shaped command profiles are generated by convolving a sequence of impulses or solving special functions for the desired command signal. In this motion, the geometry of the path is not important. However, objective is to eliminate or reduce the residual vibrations at the destination. To determine the input shaper controller commands, such information on the system parameters as estimates of the system natural frequency and damping ratio are required to make the necessary calculations. However, real systems cannot be modelled precisely, while insensitivity of the command shaper to modelling errors is an important design consideration. Many robust input shapers have been developed and reported in literature. It has been observed that the robust shapers typically have longer travelling time durations that leads to slower system responses (Vaughan et al., 2008). This creates a compromise between shaper robustness and rise/travelling time. This study presents a review of command input shaping methods and analyses the compromise between duration of motion and shaper robustness for different types of reference commands. The study also presents some theoretical and experimental results of the techniques applied to flexible robotic systems where a comparative study of robustness performance is also provided. The reviewed methods cover almost all types of positive and negative input shapers and related command generation based techniques reported in literature. Therefore, the presented study provides almost a complete picture of the topic for the researchers working in the area. The study is structured in a way that it provides all the necessary theoretical background and the implementation related details for each of the method presented.

The following procedure is used to compare some command shaping techniques. First, the mathematical model of systems is constructed. Then, the shaped command signals are generated using the command shaping methods, which are to be compared. After this, the motion equation of the flexible systems is solved for the generated inputs using MATLAB functions. In order to perform a realistic comparison of the input shaping methods, both the experimental results and results of the simulation based mathematical models are used. In experimental studies, the

system is driven using each input and the resulting residual vibrations as well as cart or servo position are measured and recorded. On the simulation side of the study, the Matlab (2009a) model of the system is also provided with the same input commands to demonstrate the correlation between the theoretical and experimental results obtained. Finally the simulation and experimental results are compared on basis of robustness and travelling time.

1.2. Research Goals

The aim of the thesis is to investigate a new robust control technique for motion control and elimination of residual vibrations in flexible robotic systems. In this thesis, it will be focused especially on the end-point position control of the flexible system using the command shaping methods presented. That is, the shape or geometry of the path is not important, and the aim of the shaped command signal is to drive system from one point to another as fast as possible and stop the system at the desired point without residual vibrations. Specifically, command shaping is concerned with the shape of the reference command and residual vibrations. If the command has an appropriate shape, then it expected to produce the desired motion, while reducing the residual vibration at destination point. For generation of such a shaped command signal, first, mathematical model of a flexible system is to be constructed. Then, a new shaped command signal is generated using physical parameters of the system model such as natural frequency, damping ratio, etc. The command shaping procedure also includes consideration of some design constraints of the system, such as robustness.

The new technique presented in this study is required to have the following specifications;

- simple and easy to implement,
- versatile and effective in reducing or eliminating residual vibrations of flexible systems
- high robustness in existence of inaccuracy of system parameters.

- no limitation on time constraints, i.e. no time limitation or time penalty

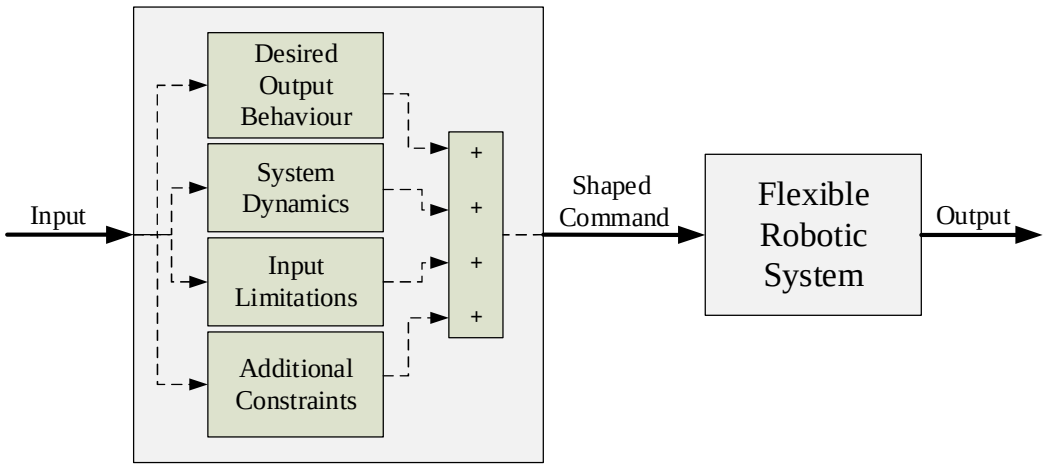

Figure 1.4. The problem to be addressed in this thesis

1.3. Thesis Contributions

This thesis makes some contributions in flexible robotic systems point to point motion control and elimination of residual vibrations in the presence of system parameters uncertainty. Major contributions include:

- **A Comparison of Command Shaping Techniques for Elimination of Residual Vibrations**

  This study presents a review of command shaping methods and investigates the compromise between rapidity of shaped motion and shaper robustness. The reviewed methods cover almost all types of positive and negative input shapers, and smoothly shaped reference commands reported in literature. Therefore, the presented review study provides almost a complete picture of the topic for the researchers working in the area. The study is structured in a way that it provides all the necessary theoretical background and the implementation related details for each of the method presented.

- **Dynamic Analysis of Gantry Cranes and Flexible Link Manipulators**

  The mathematical models of a single pendulum gantry crane and flexible link manipulator are introduced and evaluated. In addition, the flexible systems

models developed, analysed and experimentally validated. These models are also used in simulations and experimental works for comparative studies.

- **Parameter Estimation for Flexible Mechanical Systems**

  The open-loop control strategies were designed on the basis of identified natural frequencies and damping ratios of the flexible mechanical system. So, the identification of system parameters is an important factor for efficient design of an open-loop controller. The study introduces an experimental method to determine natural frequency and damping ratio of a flexible mechanical system.

- **A New Robust Command Shaping Technique to Reduce the Oscillations of A Lightly Damped Flexible Systems**

  The main contribution of this thesis is introduction of a new residual vibration elimination method developed as a part of the thesis work. This new method proves to be useful especially in case of uncertain parameters of estimated or predicted systems. It is shown that the presented new technique is capable of handling high levels of uncertainty and able to successfully eliminate or reduce residual vibrations in flexible systems. In this approach, the desired position of the system is primarily divided into two or more equal parts. The generated input signal is then used to eliminate residual vibrations. The study presents theoretical and experimental results of the techniques applied to a flexible mechanical system where a comparative study of robustness performance is also provided. The presented simulation and experimental results show that the residual vibrations are considerably decreased with a high degree of robustness in the presence of uncertainty of system parameters.

1.4. Thesis Structure

This thesis is organized as follows:

The present chapter deals with a brief introduction of vibration reduction of flexible mechanical systems and also presents the goal of the study. It also gives

some background on previously proposed command shaping schemes and presents the design philosophy that will be used throughout the thesis. At the end of this chapter, the principle contributions of the thesis are outlined.

The Chapter 2 presents the motion equation for second order systems and related residual vibrations. In addition, it provides details on how to design a shaped signal for motion control of flexible mechanical systems. It also discusses the constraint equations and presents the details on overview of different types of positive input shapers, negative input shapers and smoothly shaped reference commands. The reviewed methods cover almost all types of positive and negative input shapers, and smoothly shaped reference commands reported in literature.

The Chapter 3 describes the details of experimental setups. In addition, mathematical models and computer simulations for a gantry crane and a flexible link manipulator is developed, analysed, and experimentally validated. These models are then used in simulations in subsequent chapters. It also presents an experimental method to determine natural frequency and damping ratio of a flexible mechanical system. Chapter 3 also presents a novel robust control technique for elimination of residual vibrations in flexible systems.

The Chapter 4 illustrates theoretical and experimental results for different types of positive input shapers and smoothly shaped reference commands. It presents comparison of command shaping methods and analyses the compromise between duration of motion and shaper robustness for different types of reference commands. Advantages and drawbacks of command shaping methods are also presented.

Chapter 5 covers the conclusion, contributions and future work related details of the thesis.

2. PRELIMINARY WORK

2.1. Literature Survey

When a force is applied to a flexible mechanical system it mainly leads to motion along with vibrations. Controlling the behaviour of such mechanical systems is generally very difficult when residual vibration is not desired. Especially situation worsens if the controlled systems consist of light and flexible components mainly used for a faster response. There are some studies reported in literatures relating to control vibration of mechanical systems with flexible elements. Among these methods, command pre-shaping or input shaping based methods have attracted the attention of many researchers (Singhose and Pao, 1997; Singhose et al., 2000; Chan et al., 2003: Dharne and Jayasuriya, 2007: Gurleyuk and Cinal, 2007: Blackburn et al., 2010: Kim and Singhose, 2010). One of the solutions suggested in the literature is a feed-forward control method which alters the shape of command signal to reduce residual vibrations of the system. The earliest form of command pre-shaping technique was the use of posicast control by Smith (1957). This technique involves breaking a step input into two smaller steps, one of which is delayed in time. Superposition of the step responses results in cancellation of vibration. It also allows reduction in the settling time. However, this method is not generally favoured due to problems related to robustness in natural frequency and damping ratio uncertainties. In order to overcome this weakness, Singer and Seering (1988) proposed an acausal shaping technique for robot vibration suppression. Their work significantly extended the application range of input shaping method, in which the robustness was taken into account. In the following years, they had performed lots of works to design input shapers (Singer, 1989: Singer and Seering, 1990). Singer and Seering proposed an approach to improve the robustness of input shaping, in which the derivative of residual vibration amplitude ratio with respect to the frequency was set to zero, i.e. a three-pulse Zero Vibration and Derivative (ZVD) shaper was obtained. The ZVD shaper was much more robust; however the cost of the shaping time delay was also extended. The time delay of the Zero Vibration (ZV) shaper is half the period of the

system vibration, while the ZVD shaper extends to one complete vibration period, which means one more vibration period will be added during the system rise time if the shaper is employed.

It is obviously very difficult to suppress the residual vibration amplitude to absolute zero, and in fact such a strict requirement is seldom implemented in actual applications. If the condition of residual vibration amplitude is relaxed to non-zero, the robustness of the system can be increased notably. Based on this idea, Singhose et al. (1994) proposed Extra Insensitive (EI) input shaping approach. The EI shaper's robustness has been significantly improved compared with ZVD shaper, although they have the same time delay. Furthermore, EI input shaper will present more remarkable vibration suppression performance if it is designed according to the model error margin which can be implemented at settings level in some applications. Shan et al. (2005) presented another important method worth mentioning is called Modified Input Shaping (MIS) technique that requires the use of a certain minimum number of impulses. This technique forms modified input-shaping zero vibration (MISZV) shapers that have zero vibration at the modelled frequency, but have a larger number of impulses and longer shaper duration than the ZV shaper. Singhose et al. (1996) proposed Specified Insensitive (SI) input shaping approach. Since robustness limitation is an important consideration in SI method, the input shaper can be effectively designed according to the system robustness performance. Further details on comparison of methods for residual vibration elimination performance, such as ZV, ZVD, ZVDD and EI, are provided by Singhose et al. (1995), Vaughan et al. (2008), and Singhose (2009).

With the increase of shaper robustness, the delay of rise time is also increased, which affects the system response performance. It is obvious that there is a conflict between shaper robustness and the time delay. In order to obtain a near perfect trade-off, the shaper parameters must be selected carefully. The constraint equations used to determine the input shaper often require positive values for the impulse amplitudes. However, move time can be significantly reduced by allowing the shaper to contain negative impulses. Certain types of negative shapers have been shown to yield the time optimal control of flexible systems (Pao and Singhose,

1995). However, these negative shapers cannot be used with arbitrary commands; they must be used with step inputs. Furthermore, the impulse time locations depend on the desired move distance.

Unlike shapers containing only positive impulses, the negative shapers can lead to shaped command profiles which exceed the magnitude of the unshaped command for small periods of time. These periods of overcurrenting are not a problem for most applications because amplifiers and motors have peak current capabilities much larger than allowable steady state levels. In addition, the negative shapers have a tendency to excite un-modelled high modes (Pao and Singhose, 1996). Some researchers have formulated input shaping as a zero placement algorithm that can give rise to negative shapers (Seth et al., 1992: Jones and Ulusoy, 1994: Tuttle and Seering, 1994: Magee and Book, 1995). Because negative shapers pose the two difficulties mentioned above, the papers describing zero placement algorithms have usually included a procedure for eliminating the negative impulses. Furthermore, the negative shapers obtained with zero placements are not usually time-optimal. That is, there exist negative shapers with shorter durations which satisfy the same performance specifications. The first paper dedicated to the subject of time optimal negative input shapers required the numerical solutions of a set of simultaneous transcendental equations (Rappole et al., 1993). Singhose et al. (1994, 1997) proposed a look up method that allows the design of time optimal negative input shapers without solving a set of complicated equations.

Another approach to command shaping is the study presented by Aspinwall (1980). This method includes shaping rectangular or ‘bang-bang’ forcing function by a short, finite Fourier series to reduce residual response of a system. Swigert (1980) outlined a shaped torque method for minimizing modal vibration in a flexible satellite using shaped torque commands constructed from a finite trigonometric series. Starr (1985) reports command shaping method by suggesting a trajectory which consists of rapidly acceleration from rest to half the desired transport velocity, constant velocity, rapidly acceleration to full velocity and deceleration in a same manner. Strip (1989) suggested a motion template consist of symmetrical acceleration and deceleration profiles and the system is accelerated for a distance of

one half of acceleration times the square of natural period of oscillation. Meckl and Seering (1990) suggested construction of input signal from either ramped sinusoids or versine functions. If all harmonics of one of these template functions are added, a time optimal rectangular input function is obtained in a similar manner to the former method. However, in this method, the motion is completed in a shorter period of time owing to the shaped signal approach of the rectangular function. A more recent technique is based on shaping the input signal by inverse dynamic analysis is reported by Piazzi and Visioli (2000), who proposed a polynomial function as a desired output to produce the input signal and compared it with the bang-bang and other impulse shaping input methods. However, the suggested input function must be changed to another function at the end point to control the motion. This causes a sudden step change in acceleration at this point. In faster motion cases, this effect causes excitations and results in undesired vibrations. On the other hand, Sahinkaya (2001, 2004) suggests a third order exponential function for the output motion to shape the input signal using inverse dynamics. But the inverse dynamic analysis can be a very tedious task. Besides, it requires relatively more computation time. Alıcı et al. (1999) proposed a trajectory which consist of a half cycloid accelerating, a ramp (constant velocity) and another half cycloid decelerating is not restricted natural period of the system. In general, the major drawback of the method is due to the shaped signal being sensitive to modelling errors. Alıcı et al. (2000) have proposed a ramp superimposed onto a cycloid for input shaping in order to compare to the aforementioned input shaping method. Kapucu et al. (2001) proposed a hybrid input shaping method for undamped second order flexible system. In this method, first a cycloid plus ramp function is constructed as a pre-shaped input. Then this input is convolved this pre-shaped input with two impulse sequences, produced by using the command shaping method. The advantage of this method is due to fact that the time delay and robustness problem of the shaped signal is solved with the cost of the limitation travelling time of a half system period. Yavuz et al (2011) proposed a hybrid input shaping method to eliminate residual vibration of multi-mode system by convolving the pre-shaped input of cycloid-plus-ramped versine-ramp function with the sequence of all modes generated by two-impulse sequences. Conker et al.

(2014a) suggested an enhanced control technique for hybrid input shaping method to elimination of residual vibrations in flexible-Joint manipulators.

Command shaping is a feed-forward control technique for improving the settling time and positioning accuracy, while minimizing residual vibrations. Shaped command profiles are generated by convolving a sequence of impulses or solving special functions for the desired command signal. To determine the input shaper controller commands, estimated values of the system natural frequency and damping ratio are required to make the necessary calculations. However, real systems cannot be modelled precisely, while robustness of the shaper to modelling errors is an important design consideration. Many robust input shapers have been developed and reported in literature. It has been observed that the robust shapers typically have longer travelling time durations that leads to slower the system response. This creates a compromise between shaper robustness and rise/travelling time. This chapter presents a review of command pre-shaping methods and analyses the compromise between rapidity of motion and shaper robustness for positive input shapers, negative input shapers and smoothly shaped reference commands.

2.2. The Second Order Systems and Residual Vibrations

Second order systems are important for a number of reasons. They are the simplest systems that exhibit oscillations and overshoots. Many important systems exhibit second order system behaviour. Also second order behaviour is part of the behaviour of higher order systems and understanding second order systems helps to understand higher order systems.

For dynamic systems the vibration analysis starts with achievement of motion equation. A simplest mechanical system with arbitrary natural frequency (ω_n) and zero damping ratio ($\zeta = 0$) is selected. As seen in Figure 2.1(a), the system has an inertia element m , movable in a single coordinate $y(t)$ under the effect of position and velocity dependent forces, and an externally applied arbitrary actuation $u(t)$. Position dependent forces can be represented by the force of a spring with stiffness

*k*and the velocity dependent forces by the force of a dashpot of coefficient *b*. A great many realistic mechanical systems can effectively be reduced to have this form (Kapucu and Baysec, 1997: Mohamed and Tokhi, 2004).

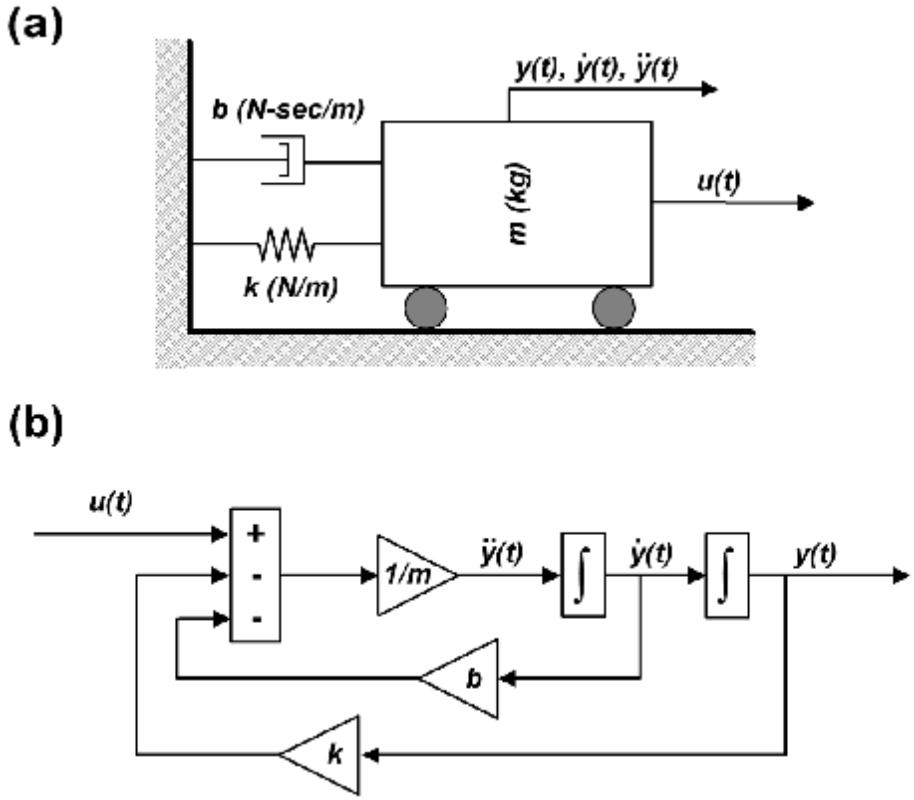

Figure 2.1. A simple, single degree of freedom, second order, linear mechanical system (a) and analogue simulation diagram of the same system (b).

The differential equation of motion of the system shown in Figure 2.l is defined as

$$m\frac{\P^2 y}{\P t^2}+b\frac{\P y}{\P t}+ky=u(t) \qquad (2.1.)$$

The transfer function of this second-order dynamical model is

$$G(s)=\frac{\mathsf{w}_n^{\,2}}{s^2+2\mathsf{z}\mathsf{w}_n s+\mathsf{w}_n^{\,2}} \qquad (2.2.a)$$

where, ω_n is the undamped natural frequency and ζ is the damping ratio. Relationship between the coefficients of transfer function and differential equation is given as:

$$\zeta = b/2\sqrt{km} \text{ and } \omega_n = \sqrt{k/m}\,. \tag{2.2.b}$$

Step or impulse response of the system generally yields damped oscillatory behaviour. Impulse response of a second order system at time t is given as (Singhose et al., 2000; Gürleyük et al., 2008; Mohamed et al., 2005):

$$x(t) = A\frac{\omega_n}{\sqrt{1-\zeta^2}} e^{-\zeta\omega_n(t-t_0)} \sin\left(\omega_n\sqrt{1-\zeta^2}\,(t-t_0)\right) \tag{2.3.}$$

where A and t_0 are the impulse amplitude and time of the impulse, respectively. For n impulses, the impulse response can be expressed as;

$$x(t) = M\sin(\omega_d t + \phi) \tag{2.4.}$$

where;

$$\omega_d = \omega_n\sqrt{1-\zeta^2} \tag{2.5.a}$$

$$M = \sqrt{\left(\sum_{j=1}^{n} B_j \cos(\omega_d t_j)\right)^2 + \left(\sum_{j=1}^{n} B_j \sin(\omega_d t_j)\right)^2} \tag{2.5.b}$$

$$B_j = \frac{A_j\omega_n}{\sqrt{1-\zeta^2}} e^{-\zeta\omega_n(t-t_i)} \tag{2.5.c}$$

$$\phi = \cos^{-1}(\zeta) \tag{2.5.d}$$

A_j and t_j are the magnitudes and times at which the impulses occur.

The residual single mode vibration amplitude of the impulse response is obtained at the time of the last impulse, t_n as

$$V_{(\omega_n,\zeta)} = e^{-\zeta\omega_n t_n}\sqrt{C_{(\omega_n,\zeta)}^{\ 2} + S_{(\omega_n,\zeta)}^{\ 2}} \tag{2.6.}$$

where

$$C_{(\omega_n,\zeta)} = \sum_{j=1}^{n} A_j e^{\zeta\omega_n t_j}\cos(\omega_d t_j) \tag{2.7.a}$$

$$S_{(\omega_n,\zeta)} = \sum_{j=1}^{n} A_j e^{\zeta\omega_n t_j}\sin(\omega_d t_j) \tag{2.7.b}$$

Equation (2.6) represents the level of vibration induced by an impulse sequence given any value of frequency and any damping ratio less than one. A constraint on residual vibration amplitude can be formed by setting equation (2.6) less than or equal to a tolerable level of residual vibration at the modelled natural frequency and damping ratio (Gürleyük et al. 2008).

2.3. The Importance of the Reference Command

The importance of the reference command can be illustrated by investigating the dynamic response of an undamped second-order harmonic oscillator. Let us assume that the desired motion is a rapid change in position from 0 to 1. Given this desired motion, the most obvious command generator produces a step function. Figure 2.2 shows the step response of an undamped oscillator (Singhose, 1997)

In an attempt to reduce vibration, a command generator that produces a ramp function in response to the desired motion could be used. Figure 2.3 shows the response to a ramp command. The vibration is reduced to 66% of the step-induced vibration. The cost of this reduced vibration is an increase in rise time.

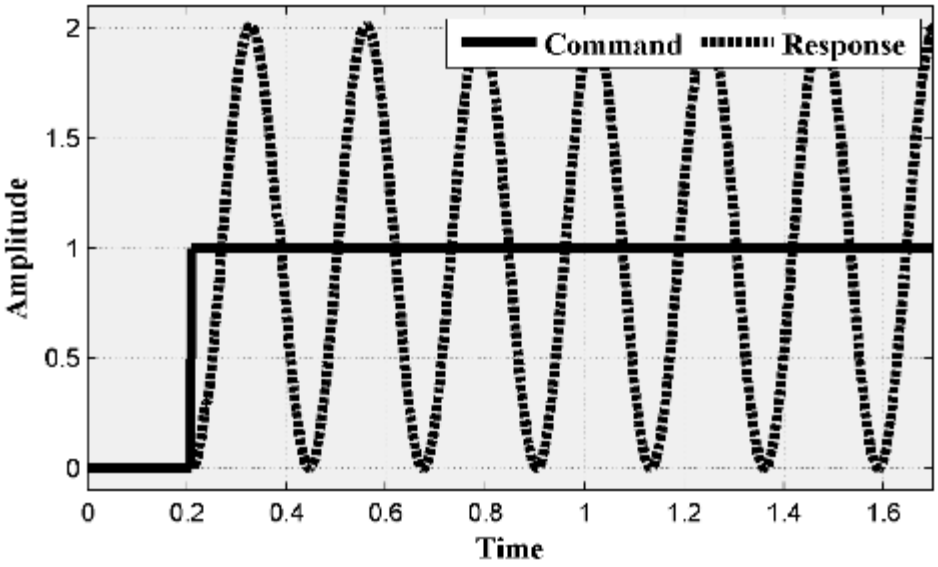

Figure 2.2. Step response of an undamped second order system

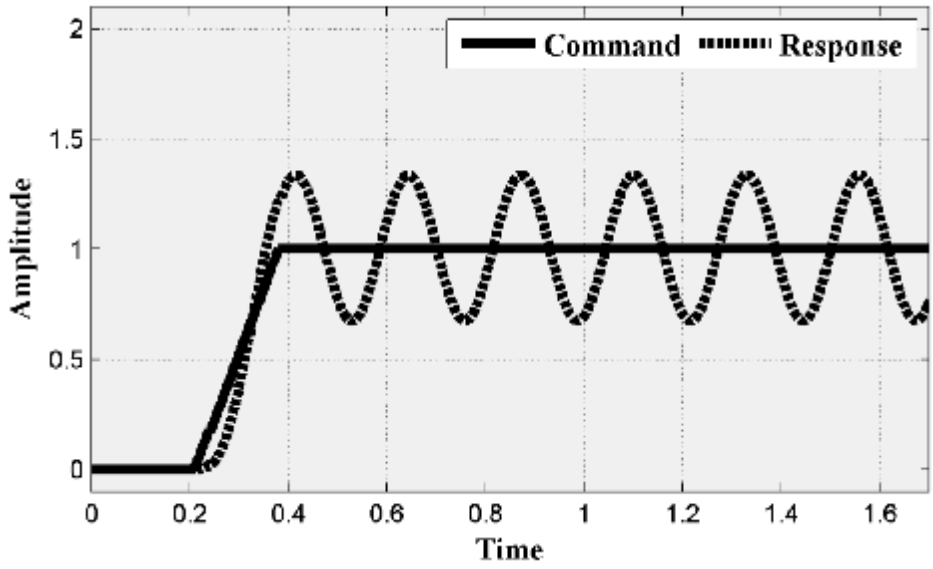

Figure 2.3. Ramp response of an undamped second order system

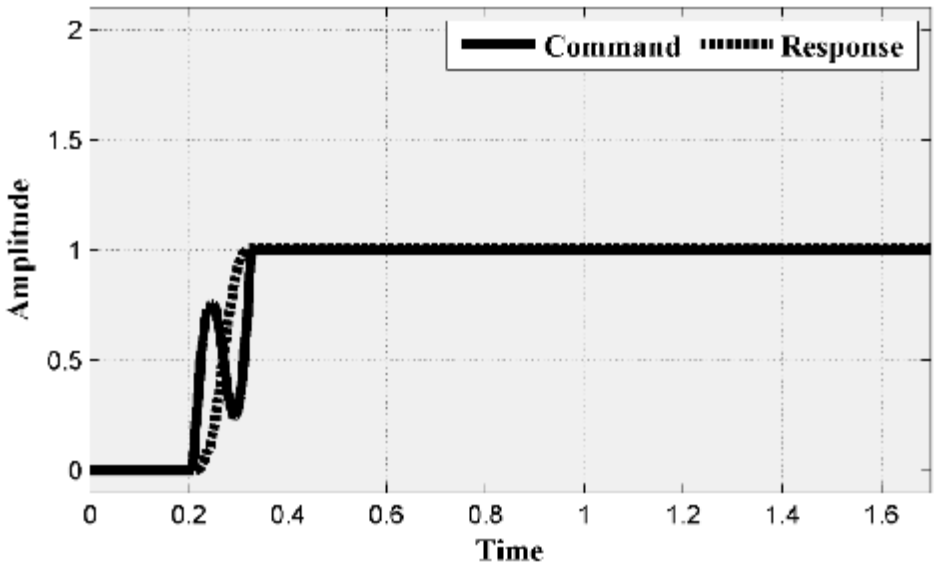

Figure 2.4. Shaped command response of an undamped second order system

If the frequency of vibration is taken into account, a command generator can be implemented that produces a special reference command. Figure 2.4 show that this shaped command causes the system to make the desired motion without any residual vibration. The price for this improved performance is increased rise time as compared to the step input. All three reference commands produce the desired motion, a rapid change in position, but the commands produce vastly different amounts of residual vibration.

Details on how to create a command generator like the one used to produce the shaped command will be given in Section 2.5.3.1. The shape of the command depends on the desired motion fed into the command generator. The distinguishing characteristic of the shaped reference commands is that they move the system to the desired position without residual vibration (Singhose, 1997).

2.4. Constraint Equations

Input shapers are designed by constructing and solving a set of constraint equations while minimizing performance criteria. The constraint equations typically set limits on: residual vibration amplitude, robustness to modelling errors and

actuator effort. The performance criteria minimized most often is the rise time, which is equivalent to the duration of the shaper.

In order to design an input shaper, or calculate impulse and time locations, a set of constraint equations must be formulated and satisfied. There are four types of constraints that are to be satisfied.

2.4.1. Residual Vibration Constraints

The maximum residual vibration amplitude from a series of impulses given in equation (2.6) can be used as a constraint equation by requiring the vibration amplitude V, to be less than some tolerable threshold. It has been shown that robustness can be improved if the vibration is limited to a small value, rather than forced to be exactly zero (Singhose et al., 1990: Singhose et al. 1994: Singhose and Kim, 2008).

2.4.2. Amplitude Constraints

The vibration caused by an input shaper can be limited by equation (2.6). However, if the input shaper impulse amplitudes are not constrained, then their values can range between positive and negative infinities. There are two possible solutions to this problem: limit the magnitude of the impulses to less than a specific value or require all the impulses to have positive values.

A second amplitude constraint must be enforced so that the shaped command reaches the desired set point; the impulse amplitudes must sum to one as follows (Singhose and Kim, 2008):

$$\sum_{i=1}^{n} A_i = 1 \qquad (2.8.)$$

If negative impulses are allowed, then the rise time will improve, but potential drawbacks such as excitation of un-modelled high modes and actuator

saturation must be addressed (Singhose and Kim, 2008). The techniques for managing the challenges of negative input shapers have been well documented by Singhose et al. (1997).

2.4.3. Robustness Constraints

Robustness to uncertainty of system parameters such as damping ratio and natural frequency are two important properties that define whether a command shaping method is superior or not. Because mathematical models of any flexible system cannot be modelled perfectly, change of the system parameters influences the shaped signal and also the system response. Therefore, robustness of shaped signal to modelling uncertainty is an important comparison tool for command shaping methods. To analyse the robustness of a command signal, the sensitivity curve and the sensitivity surface definitions are used. One key measure of robustness derived from the sensitivity curve is called as insensitivity. Insensitivity is the width of the sensitivity curve at a tolerable vibration level, with respect to the parameter of interest (Singhose et al., 1990, 1994: Vaughan et al., 2008).

2.4.3.1. Sensitivity Curve

In general, sensitivity curve is a plot of the percentage residual vibration (vibration with shaping divided by vibration without shaping) versus the normalized frequency (the actual frequency divided by the modelling frequency) as shown in Figure 2.5 where ω_x and ω are actual and modelling natural frequencies of the systems, respectively. Sensitivity curve provides a qualitative picture of the robustness of the command shaper. A sensitivity curve reveals how much residual vibration will exist when there is an error in the estimation of the vibration frequency (Convolve, Inc., 1995). One key quantitative measure of robustness derived from the sensitivity curve is Insensitivity. Insensitivity is the width of the sensitivity curve at a tolerable vibration level. If the amplitude of the residual vibration for a flexible system is less than 5 %, it is widely accepted that the system is in a vibration free

state after following the desired trajectory. To calculation of insensitivity we draw a horizontal line across the sensitivity curve at 5% as shown by the line in Figure 2.5, and the distance between the points of intersection is the insensitivity. It is shown that from figure 2.5, insensitivity varies from one method to another. For the shaping process to be effective on real systems, the shaper must have robustness to modelling errors. That is, the sensitivity curve must have zero slopes at the modelling frequency.

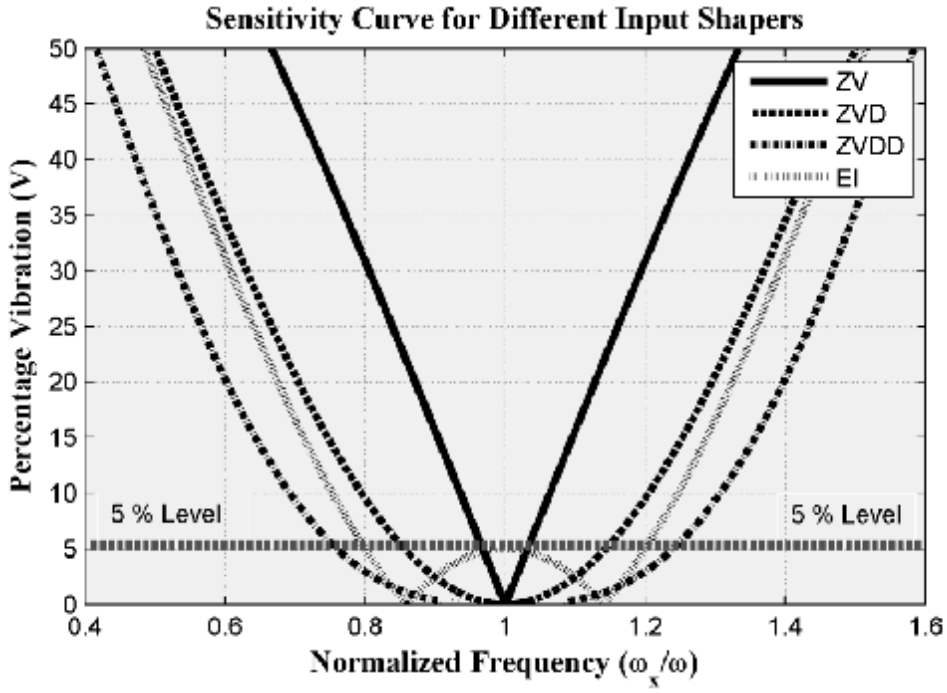

Figure 2.5. Sensitivity curves for some input shaping methods (Zero Vibration (ZV), Zero Vibration Derivative (ZVD), Zero Vibration Derivative and Derivative (ZVDD) and Extra Insensitive (EI))

2.4.3.2. Sensitivity Surface

If the sensitivity curve to both the normalized frequency (the actual frequency divided by the modelling frequency (w_x/w)) and the normalized damping ratio (the actual damping ratio divided by the modelling damping ratio (z_x/z)) is shown simultaneously, the resulting figure becomes sensitivity surface as shown in Figure 2.6 where w_x, w, z_x and z are actual frequency, modelling frequency, actual

natural frequencies and modelling natural frequencies, respectively. In Figure 2.6 the variation of the residual vibration for Zero Vibration Derivative (ZVD) input shaper is presented against estimation error in normalized natural frequency (w_x/w) and normalized damping ratio (z_x/z). Due to very low level of the damping ratio of the investigated second order system, its variation due to estimation error does not seem to affect the results as shown in Figure 2.6.

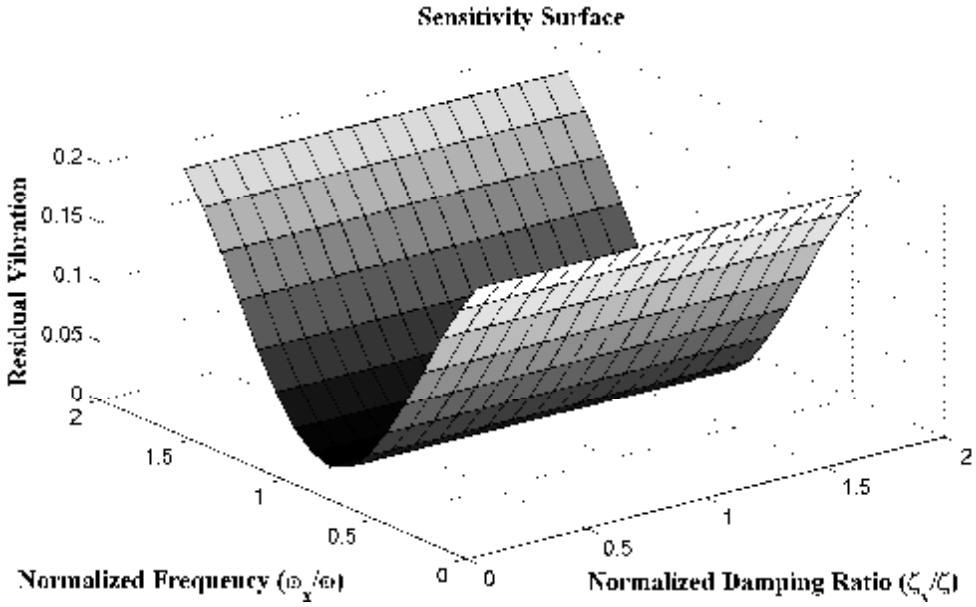

Figure 2.6. Sensitivity Surface

2.4.4. Minimization of Shaper Duration

Due to the transcendental nature of the oscillation constraint equations, there are an infinite number of solutions. To select among these solutions and to ensure that the rise time is as fast as possible, the shaper duration must be chosen as short as possible. Therefore, the final necessary design constraint minimizes the time of the final input shaper impulse as follows (Singhose and Kim, 2008):

$$\min\left(t_n\right) \tag{2.9.}$$

2.5. Shaped Reference Commands

Input shaping is a command generation technique that reduces vibration by intelligently shaping the reference signal such that the vibratory modes of the system are cancelled. To implement this method, the reference signal is convolved with a sequence of impulses, called input shapers. The timing and amplitudes of the impulses are determined using estimated properties of the system such as its frequencies and damping.

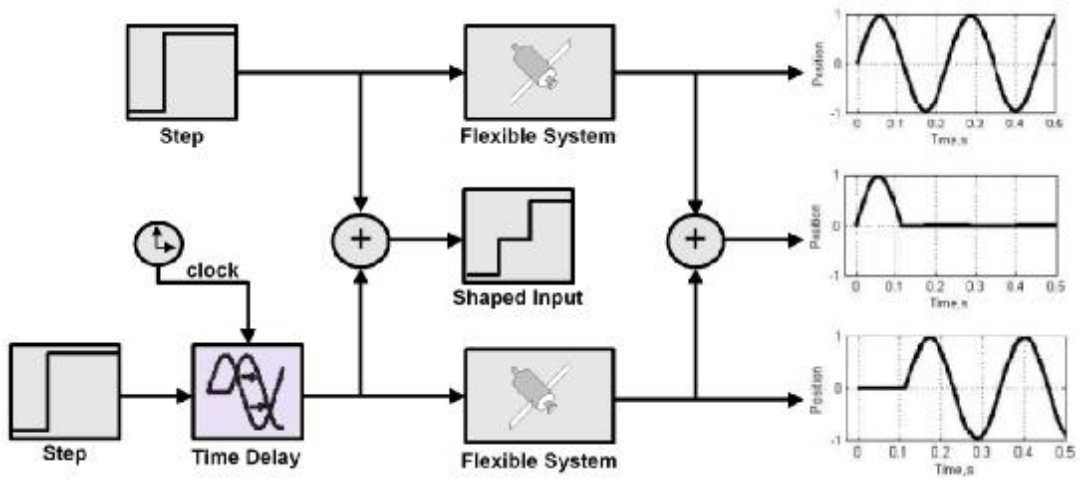

Figure 2.7. Input Shaping Process (Singh, 2010)

The simplified process of input shaping is demonstrated in Figure 2.7. Note that the rise time of the command is lengthened by the duration of the shaper. In general, the rise time of the input-shaped system will closely track the command rise time, so minimizing the shaper duration is important for achieving high-speed motion (Vaughan et al., 2007).

Input shaping's ability to cancel vibration can be viewed as destructive interference of sinusoidal waves. If two sinusoids of the same magnitude, same frequency and correct phase shift between them are added together, the resulting combination will have no oscillations. This effect can be seen in Figure 2.7. Figure 2.8 graphically indicates why the two impulse solution achieves a non-vibrating response from the system. The two responses shown can be superposed so that the

system moves forward without after the input has ended at time of the second impulse (Singer, 1989). This effect can be seen in Figure 2.8. This concept can be extended to the vibration reduction of flexible systems. If a flexible system with a constant natural frequency is given two equal inputs correctly spaced in time, then the vibration resulting from each input will add destructively cancelling each other out to yield zero residual vibration. Note that the earliest time at which the second input, or sinusoid, can be added is at one half the natural period of the system.

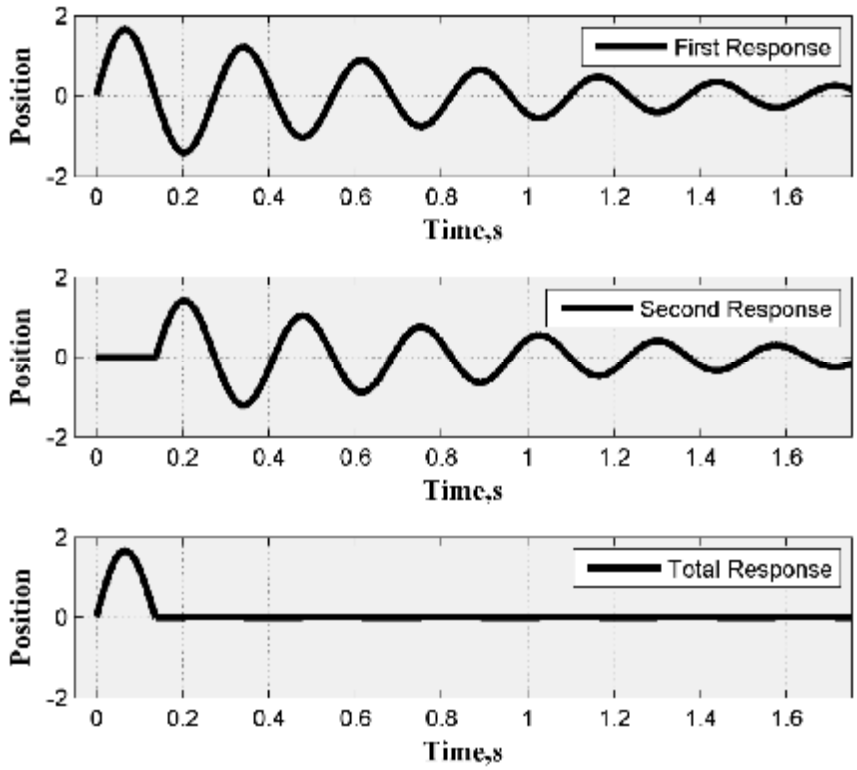

Figure 2.8. Input Shaping Process

This section will review some of the most well-known input shapers. Each of these input shapers is used within the research described in this thesis. The equations that detail the impulse times and impulse amplitudes will be written in matrix form. The first row indicates the amplitude of the impulse. The second row will indicate the time by which each impulse is delayed. Each impulse is completely defined by one column: a time delay and amplitude value.

2.5.1. Positive Input Shapers

The most common solution to the problem of large impulse amplitudes is to restrict the amplitudes to only positive values:

$$A_i \geq 0, \quad i = 1, ..., n \tag{2.10.}$$

which leads to the impulse amplitudes being less than one in order to satisfy equation (2.8). This is an attractive solution because when all positive input shaper are convolved with any unshaped input, the actuator limitations contained in the unshaped input are preserved. That is, if the unshaped command does not cause actuator limits to be exceeded, then neither will the shaped command (Singhose and Pao, 1997).

2.5.1.1. Zero Vibration (ZV) Input Shaper

A Zero Vibration (ZV), input shaper is the simplest input shaper in literature. The only constraints are minimal time and zero vibration at the modelling frequency. If Percentage Vibration (V) is set equal to zero and equation (2.6) is used to design an input shaper, then the resulting shaper is called a Zero Vibration shaper. The ZV shaper durations and amplitudes are (Vaughan et al., 2008)

$$ZV = \begin{bmatrix} A_j \\ t_j \end{bmatrix} = \begin{bmatrix} \frac{1}{1+K} & \frac{K}{1+K} \\ 0 & 0.5T_d \end{bmatrix} \tag{2.11.}$$

where $K = e^{-\frac{\zeta\pi}{\sqrt{1-\zeta^2}}}$ and $T_d = \frac{2\pi}{\omega\sqrt{(1-\zeta^2)}}$

In practice, ZV shapers can be very sensitive to modelling errors. To examine this possibility, the amplitude of residual vibration can be plotted as a function of the modelling errors.

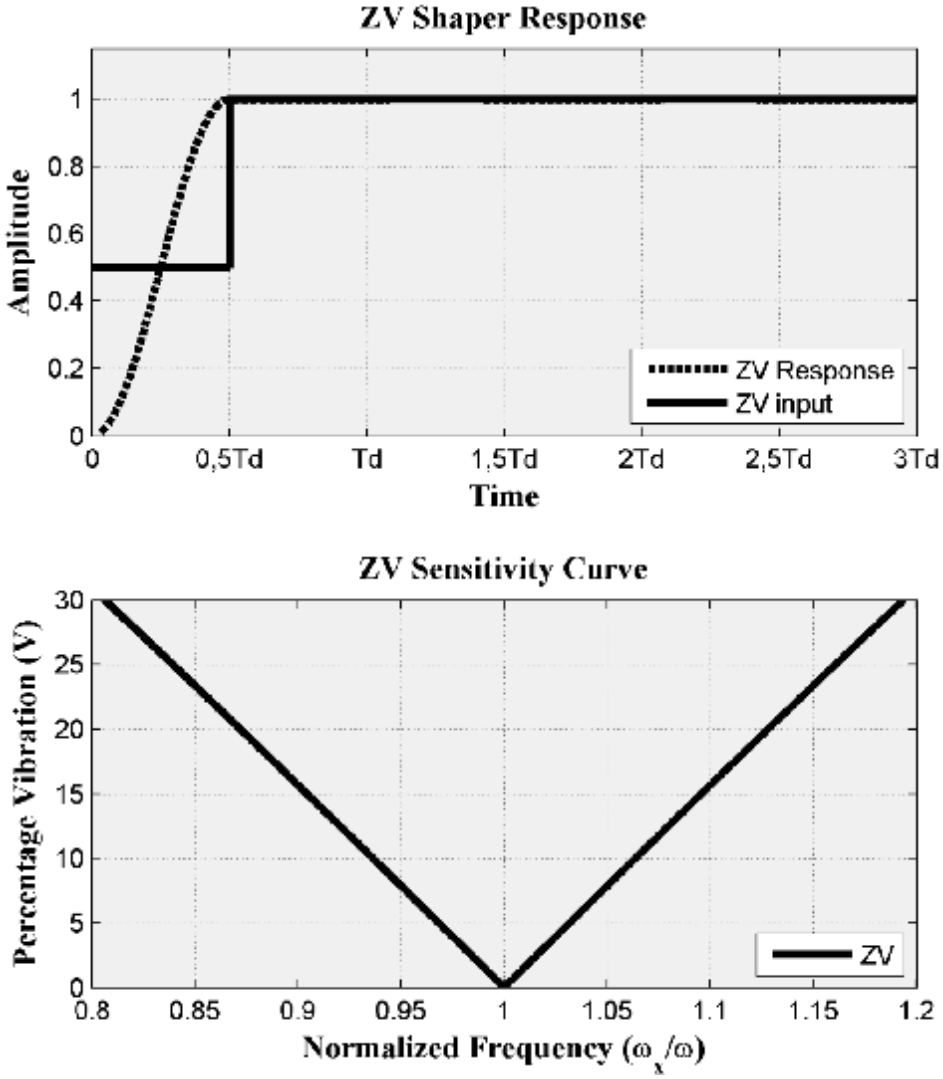

Figure 2.9. ZV input shaper and related sensitivity curve

Figure 2.9 shows such a sensitivity curve for the ZV shaper. Notice that the vibration amplitude increases rapidly as the actual frequency deviates from the modelling frequency (Singer et al., 1997). The insensitivity of ZV input shaper is 0.063 when the vibration limit (V) is set to 5%.

2.5.1.2. Derivative Methods (ZVD, ZVDD, ZVDDD Input Shapers)

The earliest form of robust input shaping was achieved by setting the derivative, with respect to the frequency, of the residual vibration equation (2.6) equal to zero.

$$\frac{d}{d\omega} e^{-\zeta\omega_n t_n} \sqrt{C_{(\omega_n,\zeta)}^{\ 2} + S_{(\omega_n,\zeta)}^{\ 2}} = 0 \tag{2.12.}$$

The resulting shaper is called a zero vibration and derivative (ZVD) shaper. The times and magnitudes for this shaper as defined by Vaughan et al. (2008) are as follows:

$$ZVD = \begin{bmatrix} A_j \\ t_j \end{bmatrix} = \begin{bmatrix} \frac{1}{1+2K+K^2} & \frac{2K}{1+2K+K^2} & \frac{K^2}{1+2K+K^2} \\ 0 & 0.5T_d & T_d \end{bmatrix} \tag{2.13.}$$

Figure 2.10 shows that the ZVD shaper is much more insensitive to modelling errors than the ZV shaper. The ZVD shaper has considerably more robustness to modelling errors. It is evident by noting that the width of the ZVD curve is much larger than the width of the ZV curve. However, the ZVD shaper has a time duration equal to one period of the vibration frequency, as opposed to the one-half period length of the ZV shaper. This trade-off is typical of the input shaper design process, increasing insensitivity usually requires increasing the length of travelling time of the input shaper (Singhose et al., 1995). The insensitivity of ZVD input shaper is 0.287 when the vibration limit (V) is set to 5%. This is approximately 4.5 times more insensitive than the ZV input shaper. The insensitivity of ZVD input shaper further increases from 0.287 to 0.4098 when the vibration limit (V) is increased from 5% to 10% (Convolve, Inc., 1995).

An input shaper with even more insensitivity than the ZVD can be obtained by setting the second derivative of equation (2.6) with respect to ω equal to zero. This shaper is called the ZVDD shaper. The algorithm can be extended indefinitely

with repeated differentiation of the percentage vibration equation. For each differentiation, an additional impulse is added to the shaper and the shaper is lengthened by one-half period of the frequency (Singhose et al., 1995).

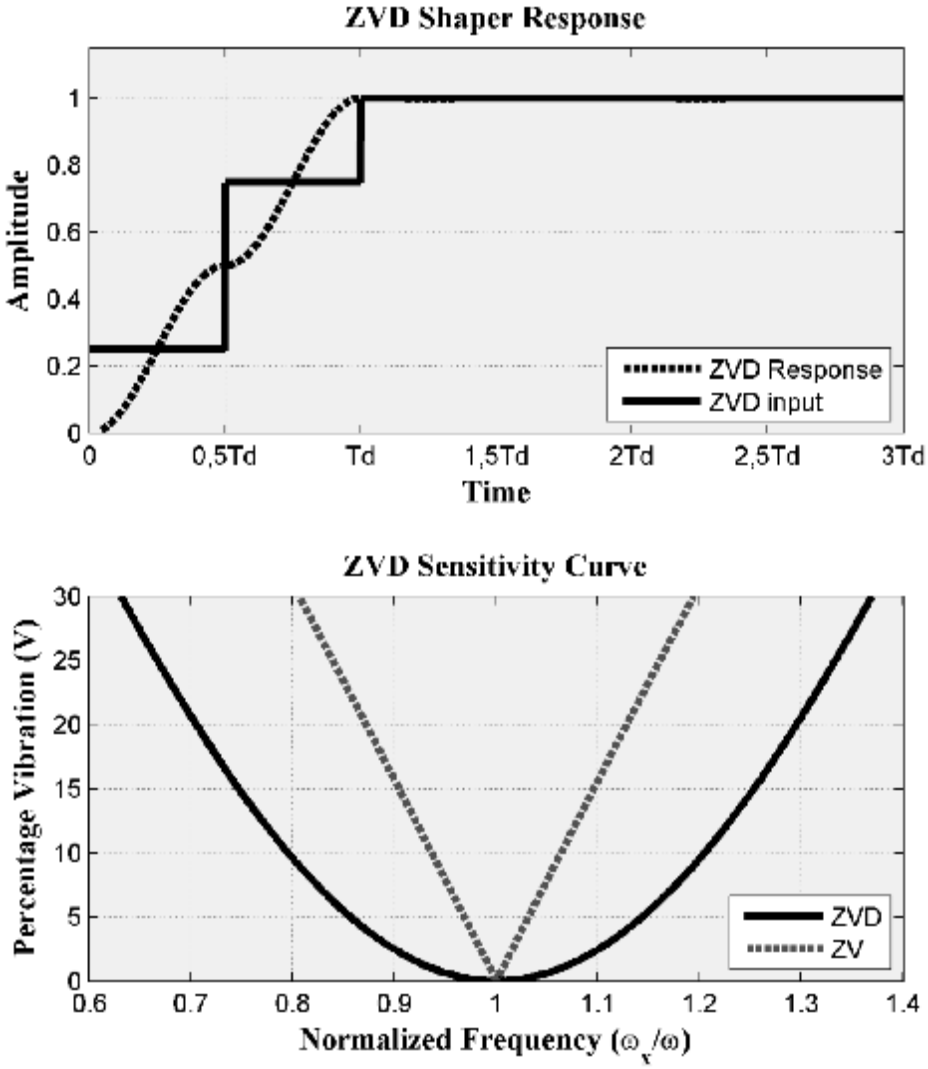

Figure 2.10. ZVD input shaper and related sensitivity curve

The times and magnitudes for ZVDD and ZVDDD shapers are defined (Vaughan et al., 2008) as follows:

$$ZVDD = \begin{bmatrix} A_j \\ t_j \end{bmatrix} = \begin{bmatrix} 1 & \frac{3K}{B} & \frac{3K^2}{B} & \frac{K^3}{B} \\ 0 & 0.5T_d & T_d & 1.5T_d \end{bmatrix} \tag{2.14.}$$

where $B = 1 + 3K + 3K^2 + K^3$

$$ZVDDD = \begin{bmatrix} A_j \\ t_j \end{bmatrix} = \begin{bmatrix} 1 & 4K & 6K^2 & 4K^3 & K^4 \\ C & C & C & C & C \\ 0 & 0.5T_d & T_d & 1.5T_d & 2T_d \end{bmatrix} \quad (2.15.)$$

where $C = 1 + 4K + 6K^2 + 4K^3 + K^4$

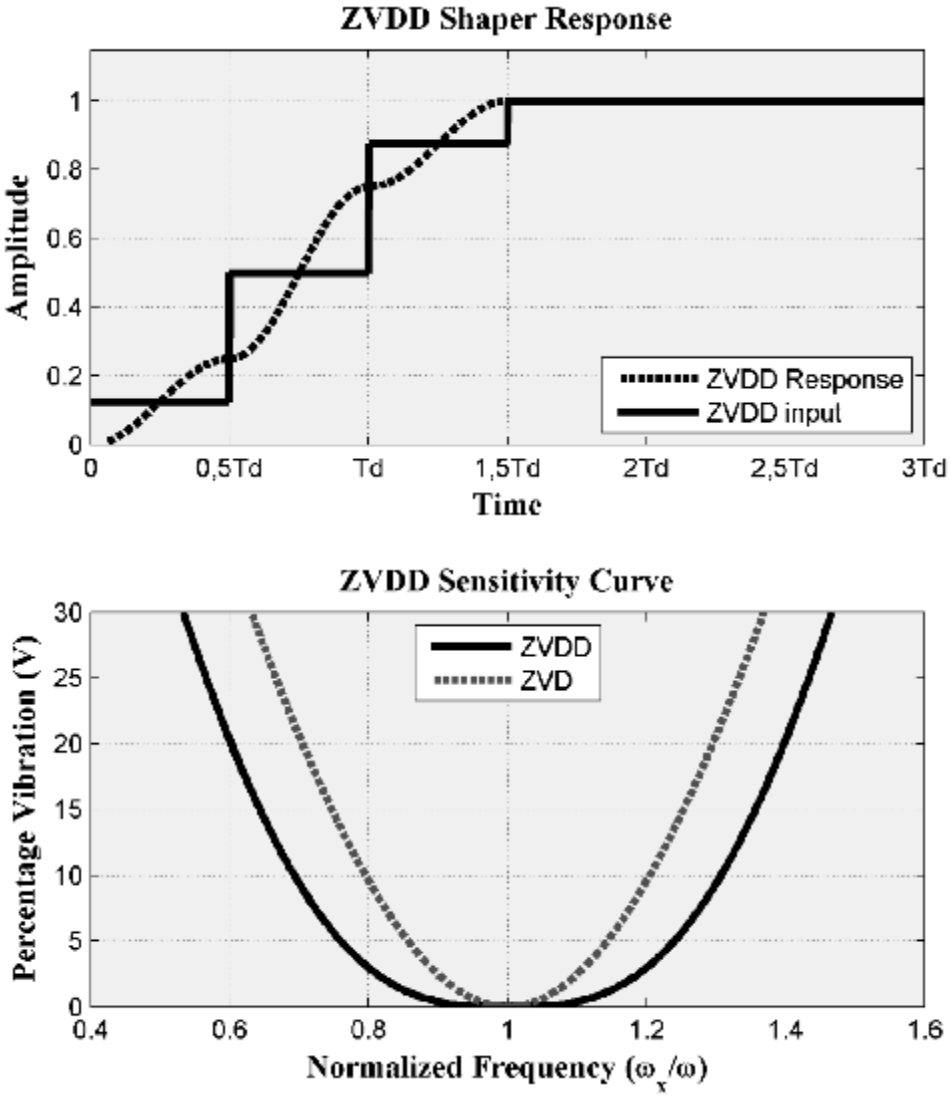

Figure 2.11. ZVDD input shaper and related sensitivity curve

Figure 2.11 shows that the ZVDD shaper is much more insensitive to modelling errors than the ZVD shaper. However, the ZVDD shaper has a time

duration equal to one and a half period of the vibration frequency, as opposed to the one period length of the ZVD shaper. The insensitivity of ZVDD input shaper is 0.48 when the vibration limit (V) is set to 5%. This is approximately 1.67 times more insensitive than the ZVD input shaper.

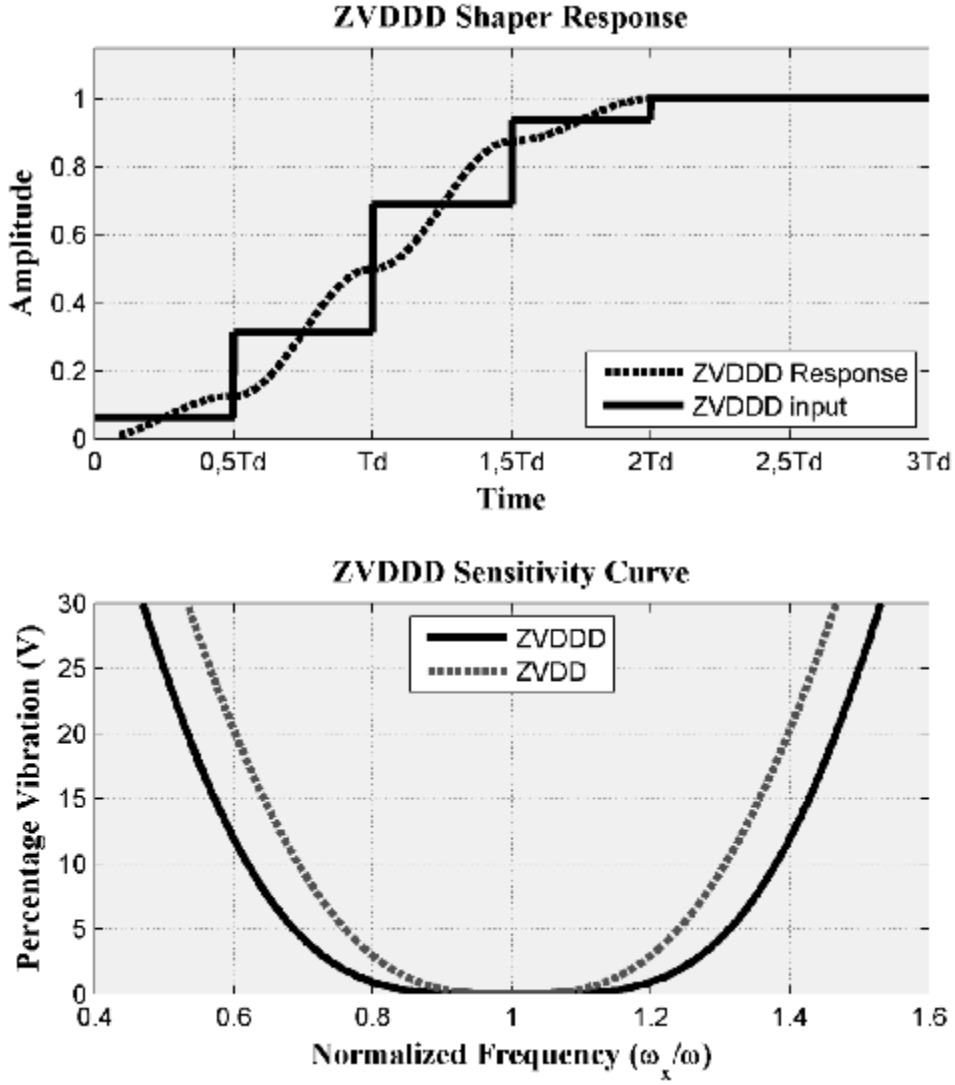

Figure 2.12. ZVDDD input shaper and related sensitivity curve

ZVDD and ZVDDD sensitivity curves are shown in Figure 2.11 and 2.12, respectively. Figure 2.12 shows that the ZVDDD shaper is much more insensitive to modelling errors than the ZVDD shaper. However, the ZVDDD shaper has a time duration equal to two period of the vibration frequency, as opposed to the one period length of the ZVDD shaper. The insensitivity of ZVDDD shaper is 0.627 when the

vibration limit (V) is set to 5%. This is approximately 1.3 times more insensitive than the ZVDD input shaper.

2.5.1.3. Extra Insensitive (EI) Input Shapers

Unlike the ZV, ZVD and ZVDD shapers, the Extra Insensitive (EI) shaper does not attempt to force the vibration to zero at the modelling frequency. Rather, the vibration is limited to some low, but acceptable level of residual vibration. The sensitivity curve for an EI shaper designed to limit vibration below 5% is shown in Figure 2.13.

The times and magnitudes for this shaper are defined as (Singhose et al. 1994; Vaughan et al., 2008):

$$EI = \begin{bmatrix} A_j \\ t_j \end{bmatrix} = \begin{bmatrix} \frac{1+V_{tol}}{4} & \frac{1-V_{tol}}{4} & \frac{1+V_{tol}}{4} \\ 0 & 0.5T_d & T_d \end{bmatrix} \tag{2.16.}$$

where V_{tol} is the tolerable level of vibration and T_d is the undamped vibration period of the system. For a system with viscous damping, the EI shaper is described by Singhose et al. (1994) and Vaughan et al. (2008).

$$EI = \begin{bmatrix} A_j \\ t_j \end{bmatrix} = \begin{bmatrix} A_1 & 1-(A_1+A_3) & A_3 \\ 0 & t_2 & T_d \end{bmatrix} \tag{2.17.}$$

where

$$A_1 = 0.24968 + 0.24961V_{tol} + 0.80008z + 1.23328V_{tol}z + ... + 0.49599z^2 + 3.17316V_{tol}z^2 \tag{2.18.a}$$

$$A_3 = 0.25149 + 0.21474V_{tol} - 0.83249z + 1.41498V_{tol}z + ... + 0.85181z^2 - 4.90094V_{tol}z^2 \tag{2.18.b}$$

$$t_2 = \frac{w\sqrt{1-z^2}}{2p}\begin{pmatrix} 0.4999 + 0.46159V_{tol}z + 4.26169V_{tol}z^2 + 1.75601V_{tol}z^3 + \dots \\ +8.57843V_{tol}^2 z - 108.644V_{tol}^2 z^2 + 336.989V_{tol}^2 z^3 \end{pmatrix} \quad (2.18.c)$$

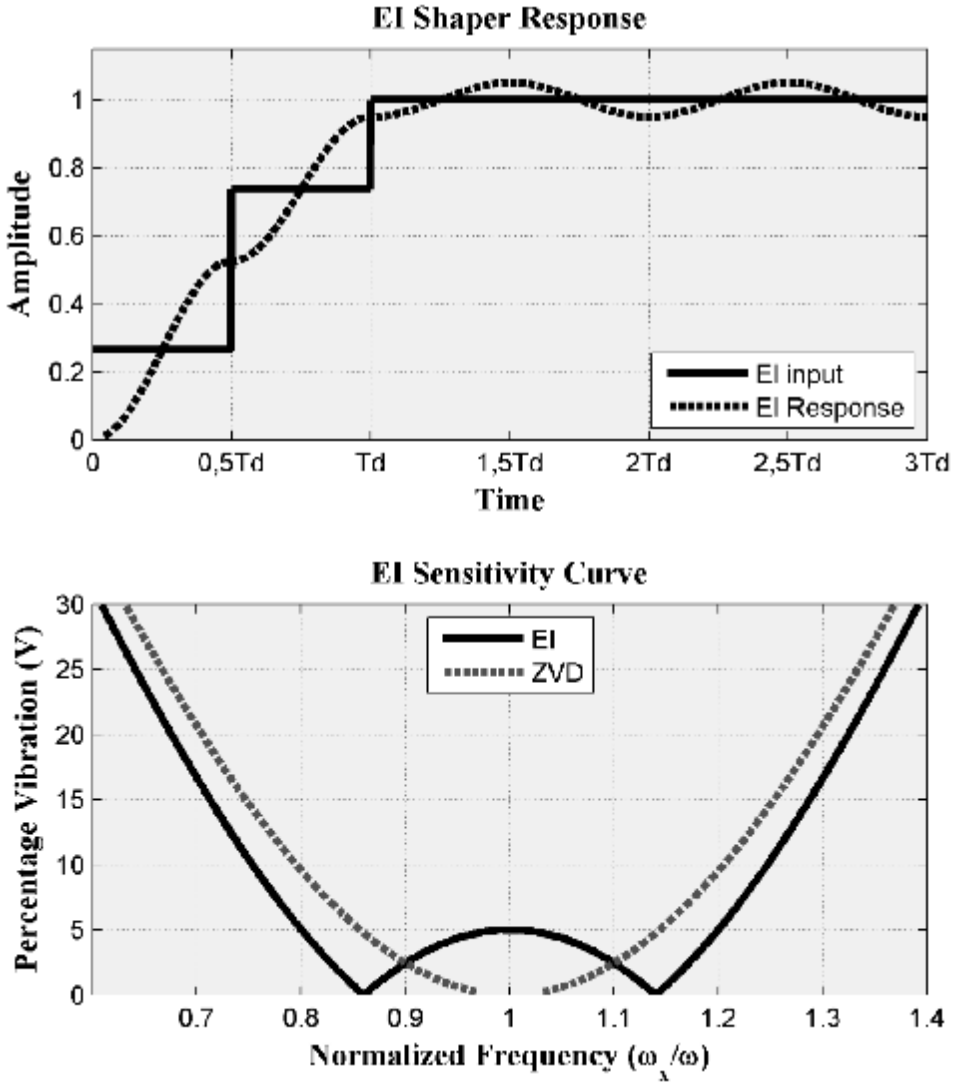

Figure 2.13. EI input shaper and related sensitivity curve

The length of the EI shaper is the same as that of the ZVD shaper, one damped cycle of vibration, but it is considerably more robust. Thus, the application of EI shapers is for systems where some small vibration is allowable, and the systems parameters are expected to change considerably. The insensitivity of EI shaper is 0.40 when the vibration limit (V) is set to 5%. This is approximately 1.4 times more

insensitive than the ZVD shaper and approximately 6.35 times more insensitive than the ZV shaper.

The ZVD problem statement requires the residual vibration to be exactly zero when the model is perfect. The EI problem statement allows there to be some small level of residual vibration when the model is perfect. The EI performance specifications are only a slight variation of the ZVD performance specifications. This can be seen by reducing the acceptable vibration in the EI formulation to zero. The EI performance specifications then converge to the ZVD specifications and the solutions are the same. This concept is demonstrated in Figure 2.14. As the acceptable limit on residual vibration is lowered, the sensitivity curve for the EI shaper approaches the sensitivity curve for the ZVD shaper (Singhose, 1997).

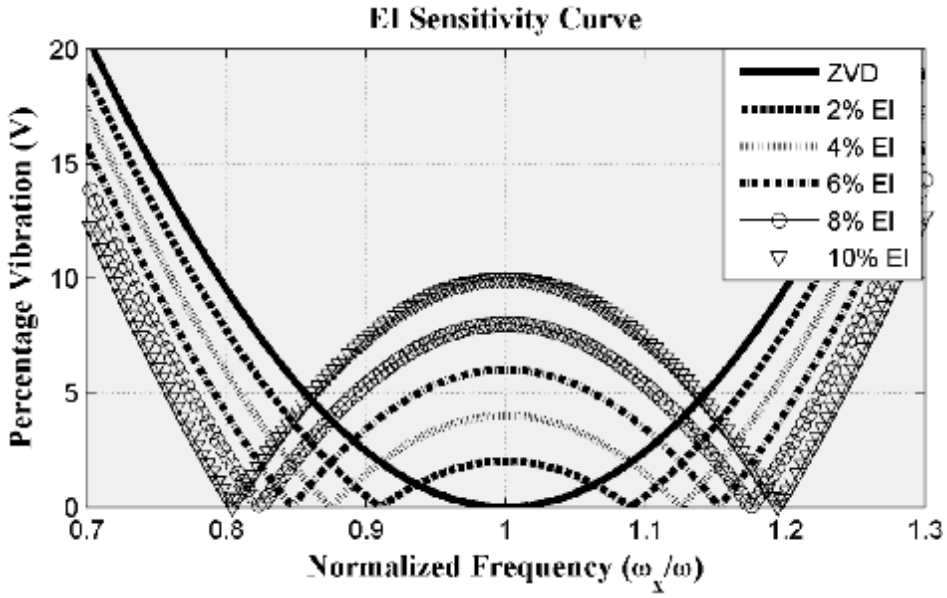

Figure 2.14. EI Sensitivity Curve as a Function of the Vibration Limit

2.5.1.4. Multi-Hump Extra Insensitive Input Shapers

The shapers that extend extra insensitive shaper idea have a progressively larger number of humps and are called multi-hump EI shapers. For undamped systems, the two-hump EI is described by Singhose et al. (1994) and Vaughan et al. (2008)

$$2H - EI = \begin{bmatrix} A_j \\ t_j \end{bmatrix} = \begin{bmatrix} A_{12H} & \frac{1}{2} - A_1 & A_2 & A_1 \\ 0 & 0.5T_d & T_d & 1.5T_d \end{bmatrix} \quad (2.19.)$$

where

$$A_1 \circ A_{12H} = \frac{3X^2 + 2X + 3V_{tol}^2}{16X} \text{ and } X = \sqrt[3]{V_{tol}^2 \left(\sqrt{1 - V_{tol}^2}\right) + 1} \quad (2.20)$$

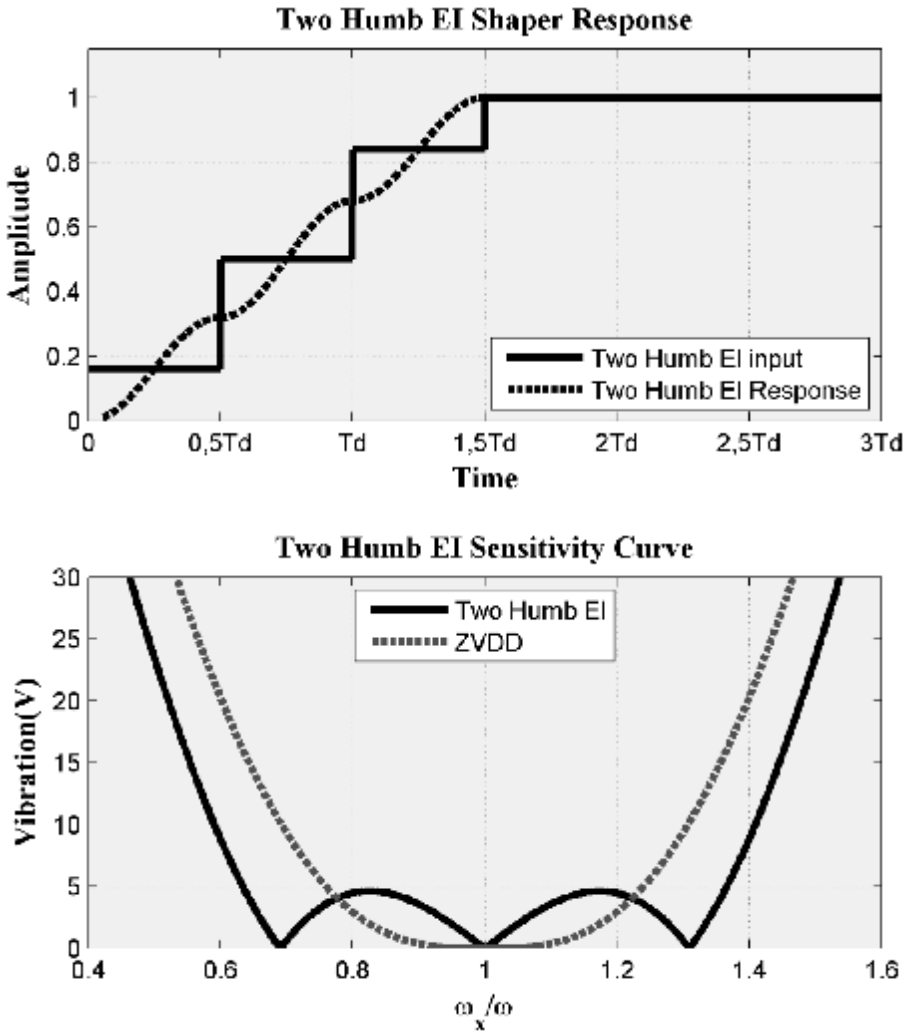

Figure 2.15. Two hump EI input shaper and related sensitivity curve

The undamped, three-hump EI shaper is described by Singhose et al. (1994) and Vaughan et al. (2008) as;

$$3H\text{-}\ EI = \begin{bmatrix} A_j \\ t_j \end{bmatrix} = \begin{bmatrix} A_{13H} & \frac{(1-V_{tol})}{4} & 1-2(A_1+A_2) & A_2 & A_1 \\ 0 & 0.5T_d & T_d & 1.5T_d & 2T_d \end{bmatrix} \quad (2.21.)$$

where

$$A_1 = A_{13H} = \frac{1+3V_{tol}+2\sqrt{2V_{tol}(V_{tol}+1)}}{16} \quad (2.22.)$$

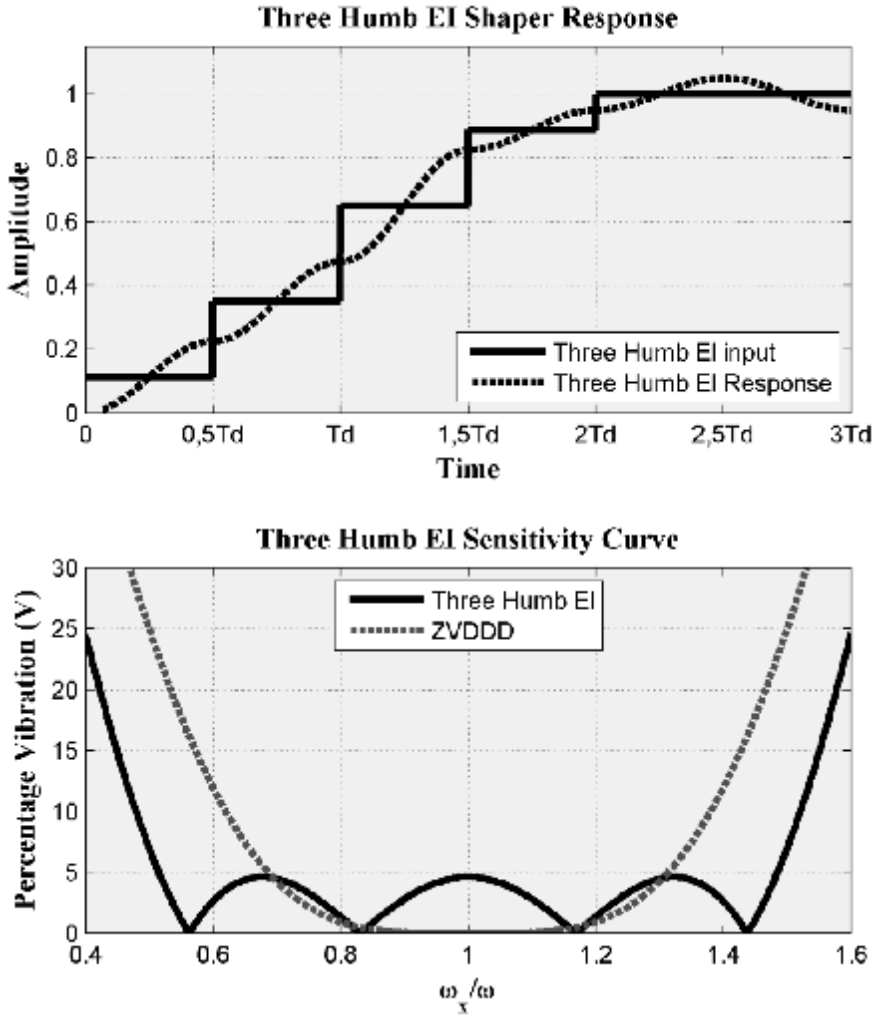

Figure 2.16. Three hump EI input shaper and related sensitivity curve

The sensitivity curves for two-hump EI and three-hump EI shapers are shown in Figure 2.15 and Figure 2.16, respectively. Note that the three-hump EI shaper

suppresses vibration over the entire range shown. As with the derivative-method shapers, the price for increased robustness is a corresponding increase in shaper duration. Note, however, that the penalty is not uniform across all shapers. The two-hump EI has the same duration as the ZVDD, and the three-hump EI and ZVDDD have the same durations. However, the EI shapers have much more robustness, as can be seen in Figure 2.15 and 2.16, where a comparative study is provided. The insensitivity of 2H-EI shaper is 0.732 when the vibration limit (V) is set to 5%. This is approximately 1.5 times more insensitive than the ZVDD input shaper.

Table 2.1. Damped multi-hump EI shapers (Singhose et al., 1994; Vaughan et al., 2008)

Shaper	$t_i = \left(M_0 + M_1 z + M_2 z^2 + M_3 z^3\right) T_d, \quad T_d = 2\pi/\omega$ $A_i = M_0 + M_1 z + M_2 z^2 + M_3 z^3$				
		M_0	M_1	M_2	M_3
Two-Hump EI	t_2	0.49890	0.16270	-0.54262	6.16180
	t_3	0.99748	0.18382	-1.58270	8.17120
	t_4	1.49920	-0.09297	-0.28338	1.85710
	A_1	0.16054	0.76699	2.26560	-1.22750
	A_2	0.33911	0.45081	-2.58080	1.73650
	A_3	0.34089	-0.61533	-0.68765	0.42261
	A_4	0.15997	-0.60246	1.00280	-0.93145
Three-Hump EI	t_2	0.49974	0.23834	0.44559	12.4720
	t_3	0.99849	0.29808	-2.36460	23.3990
	t_4	1.49870	0.10306	-2.01390	17.0320
	t_5	1.99960	-0.28231	0.61536	5.40450
	A_1	0.11275	0.76632	3.29160	-1.44380
	A_2	0.23698	0.61164	-2.57850	4.85220
	A_3	0.30008	-0.19062	-2.14560	0.13744
	A_4	0.23775	-0.73297	0.46885	-2.08650
	A_5	0.11244	-0.45439	0.96382	-1.46000

The insensitivity of 3H-EI shaper is 0.97 when the vibration limit (V) is set to 5%. This is approximately 1.55 times more insensitive than the ZVDDD input shaper and approximately 1.32 times more insensitive than the 2H-EI input shaper.

Singhose et al. (1995) solved the multi hump EI constraints over a suitable range of vibration constraint, damping ratio and Amplitude constraint. The amplitudes and time locations for the damped two-hump EI ($V_{tol} = 5$ percent) shaper and the three-hump EI ($V_{tol} = 5$ percent) shaper are given in Table 2.1.as a function of system damping. The curve fits for the two-hump EI shaper have maximum errors in the impulse times and amplitudes of less than 0.5 percent over the range $0 \le \zeta \le 0.3$. The curve fits for the three-hump EI shaper are accurate to within 0.4 percent over the range of $0 \le \zeta \le 0.2$ (Singhose et al., 1995; Vaughan et al., 2008).

2.5.1.5. Modified Input Shaping (MIS) Techniques

A modified input shaping (MIS) technique has been proposed that relaxes the constraint requiring the use of the minimum number of impulses. This technique forms modified input-shaping zero vibration (MISZV) shapers that have zero vibration at the modelled frequency, but have a larger number of impulses and longer shaper duration than the ZV shaper (Vaughan et al., 2008). An N-impulse MISZV shaper is described by Shan et al. (2005).

$$N\text{-}impulse\ MISZV = \begin{bmatrix} A_j \\ t_j \end{bmatrix} = \begin{bmatrix} \frac{1}{1+M} & \frac{K_m}{1+M} & \cdots & \frac{K_m^{i-1}}{1+M} & \frac{K_m^{N-1}}{1+M} \\ 0 & \frac{T_d}{N} & \cdots & \frac{(i-1)T_d}{N} & \frac{(N-1)T_d}{N} \end{bmatrix} \quad (2.23.)$$

where

$$K_m = e^{-2\zeta\pi/N\sqrt{1-\zeta^2}},\ M = K_m + \ldots + K_m^{i-1} + K_m^{N-1} \text{ and } T_d = 2\pi/\omega\sqrt{1-\zeta^2} \quad (2.24.)$$

The sensitivity plots for two to five-impulse MISZV shapers are shown in Figure 2.17 and 2.18. One can see that the additional impulses only provide a minimal increase in shaper insensitivity.

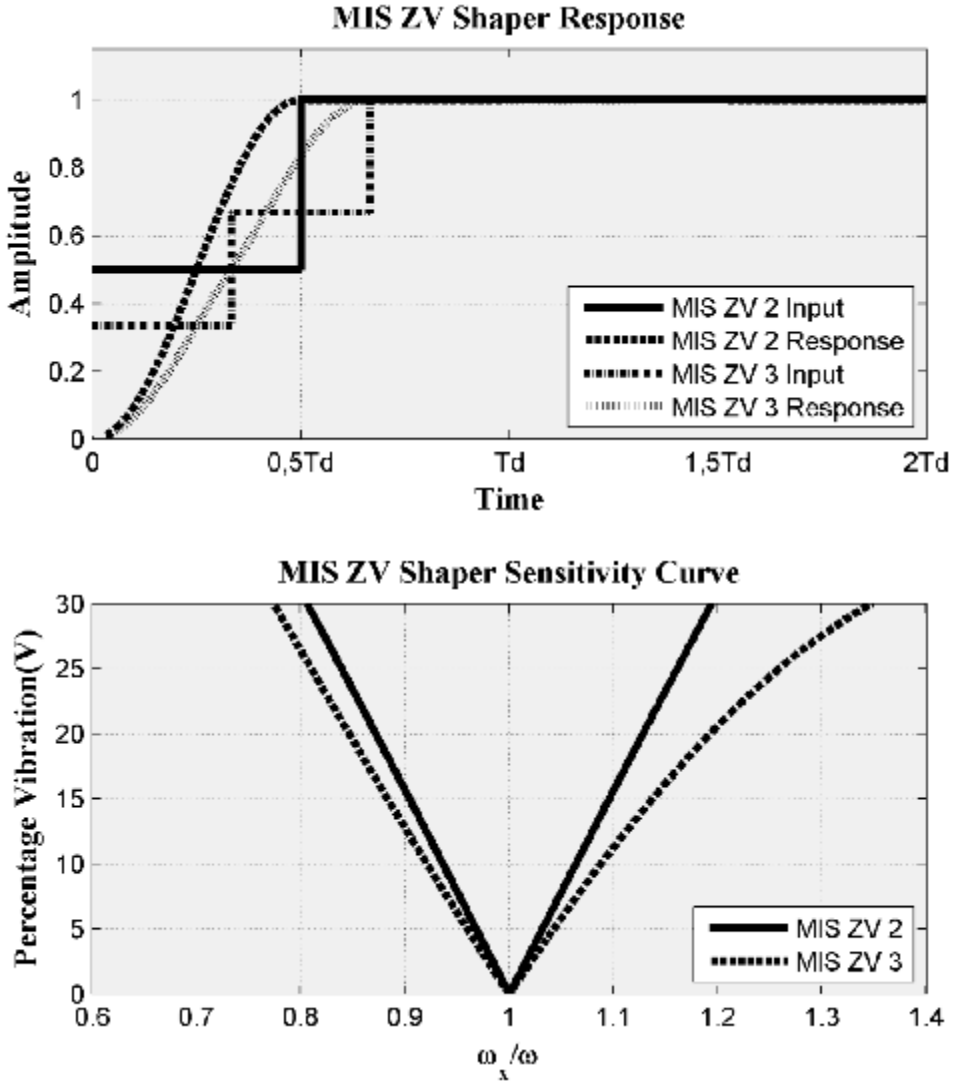

Figure 2.17. MIS 2 and 3 Impulse ZV shaper and related sensitivity curve

The performance of Modified Input Shaping (MIS) Zero Vibration (ZV) techniques stands between ZV and ZVD. The travelling time and robustness properties of the MISZV method stand in between ZV and ZVD methods. Each additional impulse to the reference command improves the robustness performance while extending the travelling time. Travelling time of the Zero Vibration Modified

Input Shapers for 2 impulse, 3 impulse, 4 impulse and 5 impulse is $0.5T_d$, $0.665T_d$, $0.749T_d$ and $0,799T_d$, respectively. The insensitivity of 2 to 5 impulse MIS-ZV shaper is 0.063, 0.082, 0.090 and 0.094, respectively. The additional impulses only provide a minimal increase in shaper insensitivity.

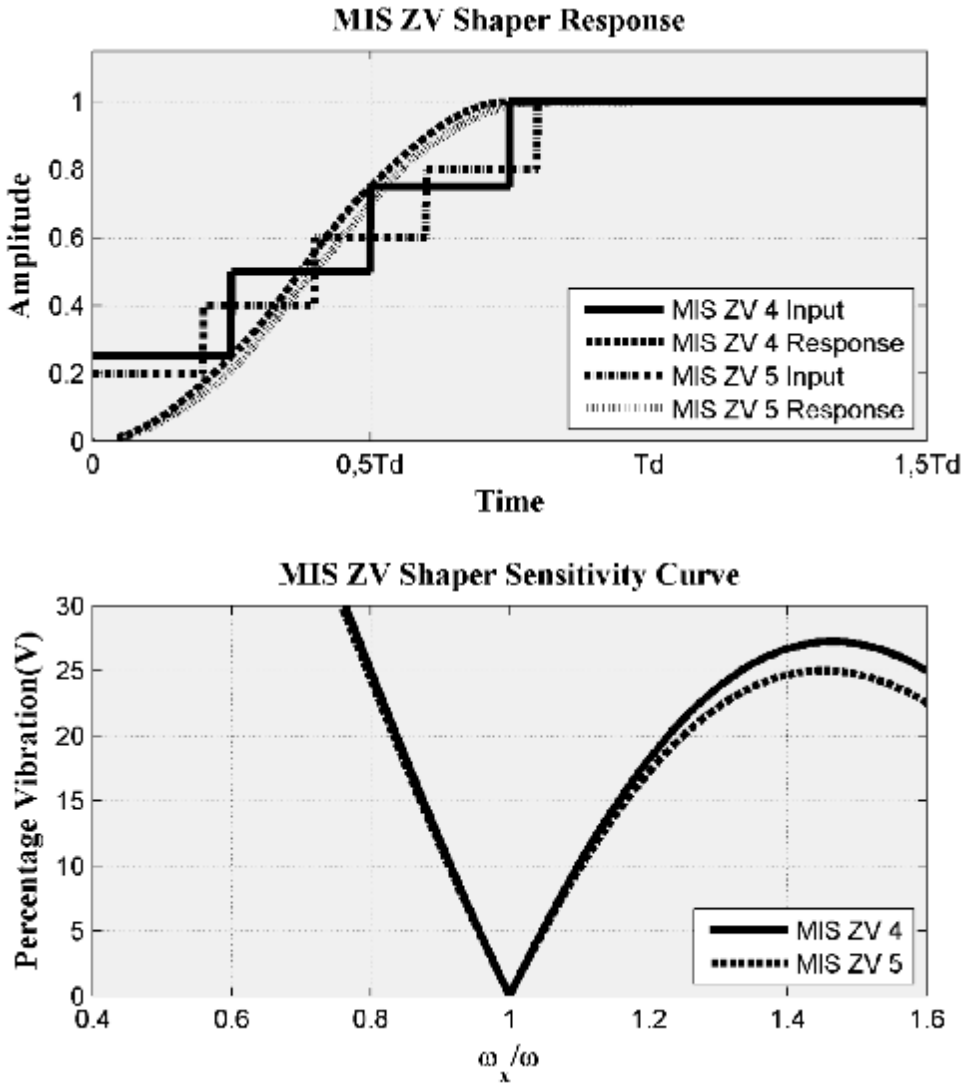

Figure 2.18. MIS 4 and 5 Impulse ZV shaper and related sensitivity curve

Zero-derivative MIS (MISZVD) shapers are formed by convolving two MISZV shapers designed for the same frequency. The resulting MISZVD shaper is indicated by the number of impulses of each of the MISZV shapers used to create it. An $N' M$ -impulse MISZVD is formed by convolving an MISZV shaper containing

N impulses with an MISZV shaper with M impulses (Vaughan et al., 2008; Shan et al. 2005). Convolving MISZV shapers of higher number of impulses results in more robust MISZVD shapers, at the cost of increased shaper duration. It should be noted that a $2' 2$-impulse MISZVD shaper is the traditional ZVD shaper. The sensitivity plots for $2' 2$ and $2' 3$ impulse MISZVD shapers are shown in Figure 2.19. When the vibration limit (V) is set to 5%, the insensitivity of $2' 2$ and $2' 3$ impulse MISZVD shapers are 0.287 and 0.332, respectively. $2' 3$ Impulse MISZVD shaper is approximately 1.15 times more insensitive than the $2' 2$ Impulse MISZVD shaper.

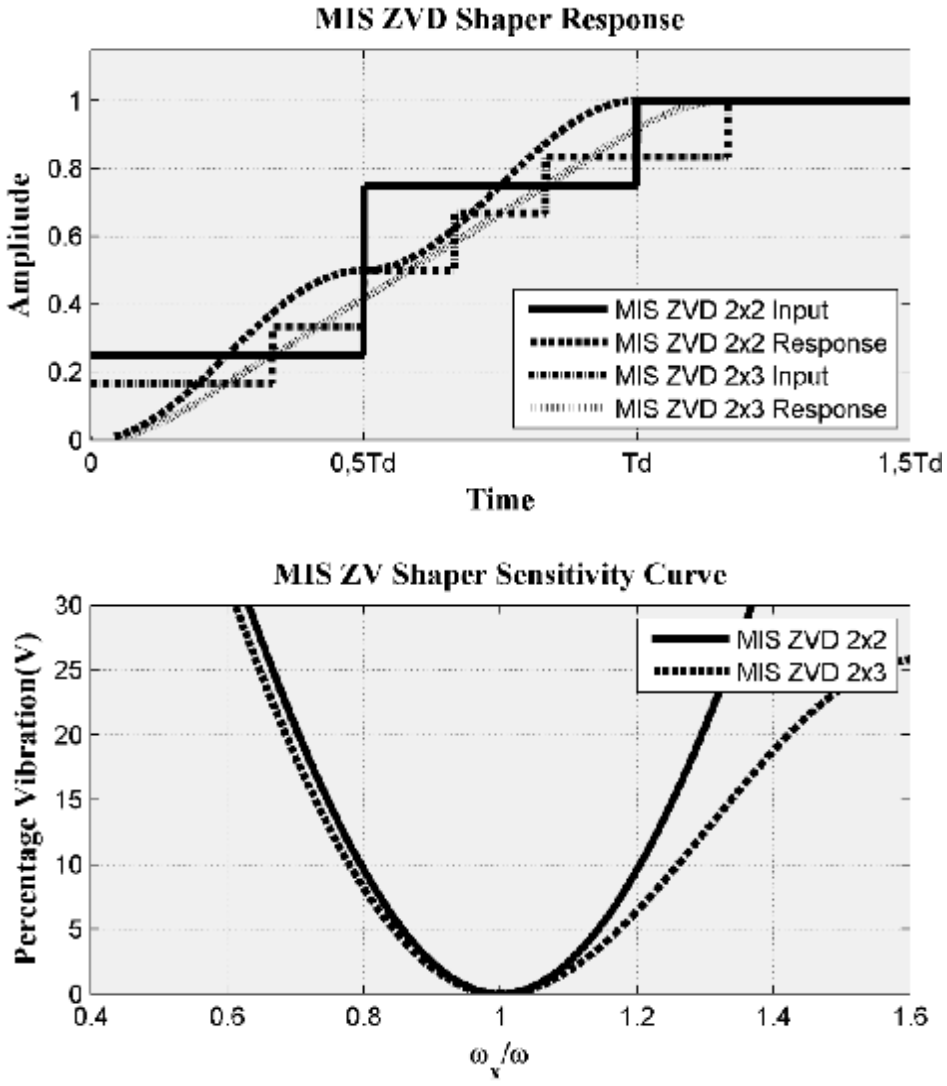

Figure 2.19. MIS $2' 2$ and $2' 3$ Impulse ZVD shaper and related sensitivity curve

2.5.2. Negative Input Shapers

In the previous sections the constraint equations used to determine the input shapers required positive values for the impulse amplitudes. Although positive input shapers are well-behaved, they move the system more slowly than shapers containing negative impulses (Singhose and Pao, 1997).

If negative impulses are allowed, then the rise time will improve, but potential drawbacks such as excitation of un-modelled high modes and actuator saturation must be addressed (Singhose and Kim, 2008). Techniques for managing the challenges of negative input shapers have been well documented by Singhose et al. (1997).

It has been reported that, for most of the negative input shapers mentioned in literature, a closed-form solution cannot be derived easily (Singhose et al., 1997: Singhose, 1997). It was also reported that, some means of numerical solution can be obtained by using programmes such as the MATLAB Optimization Toolbox. The analytical solutions to negative input shapers are listed in Tables 2.2 to 2.4, results of which are presented in Figures 2.22 to 2.29. For further details on the analytical solutions, refer to papers by Singhose et al. (1994), Singhose et al. (1997), Singhose and Pao (1997), Singhose (1997).

2.5.2.1. Partial-Sum (PS) Constraint

If the positive amplitude constraint equation (2.10.) is abandoned, another amplitude constraint must be used to limit the impulses to finite values. If the unshaped command is a step function in actuator force, constraining the partial sums of the amplitudes of the impulses to be less than one will guarantee that actuator limits are not exceeded (Singhose et al., 1994: Singhose and Pao, 1997). This requirement can be expressed as:

$$\left| \sum_{i=1}^{n} A_i \right| \leq 1, \quad n = 1, 2, ..., k \tag{2.25.}$$

When solving for the negative input shaper with constraints equation (2.8.) and (2.25.), while minimizing the shaper length, the impulse amplitudes are such that the equality sign in equation (2.25.) holds, giving impulse amplitudes of given below (Singhose and Pao, 1997):

$$A_i = \begin{bmatrix} 1 & -2 & 2 & -2 & 2 \end{bmatrix} \tag{2.26.}$$

When convolving the partial sum negative shaper given by equation (2.26.) with a step command in acceleration, the result of the convolution is a series of alternating negative pulses with magnitudes equal to the magnitude of the step. Unfortunately, most real inputs contain many step changes in acceleration. Figure 2.20 shows that when a shaper having amplitudes described by equation (2.25.) is convolved with a bang-off-bang acceleration command, there will be short periods of overcurrenting. That is, the magnitude of the shaped command exceeds that of the unshaped command (Singhose and Pao, 1997).

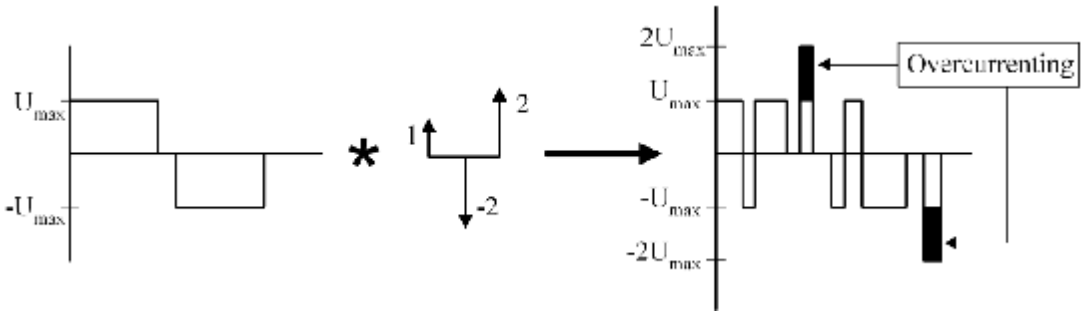

Figure 2.20. Shaping with partial sum negative shapers leads to overcurrenting (Singhose and Pao, 1997)

2.5.2.2. Unity-Magnitude (UM) Constraint

The presence of the overcurrenting is tolerable for many applications because most systems have peak current capabilities that greatly exceed the steady state levels. However, elimination of the overcurrenting altogether is desirable, and has motivated the development of an amplitude constraint that accommodates a larger class of command inputs (Pao and Singhose, 1996: Singhose and Pao, 1997). This

alternate constraint requires the impulses amplitudes to have unity magnitude (Singhose and Pao, 1997):

$$A_i = (-1)^{i+1}, \quad i = 1,...,n \tag{2.27.}$$

where n is odd. For example, if n = 5, then

$$A_i = [1 \quad -1 \quad 1 \quad -1 \quad 1] \tag{2.28.}$$

Note that a shaper meeting the amplitude constraint of equation (2.27) automatically satisfies equation (2.8). Because the unity magnitude negative shapers offer considerable advantages over the partial-sum shapers given by equation (2.25), only the unity magnitude negative shapers will be addressed here. Figure 2.21 shows the shaped command resulting from the convolution of a unity-magnitude negative shaper with a bang-bang command (Singhose and Pao, 1997).

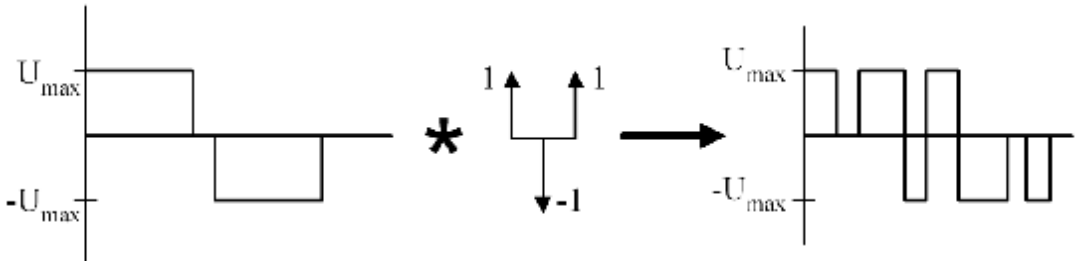

Figure 2.21. Input shaping a bang-bang command with a negative unity magnitude EI shaper yields a command which does not cause overcurrenting (Singhose et al., 1994)

2.5.2.3. Negative Zero Vibration (ZV) Shapers

ZV shapers do not work well on most real systems, but they are the shortest and, therefore, the highest performance shapers when the system frequencies are known very accurately (Singhose et al., 1997). Combining the partial sum amplitude constraint of equation (2.25.) and unity magnitude amplitude constraint of equation

(2.27.) with the vibration constraint of equation (2.6.), the impulse time locations of the partial sum (PS) and Unity-Magnitude (UM) ZV shaper can be determined, respectively. A detailed closed-form description is provided by Singhose and Pao (1997), Singhose et al. (1997) and Pao and Singhose (1996).

The amplitudes and time locations for the PS-ZV and UM-ZV shaper are given in Table 2.2 as a function of the system damping (Singhose et al., 1997; Singhose; 1997). The curve fits for the PS-ZV and UM-ZV shaper have maximum errors in the impulse times and amplitudes of less than 0.5 percent over the range $0 \leq z \leq 0.3$.

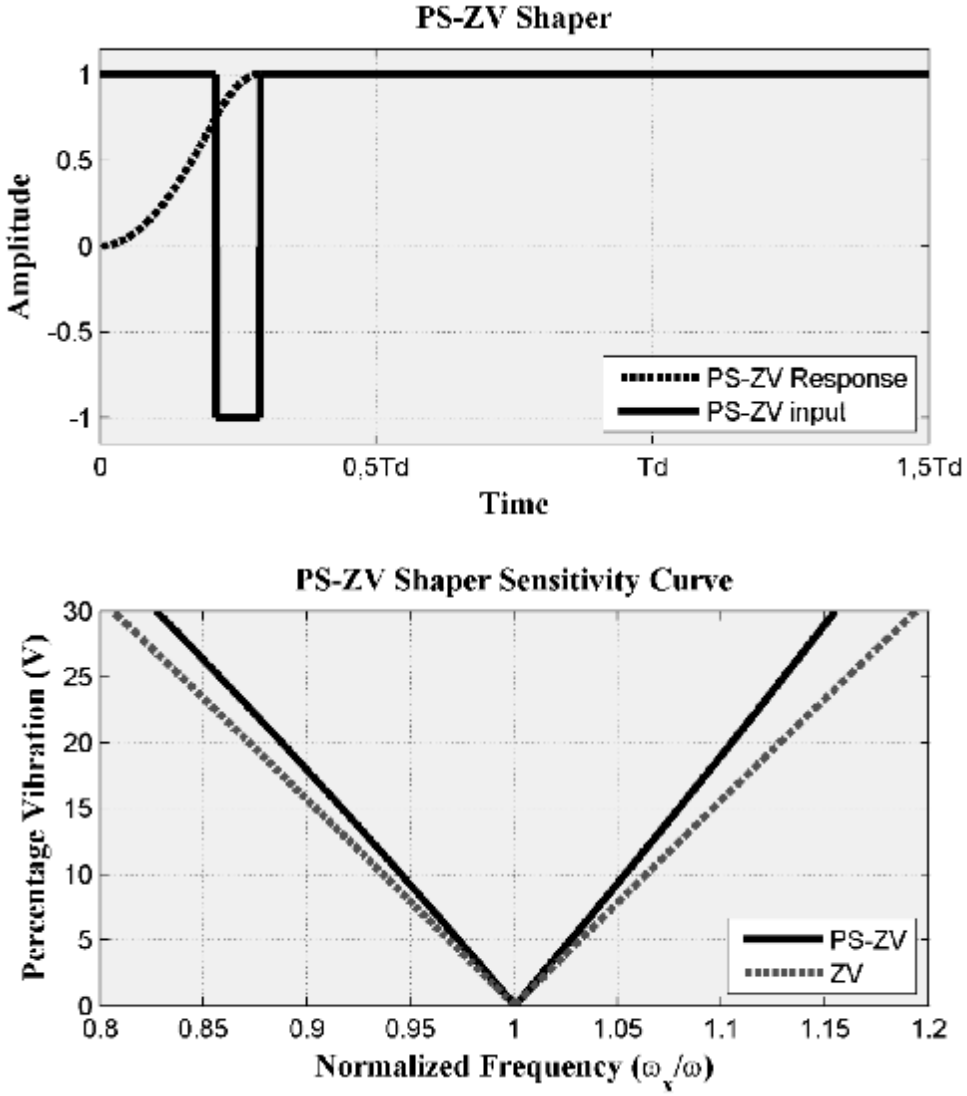

Figure 2.22. Partial Sum ZV input shapers and related sensitivity curve

When $A=1$, the length of PS-ZV shaper is $0.29T_d$, where T_d is the period of vibration. The UM-ZV shaper has a length of $0.33T_d$, while the positive ZV shaper has length of $0.5T_d$. A negative shaper will have slightly poorer performance than a positive shaper in the presence of modelling errors, even though they satisfy the same robustness constraints (Singhose et al., 1997). For example, the sensitivity curves for the positive ZV shaper, PS-ZV shaper and UM-ZV shaper are shown in Figure 2.7, Figure 2.22 and Figure 2.23, respectively.

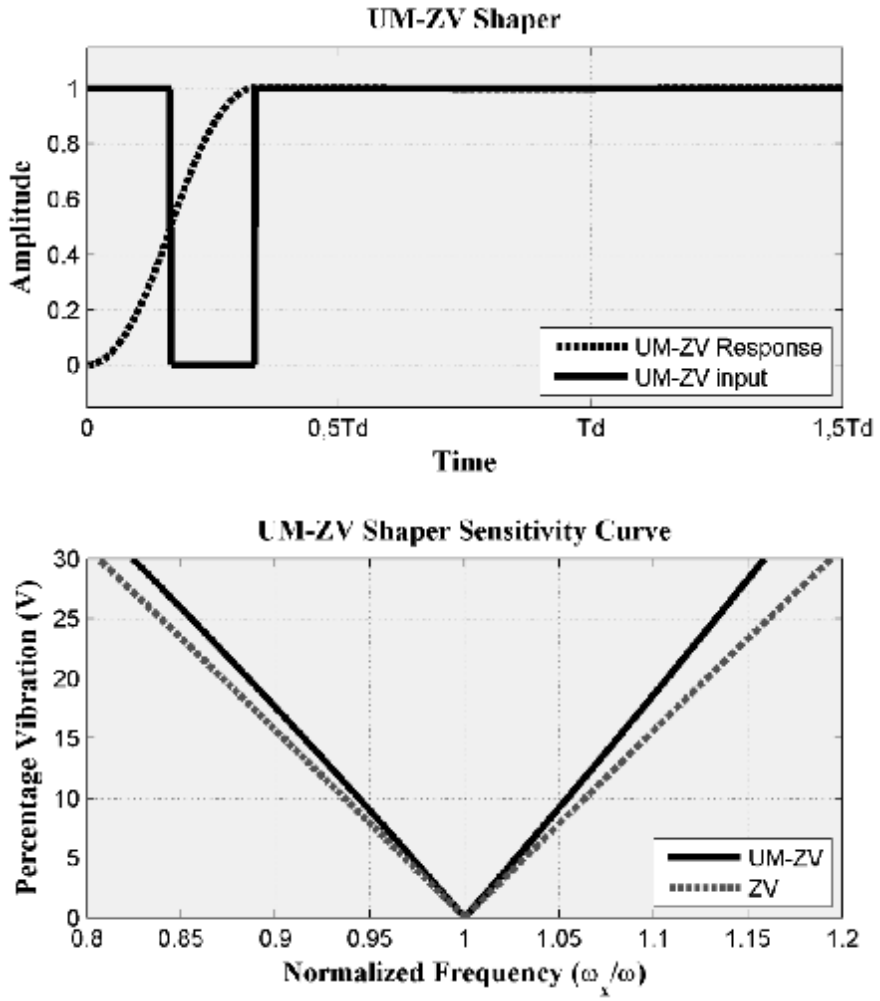

Figure 2.23. Unity Magnitude ZV input shapers and related sensitivity curve

When the vibration limit (V) is set to 5%, the insensitivity of PS-ZV and UM-ZV shapers are 0.054 and 0.0548, respectively. The positive ZV shaper is

approximately 1.16 times more insensitive than the PS-ZV input shaper and approximately 1.15 times more insensitive than the UM-ZV input shaper.

Table 2.2. Numerically determined Negative ZV input shapers (Singhose et al., 1997; Singhose, 1997)

	$t_j = \left(M_0 + M_1 z + M_2 z^2 + M_3 z^3\right) T_d, \quad T_d = 2\pi/\omega$					
Shaper	A_j	t_j	M_0	M_1	M_2	M_3
PS-ZV	1	t_1	0	0	0	0
	-2	t_2	0.20970	0.22441	0.08028	0.23124
	2	t_3	0.29013	0.09557	0.10346	0.24624
UM-ZV	1	t_1	0	0	0	0
	-1	t_2	0.16658	0.29277	0.07544	0.21335
	1	t_3	0.33323	0.00533	0.17914	0.20125

2.5.2.4. Negative Zero Vibration and Derivative (ZVD) Shapers

To satisfy the ZVD constraints, a negative shaper must contain five impulses. For the UM-ZVD and PS-ZVD shaper the amplitudes are:

$$PS\text{-}\ ZVD = A_j = \begin{bmatrix} 1 & -2 & 2 & -2 & 2 \end{bmatrix} \tag{2.29.}$$

$$UM\text{-}\ ZVD = A_j = \begin{bmatrix} 1 & -1 & 1 & -1 & 1 \end{bmatrix} \tag{2.30.}$$

The time location of each impulse is a complex function of z . Solutions are obtained by Singhose (1997) over a wide range of z for both the UM and the PS amplitude constraints. The curve fits to t_2, t_3, t_4, and t_5 for the UM and the PS ZVD shapers are shown in Table 2.3. The length of the UM-ZVD shaper is 73% of the positive ZVD, while the length of the PS-ZVD shaper is only 68% of the positive ZVD input shaper when $A=1$ (Singhose, 1997).

Table 2.3. Numerically determined Negative ZVD input shapers (Singhose et al., 1997; Singhose, 1997)

$t_j = \left(M_0 + M_1 z + M_2 z^2 + M_3 z^3\right) T_d, \quad T_d = 2\pi/\omega$

Shaper	A_j	t_j	M_0	M_1	M_2	M_3
PS-ZVD	1	t_1	0	0	0	0
	-2	t_2	0.15234	0.23397	0.15168	0.21310
	2	t_3	0.27731	0.11147	0.04614	0.28786
	-2	t_4	0.63114	0.34930	0.11840	0.52558
	2	t_5	0.67878	0.19411	0.27432	0.48505
UM-ZVD	1	t_1	0	0	0	0
	-1	t_2	0.08945	0.28411	0.23013	0.16401
	1	t_3	0.36613	-0.08833	0.24048	0.17001
	-1	t_4	0.64277	0.29103	0.23262	0.43784
	1	t_5	0.73228	0.00992	0.49385	0.38633

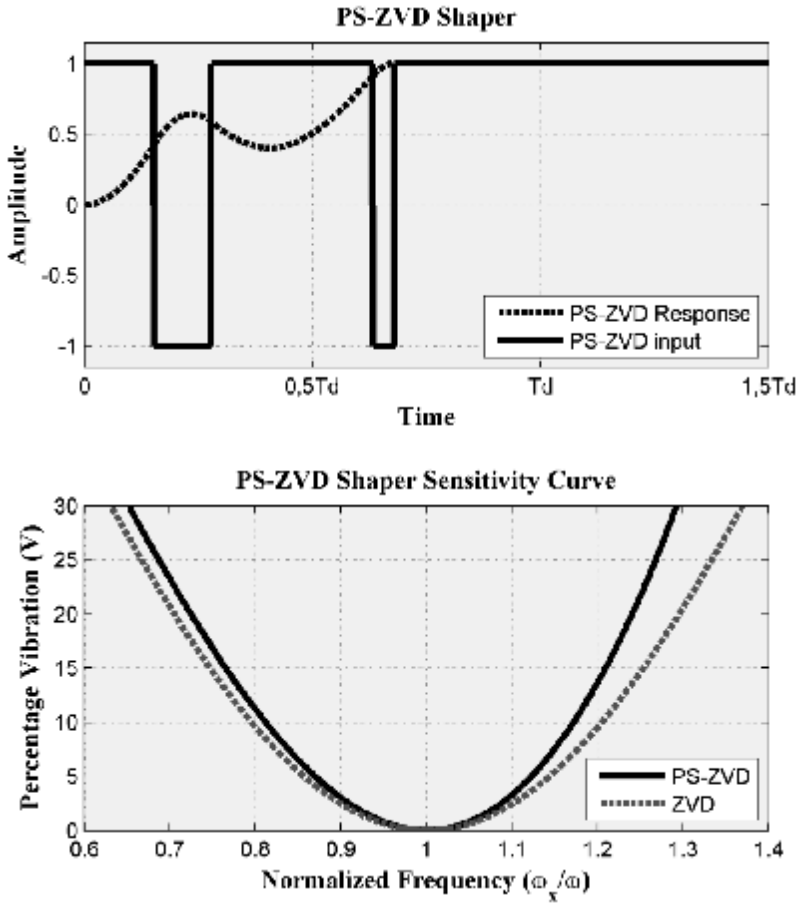

Figure 2.24. Partial Sum ZVD input shapers and related sensitivity curve

When amplitude of the input signal is equal to one $(A=1)$, the length of PS-ZVD shaper is $0.67T_d$, where T_d is the period of vibration. The UM-ZVD shaper has a length of $0.73T_d$, while the positive ZVD shaper has length of T_d. A negative shaper will have slightly poorer performance than a positive shaper in the presence of modelling errors, even though they satisfy the same robustness constraints. For example, the sensitivity curves for the positive ZVD shaper, PS-ZVD shaper and UM-ZVD shaper are shown in Figure 2.8, Figure 2.24 and Figure 2.25, respectively. When the vibration limit (V) is set to 5%, the insensitivity of PS-ZVD and UM-ZVD shapers are 0.2535 and 0.2585, respectively. The positive ZVD shaper is approximately 1.135 times more insensitive than the PS-ZVD input shaper and approximately 1.113 times more insensitive than the UM-ZVD input shaper.

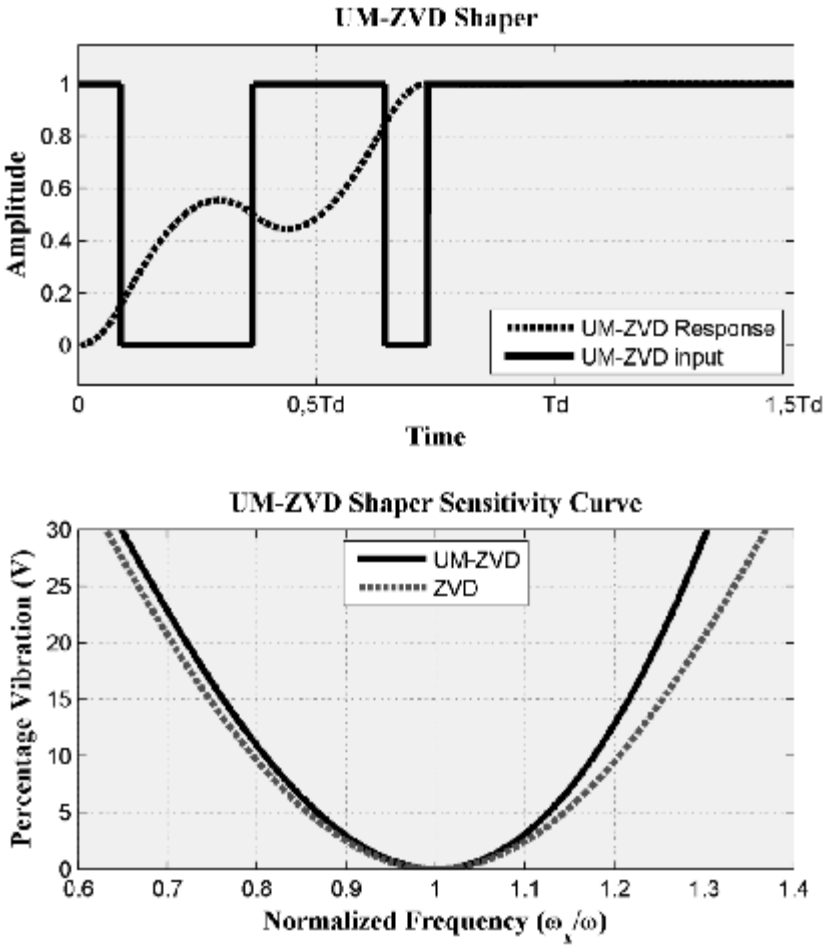

Figure 2.25. Unity Magnitude ZVD input shapers and related sensitivity curve

2.5.2.5. Negative Extra-Insensitive (EI) Shapers

Singhose et al. (1997) solved the UM and PS EI constraints over a suitable range of vibration constraint, damping ratio and amplitude constraint. Table 2.4 includes curve fits to the time locations of the negative EI shapers when residual vibration is 5%. By examining Table 2.4, it can be seen that the EI shapers are essentially the same length as the ZVD shapers regardless of the values of z . However EI shapers are more insensitive to modelling errors than that of ZVD input shapers.

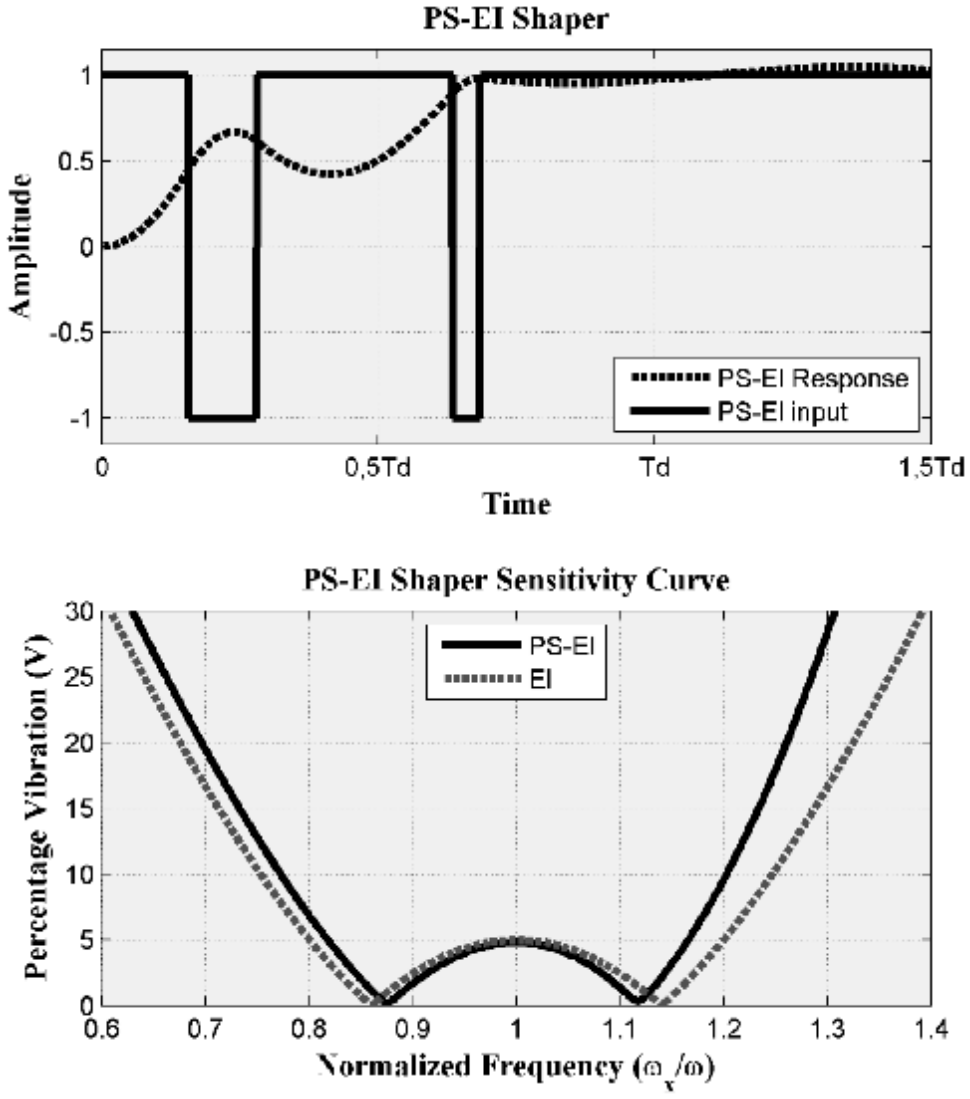

Figure 2.26. Partial Sum EI input shapers and related sensitivity curve

Table 2.4. Numerically determined Negative EI input shapers (Singhose et al., 1997; Singhose, 1997)

	$t_j = \left(M_0 + M_1 z + M_2 z^2 + M_3 z^3\right) T_d, \quad T_d = 2\pi/\omega$					
Shaper	A_j	t_j	M_0	M_1	M_2	M_3
PS-EI V=5%	1	t_1	0	0	0	0
	-2	t_2	0.15631	0.26556	0.05324	0.69457
	2	t_3	0.28080	0.13931	-0.05627	0.75423
	-2	t_4	0.63427	0.34142	0.15371	0.32904
	2	t_5	0.68410	0.18498	0.31059	0.28565
UM-EI V=5%	1	t_1	0	0	0	0
	-1	t_2	0.09374	0.31903	0.13582	0.65274
	1	t_3	0.36798	-0.05894	0.13641	0.63266
	-1	t_4	0.64256	0.28595	0.26334	0.24999
	1	t_5	0.73664	0.00162	0.52749	0.19208
2 Hump PS-EI V=5%	1	t_1	0	0	0	0
	-1	t_2	0.12952	0.29981	0.08010	1.7913
	1	t_3	0.27452	0.22452	-0.20059	1.8933
	-1	t_4	0.58235	0.51403	-0.00620	1.6106
	1	t_5	0.68355	0.26308	0.08029	1.7095
	-1	t_6	1.08870	0.39342	0.14197	0.48868
	1	t_7	1.12080	0.25926	0.35816	0.35035
2 Hump UM-EI V=5%	1	t_1	0	0	0	0
	-2	t_2	0.05970	0.31360	0.31759	1.5872
	2	t_3	0.40067	-0.08570	0.14685	1.6059
	-2	t_4	0.59292	0.38625	0.34296	1.2889
	2	t_5	0.78516	-0.08828	0.54174	1.3883
	-2	t_6	1.12640	0.20919	0.44217	0.30771
	2	t_7	1.18640	-0.02993	0.79859	0.10478

Partial Sum EI and Unity Magnitude EI input shapers are shown in Figure 2.26 and Figure 2.27, respectively. The length of the Unity Magnitude EI shaper is 73% of the positive EI input shaper, while the length of the Partial Sum EI shaper is only 68% of the positive EI input shaper when amplitude of the input signal is equal

to one $(A=1)$. When the vibration limit (V) is set to 5%, the insensitivity of PS-EI and UM-EI shapers are 0.348 and 0.355, respectively. The positive EI shaper is approximately 1.15 times more insensitive than the PS-EI input shaper and approximately 1.127 times more insensitive than the UM-EI input shaper.

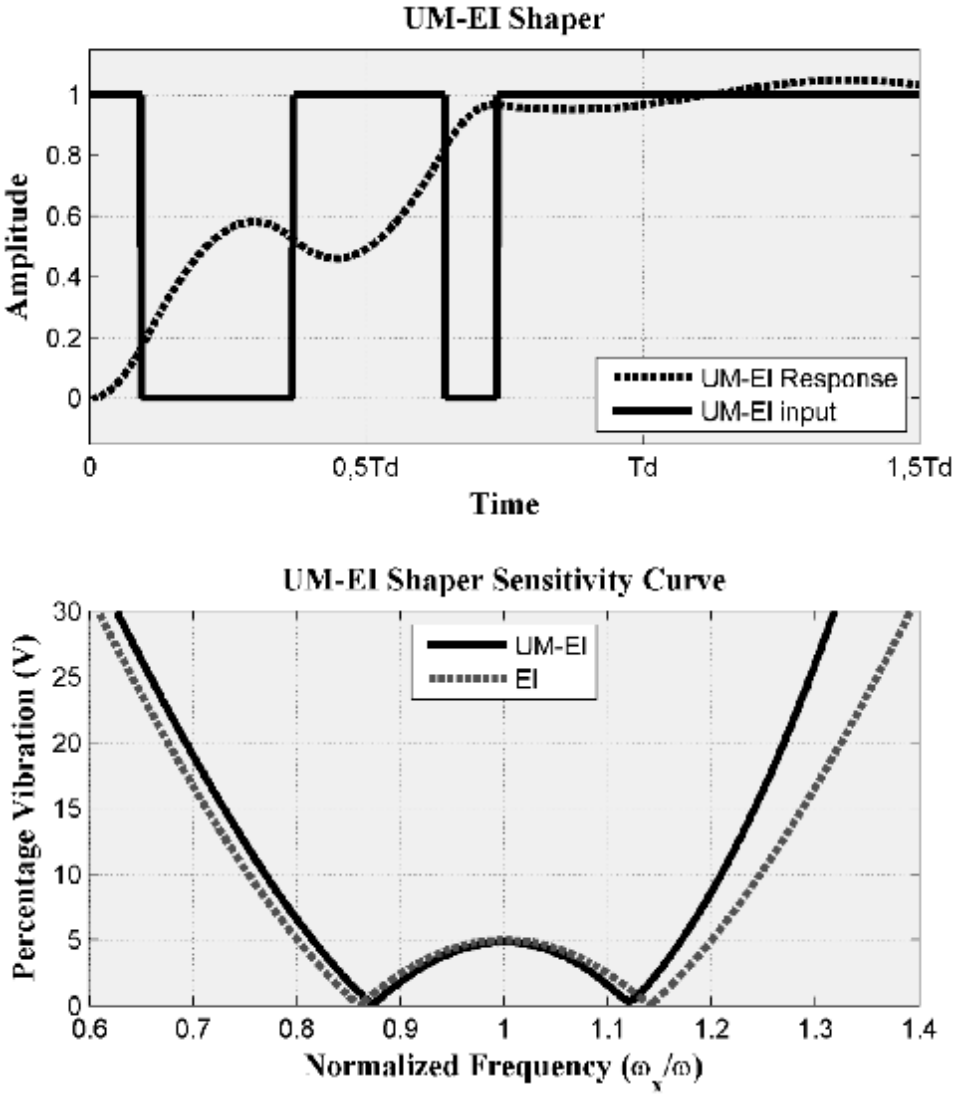

Figure 2.27. Unity Magnitude EI input shapers and related sensitivity curve

A negative shaper will have slightly poorer performance than a positive shaper in the presence of modelling errors, even though they satisfy the same robustness constraints (Singhose et al., 1997). For example, the sensitivity curves for

the positive EI shaper, PS-EI shaper and UM-EI shaper are shown in Figure 2.13, Figure 2.26 and Figure 2.27, respectively.

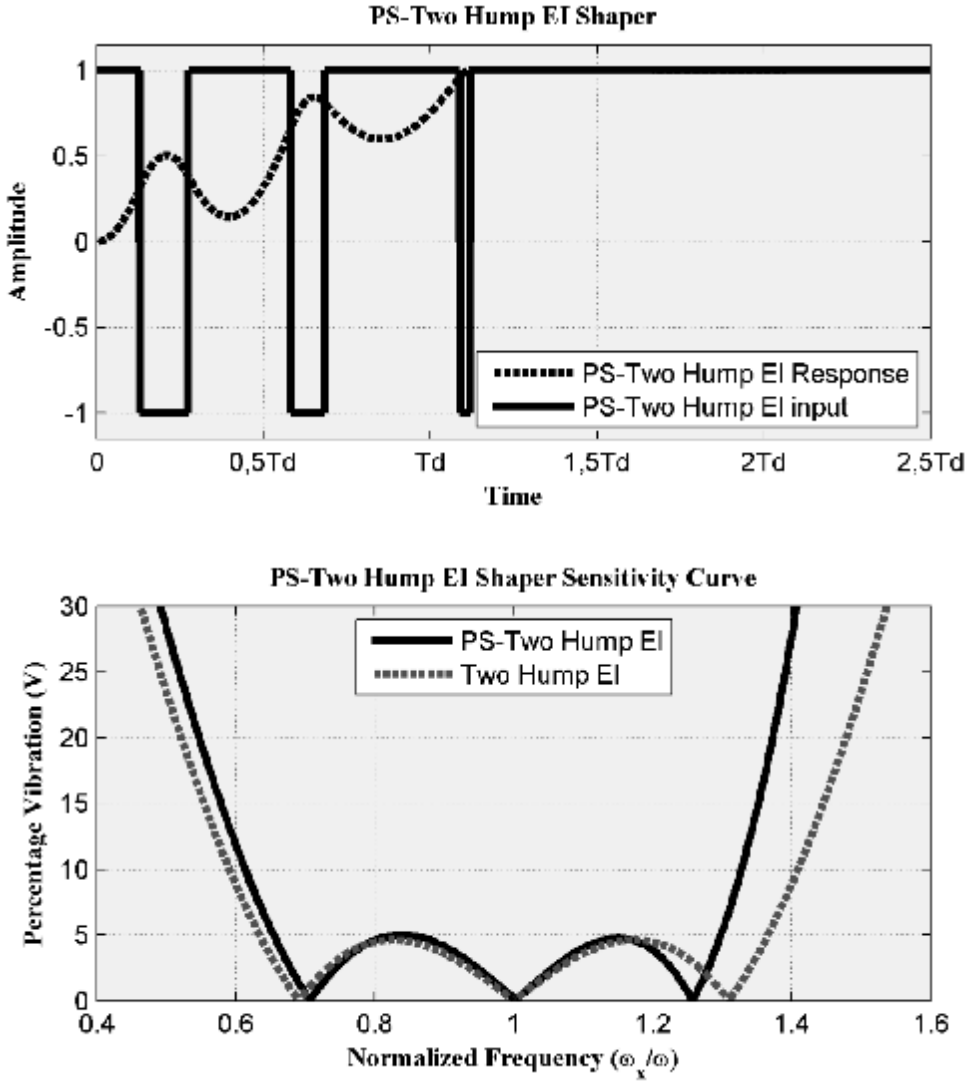

Figure 2.28. Partial Sum 2 Hump EI input shapers and related sensitivity curve

Partial Sum 2 hump EI and Unity Magnitude 2 hump EI input shapers are shown in Figure 2.28 and Figure 2.29, respectively. The length of the UM 2 Hump EI shaper is 79% of the positive 2 hump EI input shaper, while the length of the PS 2 Hump EI shaper is only 74% of the positive 2 Hump EI input shaper when amplitude of the input signal is equal to one $(A=1)$. When the vibration limit (V) is set to 5%, the insensitivity of PS-Two Hump EI and UM-Two Hump EI shapers are

0.6437 and 0.659, respectively. The positive Two Hump EI shaper is approximately 1.138 times more insensitive than the PS-Two Hump EI input shaper and approximately 1.11 times more insensitive than the UM-Two Hump EI input shaper.

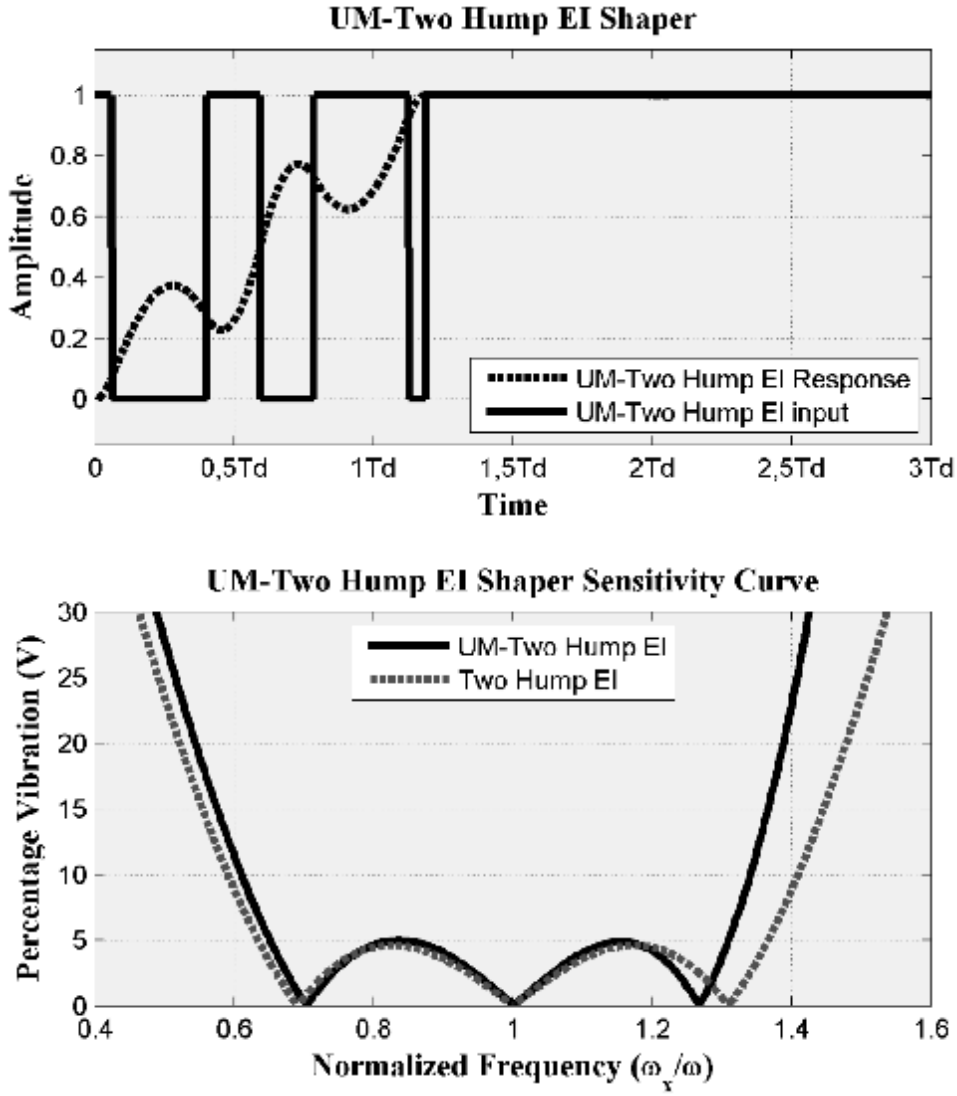

Figure 2.29. Unity Magnitude 2 Hump EI input shapers and related sensitivity curve

2.5.3. Smoothly Shaped Reference Commands

This kind of shaped signal is produced by adding more than one template functions using the model parameters. In this technique, the amplitude of each function is designed such that the oscillations of them cancel each other out. Thus, a vibration free motion is obtained at the end of the move. The details of reference

command functions such as a cycloid plus ramped versine plus ramp (CPRVPR), multi cycloid plus ramped versine plus ramp and hybrid input shaping technique is described in section 2.5.3.1, 2.5.3.2 and 2.5.3.3, respectively.

2.5.3.1. Cycloid Plus Ramped Versine Plus Ramp (CPRVPR) Function

Cycloid plus ramped versine plus ramp (CPRVPR) input is made up of three functions. The total distance to be covered from the beginning to end of a move within a specified time is the sum of the distances to be travelled by each of the three functions within the same travel time. By adjusting excursion distance of each function, vibration can be eliminated provided that the specified move time and the total distance are unchanged. Each component of the reference input creates oscillations such that these oscillations cancel each other out resulting in reduction or elimination of residual vibration.

A motion profile of a CPRVPR function is expressed as (Kapucu et al., 2008)

$$Y = \frac{L_1 Rt}{2\pi} + \frac{L_2}{2\pi}\left[Rt - \sin(Rt)\right] + \frac{L_3 Rt}{2\pi} + \frac{L_3}{2\pi}\left[1 - \cos(Rt)\right] \qquad (2.31.)$$

where L_1 is the maximum excursion distance to be travelled by ramp motion profile, L_2 is the maximum excursion distance to be travelled by cycloid motion profile, L_3 is the maximum excursion distance to be travelled by ramped versine motion profile, t is time into motion, t is the travelling time, and $R = 2\pi / t$. Furthermore, total distance can be written as $L = L_1 + L_2 + L_3$, then arranging the equation above becomes

$$Y(t) = \frac{LRt}{2\pi} - \frac{L_2}{2\pi}\sin(Rt) + \frac{L_3}{2\pi}\left(1 - \cos(Rt)\right) \qquad (2.32.)$$

The corresponding velocity profile is defined as:

$$\dot{r}(t) = \frac{LR}{2\pi} - \frac{L_2 R}{2\pi}\cos(Rt) - \frac{L_3 R}{2\pi}\sin(Rt) \tag{2.33.}$$

The solution of the equation of motion provided in equation (2.1.) under the effect of the positional input equation (2.32.) and corresponding velocity equation (2.33.) yields the following excursion distance values (L_1 , L_2 and L_3) for zero residual vibration with zero initial conditions (Kapucu et al., 2008).

$$\begin{aligned} L_1 &= \frac{LR\left(R - 2\zeta\omega_n\right)}{\omega_n^{\,2}} = \frac{Lt_n\left(t_n - 2\zeta t\right)}{t^2} \\ L_2 &= L\left(1 - \frac{R^2}{\omega_n^{\,2}}\right) = L\left(1 - \frac{t_n^{\,2}}{t^2}\right) \\ L_3 &= \frac{2L\zeta R}{\omega_n} = \frac{2L\zeta t_n}{t} \\ L &= L_1 + L_2 + L_3 \end{aligned} \tag{2.34.}$$

where ω_n is the natural frequency, and t_n is the natural period. Variations of L_1 , L_2 and L_3 is possible with traveling time t to result in an oscillation free displacement of the system.

Cycloid plus ramped versine plus ramp function motion profile and related sensitivity curve is shown in Figure 2.30. Figure 2.30 shows that the vibration amplitude increases rapidly as the actual frequency deviates from the modelling frequency. The length of the CPRVPR reference function is the same as that of the ZV shaper, half damped cycle of vibration. However, the ZV shaper has slightly more robustness to modelling errors. The insensitivity of CPRVPR function is 0.0585 when the vibration limit (V) is set to 5%. The insensitivity further increases from 0.0585 to 0.1175 when V is increased from 5% to 10%. ZV shaper is approximately 1.076 times more insensitive than the CPRVPR reference function.

On the other hand, theoretically, there is no travelling time restriction on the system and this is the main advantages of this reference command (Kapucu et al., 2008).

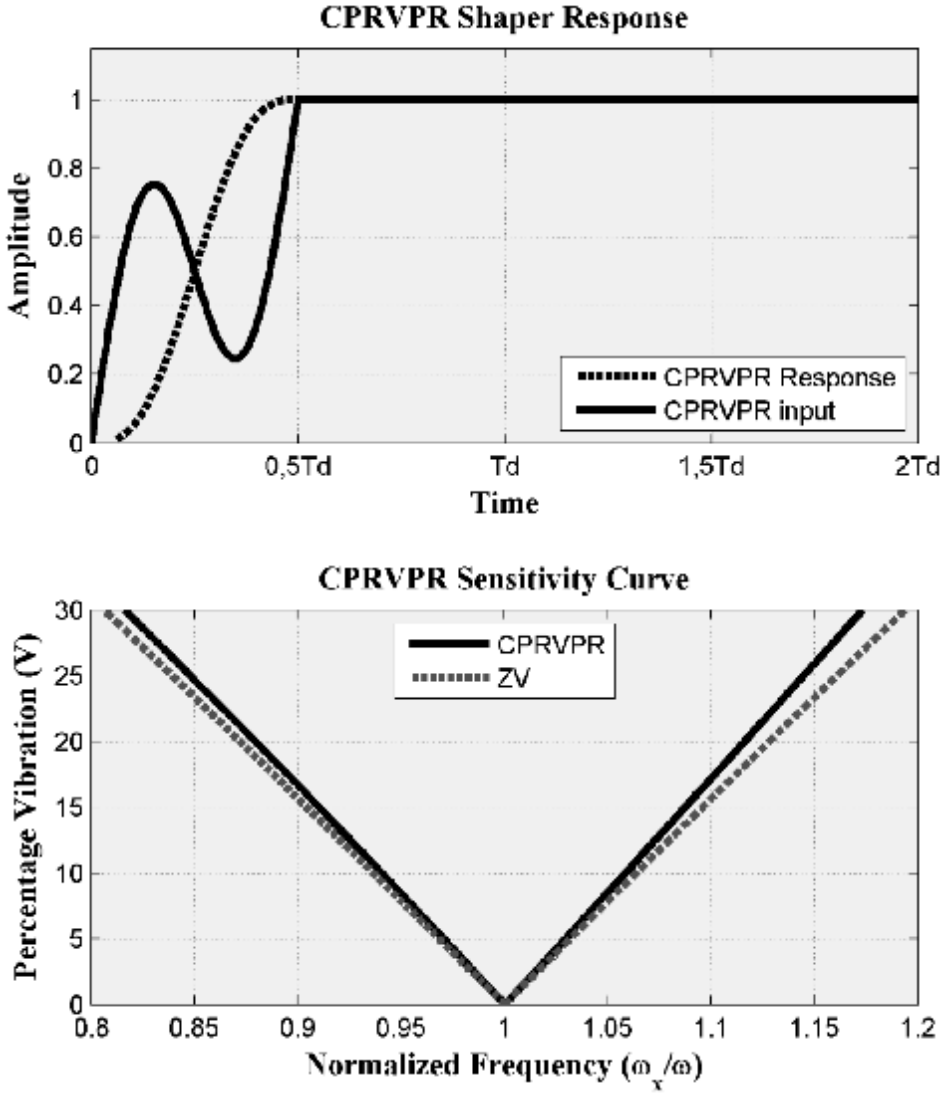

Figure 2.30. Cycloid plus ramped versine plus ramp function and related sensitivity curve for a total travelling distance $L=1$ and travelling time of $t = 0.5T_d$

2.5.3.2. Multi Cycloid Plus Ramped Versine Plus Ramp (CPRVPR) Function

The cycloid plus ramped versine plus ramp function, described in section 2.5.3.1, can be extended to drive for multi degree of freedom systems. The shaped reference commands for these systems can be written as

$$
\begin{aligned}
Y_1(t) &= \frac{L_1^T}{2\pi} Rt - \frac{L_{2_1}}{2\pi}\sin(Rt) + \frac{L_{3_1}}{2\pi}\left(1 - \cos(Rt)\right) \\
Y_2(t) &= \frac{L_2^T}{2\pi} Rt - \frac{L_{2_2}}{2\pi}\sin(Rt) + \frac{L_{3_2}}{2\pi}\left(1 - \cos(Rt)\right) \\
\ldots\ldots &= \ldots\ldots\ldots\ldots\ldots\ldots + \ldots\ldots\ldots\ldots\ldots\ldots \\
Y_i(t) &= \frac{L_i^T}{2\pi} Rt - \frac{L_{2_i}}{2\pi}\sin(Rt) + \frac{L_{3_i}}{2\pi}\left(1 - \cos(Rt)\right)
\end{aligned}
\tag{2.35.}
$$

The excursion distance values are found as;

$$
\begin{aligned}
L_{1_i} &= \frac{L_i^T R\left(R - 2\zeta_i \omega_{ni}\right)}{\omega_{ni}^{\,2}} = \frac{L_i^T \tau_{ni}\left(\tau_{ni} - 2\zeta_i \tau\right)}{\tau^2} \\
L_{2_i} &= L_i^T\left(1 - \frac{R^2}{\omega_{ni}^{\,2}}\right) = L\left(1 - \frac{\tau_{ni}^{\,2}}{\tau^2}\right) \\
L_{3_i} &= \frac{2L_i^T \zeta_i R}{\omega_{ni}} = \frac{2L_i^T \zeta_i \tau_{ni}}{\tau} \\
L_i^T &= L_{1_i} + L_{2_i} + L_{2_i}
\end{aligned}
\tag{2.36.}
$$

where L_{1_i} is the maximum excursion distance to be travelled by ramp motion profile, L_{2_i} is the maximum excursion distance to be travelled by cycloid motion profile, L_{3_i} is the maximum excursion distance to be travelled by ramped versine motion profile for ith preshaped input. Also, ζ_i, ω_{ni}, τ_{ni} are damping ratio, natural frequency, period of natural oscillation for ith preshaped input, respectively.

2.5.3.3. Hybrid Input Shaper

In this method, a preshaped command is produced by combining the different template functions to allow the resulting trajectory and the travelling time being adjustable. Then, this preshaped input is convolved with sequence of impulses. This sequence of impulses is obtained using the input shaping described in section 2.5.1.1 to increase the robustness of the signal. The method suggested by Yavuz et al. (2011)

is named as hybrid input shaping. For a specified travelling time and displacement, hybrid-shaping technique is implemented as follows;

1. Travelling time for the template function is calculated from $t_1 = t_t - t_{delay}$ in order to satisfy the total travelling time t_t.Note that t_t should be greater than the t_{delay}.
2. The distances L_1, L_2 and L_3 for the template functions are calculated from equation (2.34),
3. The resulting trajectory is convolved with the two impulse sequence defined by equation (2.11).

The motion profile and related sensitivity curve for hybrid input shaping method are shown in Figure 2.31 for travelling time $t = T_d$. It can be seen from Figure 2.31 that the vibration is considerably eliminated by convolving the pre-shaped input of cycloid plus ramped versine ramp function with the sequence of all modes generated by two impulse sequences. In generation of the convolved input signal, cycloid-plus-ramped and versine-plus-ramp functions are used. This reference input is composed of three functions. Considering the total distance to be covered within a specified time is divided into three parts. Each part is travelled by each of the three functions within the same travel time. Provided that the specified move time and the total distance are unchanged, vibration can be eliminated by adjusting excursion distance of each function. Each component of input creates such oscillations that they cancel each other out. The details of cycloid-plus-ramped and versine-plus-ramp functions are presented in Section 2.5.3.1. The increase in travelling time improves the robustness and also causes variations on the input function profile. The length of the Hybrid input shaper is the same as that of the ZVD shaper, one damped cycle of vibration, but ZVD shaper is slightly more robust to modelling errors. The insensitivity of Hybrid input shaper is 0.2754 when the vibration limit (V) is set to 5%. The insensitivity further increases from 0.2754 to 0.3927 when V is increased from 5% to 10%. ZVD shaper is approximately 1.044

times more insensitive than the Hybrid input shaper. On the other hand theoretically, the main advantage of hybrid input shaping method is that there is no travelling time restriction in application of the method (Yavuz et al., 2011).

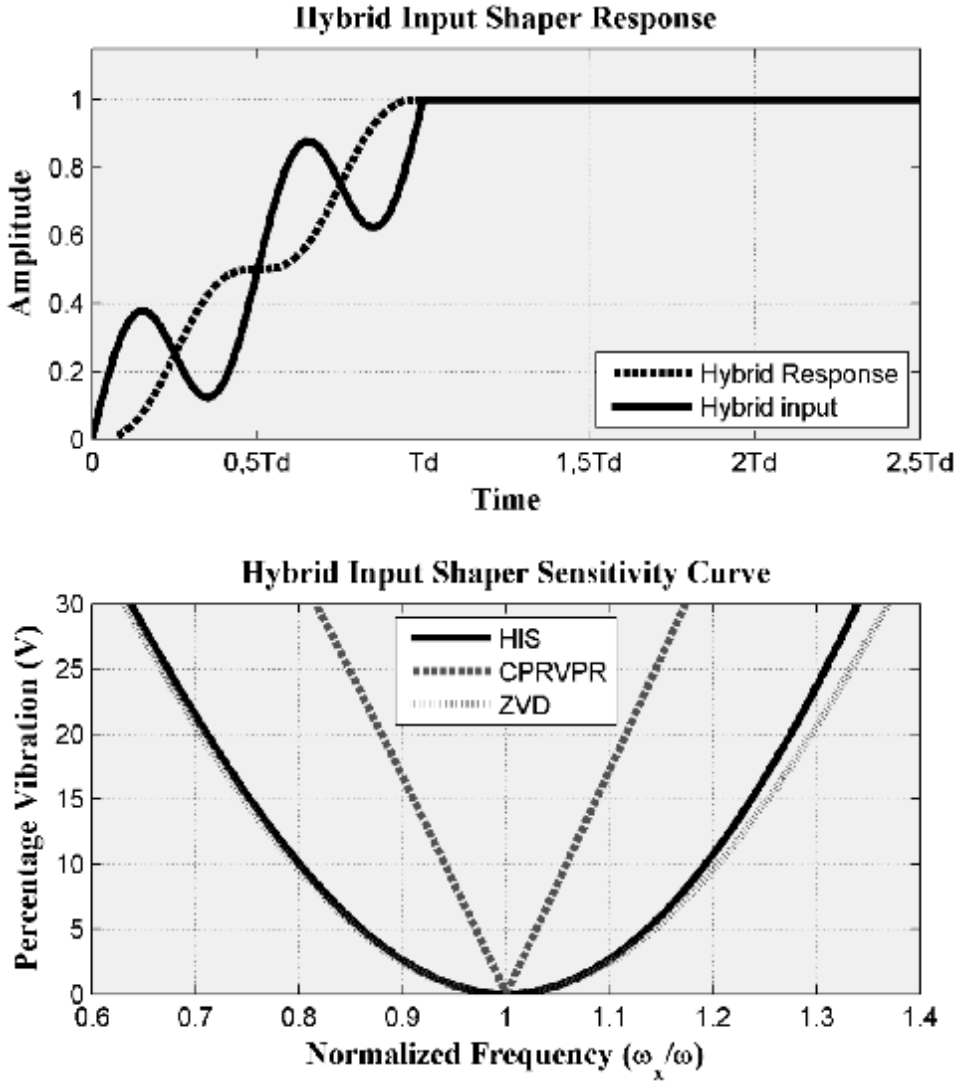

Figure 2.31. Hybrid input shaper and related sensitivity curve for a total travelling distance $L=1$ and travelling time of $t = T_d$

2.6. Multi Mode Input Shapers

Single mode shapers can be obtained by simply plugging the natural frequency and damping ratio of the system into simple equations like those derived in the Section 2.5. The equations provide the amplitudes and time locations of the

impulses that comprise the input shaper. A simple method to obtain a two-mode shaper is to convolve two single-mode shapers together. For example, suppose a system has undamped modes at 1 Hz and 2.5 Hz, then ZV shapers for each mode are

$$ZV = \begin{bmatrix} A_j \\ t_j \end{bmatrix} = \begin{bmatrix} A_1 & A_2 \\ t_{a1} & t_{a2} \end{bmatrix} \tag{2.37.}$$

$$ZV = \begin{bmatrix} A_j \\ t_j \end{bmatrix} = \begin{bmatrix} B_1 & B_2 \\ t_{b1} & t_{b2} \end{bmatrix} \tag{2.38.}$$

When describing a two-mode shaper, the constraints used to eliminate each mode will be stated explicitly. For example, if ZVD constraints are used for the first mode and ZV constraints are used for the second mode, then the result is a ZVD-ZV shaper.

Convolving the shapers defined by equation 2.37 and 2.38; one can generate a ZV-ZV shaper defined as follows:

$$ZV - ZV = \begin{bmatrix} A_j \\ t_j \end{bmatrix} = \begin{bmatrix} A_1 * B_1 & A_1 * B_2 & A_2 * B_1 & A_2 * B_2 \\ t_{a1} + t_{b1} & t_{a1} + t_{b2} & t_{a2} + t_{b1} & t_{a2} + t_{b2} \end{bmatrix} \tag{2.39.}$$

The sensitivity curves for the single-mode shapers and the convolved two-mode shaper for ZV and ZVD techniques are shown in Figure 2.32 and 2.33, respectively. The convolved ZVD-ZVD shaper is more robust then the ZV-ZV shaper for all mode ratios. Figure 2.32 and Figure 2.33 shows that convolved shapers have greater robustness to second mode modelling errors. Note that the vibration suppression of the convolved two mode ZVD-ZVD shaper near 6 Hz is due to the contribution from the 1 Hz shaper. Single mode shapers suppress vibration at odd multiplies of their design frequency. When an input shaper is convolved with a second shaper, the vibration suppression properties at these higher frequencies are passed on to the resulting two mode shaper (Singhose, 1997: Singhose et al, 1997).

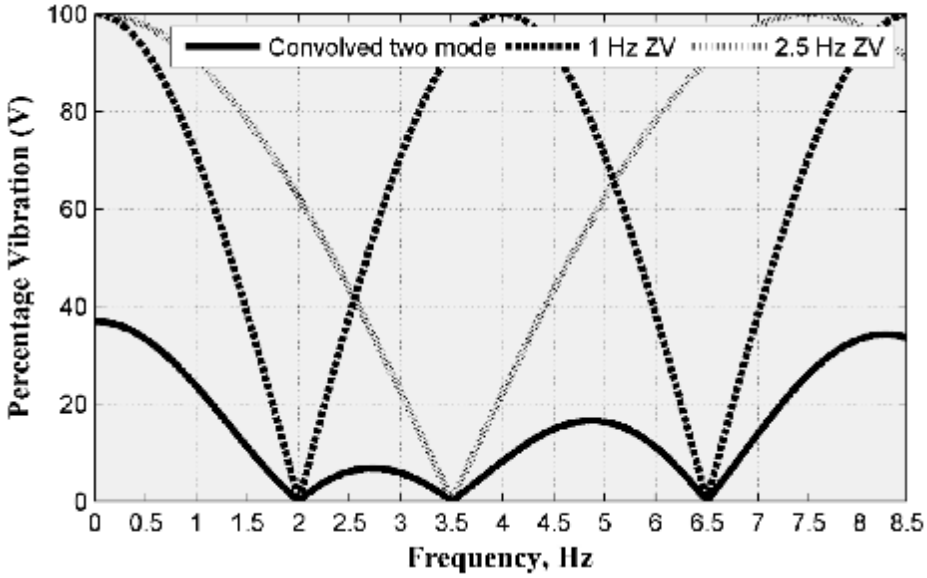

Figure 2.32. Convolved two mode ZV-ZV shapers for 1 Hz and 2.5 Hz

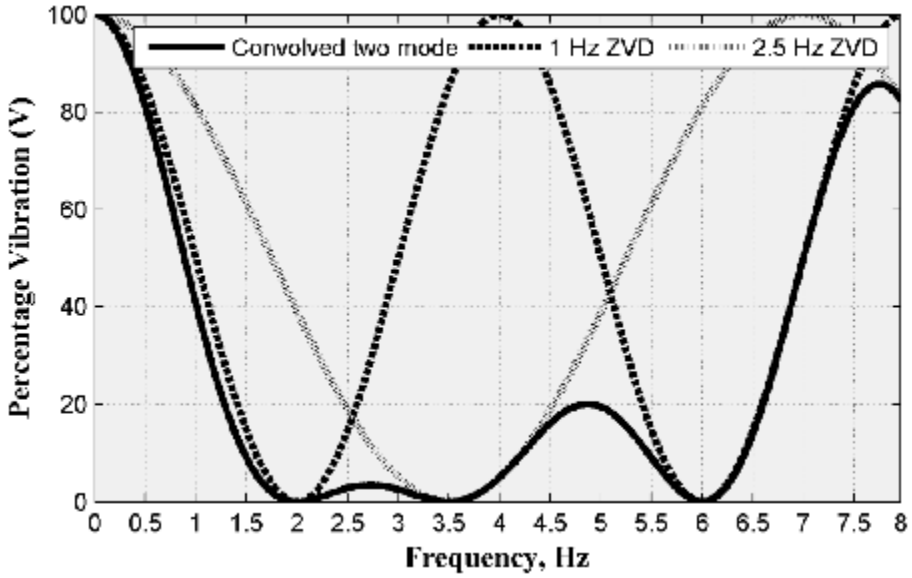

Figure 2.33. Convolved two mode ZVD-ZVD shapers for 1 Hz and 2.5 Hz

2.7. Comparison of Conventional Command Shaping Techniques

In the previous sections some selected positive, negative and smoothly shaped reference command methods are introduced. The successful implementation of the introduced command shaping methods requires accurate estimation or

determination of the natural frequency and damping ratio of the system in concern. In addition to this, the mathematical models of any flexible system cannot be modelled perfectly. The variations or change of the system parameters influences the shaped signal and also the system response. Therefore, the robustness of shaped signal to modelling uncertainty is an important performance comparison tool for command shaping methods. In this section, the presented methods are compared for length of travelling time and also their robustness for system natural frequency estimation errors.

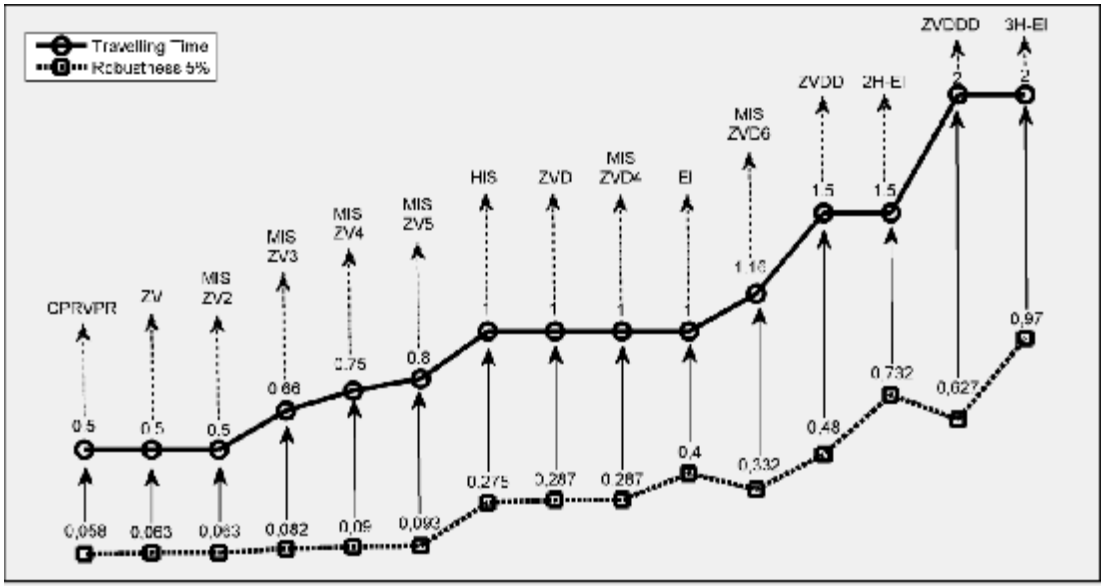

Figure 2.34. Performance criteria for comparison of positive and smoothly shaped reference commands

This Section presents a comparison of conventional command pre-shaping methods and investigates the compromise between rapidity of motion and shaper robustness. In this study, in total of 23 different input shaping methods are reviewed. The compared methods cover almost all types of positive shapers and smoothly shaped reference commands reported in literature. Therefore, the presented review study provides almost a complete picture of the topic for the researchers working in the area. The study is structured in a way that it provides all the necessary theoretical background and the implementation related details for each of the method presented.

In addition, the presented methods are also used for comparative study of robustness and travelling time features.

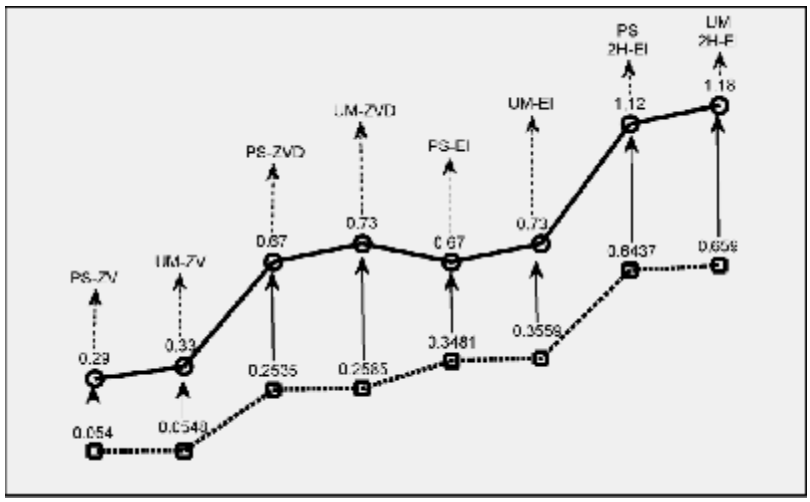

Figure 2.35. Performance criteria for comparison of negative input shapers

From the details of the Figure 2.34 and 2.35 it can be concluded from simulation results that (Conker et al., 2014b):

- The robust shapers typically have longer travelling times that leads to slower the system response. This creates a compromise between shaper robustness and rise/travelling time.
- The increasing travelling time appears to cause increasing robustness that is mostly method dependent. Hence, the compromise on increasing travelling time gains increasing robustness that varies from a method to another. In other words, the efficiency of methods varies from one method to another.
- The comparative study of the methods for robustness indicate that the best method for positive input shapers is three hump extra insensitive (3H-EI) with value of '0.97', and for negative input shapers is Unity Magnitude two hump extra insensitive with value of '0.659'.

2.8. Applications of Command Shaping

Due to its ease of implementation and robustness to system uncertainty, input shaping has been applied with great success to many types of real world systems. Many researchers applied their methods on real system such as robotic manipulators, cranes, coordinate measuring machines, spacecraft etc. to verify them with experimental results. Some of the applications that have been reported in the literature are summarized here.

Successful applications of command shaping techniques have been reported on problems of controlling XY stages (Singhose and Singer, 1996: Fortgang et al., 2005: Park et al., 2007: Vaughan et al., 2009), flexible robotic manipulators (Starr, 1985: Tzes et al., 1989: Singer and Seering, 1990: Hillsley and Yurkovich, 1991: Magee and Book, 1993: Feddema, 1993: Kwon et al., 1994: Zou et al., 1995: Wilson et al. 1996: Grosser and Singhose, 2000: Chang et al, 2003: Mohamed and Tokhi, 2004: Yano and Terashima, 2005: Kapucu et al., 2005: Alici et al., 2006: Kapucu et al., 2006: Sung and Lee, 2006: Freese et al., 2007: Gurleyuk, 2007: Park and Rhim, 2008: Huey et al., 2008: Yavuz et al., 2011: Conker et al., 2014a) and voice coil motors (Jung et al., 2009). Command shaping has also proven beneficial for spacecraft (Liu and Wie, 1992: Banerjee, 1993: Singh and Vadali, 1993: Wie et al., 1993: Singhose et al., 1996: Gorinevsky and Vukovich, 1998: Song et al., 1999: Parman and Koguchi, 1999: Banerjee et al., 2001: Biediger et al., 2003: Robertson et al., 2005). Command shaping has been implemented on tower cranes (Vaughan et al., 2007), boom cranes (Parker et al., 1999: Danielson et al., 2008), container cranes (Park et al., 2000: Hong and Hong, 2004: Zrnić et al., 2005: Masoud and Daqaq, 2006: Daqaq and Masoud, 2006), as well as several portable cranes.

Input shapers for multi-mode systems have also been designed for specific applications such as robots (Yurkovich et al., 1990: Hillsley and Yurkovich, 1991: Magee and Book, 1993: Hillsley and Yurkovich, 1993: Magee and Book, 1994: Magee and Book, 1995), spacecraft (Banerjee, 1993: Singh and Vadali, 1993: Sung and Wander, 1993: Tuttle and Seering, 1995: Banerjee and Singhose, 1998: Banerjee et al., 2001: Robertson et al., 2005: Hu, 2008) and cranes (Kim and Singhose, 2007:

Manning et al., 2008: Singhose et al., 2008). In addition, some work has addressed the use of input shaping on nonlinear systems (Gorinevsky and Vukovich, 1998: Smith et al., 2002: Kozak et al., 2004). Input shaping has also been applied to systems with varying parameters (Magee and Book, 1992: Pao and Lau, 2000).

3. MATERIALS AND METODS

3.1. Materials

3.1.1. Experimental Setup of Flexible Robot Systems

In this study, Quanser linear pendulum gantry system and Quanser flexible link manipulator systems are used for experimental study of flexible robotic systems, shown in Figures 3.1 and 3.5, respectively. For further validation of the proposed techniques and to demonstrate the practical effectiveness of the proposed techniques over the conventional methods, a set of experiments are performed. Experimental setups used for performance analysis of the techniques with the Quanser linear pendulum gantry and flexible-link laboratory positioning mechanisms are presented in this section.

3.1.1.1. Single Pendulum Gantry System

A picture of the linear single pendulum gantry system and its schematic illustration is shown in Figure 3.1. The pendulum has a pivot on the cart, and the angular position of the pendulum (α) is measured using an encoder. The centre of mass of the pendulum is at length, l_p, and the moment of inertia about the centre of mass is j_p. The pendulum angle, α, is zero when it is suspended perfectly vertically and increases positively when rotated counter-clockwise (CCW). The positive direction of linear displacement of the cart, x_c, is to the right when facing the cart. The position of the pendulum centre of gravity is denoted as the (x_p, y_p) coordinate (Quanser Inc., 2012a).

The experimental block diagram of single pendulum gantry details of which are presented by Quanser Consulting Inc. is shown in Figure 3.2. The experimental setup consists of a compound pendulum bonded to the sliding member (cart) moving horizontally, which is driven by a high quality DC motor equipped with a planetary

gearbox. The cart slides along a stainless steel shaft using linear bearings. The DC motor is equipped with internal brakes, which are engaged when the power is disabled. On the single pendulum gantry system, both cart and pendulum positions are measured with two optical encoders. The encoder measuring the cart linear position does so through a rack-pinion system. Both encoders are typically identical. The encoder model used in the experimental setup is a single-ended optical shaft encoder. It offers a high resolution of 4096 counts per revolution. These encoders are connected to digital counters built in the interfacing board; the result of the measurement is then sent to the PC.

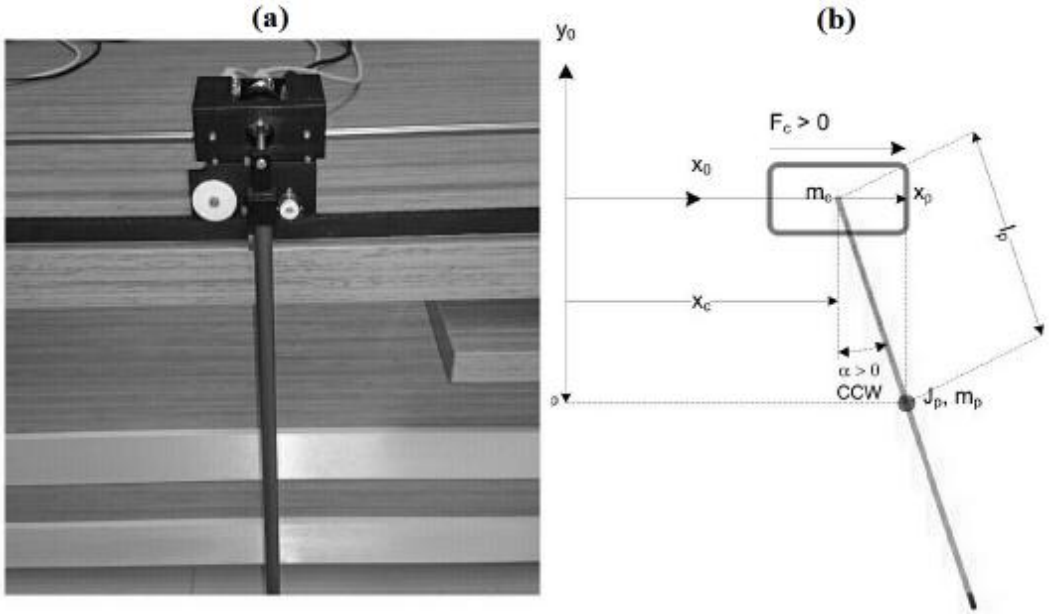

Figure 3.1.a). Single pendulum gantry electromechanical model; and b) its schematic illustration

An interfacing board is used to link the computer with the single pendulum gantry system, as shown in the experimental setup diagram in Figure 3.2. The controller developed by user is implemented using MATLAB/SIMULINK, which is integrated with the real time plant by Quarc software. The results of experiments are obtained in SIMULINK environment. The whole system, whose parameters are shown in Table 3.1, is illustrated in Figure 3.1. The detailed information upon the utilized single pendulum gantry can be found in reference (Quanser Inc., 2012a).

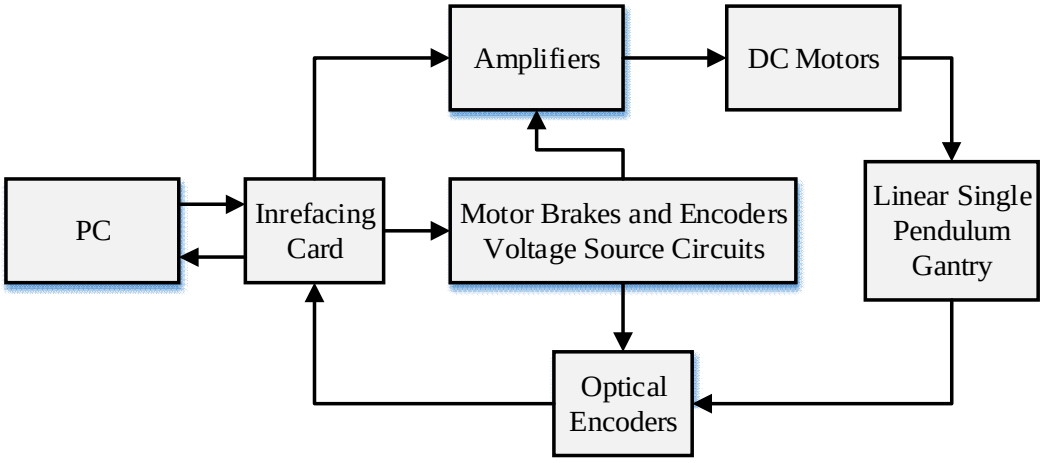

Figure 3.2. Linear single pendulum gantry crane diagram

3.1.1.2. Modelling of the Single Pendulum Gantry Crane System

Instead of using classical mechanics, the Lagrange method is used to find the equations of motion of the system. This systematic method is often used for more complicated systems such as robotic manipulators with multiple joints.

More specifically, the dynamics equations that describe the motion of the linear cart and pendulum with respect to the motor voltage will be obtained using the Euler-Lagrange equation:

$$\frac{\partial^2 L}{\partial t \partial \dot{q}_i} - \frac{\partial L}{\partial q_i} = Q_i \qquad (3.1.)$$

The variable q_i is called generalized coordinate. For this system let

$$q(t)^T = \begin{bmatrix} x_c(t) & \alpha(t) \end{bmatrix} \qquad (3.2.)$$

where $x_c(t)$ is the cart position and $\alpha(t)$ is the pendulum angle. The corresponding velocities are

$$\dot{q}(t)^T = \begin{bmatrix} \frac{\partial x_c(t)}{\partial t} & \frac{\partial \alpha(t)}{\partial t} \end{bmatrix} \tag{3.3.}$$

With the generalized coordinates defined, the Euler-Lagrange equations for the linear pendulum gantry are:

$$\begin{aligned} \frac{\partial^2 L}{\partial t \partial \dot{x}_c} - \frac{\partial L}{\partial x_c} &= Q_{x_c} \\ \frac{\partial^2 L}{\partial t \partial \dot{\alpha}} - \frac{\partial L}{\partial \alpha} &= Q_{\alpha} \end{aligned} \tag{3.4.}$$

The Lagrangian of the system, L, is described as,

$$L = T - V \tag{3.5.}$$

where T is the total kinetic energy of the system and V is the total potential energy of the system. Therefore, the Lagrangian represents the difference between the kinetic and potential energy of the system.

According to the reference frame definition shown in Figure 3.1, the Cartesian coordinates of the centre of gravity of the pendulum are defined by:

$$\begin{aligned} x_p &= x_c + l_p \sin(\alpha) \\ y_p &= -l_p \cos(\alpha) \end{aligned} \tag{3.6.}$$

Since the linear motion of the cart is fixed vertically, the total potential energy of the system can be expressed as the gravitational potential energy of the pendulum:

$$V_T = -M_p g l_p \cos(\alpha) \tag{3.7.}$$

The total kinetic energy of the system is the sum of the translational and rotational kinetic energies arising from the cart and pendulum. The translational kinetic energy of the cart, T_{ct}, can be expressed as:

$$T_{ct} = \frac{1}{2} M \dot{x}_c^2 \tag{3.8.}$$

and the rotational energy due to the DC motor, T_{cr}, is:

$$T_{cr} = \frac{\eta_g J_m K_g^2 \dot{x}_c^2}{2 r_{mp}^2} \tag{3.9.}$$

where the corresponding experimental setup parameters are defined in the User Manual (Quanser Inc., 2012a). If the kinetic energy equations are combined, the resultant total kinetic energy of the cart can be defined as:

$$T_c = \frac{1}{2} J_{eq} \dot{x}_c^2 \tag{3.10.}$$

where

$$J_{eq} = M + \frac{\eta_g K_g^2 J_m}{r_{mp}^2} \tag{3.11.}$$

The pendulum translational kinetic energy can be expressed as a function of the linear velocity of the centre of gravity:

$$T_{pt} = \frac{1}{2} M_p \sqrt{\dot{x}_p^2 + \dot{y}_p^2} \tag{3.12.}$$

where the components of the linear velocity of the pendulum centre of gravity are defined by:

$$\begin{aligned} \dot{x}_p &= \dot{x}_c + l_p \cos(\theta)\dot{\theta} \\ \dot{y}_p &= l_p \sin(\theta)\dot{\theta} \end{aligned} \tag{3.13.}$$

The rotational kinetic energy of the pendulum is defined as:

$$T_{pr} = \frac{1}{2} J_p \dot{\theta}^2 \tag{3.14.}$$

where the parameters of the pendulum are listed in the User Manual (Quanser Inc., 2012a).

The total kinetic energy of the system can be found by combining the kinetic energy of the cart in Equation (3.10), with the pendulum kinetic energy in Equations (3.12) and (3.14):

$$T_T = \frac{1}{2}\left(J_{eq} + M_p\right)\dot{x}_c^2 + M_p l_p \cos(\theta)\dot{\theta}\dot{x}_c + \frac{1}{2}\left(J_p + M_p l_p^2\right)\dot{\theta}^2 \tag{3.15.}$$

The generalized forces, Q_{x_c} and Q, are used to describe the non-conservative forces (e.g., friction) applied to a system with respect to the generalized coordinates. The generalized force acting on the linear cart is:

$$Q_{x_c} = F_c - B_{eq}\dot{x}_c \tag{3.16.}$$

and acting on the pendulum is

$$Q_\theta = - B_p\dot{\theta} \tag{3.17.}$$

The nonlinear Coulomb friction applied to the linear cart, and the forces on the linear cart due to the pendulum's action have been neglected in the dynamic model. By substituting the total kinetic and potential energy of the system shown in Equation (3.7.) and Equation (3.15.), and the generalized forces into the Euler-Lagrange formulation, the nonlinear Equations of Motion (EOM) are becomes as follows:

$$\left(J_{eq}+M_p\right)\ddot{x}_c+M_p l_p\cos(\alpha)\ddot{\alpha}-M_p l_p\sin(\alpha)\dot{\alpha}^2=F_c-B_{eq}\dot{x}_c \qquad (3.18.)$$

$$M_p l_p\cos(\alpha)\ddot{x}_c+\left(J_p+M_p l_p{}^2\right)\ddot{\alpha}+M_p l_p g\sin(\alpha)=-B_p\dot{\alpha} \qquad (3.19.)$$

Table 3.1. Physical parameters of the linear single pendulum gantry crane system

Symbol	Description	Value	Unit
x_c	Cart position		mm
α	Link angle		rad
g	Gravitational constant of earth	9.81	m/s^2
M_p	Pendulum mass	0.230	kg
l_p	Pendulum length from pivot to center of gravity	0.3302	m
J_{eq}	Lumped mass of the cart system	1.07313	kg
J_p	Pendulum moment of inertia	$7.89*10^{-3}$	$kg.m^2$
J_m	Rotor inertia	$3.9*10^{-7}$	$kg.m^2$
B_{eq}	Equivalent viscous damping coefficient	5.4	N.m.s/rad
B_p	Viscous damping coefficient, as seen at the pendulum axis	0.0024	N.m.s/rad
η_g	Planetary gearbox efficiency	0.90	
η_m	Motor efficiency	0.69	
K_g	Planetary gearbox gear ratio	3.71	
K_m	Motor back-emf constant	$7.68 * 10^{-3}$	V/(rad/s)
K_t	Motor current-torque constant	$7.68 * 10^{-3}$	N.m/A
R_m	Motor armature resistance	2.6	Ω
r_{mp}	Motor pinion radius	$6.35*10^{-3}$	m
F_c	Driving force		N

The linear force applied to the cart, F_c, is generated by the servo motor and described by the equation:

$$F_c = \left(\frac{\eta_g K_g K_t}{R_m r_{mp}}\right)\left(-\frac{K_g K_m \dot{x}_c}{r_{mp}} + \eta_m V_m\right) \tag{3.20.}$$

where the servo motor parameters are defined in the User Manual (Quanser Inc., 2012a).

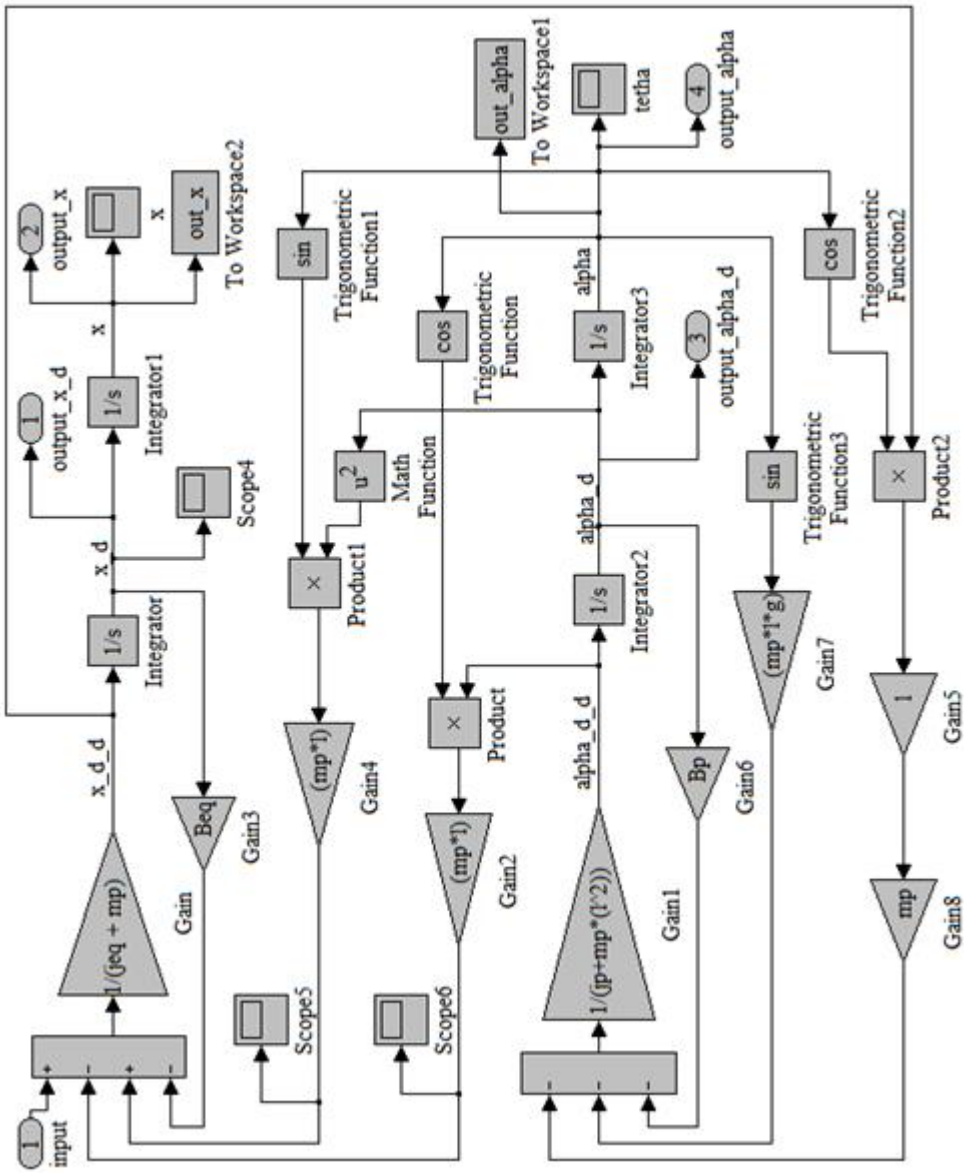

Figure 3.3. Simulink diagram of single pendulum gantry crane system

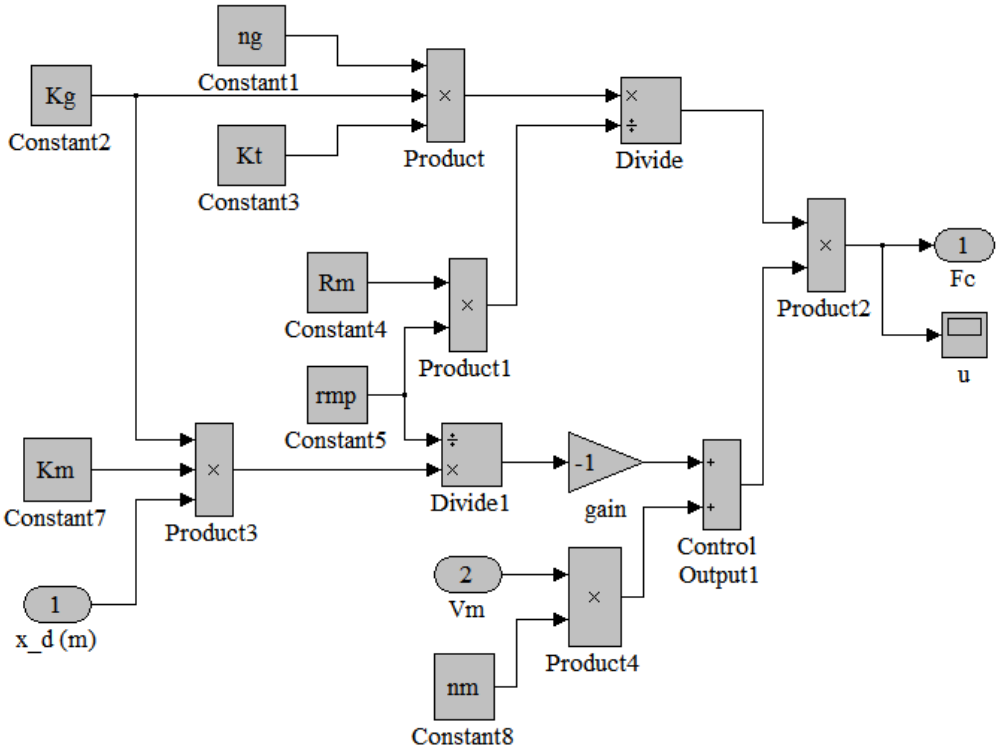

Figure 3.4. Simulink diagram of DC motor for single pendulum gantry system

3.1.1.3. Flexible-Link Robotic Manipulator

The Figure 3.5 shows the modular flexible link apparatus manufactured by Quanser Consulting, Inc (Quanser Inc., 2012b). The manipulator arm is a spring steel bar that moves in the horizontal plane due to the action of a DC motor. A potentiometer measures the angular position of the system, and the arm deflections are measured by means of a strain gauge mounted near its base. The whole system, whose parameters are shown in Table 3.2., is shown in Fig. 3.5.

The base of the flexible link is mounted on the load gear of the system. The servo angle, q increases positively when it rotates counter-clockwise (CCW). The servo and the link turn in the CCW direction when the control voltage is positive. The flexible link has a total length of L_l, a mass of m_l, and its moment of inertia about the center of mass is J_l. The deflection angle of the link is denoted as a and increases positively when rotated in CCW direction (Quanser Inc., 2012b).

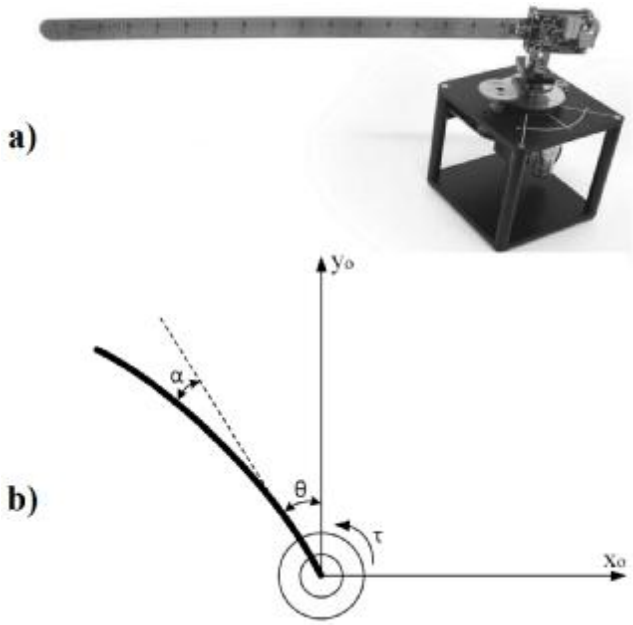

Figure 3.5. a) Flexible-link manipulator electromechanical model; and b) its schematic illustration

The flexible link system can be represented by the diagram shown in Figure 3.6. Our control variable is the input servo motor voltage, V_m. This generates a torque, t, at the load gear of the servo that rotates the base of the link. The viscous friction coefficient of the servo is denoted by B_{eq}. This is the friction that opposes the torque being applied at the servo load gear. The friction acting on the link is represented by the viscous damping coefficient B_l. Finally, the flexible link is modelled as a linear spring with the stiffness K_S.

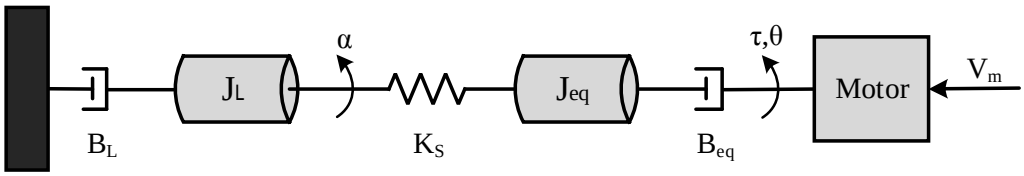

Figure 3.6. Flexible-link manipulator model

The experimental block diagram of flexible link manipulator is shown in Figure 3.7. This manipulator arm, fabricated by Quanser Consulting Inc., is a spring steel bar that moves in the horizontal plane due to the action of a DC motor. The DC

motor is equipped with a gear box. The gearbox output drives external gears. The unit is equipped with tachometer, potentiometer and optical encoder to measure the output angular speed and position. The arm deflection of flexible link is measured via a strain gauge mounted at the clamped end of the flexible arm. The output of this strain gauge is an analogue signal proportional to the deflection of the link. The installation and calibration of this gauge is done by the manufacturer, Quanser. The deflection output is available in the specific software. The controller developed by user is implemented using MATLAB/SIMULINK which is integrated with the real time plant by Quarc software. The results of experiments are obtained in SIMULINK environment. The detailed information upon the utilized flexible link manipulator can be found in reference (Quanser Inc., 2012b).

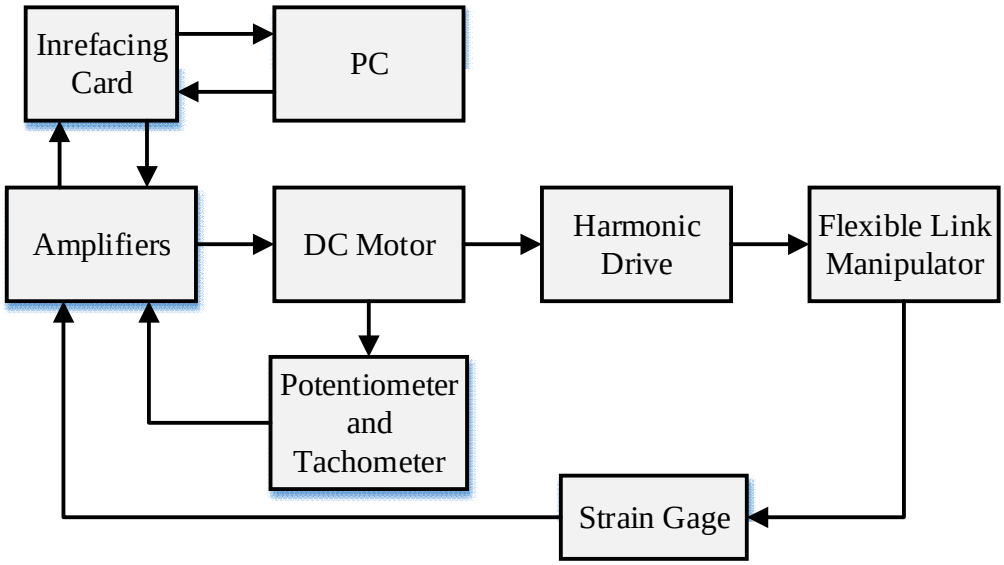

Figure 3.7. Flexible link robotic manipulator diagram

3.1.1.4. Modelling of the Flexible-Link Robotic Manipulator

Instead of using classical mechanics, the Lagrange method is used to find the equations of motion of the system. This systematic method is often used for more complicated systems such as robot manipulators with multiple joints.

More specifically, the equations that describe the motions of the servo and the link with respect to the servo motor voltage, i.e. the dynamics, will be obtained using the Euler-Lagrange equation:

$$\frac{\partial^2 L}{\partial t \partial \dot{q}_i} - \frac{\partial L}{\partial q_i} = Q_i \tag{3.21.}$$

The variables q_i are called generalized coordinates. For this system let

$$q(t)^T = \begin{bmatrix} \theta(t) & \alpha(t) \end{bmatrix} \tag{3.22.}$$

where, as shown in Figure 3.6, $\theta(t)$ is the servo angle and $\alpha(t)$ is the flexible link angle. The corresponding velocities are

$$\dot{q}(t)^T = \begin{bmatrix} \frac{\partial \theta(t)}{\partial t} & \frac{\partial \alpha(t)}{\partial t} \end{bmatrix} \tag{3.23.}$$

With the generalized coordinates defined, the Euler-Lagrange equations for the rotary flexible link system are

$$\begin{aligned} \frac{\partial^2 L}{\partial t \partial \dot{\theta}} - \frac{\partial L}{\partial \theta} &= Q_1 \\ \frac{\partial^2 L}{\partial t \partial \dot{\alpha}} - \frac{\partial L}{\partial \alpha} &= Q_2 \end{aligned} \tag{3.24.}$$

The Lagrangian of a system is defined

$$L = T - V \tag{3.25.}$$

where T is the total kinetic energy of the system and V is the total potential energy of the system. Thus the Lagrangian is the difference between a system's kinetic and potential energies.

The generalized forces Q_i are used to describe the non-conservative forces (e.g., friction) applied to a system with respect to the generalized coordinates. In this case, the generalized force acting on the rotary arm is

$$Q_1 = \tau - B_{eq}\dot{\theta} \tag{3.26.}$$

and acting on the link is

$$Q_2 = -B_l\dot{\alpha} \tag{3.27.}$$

The torque applied at the base of the rotary arm (i.e., at the load gear) is generated by the servo motor as described by the equation

$$\tau = \frac{\eta_g K_g \eta_m k_t \left(V_m - K_g k_m \dot{\theta}\right)}{R_m} \tag{3.28.}$$

Again, the Euler-Lagrange equations is a systematic method of finding the equations of motion (EOMs) of a system. Once the kinetic and potential energy are obtained and the Lagrangian is found, then the task is to compute various derivatives to get the EOMs.

Translational kinetic equation is defined as

$$T = \frac{1}{2}mv^2 \tag{3.29.}$$

where m is the mass of the object and v is the linear velocity. Rotational kinetic energy is described as

$$T = \frac{1}{2} J \omega^2 \tag{3.30.}$$

where J is the moment of inertia of the object and ω is its angular rate.

Potential energy comes in different forms. Typically in mechanical system we deal with gravitational and elastic potential energy. The relative gravitational potential energy of an object is

$$V_g = mg\Delta h \tag{3.31.}$$

where m is the object mass and Δh is the change in altitude of the object. The equation for elastic potential energy, i.e., the energy stored in a spring, is

$$V_e = \frac{1}{2} K \Delta x^2 \tag{3.32.}$$

where K is the spring stiffness and Δx is the linear or angular change in position. Using Equation (3.32.), the elastic energy stored in the spring equals

$$V = \frac{1}{2} K_s \theta^2 \tag{3.33.}$$

This is the total potential energy that is store in the system.
Using the Equation (3.30), the total kinetic energy from the SRV02 rotating and the deflection of the link is defined as

$$T = \frac{1}{2} J_{eq} \dot{\theta}^2 + \frac{1}{2} J_l \left(\dot{\theta} + \dot{\alpha} \right)^2 \tag{3.34.}$$

Using Equation (3.25), the total kinetic energy from the SRV02 rotating and the deflection of the link is

$$L = \frac{1}{2} J_{eq} \dot{\theta}^2 + \frac{1}{2} J_l \left(\dot{\theta} + \dot{\alpha} \right)^2 - \frac{1}{2} K_s \alpha^2 \tag{3.35.}$$

Compute the derivatives required by Equation (3.24.) and substitute the generalized force, Q_1, given in Equation (3.26.). The derivatives are

$$\begin{aligned} \frac{\partial L}{\partial \dot{\theta}} &= J_{eq} \dot{\theta} + J_l \left(\dot{\theta} + \dot{\alpha} \right) \\ \frac{\partial^2 L}{\partial t \partial \dot{\theta}} &= J_{eq} \ddot{\theta} + J_l \left(\ddot{\theta} + \ddot{\alpha} \right) \\ \frac{\partial L}{\partial \theta} &= 0 \end{aligned} \tag{3.36.}$$

Substituting the above answers and Equation (3.26.) into Equation (3.24.) gives the first equation of motion

$$\left(J_{eq} + J_l \right) \ddot{\theta} + J_l \ddot{\alpha} + B_{eq} \dot{\theta} = \tau \tag{3.37.}$$

Compute the derivatives required by Equation (3.24.) and substitute the generalized force, Q_2, given in Equation (3.27.). The derivatives are

$$\begin{aligned} \frac{\partial L}{\partial \dot{\alpha}} &= J_l \left(\dot{\theta} + \dot{\alpha} \right) \\ \frac{\partial^2 L}{\partial t \partial \dot{\alpha}} &= J_l \left(\ddot{\theta} + \ddot{\alpha} \right) \\ \frac{\partial L}{\partial \alpha} &= K_s \alpha \end{aligned} \tag{3.38.}$$

Substituting the above derivative and Equation (3.27.) into Equation (3.24.) gives the second equation of motion

$$J_l \ddot{\theta} + J_l \ddot{\alpha} + B_l \dot{\theta} + K_s \alpha = 0 \tag{3.39.}$$

Subtract equation (3.37.) from (3.39.) and set $B_l = 0$ to obtain the first equation of motion

$$\ddot{\theta} = -\frac{B_{eq}}{J_{eq}}\dot{\theta} + \frac{K_s}{J_{eq}}\alpha + \frac{1}{J_{eq}}\tau \tag{3.40.}$$

Substitute this into Equation (3.39.)

$$\begin{aligned} J_l\left(-\frac{B_{eq}}{J_{eq}}\ddot{\theta} + \frac{K_s}{J_{eq}}\alpha + \frac{1}{J_{eq}}\tau\right) + J_l\ddot{\alpha} + K_s\alpha = 0 \\ -\frac{J_l B_{eq}}{J_{eq}}\ddot{\theta} + J_l\ddot{\alpha} + K_s\left(\frac{J_l}{J_{eq}} + 1\right)\alpha = -\frac{J_l}{J_{eq}}\tau \end{aligned} \tag{3.41.}$$

Table 3.2. Physical parameters of the flexible-link robotic manipulator

Symbol	Description	Value	Unit
L_l	Flexible link length	41.9	Cm
m_l	Flexible link mass	0.065	kg
J_l	Flexible link moment of intertia	0.0038	kg.m^2
R_m	Motor armature resistance	2.6	Ω
K_g	Total gear ratio	70	
k_t	Motor torque constant	0.00767	N.m/A
k_m	Motor back-EMF constant	0.00767	V.s/rad
η_g	Gearbox efficiency	0.90	
η_m	Motor efficiency	0.69	
J_{eq}	Equivalent moment of inertia	0.002	kg.m^2
B_{eq}	Equivalent viscous damping coefficient	0.004	N.m.s/rad
K_s	Experimentally determined stiffness for flexible link	1.3	N.m./rad
α	Tip deflection		rad
θ	Position of load angle		rad
V_m	DC input voltage		V

Solve for $\ddot{\alpha}$ to obtain the second equation of motion

$$\ddot{\alpha} = \frac{B_{eq}}{J_{eq}}\dot{\theta} - K_s\left(\frac{J_l + J_{eq}}{J_l J_{eq}}\right)\alpha - \frac{1}{J_{eq}}\tau \qquad (3.42.)$$

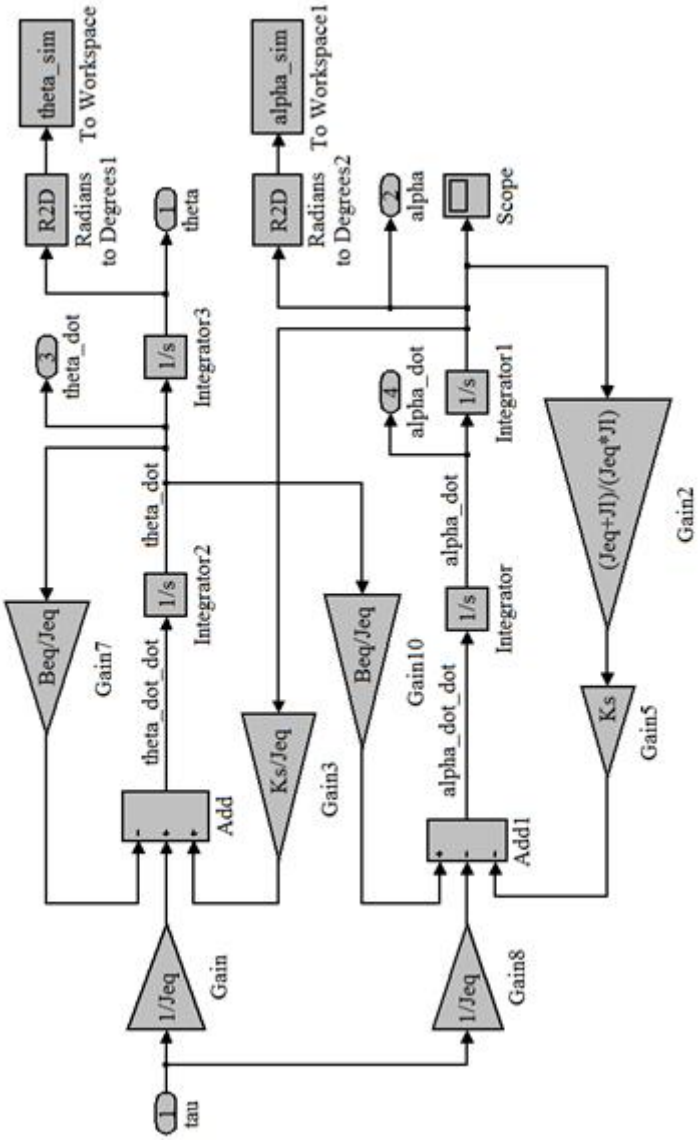

Figure 3.8. Simulink diagram of flexible link robotic manipulator

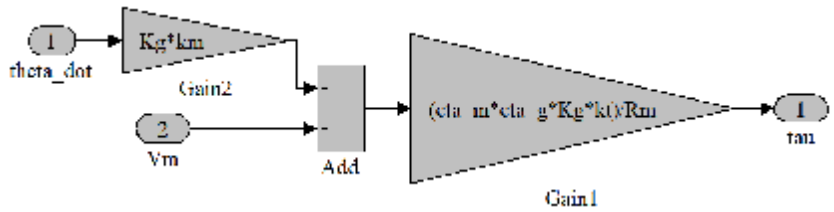

Figure 3.9. Simulink diagram of DC motor for flexible link manipulator

3.1.2. Verification and Validation of Simulation Models

In order to perform a comparative study of the input shaping methods and the experimental results of the techniques, previously described experimental setups and the presented mathematical model of the systems are used. The experimental setups are driven using step input and the resulting residual vibrations as well as cart/servo position are measured. The Matlab (2009a) models of the systems are also provided with the same input commands to demonstrate the correlation between the theoretical and experimental results obtained. The results of step input for the Matlab models of the systems and the experimental setups are presented in Figures 3.10 and 3.11.

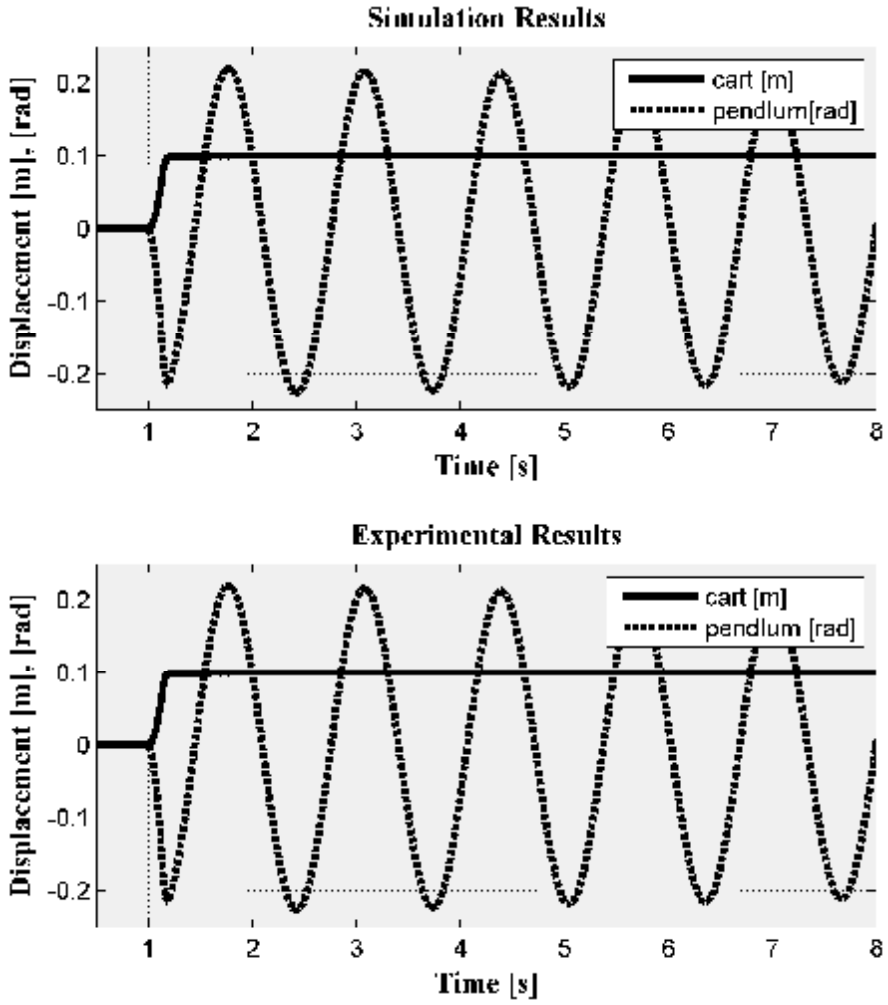

Figure 3.10. Simulation and experimental results of single pendulum gantry system for step input

In Figure 3.10, the reference input and displacement of cart are given in meters. On the other hand, the pendulum oscillation is given in unit of radians.

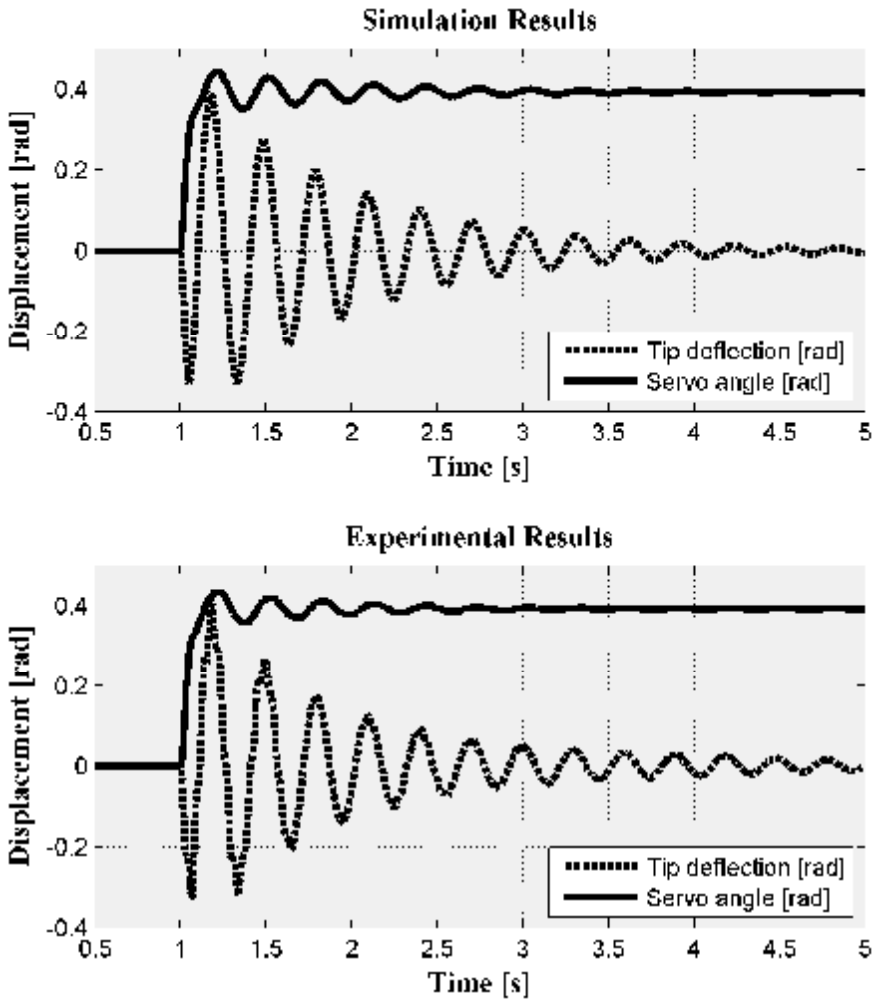

Figure 3.11. Simulation and experimental results of flexible link manipulator for step input

In Figure 3.11, the reference input, servo motor angle and flexible link tip deflection are given in unit of radians. In Figures 3.10 and 3.11, it can be seen that the simulation and test results match up very closely. This simply indicates that the behavior of the developed Matlab model and the experimental setup are very much the same. This is mainly due to the accurate mathematical model of the mechanical and the electronic systems.

3.1.3. Parameter Estimation from Experimental Data

Input shaping is a command generation technique that reduces vibration by suitably shaping the reference signal such that the vibratory modes of the system are cancelled. Shaped command profiles are generated by convolving a sequence of impulses or solving special functions for the desired command signal. Shaped command profiles are generated by using estimates of the system frequencies and damping. In contrast, most systems have errors in estimated damping and natural frequencies which can result in significant residual errors when a rest-to-rest manoeuvre is performed.

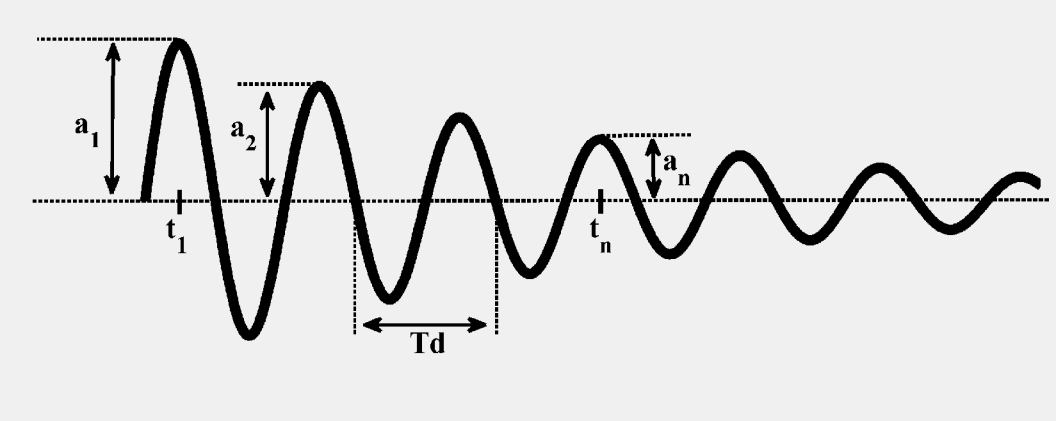

Figure 3.12. Illustrative decaying displacement time history

The logarithmic decrement is often used to estimate frequency and damping values from the transient response of a single degree of freedom system. The technique is very simple to employ and provides quick estimates without the need for extensive computation. Figure 3.12 represents a typical decaying time history trace for a single degree of freedom oscillator in which a_1, a_2, etc, are successive amplitude peaks at times t_1, t_2, etc. Td and ω_d are the damped natural period and frequency, respectively. The period of oscillation, $Td = 2\pi/\omega_d$, can be measured directly from crossing points on the zero axis, as shown in Figure 3.12.
To determine the damping ratio from the rate of decay of the oscillation,

$$\frac{a_1}{a_2} = \frac{e^{-\zeta\omega_n t_1}}{e^{-\zeta\omega_n (t_1+Td)}} = e^{-\zeta\omega_n Td} \tag{3.43.}$$

$$\frac{a_1}{a_n} = \frac{1}{e^{-\zeta\omega_n (n-1)Td}} = e^{-\zeta\omega_n Td(n-1)} \tag{3.44.}$$

The logarithm of the ratio of succeeding amplitudes is called the logarithmic decrement. Thus,

$$\ln\frac{a_1}{a_2} = \frac{1}{(n-1)}\ln\frac{a_1}{a_n} = \zeta\omega_n Td = \zeta\omega_n\frac{2\pi}{\omega_d} = \frac{2\pi}{\sqrt{1-\zeta^2}} \tag{3.45.}$$

Once the amplitudes a_1 and a_n are measured and the logarithmic decrement is calculated, the damping ratio ζ is found from (Ogata, 2003)

$$\zeta = \frac{\frac{1}{n-1}\ln\frac{a_1}{a_n}}{\sqrt{4\pi^2 + \left[\frac{1}{n-1}\ln\frac{a_1}{a_n}\right]^2}} \tag{3.46.}$$

Figures 3.10 and 3.11, shows the step response of the single pendulum gantry and flexible link manipulator, respectively. The logarithmic decrement method was applied to data obtained from experimental setup systems effectively. The resulting damping ratios and frequencies for the Single pendulum gantry and flexible link manipulator are shown in table 3.3.

Table 3.3. Command shaping calculation parameters for experimental setups

Experimental Setup	ζ	ω_d
Single Pendulum Gantry	0.004	4.789
Flexible-Link Robotic Manipulator	0.07	20.4

3.2. Methods

3.2.1. Proposed Input Shaping Technique: Modified Cycloid Plus Ramped Versine Plus Ramp (M-CPRVPR) Reference Function

The proposed input shaping method (M-CPRVPR) utilises the cycloid plus ramped versine plus ramp (CPRVPR) reference function presented in section 2.5.3.2. The CPRVPR reference input consists of three functions. The total distance to be covered from the beginning to end of a move within a specified time is the sum of the distances to be travelled by each of the three functions within the same travel time. By adjusting excursion distance of each function, vibration can be eliminated provided that the specified move time and the total distance are unchanged. Each component of the reference command creates oscillations such that these oscillations cancel each other and no vibration results. CPRVPR Method, the Equations (2.33), (2.34), (2.35) and (2.36) are used to generate the command input required for the system. The proposed method, on the other hand, divides the travelling time into two or more sections and calculates the command input as two or more separate inputs and then joins them to form the new input. The calculations for the new method are as follows where the input is divided into two or more sections and each one is calculated independently to form the other part of the input signal.

$$\begin{aligned} L &= L_a + L_b + ... + L_n \\ L_a &= L_b = ... = L/n \end{aligned} \tag{3.47.}$$

$$\begin{aligned} t &= t_a + t_b + ... + t_n \\ t_a &= t_b = ... = t/n \end{aligned} \tag{3.48.}$$

$$R_{a,b,...,n} = 2p/t_{a,b,...,n} \tag{3.49.}$$

where L is total travelling distance and t is total travelling time.

$$L_{1_{(a,b,\ldots,n)}} = \frac{LR_{a,b,\ldots,n}\left(R_{a,b,\ldots,n} - 2\zeta\omega_n\right)}{\omega_n^{\,2}}$$
$$L_{2_{(a,b,\ldots,n)}} = \frac{L\left(1 - R_{a,b,\ldots,n}\right)}{\omega_n^{\,2}} \qquad (3.50.)$$
$$L_{3_{(a,b,\ldots,n)}} = \frac{2L\zeta R_{a,b,\ldots,n}}{\omega_n}$$

where L_1 is the maximum excursion distance to be travelled by ramp motion profile, L_2 is the maximum excursion distance to be travelled by cycloid motion profile, L_3 is the maximum excursion distance to be travelled by ramped versine motion profile. Variations of L_1, L_2 and L_3 is possible with traveling time t to result in an oscillation free displacement of the system. Furthermore, total distance can be written as $L = L_1 + L_2 + L_3$.

$$Y = \begin{cases} 0 \le t \le \frac{t_1}{n} \Rightarrow Y = \frac{L_{1a}R_a t}{2\pi} + \frac{L_{2a}}{2\pi}\left(R_a t - \sin(R_a t)\right) \\ \qquad\qquad + \frac{L_{3a}R_a t}{2\pi} + \frac{L_{3a}}{2\pi}\left(1 - \cos(R_a t)\right) \\ \frac{t_1}{n} \le t \le \frac{t_2}{n} \Rightarrow Y = \frac{L_{1b}R_b t}{2\pi} + \frac{L_{2b}}{2\pi}\left(R_b t - \sin(R_b t)\right) \\ \qquad\qquad + \frac{L_{3b}R_b t}{2\pi} + \frac{L_{3b}}{2\pi}\left(1 - \cos(R_b t)\right) \\ \ldots\ldots\ldots\ldots\ldots\ldots\ldots\ldots\ldots\ldots\ldots\ldots\ldots\ldots\ldots\ldots\ldots\ldots \\ \frac{t_n}{n} \le t \le t \Rightarrow Y = \frac{L_{1n}R_n t}{2\pi} + \frac{L_{2n}}{2\pi}\left(R_n t - \sin(R_n t)\right) \\ \qquad\qquad + \frac{L_{3n}R_n t}{2\pi} + \frac{L_{3n}}{2\pi}\left(1 - \cos(R_n t)\right) \end{cases} \qquad (3.51.)$$

As defined in Equations (3.47) to (3.51), the new method allows virtually division of the motion of the system into two or more steps. Because the first step completes with almost steady motion with relatively reduced vibration levels, the second part of the motions starts with the advantage of very little or almost no

residual vibrations. Consequently, the result of the second part of the motion yields better performance relative to the CPRVPR reference function.

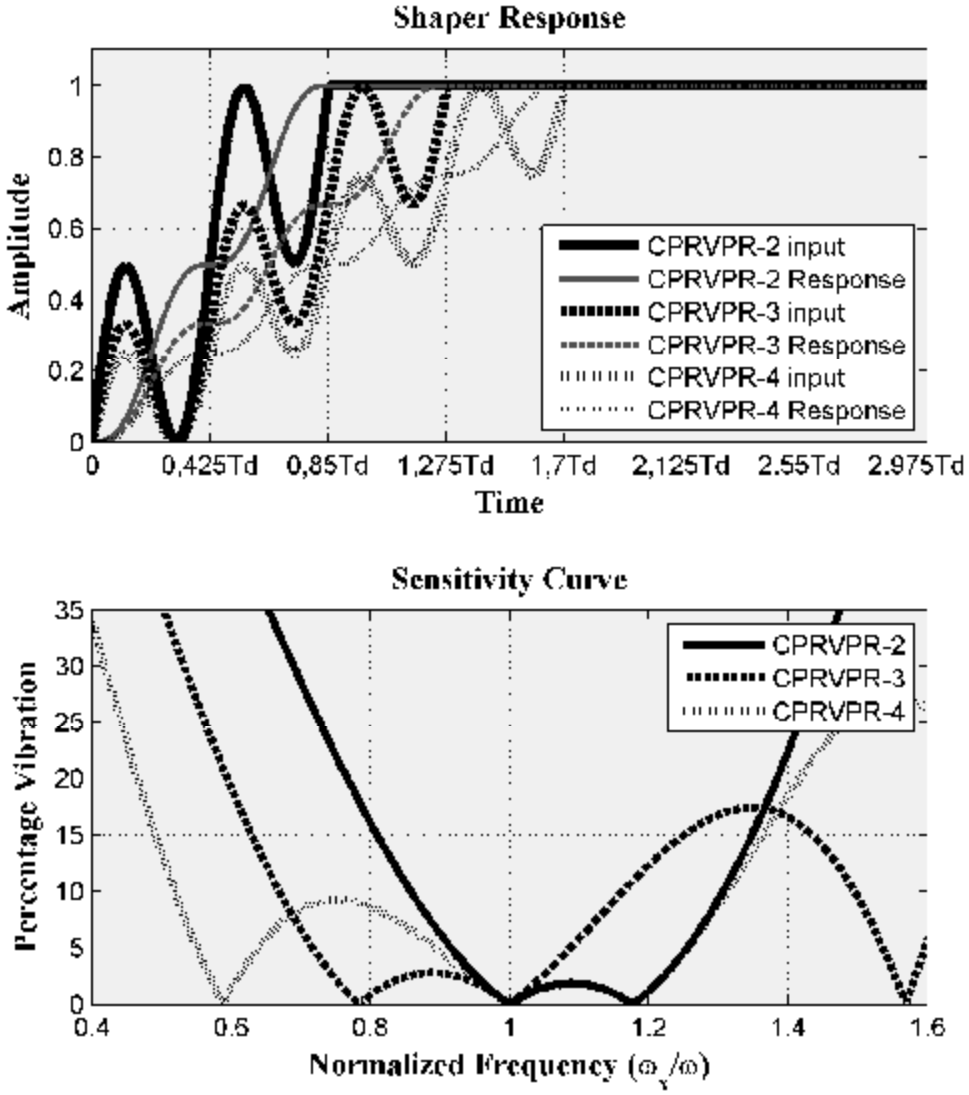

Figure 3.13. Recursion of cycloid plus ramped versine plus ramp function and sensitivity curve for a total travelling distance $L = 1$ and travelling time of $t = 0.425T_d$

As illustrated in Figures 3.13 and 3.14, the presented method consists of two or more components where the resulting residual vibration cancels out due to reverse act. There is no difference between the signals applied to the system in two or more parts of the input signal. In fact, the same signal is repeated in each part. By doing this, it is not the natural period of the system used in calculation of the signal timing

and related calculations; it is the arbitrarily chosen travelling time that is divided into two or more equal parts that is used in application of the input signal. These features of the input signals can be seen clearly in the figures.

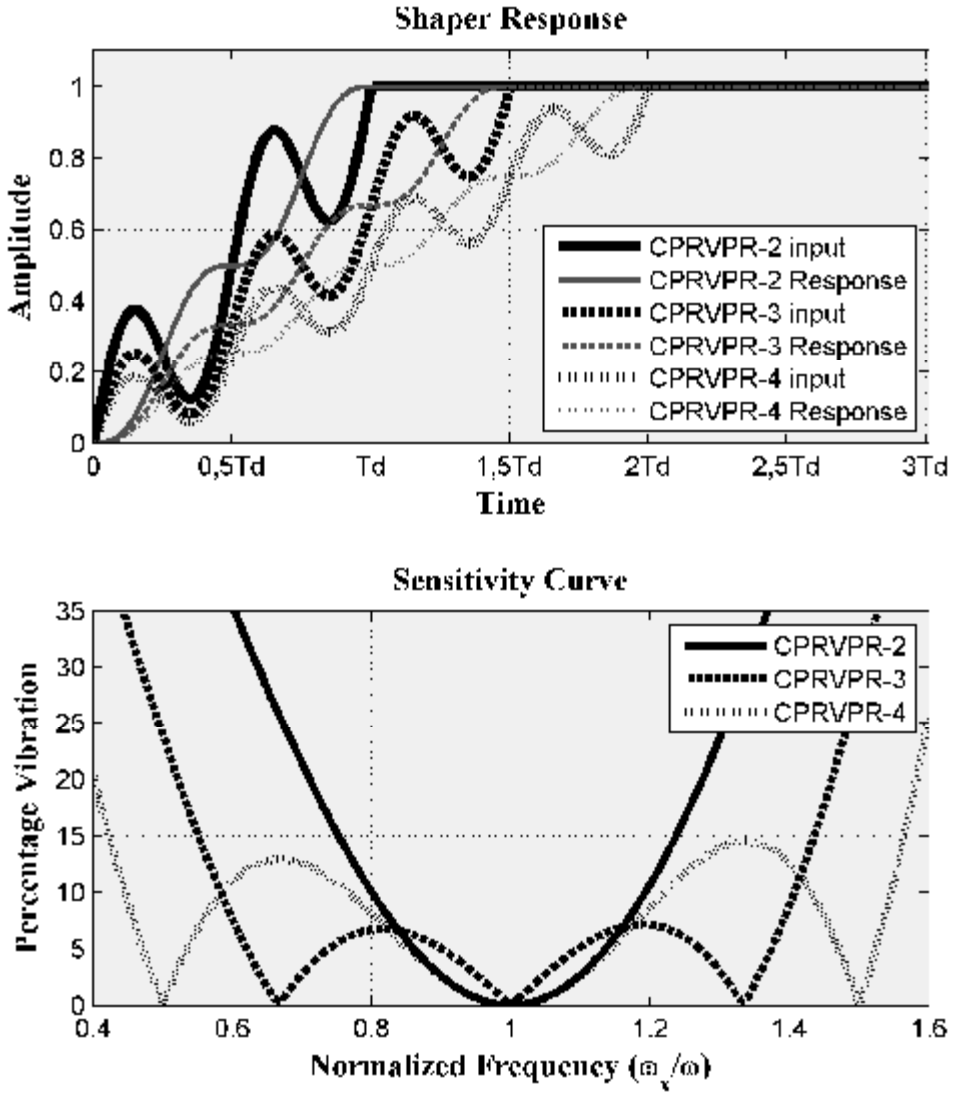

Figure 3.14. Recursion of cycloid plus ramped versine plus ramp function and sensitivity curve for a total travelling distance $L = 1$ and travelling time oft $= 0.5T_d$

The proposed method considers a trajectory based on a cycloidal and versine motion, which is commonly used as a high speed cam profile, continuous throughout one cycle, plus a ramp. The amplitude of the ramp, the cycloidal function and versine function are determined such that total travelling distance and the transportation time

conditions are satisfied. Then the resulting trajectory is convolved desired times to obtain a twice or more shaped input. The algorithm can be extended indefinitely with repeated recursion of the motion profile equation. For each recursion, an additional part is added to the shaper and the shaper is lengthened by recursion period of the frequency. This trade-off is typical of the input shaper design process, increasing insensitivity usually requires increasing the length of travelling time of the input shaper. These features of the input signals can be seen clearly in the Figures 3.13 and 3.14. It is believed that this method contributes to the efforts in reducing the vibration of multi mode systems in the presence of uncertainty in the dynamic parameters of flexible system such as its modal natural frequencies and the damping ratios.

Figures 3.13 and 3.14 simulation results shows that proposed new technique is simple and easy to implement, and can be considered as a versatile and effective way to determine a trajectory resulting in reduced or eliminated residual vibrations of flexible systems with high robustness. The advantage of the proposed technique is that it neither limits nor increases the move time, i.e. no time limitation or time penalty. Most conventional input shaping methods, however, tend to increase the travelling time by at least a half damped period or more.

4. RESULTS AND DISCUSSIONS

One of the methods used to reduce or eliminate the residual vibrations is to modify the input command by using the system parameters that are known beforehand. In order to eliminate the residual vibrations completely, the system parameters must be known very accurately. In realistic systems, achieving such level of accuracy may not always be possible. To address the problem and to provide practical solutions, in this thesis, new residual vibration elimination methods are introduced. In this section of the presented work, the simulations and the experimental results of the new methods are presented. The simulation and the experimental results show that the residual vibrations are considerably decreased with a high degree of robustness in the presence of system parameters uncertainty. These new methods prove to be useful especially in the case of uncertain parameters of estimated or predicted systems. It is shown that the presented new technique is capable of handling high levels of uncertainty and able to successfully eliminate or reduce residual vibrations in flexible systems. The present chapter provides details on theoretical and experimental results of these techniques applied to the single pendulum gantry crane and flexible link robotic manipulator systems where a comparative study of robustness performance is also provided. Simulation and experimental results show that the oscillations are considerably decreased with a high degree of robustness in the presence of system parameters uncertainty.

In order to perform a comparison amongst the input shaping methods and the experimental results of the techniques, previously described experimental setups and the mathematical models of the systems are used. The experimental setups are driven using each input command shaping method individually. The resulting residual vibrations as well as cart or servo positions are also measured during each trial. In order to demonstrate the correlation between the theoretical and experimental results obtained, the Matlab (2009a) models of the systems are also provided with the same input commands as the experimental models. In order to demonstrate the effectiveness of the proposed techniques, the simulation and the experimental results are compared with the conventional input shaping methods.

4.1. Results

4.1.1. Experiment Set 1: Single Pendulum Gantry System

In this section, to validate the proposed techniques and to demonstrate the practical effectiveness of it over the discussed conventional methods, it has been tested in real time experiments using a single pendulum gantry system. This gantry system is fabricated by Quanser Inc. (Quanser Inc., 2012a). The detailed information upon the utilized gantry system can be found in Section 3.1.1 and from the website of the company (Quanser Inc.).

4.1.1.1. Zero Vibration (ZV) Shaper

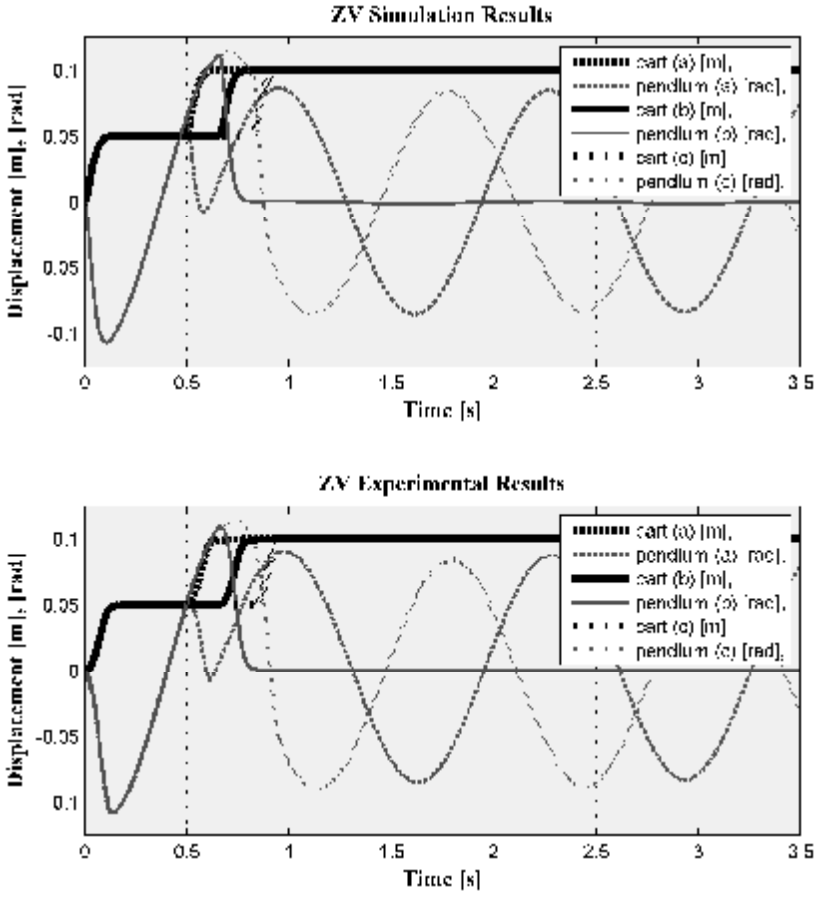

Figure 4.1. ZV shaper with experimental and simulation results for (a) -%25, (b) %0, (c) +%25 estimation error of natural frequency

In Figures 4.1, the simulation and experimental results of ZV shaper are illustrated. In the figure, estimation error of ±%25 is introduced to natural frequency of the system used in calculation of the input signals. Figure 4.1 is plotted with estimation errors of (a) -%25, (b) %0, (c) +%25, respectively.

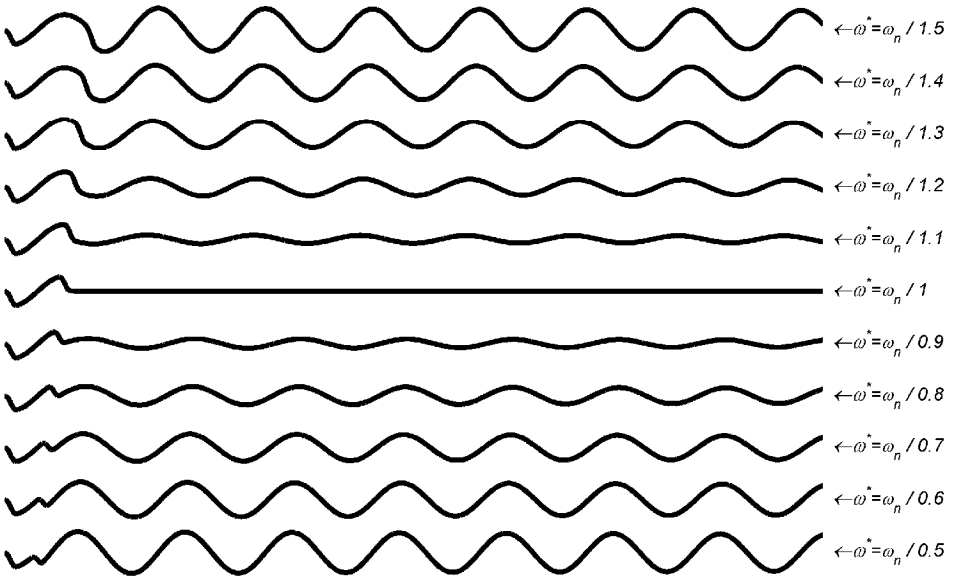

Figure 4.2. Pendulum positions of different predicted natural frequencies for ZV shaper related experimental results

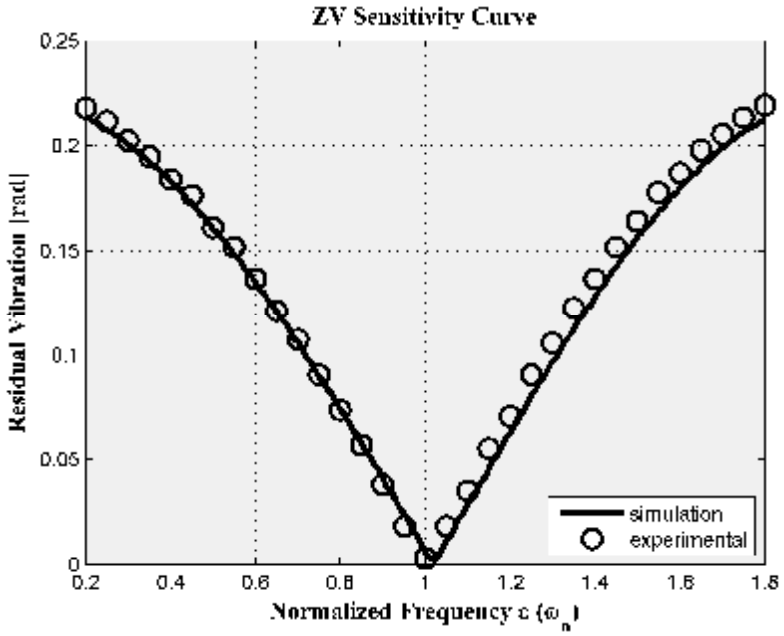

Figure 4.3. Theoretical and experimental sensitivity curves for the ZV shaper

In Figure 4.1, it can be seen that, the estimation error causes increasing residual vibrations of pendulum ranging from 0.948 to 0.839 rad. It can be seen that increasing error in estimation of the natural frequency of the system causes increasing residual vibrations. These results are also validated in Figure 4.2, where pendulum position of different predicted natural frequencies and related sensitivity curves are presented, respectively.

The theoretical and experimental sensitivity curves for the ZV shaper are shown in Figure 4.3. The experimental results closely match those predicted by the theoretical study. Figure 4.3 shows that the vibration amplitude increases rapidly as the estimated frequency deviates from the actual system frequency.

4.1.1.2. Zero Vibration Derivative (ZVD) Shaper

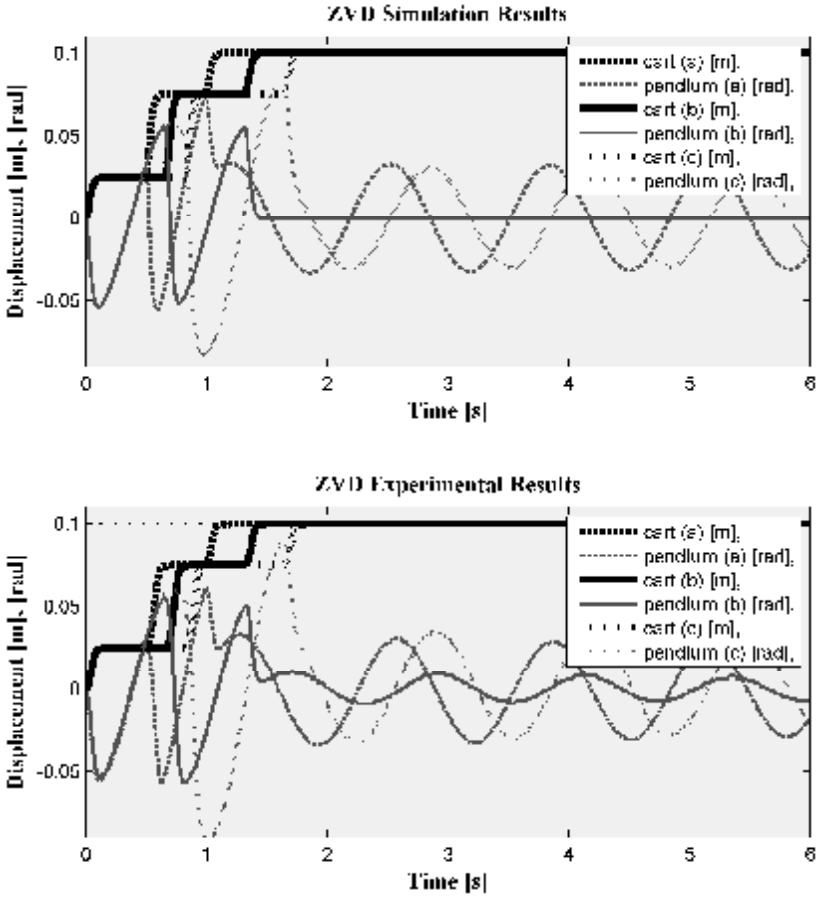

Figure 4.4. ZVD shaper with experimental and simulation results for (a) -%25, (b) %0, (c) +%25 estimation error of natural frequency

In Figures 4.4, the simulation and experimental results of ZVD shaper are illustrated. In the figure, estimation error of ±%25 is introduced to natural frequency of the system used in calculation of the input signals. Figure 4.4 is plotted with estimation errors of (a) -%25, (b) %0, (c) +%25, respectively.

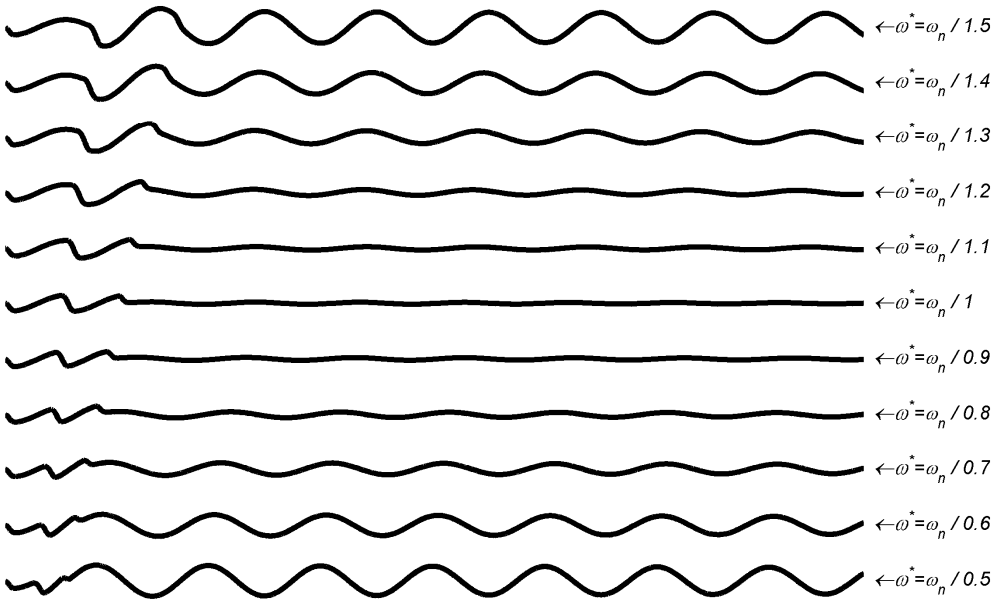

Figure 4.5. Pendulum positions of different predicted natural frequencies for ZVD shaper related experimental results

In Figure 4.4, it can be seen that, the estimation error causes increasing residual vibrations of pendulum ranging from 0.0352 to 0.0306 rad. It can be seen that increasing error in estimation of the natural frequency of the system causes increasing residual vibrations. These results are also validated in Figure 4.5 and 4.6 where pendulum position of different predicted natural frequencies and related sensitivity curves are presented, respectively.

The theoretical and experimental sensitivity curves for the ZVD shaper are shown in Figure 4.6. The experimental results closely match those predicted by the theoretical study. Figure 4.6 shows that the ZVD shaper is much more insensitive to modelling errors than the ZV shaper. However, the ZVD shaper has a time duration equal to one period of the vibration frequency, as opposed to the one-half period length of the ZV shaper. This trade-off is typical of the input shaper design process,

increasing insensitivity usually requires increasing the length of travelling time of the input shaper.

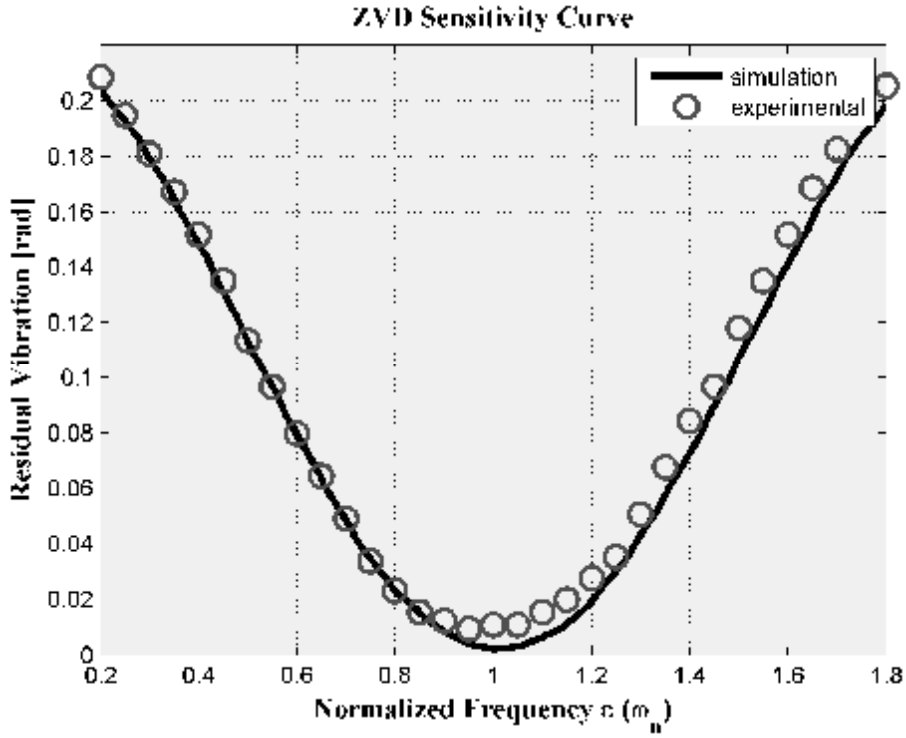

Figure 4.6. Theoretical and experimental sensitivity curves for the ZVD shaper

4.1.1.3. Zero Vibration Derivative and Derivative (ZVDD) Shaper

In Figures 4.7, the simulation and experimental results of ZVDD shaper are illustrated. In the figure, estimation error of ±%25 is introduced to natural frequency of the system used in calculation of the input signals. Figure 4.7 is plotted with estimation errors of (a) -%25, (b) %0, (c) +%25, respectively. In Figure 4.7, it can be seen that, the estimation error causes increasing residual vibrations of pendulum ranging from 0.0138 to 0.0107 rad. It can be seen that increasing error in estimation of the natural frequency of the system causes increasing residual vibrations. These results are also validated in Figure 4.8 and 4.9, where pendulum position of different predicted natural frequencies and related sensitivity curves are presented, respectively.

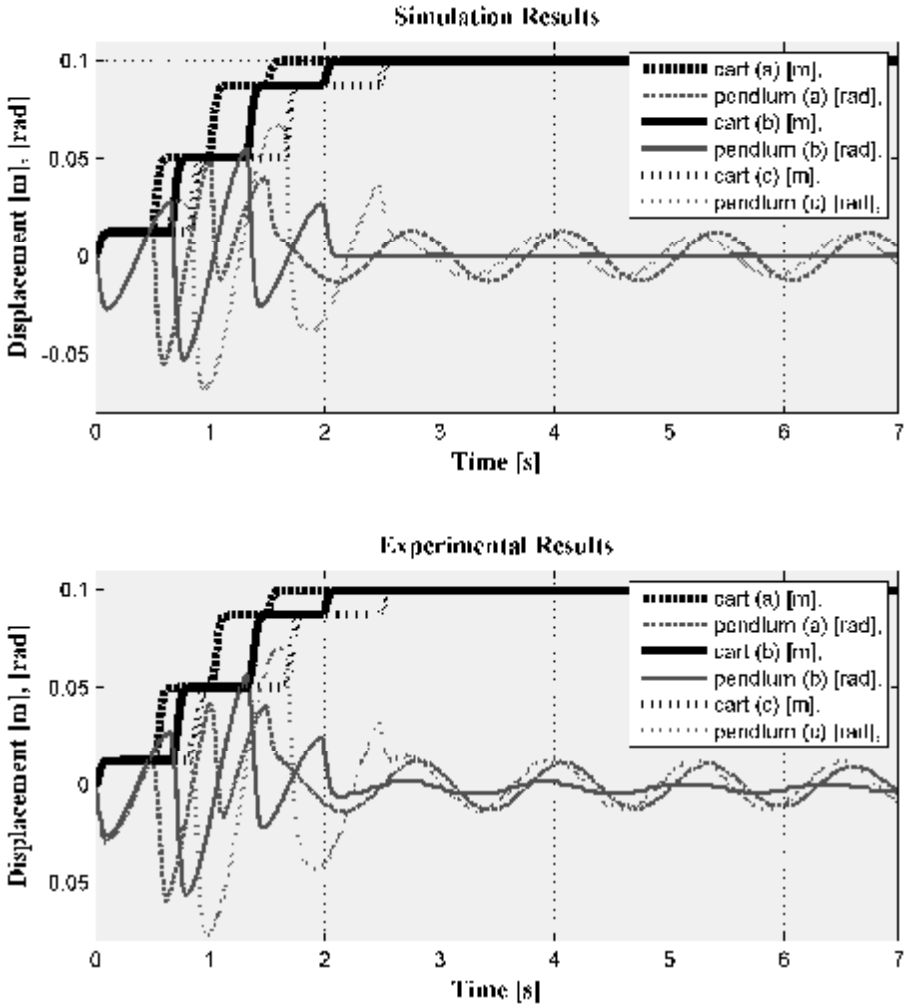

Figure 4.7. ZVDD shaper with experimental and simulation results for (a) -%25, (b) %0, (c) +%25 estimation error of natural frequency

The theoretical and experimental sensitivity curves for the ZVDD shaper are shown in Figure 4.9. The experimental results closely match those predicted by the theoretical study. Figure 4.8 and 4.9 shows that the ZVDD shaper is much more insensitive to modelling errors than the ZVD shaper. However, the ZVDD shaper has a time duration equal to one and a half period of the vibration frequency, as opposed to the one period length of the ZVD shaper. The additional robustness gained from each higher-order derivative is evident in the plot.

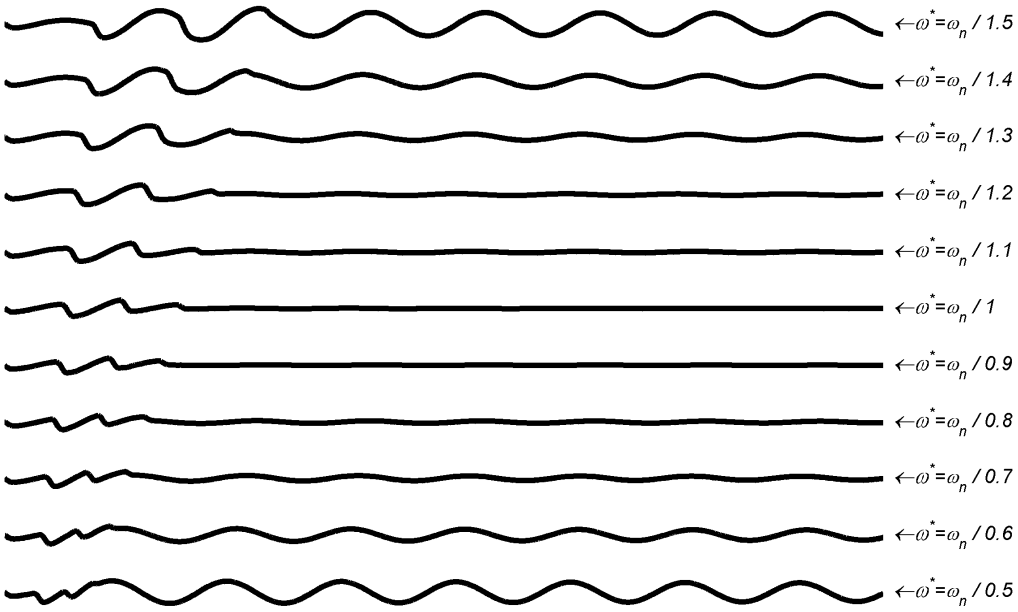

Figure 4.8. Pendulum positions of different predicted natural frequencies for ZVDD shaper related experimental results

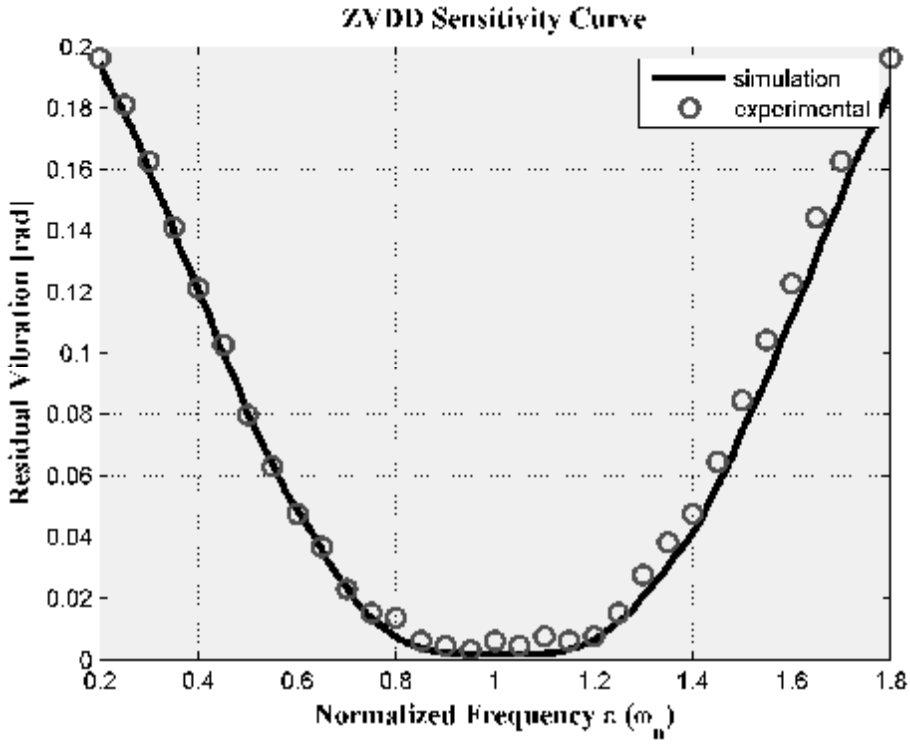

Figure 4.9. Theoretical and experimental sensitivity curves for the ZVDD shaper

4.1.1.4. Zero Vibration Derivative Derivative Derivative (ZVDDD) Shaper

In Figures 4.10, the simulation and experimental results of ZVDDD shaper are illustrated. In the figure, estimation error of ±%25 is introduced to natural frequency of the system used in calculation of the input signals. Figure 4.10 is plotted with estimation errors of (a) -%25, (b) %0, (c) +%25, respectively.

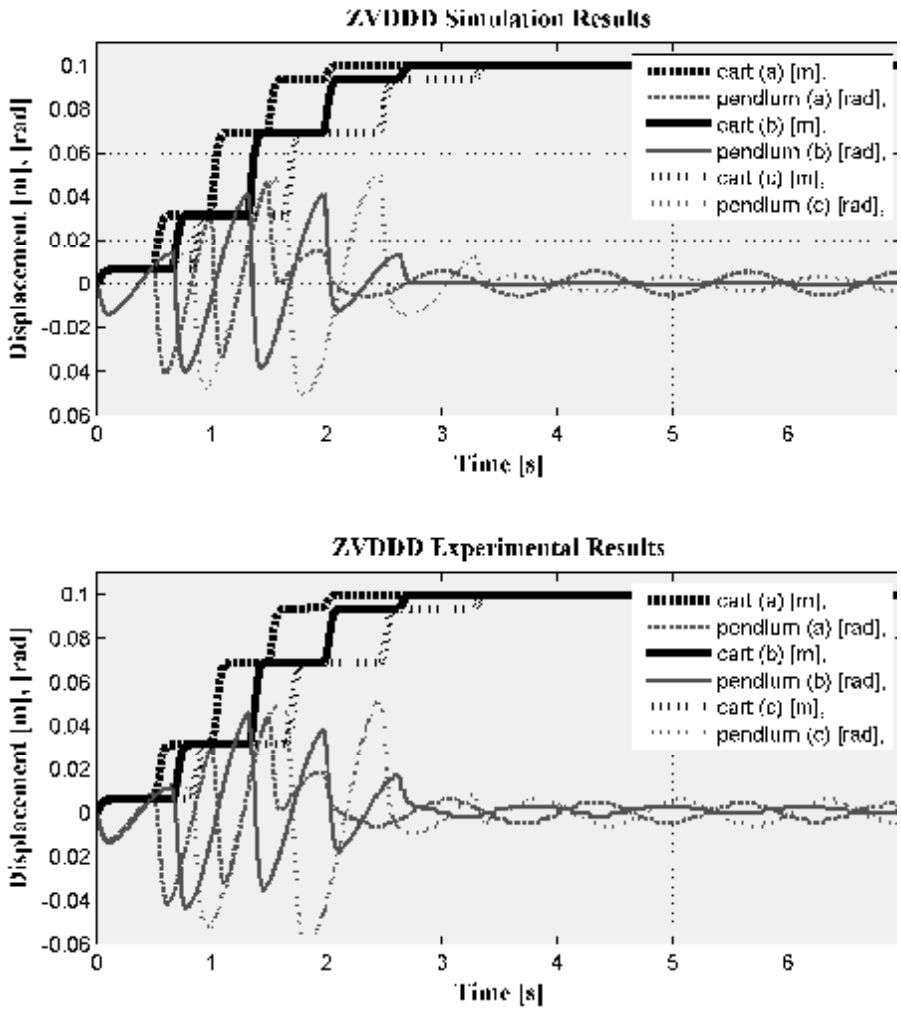

Figure 4.10. ZVDD shaper with experimental and simulation results for (a) -%25, (b) %0, (c) +%25 estimation error of natural frequency

In Figure 4.10, it can be seen that, the estimation error causes increasing residual vibrations of pendulum ranging from 0.0061 to 0.0046 rad. It can be seen that increasing error in estimation of the natural frequency of the system not effect residual

vibrations. These results are also validated in Figure 4.11 and 4.12 where pendulum position of different predicted natural frequencies and related sensitivity curves are presented, respectively.

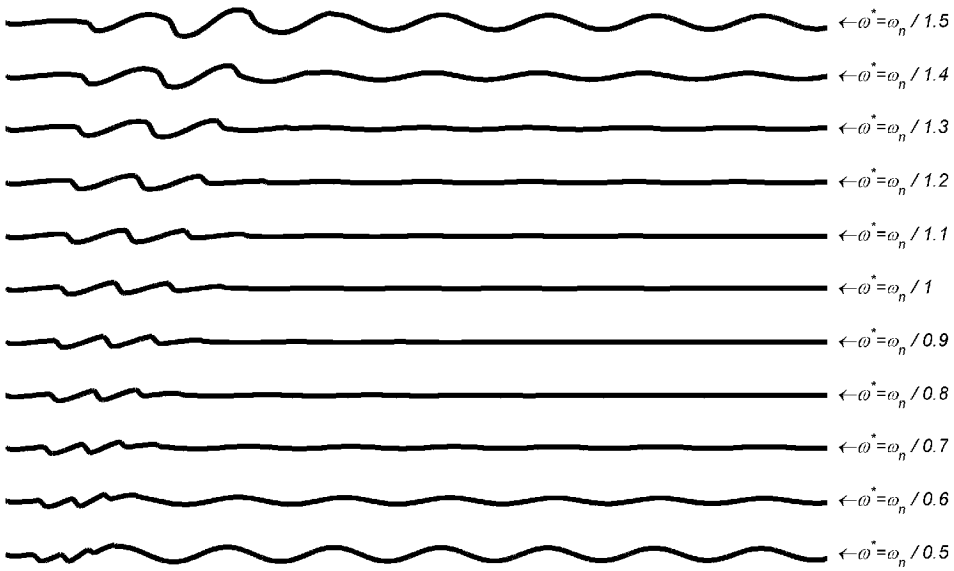

Figure 4.11. Pendulum positions of different predicted natural frequencies for ZVDDD shaper related experimental results

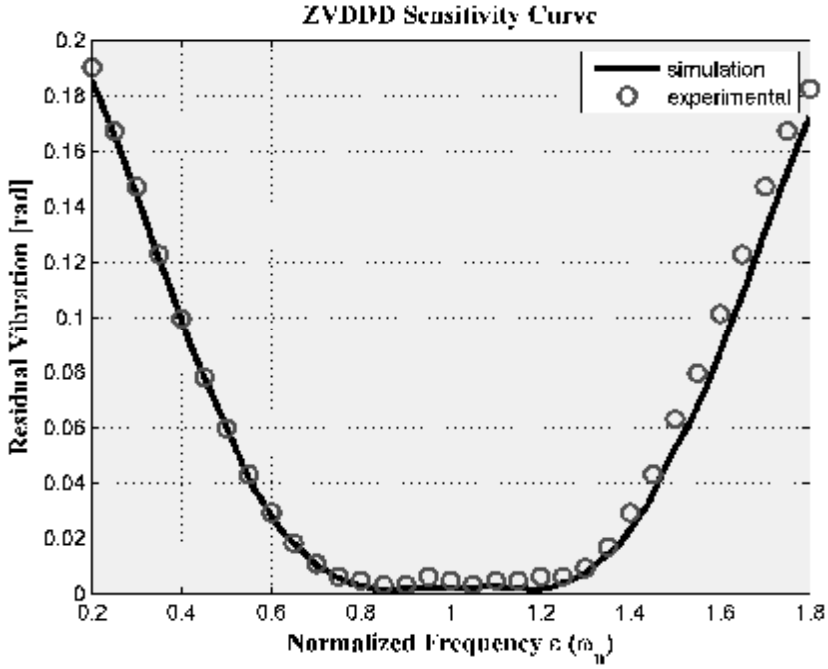

Figure 4.12. Theoretical and experimental sensitivity curves for the ZVDDD shaper

Figure 4.11 and 4.12, shows that the ZVDDD shaper is much more insensitive to modelling errors than the ZVDD shaper. However, the ZVDDD shaper has a time duration equal to two period of the vibration frequency, as opposed to the one and a half period length of the ZVDD shaper. The additional robustness gained from each higher-order derivative is evident in the plot. The algorithm can be extended indefinitely with repeated differentiation of the percentage vibration equation. For each differentiation, an additional impulse is added to the shaper and the shaper is lengthened by one-half period of the frequency.

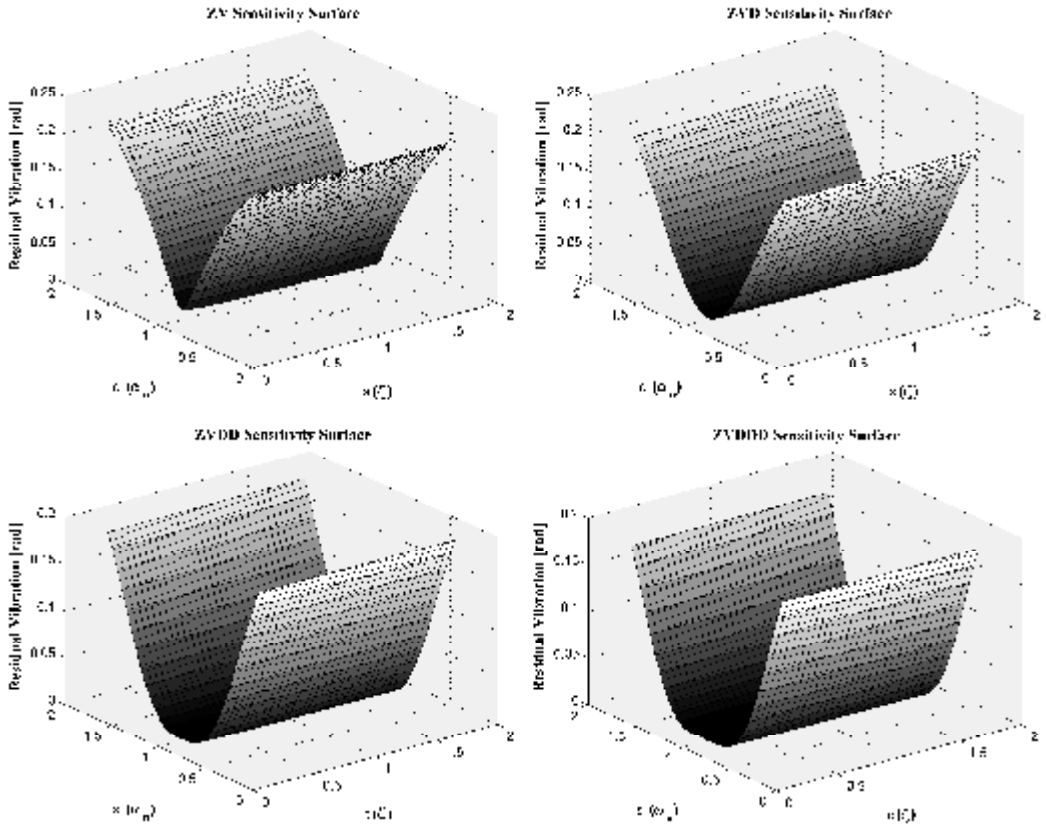

Figure 4.13. Robustness of the system to uncertainties in the mode frequencies and the damping ratios for the ZV, ZVD, ZVDD and ZVDDD Shapers

In Figure 4.13, the variation of the residual vibration is presented against estimation error in natural frequency and damping ratio of the system for the ZV, ZVD, ZVDD and ZVDDD input shapers. It can clearly be seen that the variation of estimation error (or increasing uncertainty) of damping ratio has relatively reduced the effect on the residual vibration of the system. Therefore, the uncertainties on the

damping ratio do not play an important role in affecting the behavior of the system mainly due to its very low value, i.e. ζ =0.004. On the other hand, the estimation error in natural frequency of the system appears to affect the motion of the system and the resulting residual vibration levels.

4.1.1.5. Extra Insensitive (EI) Shaper

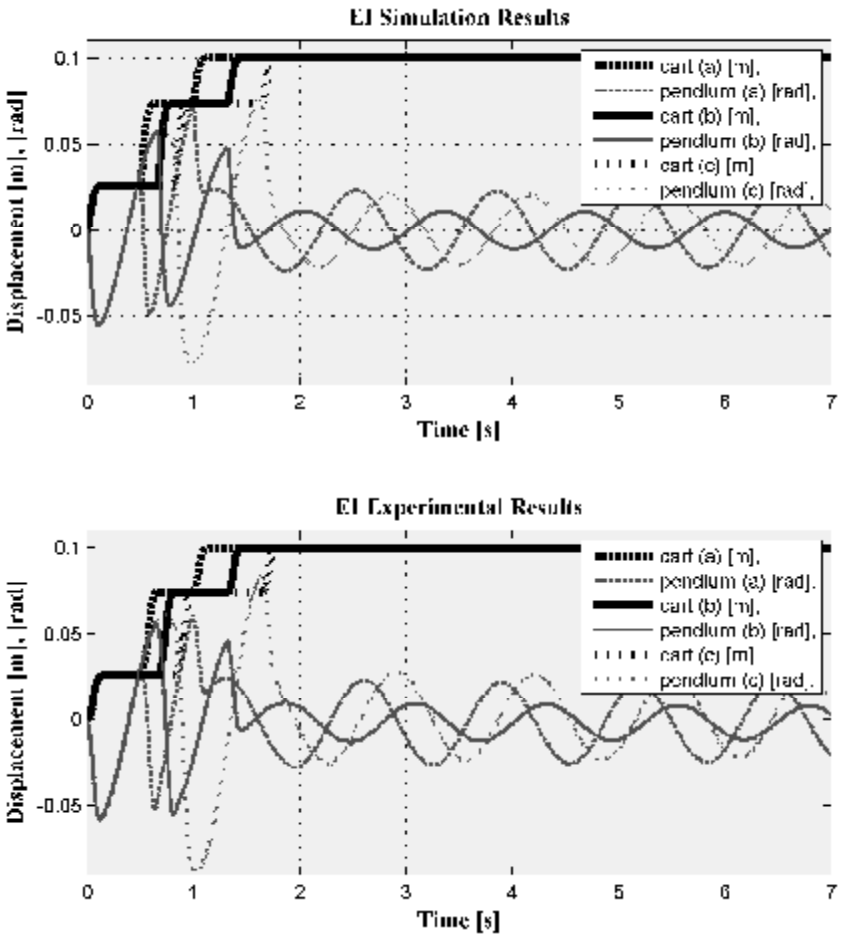

Figure 4.14. EI shaper with experimental and simulation results for (a) -%25, (b) %0, (c) +%25 estimation error of natural frequency

In Figures 4.14, the simulation and experimental results of EI shaper are illustrated. In the figure, estimation error of ±%25 is introduced to natural frequency of the system used in calculation of the input signals. Figure 4.14 is plotted with estimation errors of (a) -%25, (b) %0, (c) +%25, respectively. In Figure 4.14, it can be

seen that, the estimation error causes increasing residual vibrations of pendulum ranging from 0.023 to 0.0276 rad. It can be seen that increasing error in estimation of the natural frequency of the system causes increasing residual vibrations.

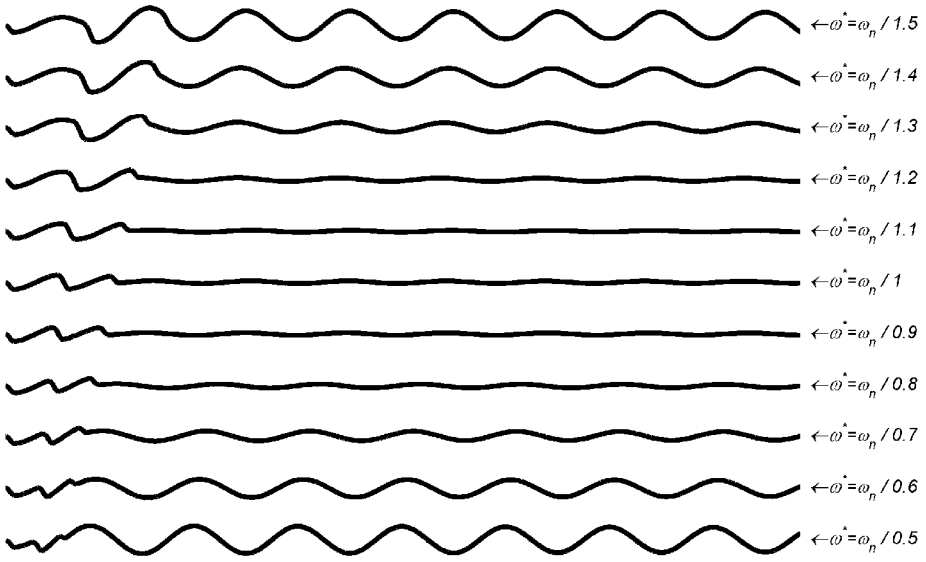

Figure 4.15. Pendulum positions of different predicted natural frequencies for EI shaper related experimental results

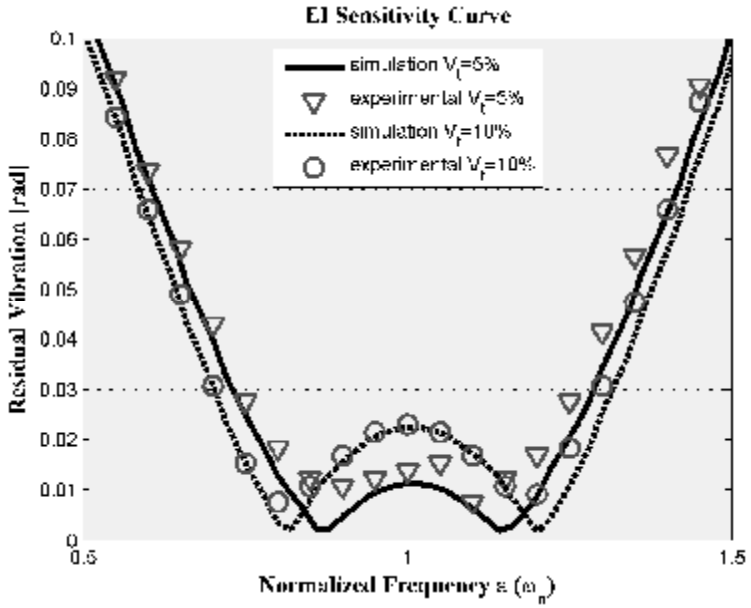

Figure 4.16. Theoretical and experimental sensitivity curves for the 5% and 10% EI shaper

These results are also validated in Figure 4.15 and 4.16 where pendulum position of different predicted natural frequencies and related sensitivity curves are presented, respectively.

Unlike the ZV, ZVD, ZVDD and ZVDDD shapers, the Extra Insensitive (EI) shaper does not attempt to force the vibration to zero at the modelling frequency. Rather, the vibration is limited to some low, but acceptable level of residual vibration. The sensitivity curve for an EI shaper designed to limit vibration below 5% and 10% is shown in Figure 4.16. The length of the EI shaper is the same as that of the ZVD shaper, one damped cycle of vibration, but it is considerably more robust. Thus, the application of EI shapers is for systems where some small vibration is allowable, and the systems parameters are expected to change considerably.

4.1.1.6. Two Hump Extra Insensitive (2H-EI) Shaper

In Figures 4.17, the simulation and experimental results of Two Hump EI (2H-EI) shaper are illustrated. In the figure, estimation error of ±%25 is introduced to natural frequency of the system used in calculation of the input signals. Figure 4.17 is plotted with estimation errors of (a) -%25, (b) %0, (c) +%25, respectively. In Figure 4.17, it can be seen that, the estimation error causes increasing residual vibrations of pendulum ranging from 0.0061 to 0.0107 rad. It can be seen that increasing error in estimation of the natural frequency of the system does not seem to important affect the residual vibrations. These results are also validated in Figure 4.18 and 4.19 where pendulum position of different predicted natural frequencies and related sensitivity curves are presented, respectively.

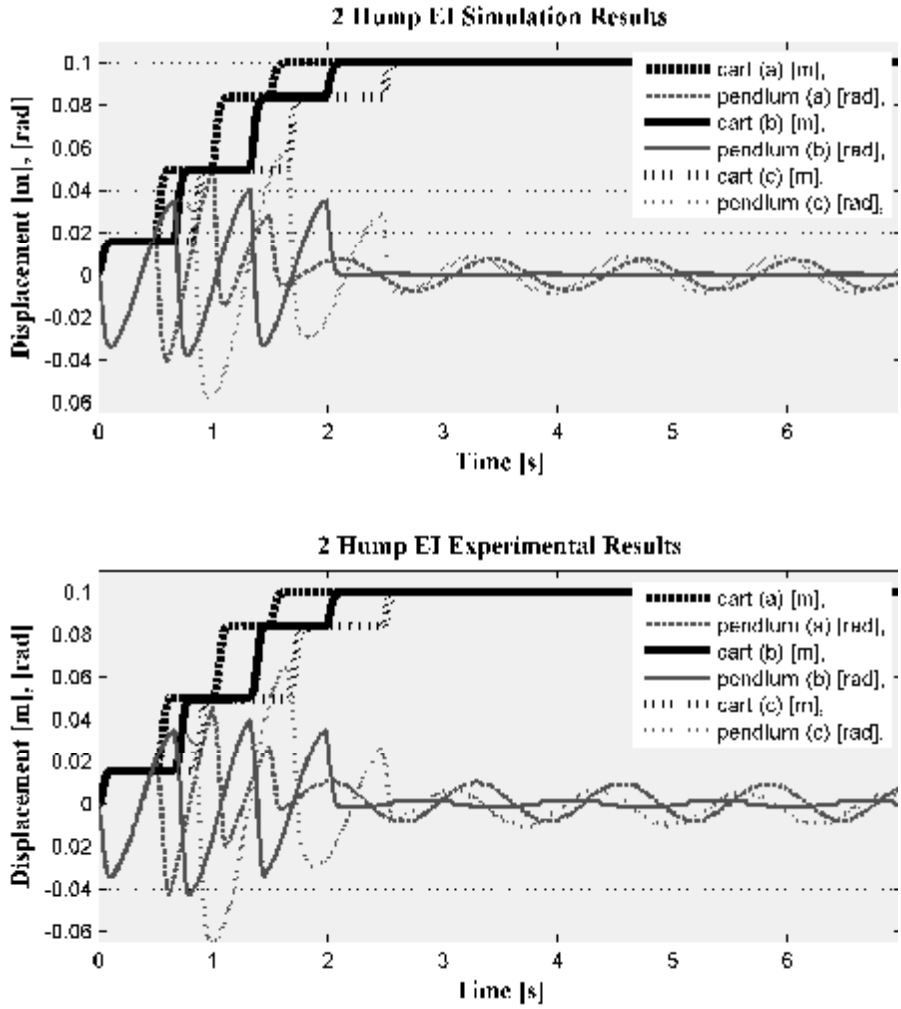

Figure 4.17. Two Hump EI shaper with experimental and simulation results for (a) -%25, (b) %0, (c) +%25 estimation error of natural frequency

The theoretical and experimental sensitivity curves for two-hump EI shapers designed to limit vibration below 5% and 10% are shown in Figure 4.19. The experimental results closely match those predicted by the theoretical study. As with the derivative-method (ZVD, ZVDD and ZVDDD) shapers, the price for increased robustness is a corresponding increase in shaper duration. Note, however, that the penalty is not uniform across all shapers. The Two-Hump EI shaper has the same duration as the ZVDD shaper. However, the Two-Hump EI shapers have much more robustness, as can be seen in Figure 4.18 and 4.19.

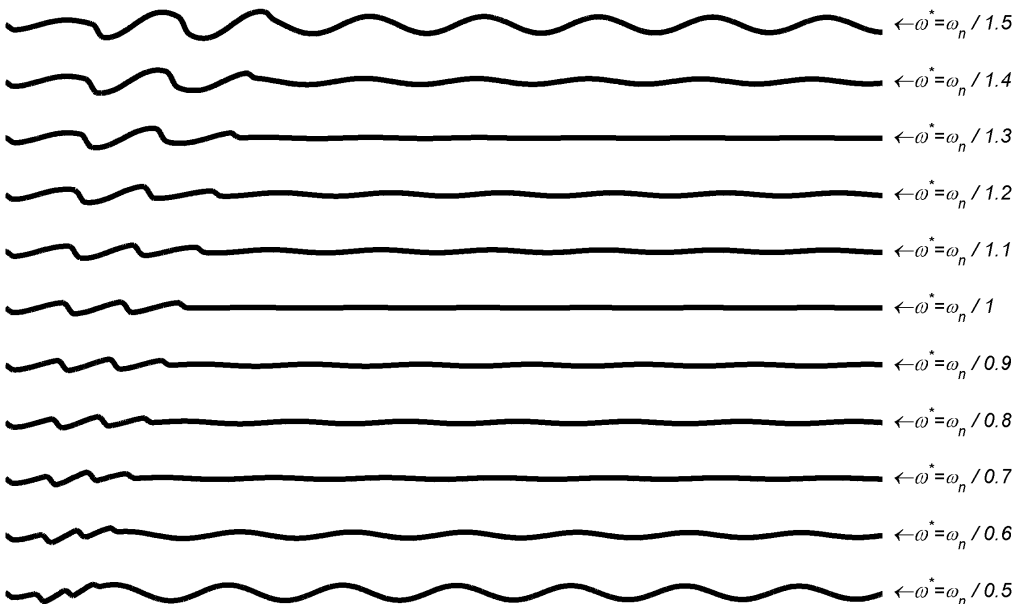

Figure 4.18. Pendulum positions of different predicted natural frequencies for Two Hump EI shaper related experimental results

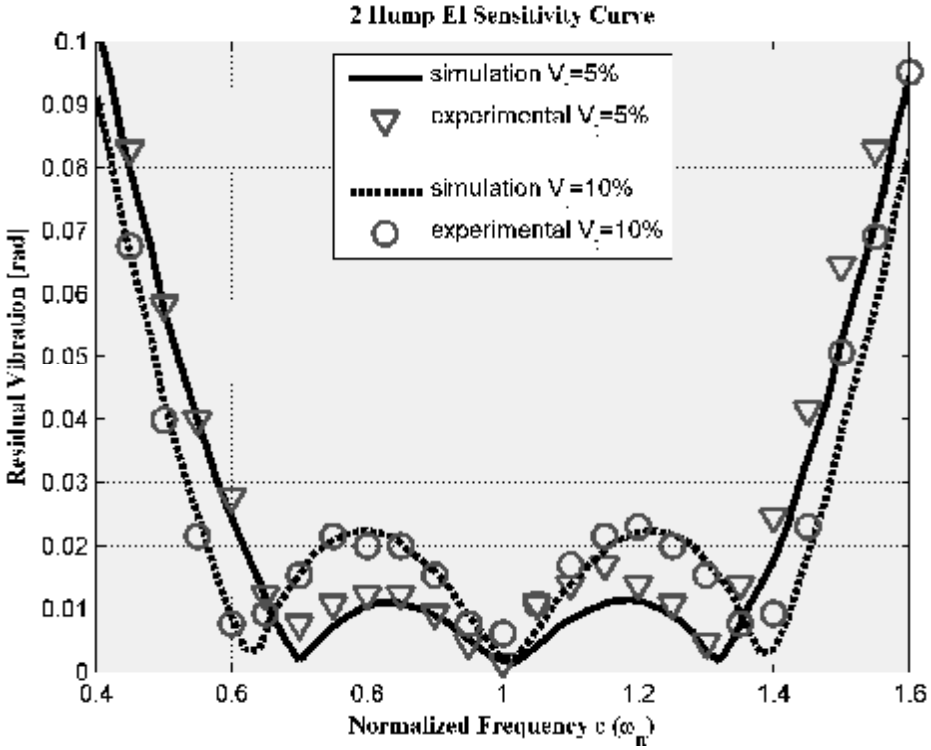

Figure 4.19. Theoretical and experimental sensitivity curves for the 5% and 10% Two Hump EI shaper

4.1.1.7. Three Hump Extra Insensitive (3H-EI) Shaper

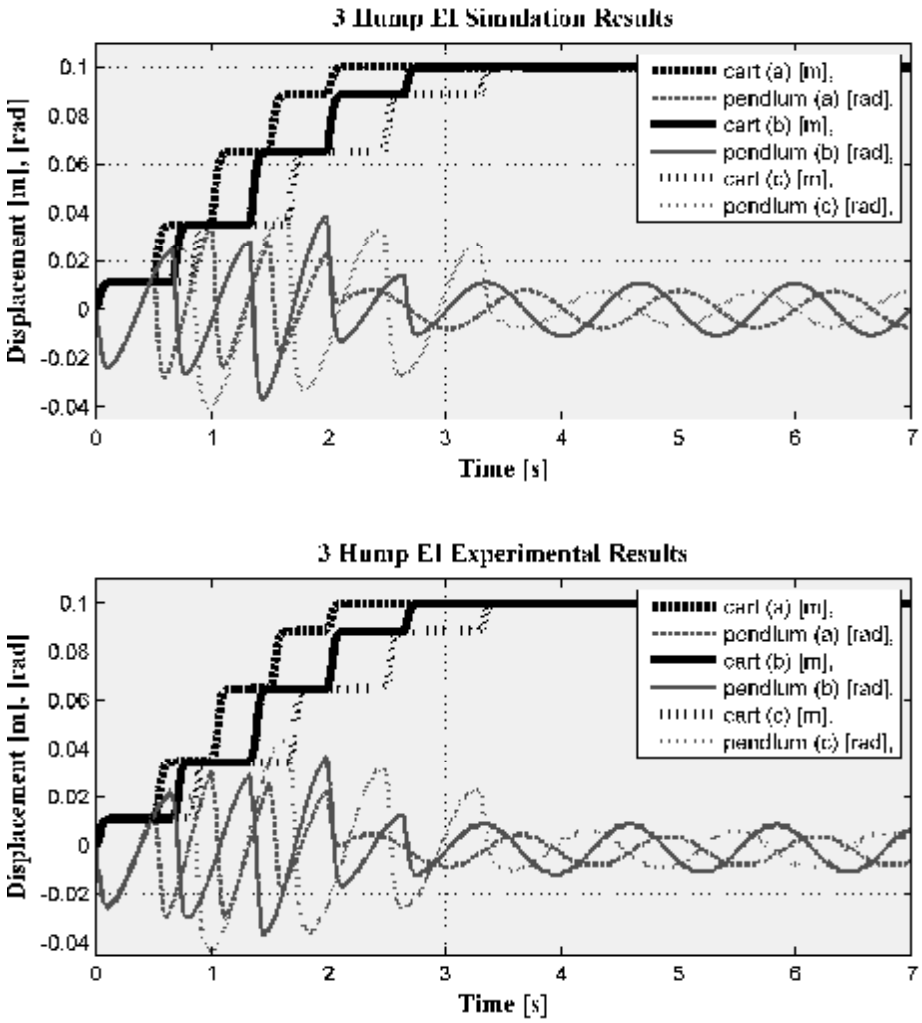

Figure 4.20. Three Hump EI shaper with experimental and simulation results for (a) -%25, (b) %0, (c) +%25 estimation error of natural frequency

In Figures 4.20, the simulation and experimental results of Three Hump EI shaper (3H-EI) are illustrated. In the figure, estimation error of ±%25 is introduced to natural frequency of the system used in calculation of the input signals. Figure 4.20 is plotted with estimation errors of (a) -%25, (b) %0, (c) +%25, respectively. In Figure 4.20, it can be seen that, the estimation error causes increasing residual vibrations of pendulum ranging from 0.0061 to 0.0092 rad. It can be seen that increasing error in estimation of the natural frequency of the system does not seem to important affect the residual vibrations. These results are also validated in Figure 4.21 and 4.22 where

pendulum position of different predicted natural frequencies and related sensitivity curves are presented, respectively.

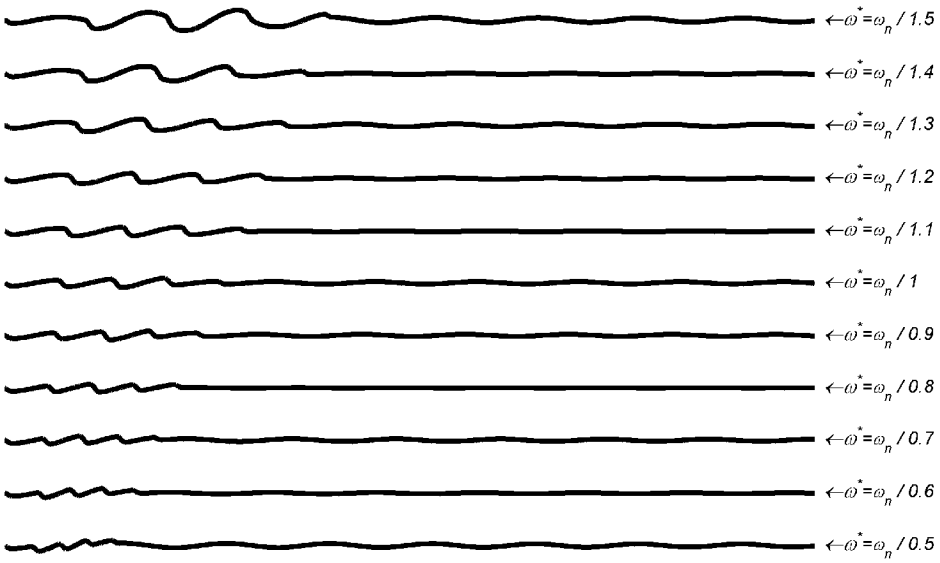

Figure 4.21. Pendulum positions of different predicted natural frequencies for Three Hump EI shaper related experimental results

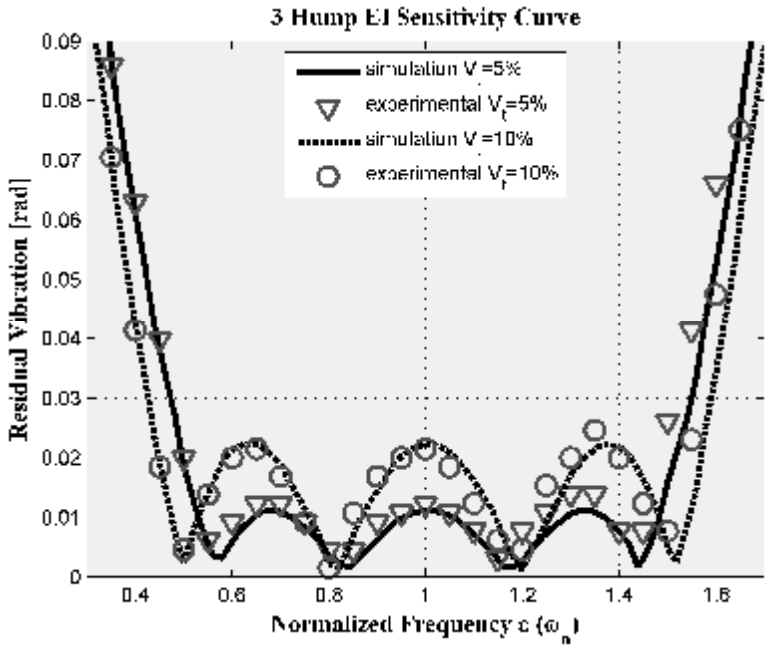

Figure 4.22. Theoretical and experimental sensitivity curves for the 5% and 10% Three Hump EI shaper

The sensitivity curves for three-hump EI shapers designed to limit vibration below 5% and 10% are shown in Figure 4.22. Note that the three-hump EI shaper suppresses vibration over the entire range shown. As with the derivative-method shapers (ZVD, ZVDD and ZVDDD), the price for increased robustness is a corresponding increase in shaper duration. Note, however, that the penalty is not uniform across all shapers. The Three-Hump EI shaper has the same duration as the ZVDDD shaper. However, the Three-Hump EI shapers have much more robustness, as can be seen in Figure 4.21 and 4.22.

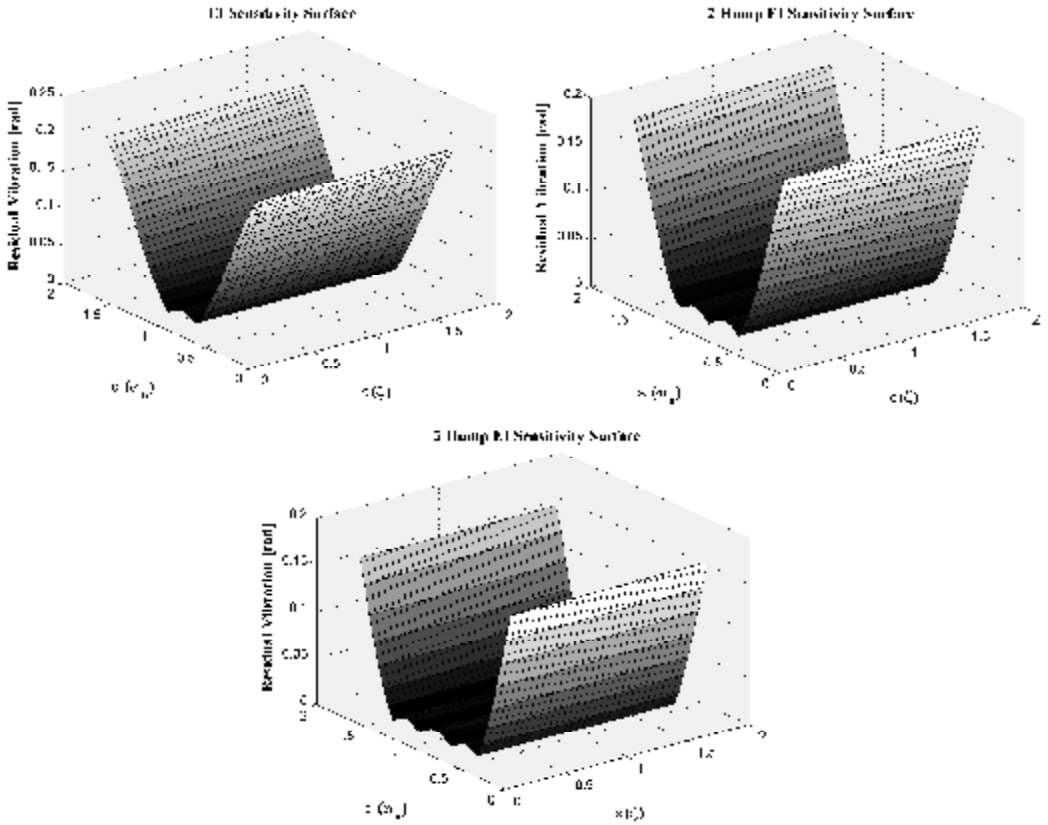

Figure 4.23. Robustness of the system to uncertainties in the mode frequencies and damping ratios for the EI, Two Hump EI and Three Hump EI input shapers

In Figure 4.23, the variation of the residual vibration is presented against estimation error in natural frequency and damping ratio of the system for the EI, 2H-EI and 3H-EI input shapers. It can clearly be seen that the variation of estimation error (or increasing uncertainty) of damping ratio has relatively reduced the effect on

the residual vibration of the system. Therefore, the uncertainties on the damping ratio do not play an important role in affecting the behavior of the system mainly due to its very low value, i.e. ζ =0.004.

4.1.1.8. Modified Input Shaper (MIS)

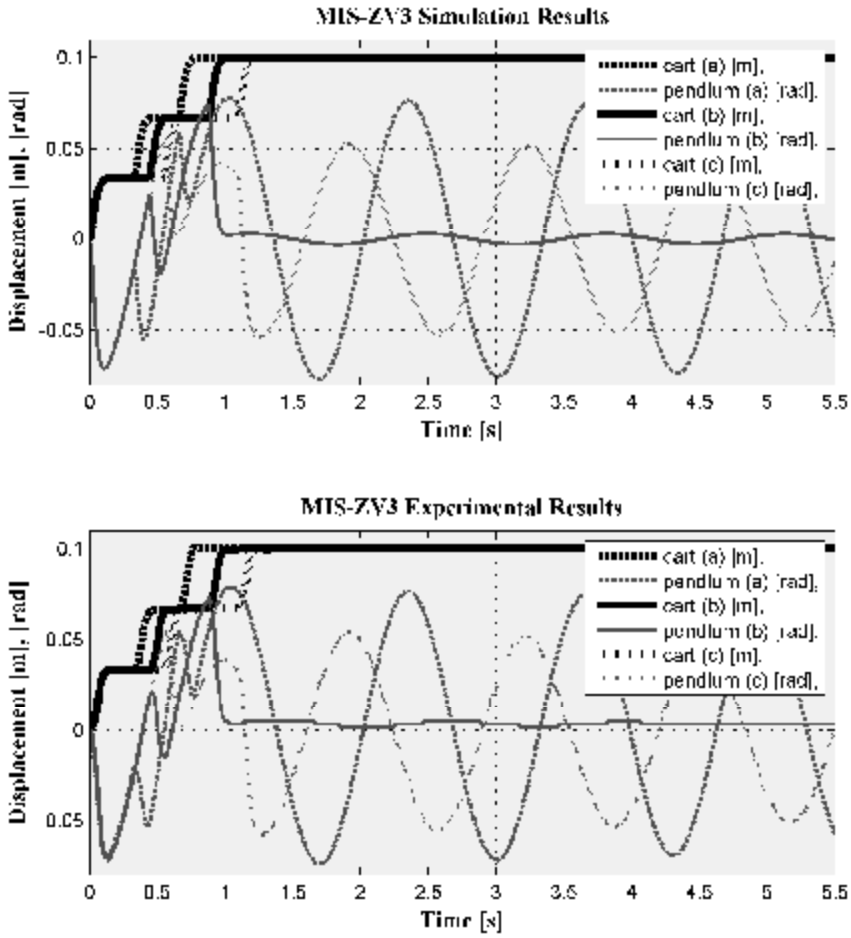

Figure 4.24. MIS-ZV-3 Impulse shaper with experimental and simulation results for (a) -%25, (b) %0, (c) +%25 estimation error of natural frequency

In Figures 4.24, the simulation and experimental results of MIS ZV 3 Impulse shaper are illustrated. In the figure, estimation error of ±%25 is introduced to natural frequency of the system used in calculation of the input signals. Figure 4.24 is plotted with estimation errors of (a) -%25, (b) %0, (c) +%25, respectively. In Figure 4.24, it can be seen that, the estimation error causes increasing residual vibrations of pendulum

ranging from 0.0536 to 0.0767 rad. It can be seen that increasing error in estimation of the natural frequency of the system causes increasing residual vibrations. These results are also validated in Figure 4.26 and 4.32 where pendulum position of different predicted natural frequencies and related sensitivity curves are presented, respectively.

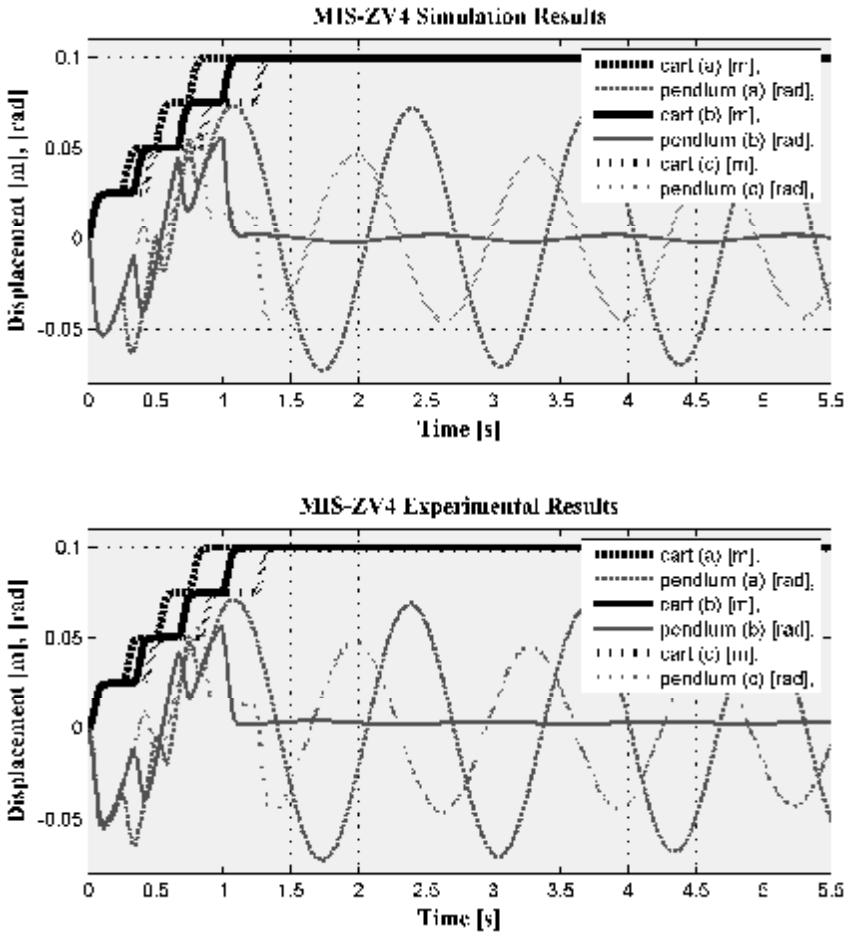

Figure 4.25. MIS-ZV-4 Impulse shaper with experimental and simulation results for (a) -%25, (b) %0, (c) +%25 estimation error of natural frequency

In Figures 4.25, the simulation and experimental results of MIS ZV 4 impulse shaper are illustrated. In the figure, estimation error of ±%25 is introduced to natural frequency of the system used in calculation of the input signals. Figure 4.25 is plotted with estimation errors of (a) -%25, (b) %0, (c) +%25, respectively. In Figure 4.25, it can be seen that, the estimation error causes increasing residual vibrations of pendulum ranging from 0.0447 to 0.069 rad. It can be seen that increasing error in estimation of

the natural frequency of the system causes increasing residual vibrations. These results are also validated in Figure 4.27 and 4.32 where pendulum position of different predicted natural frequencies and related sensitivity curves are presented, respectively.

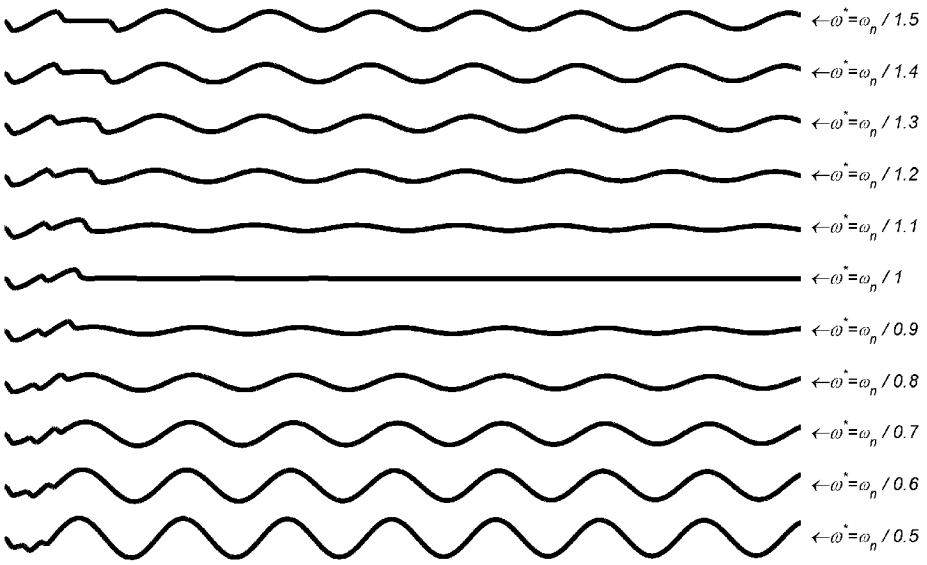

Figure 4.26. Pendulum positions of different predicted natural frequencies for MIS-ZV-3 Impulse shaper related experimental results

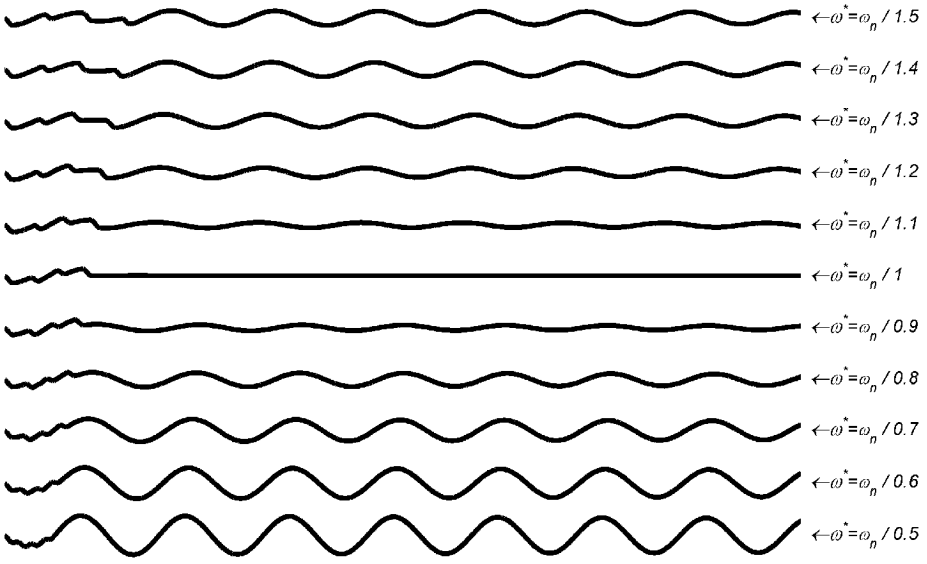

Figure 4.27. Pendulum positions of different predicted natural frequencies for MIS-ZV-4 Impulse shaper related experimental results

In Figures 4.28, the simulation and experimental results of MIS ZV 5 impulse shaper are illustrated. In the figure, estimation error of ±%25 is introduced to natural frequency of the system used in calculation of the input signals. Figure 4.33 is plotted with estimation errors of (a) -%25, (b) %0, (c) +%25, respectively. In Figure 4.33, it can be seen that, the estimation error causes increasing residual vibrations of pendulum ranging from 0.0429 to 0.069 rad. It can be seen that increasing error in estimation of the natural frequency of the system causes increasing residual vibrations. These results are also validated in Figure 4.30 and 4.32 where pendulum position of different predicted natural frequencies and related sensitivity curves are presented, respectively.

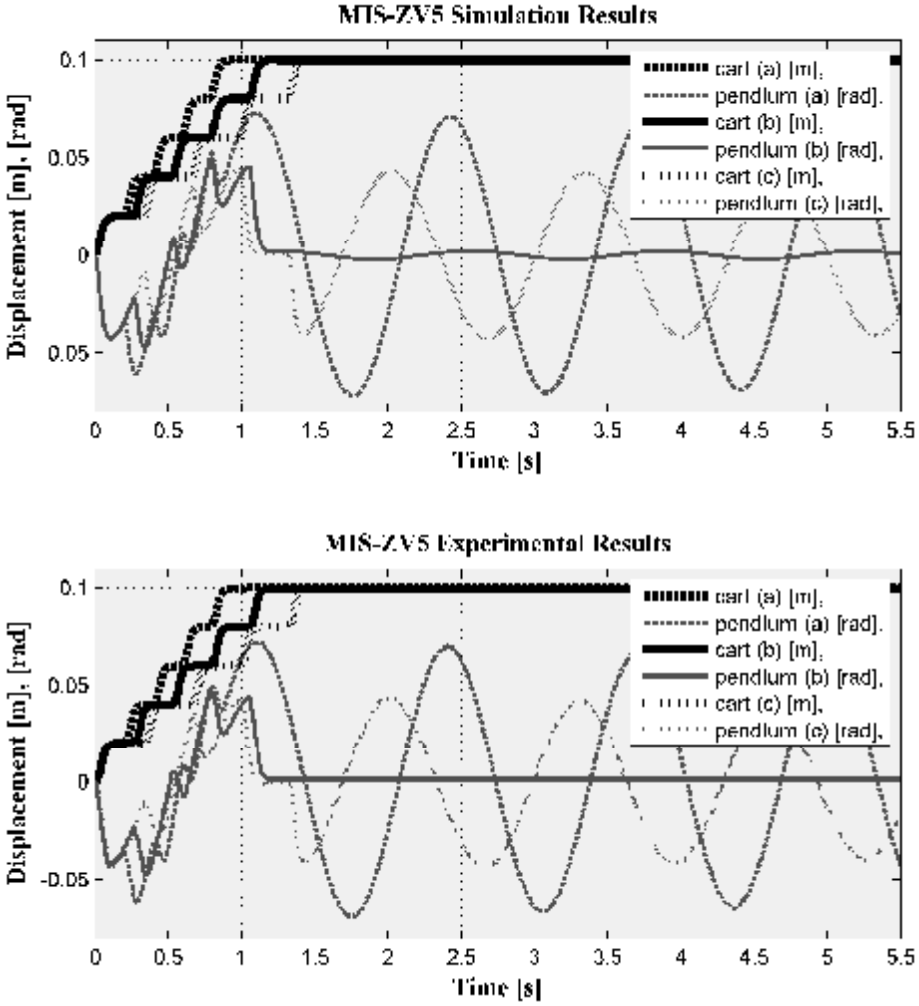

Figure 4.28. MIS-ZV-5 Impulse shaper with experimental and simulation results for (a) -%25, (b) %0, (c) +%25 estimation error of natural frequency

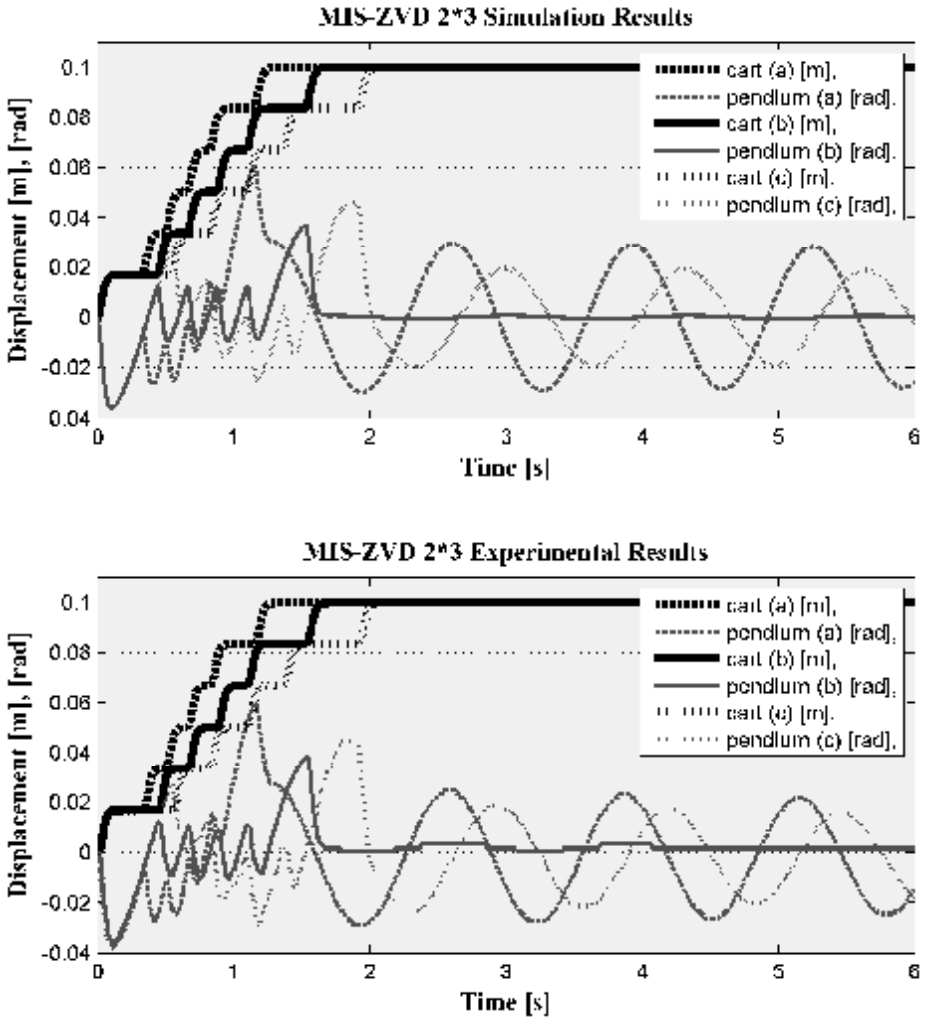

Figure 4.29. MIS-ZVD-6 Impulse shaper with experimental and simulation results for (a) -%25, (b) %0, (c) +%25 estimation error of natural frequency

In Figures 4.29, the simulation and experimental results of MIS ZVD 6 impulse shaper are illustrated. In the figure, estimation error of ±%25 is introduced to natural frequency of the system used in calculation of the input signals. Figure 4.29 is plotted with estimation errors of (a) -%25, (b) %0, (c) +%25, respectively. In Figure 4.29, it can be seen that, the estimation error causes increasing residual vibrations of pendulum ranging from 0.0184 to 0.0245 rad. It can be seen that increasing error in estimation of the natural frequency of the system causes increasing residual vibrations. Figure 4.29 shows that the MIS-ZVD shaper is much more insensitive to modelling errors than the MIS-ZV shaper. These results are also validated in Figure 4.31 and 4.32 where

pendulum positions of different predicted natural frequencies and related sensitivity curves are presented, respectively.

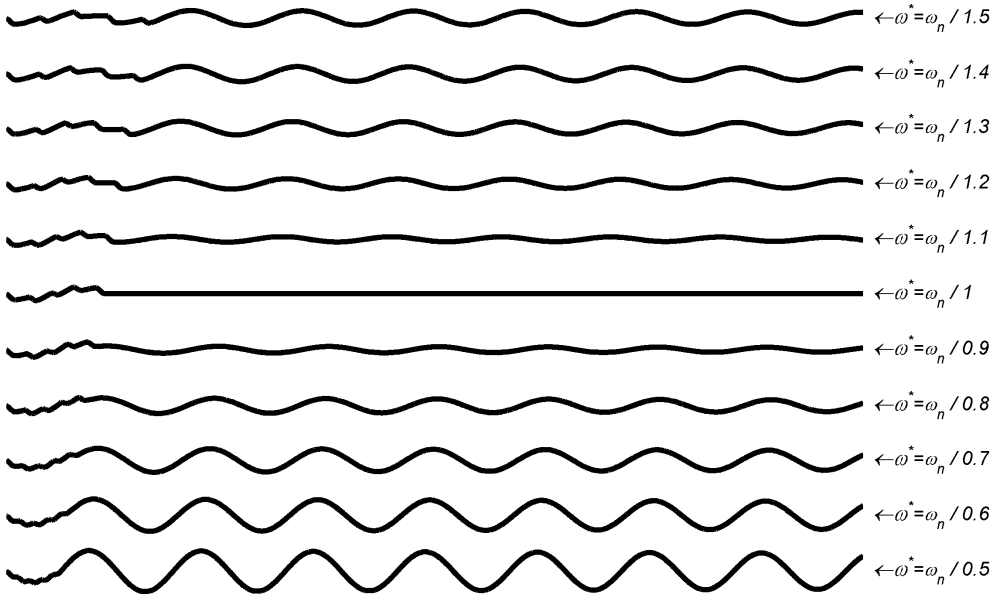

Figure 4.30. Pendulum positions of different predicted natural frequencies for MIS-ZV-5 Impulse shaper related experimental results

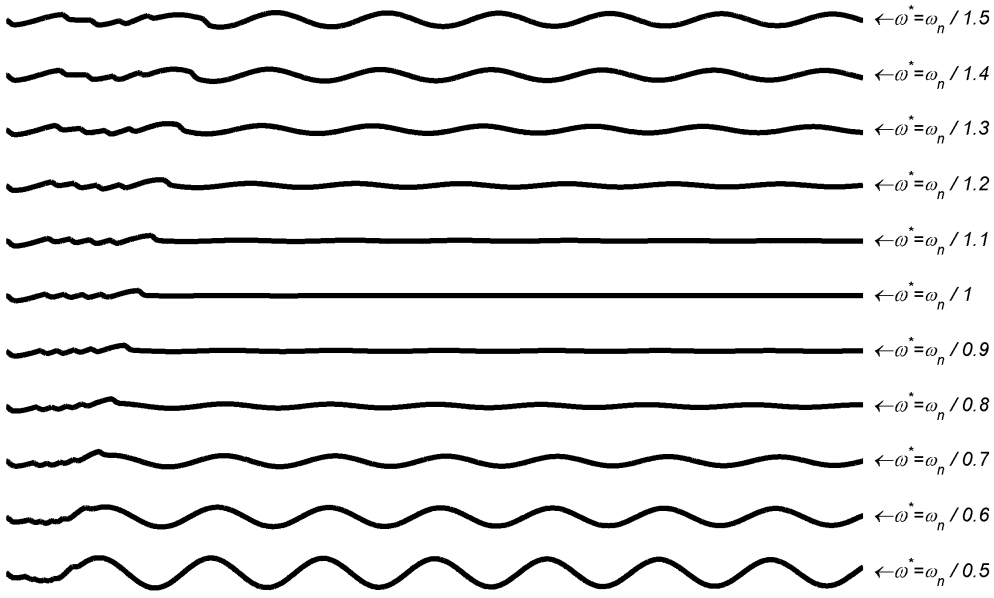

Figure 4.31. Pendulum positions of different predicted natural frequencies for MIS-ZVD-6 Impulse shaper related experimental results

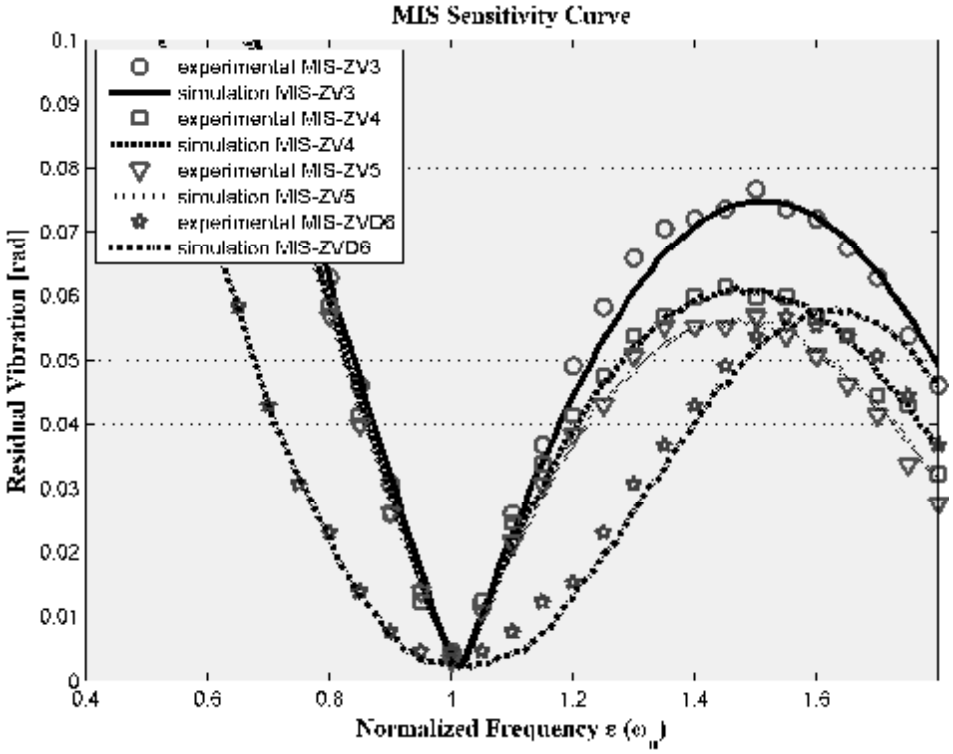

Figure 4.32. Theoretical and experimental sensitivity curves for the Modified Input Shapers

Theoretical and experimental sensitivity plots for three to five-impulse MIS-ZV shapers and six impulse MIS-ZVD shaper are shown in Fig. 4.32. For each shaper, the experimental results closely follow the theoretical results. Convolving MISZV shapers of higher number of impulses results in more robust MISZVD shapers, at the cost of increased shaper duration. One can see that the additional impulses only provide a minimal increase in shaper insensitivity for MIS-ZV shapers. The 6-Impulse MISZVD shaper, however, exhibits good robustness to modelling errors in natural frequency. It should be noted that a 4-impulse MISZVD shaper is the traditional ZVD shaper.

In Figure 4.33, the variation of the residual vibration is presented against estimation error in natural frequency and damping ratio of the system for various MIS techniques. It can clearly be seen that the variation of estimation error (or increasing uncertainty) of damping ratio has relatively reduced effect on the residual vibration of the system. Therefore, the uncertainties on the damping ratio do not play an important role in affecting the behavior of the system due to its very low value,

i.e. ζ =0.004. On the other hand, the estimation error in natural frequency of the system appears to affect the motion of the system and the resulting residual vibration levels.

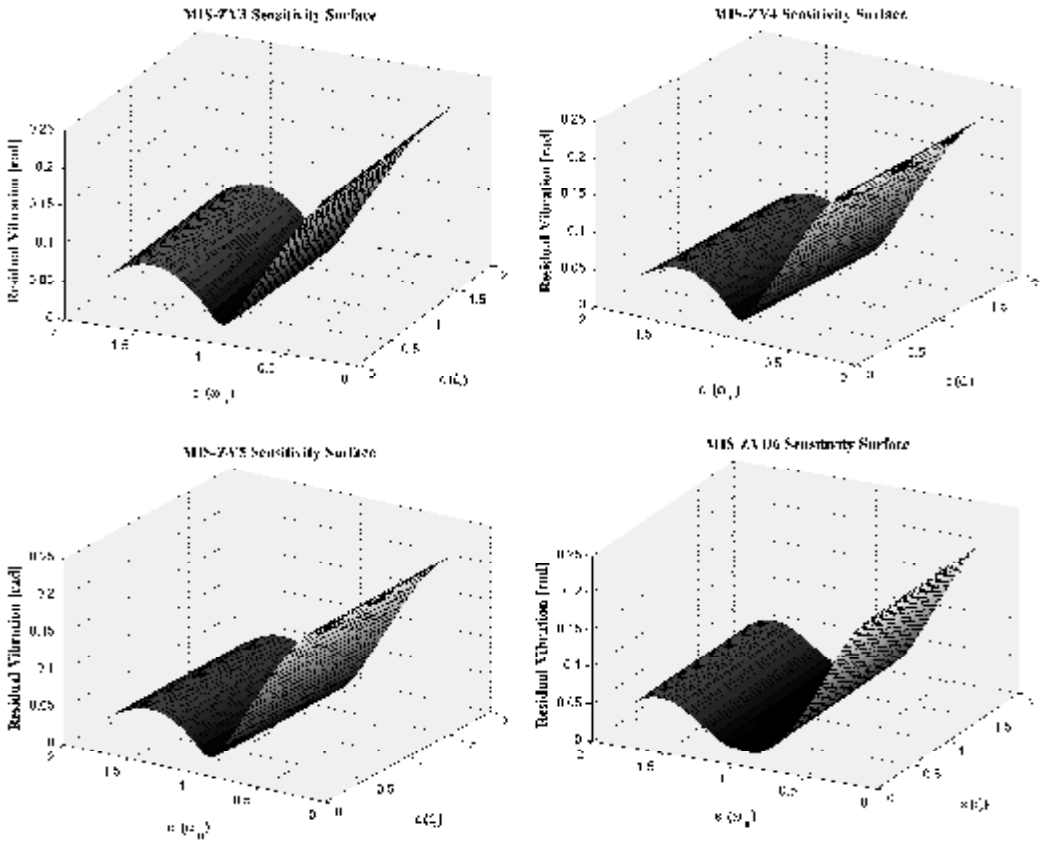

Figure 4.33. Robustness of the system to uncertainties in the mode frequencies and damping ratios for the Modified Input Shapers

4.1.1.9. Cycloid Plus Ramped Versine Plus Ramp (CPRVPR) Function

In Figures 4.34, the simulation and experimental results of CPRVPR reference function are illustrated. In the figure, estimation error of ±%25 is introduced to natural frequency of the system used in calculation of the input signals. Figure 4.34 is plotted with estimation errors of (a) -%25, (b) %0, (c) +%25, respectively. Figure 4.34 shows that the length of the CPRVPR reference function is the same as that of the ZV shaper, half damped cycle of vibration. In Figure 4.34, it can be seen that, the estimation error causes increasing residual vibrations of pendulum ranging from

0.0935 to 0.1058 rad. It can be seen that increasing error in estimation of the natural frequency of the system causes increasing residual vibrations. These results are also validated in Figure 4.35 and 4.36 where pendulum positions of different predicted natural frequencies and related sensitivity curves are presented, respectively.

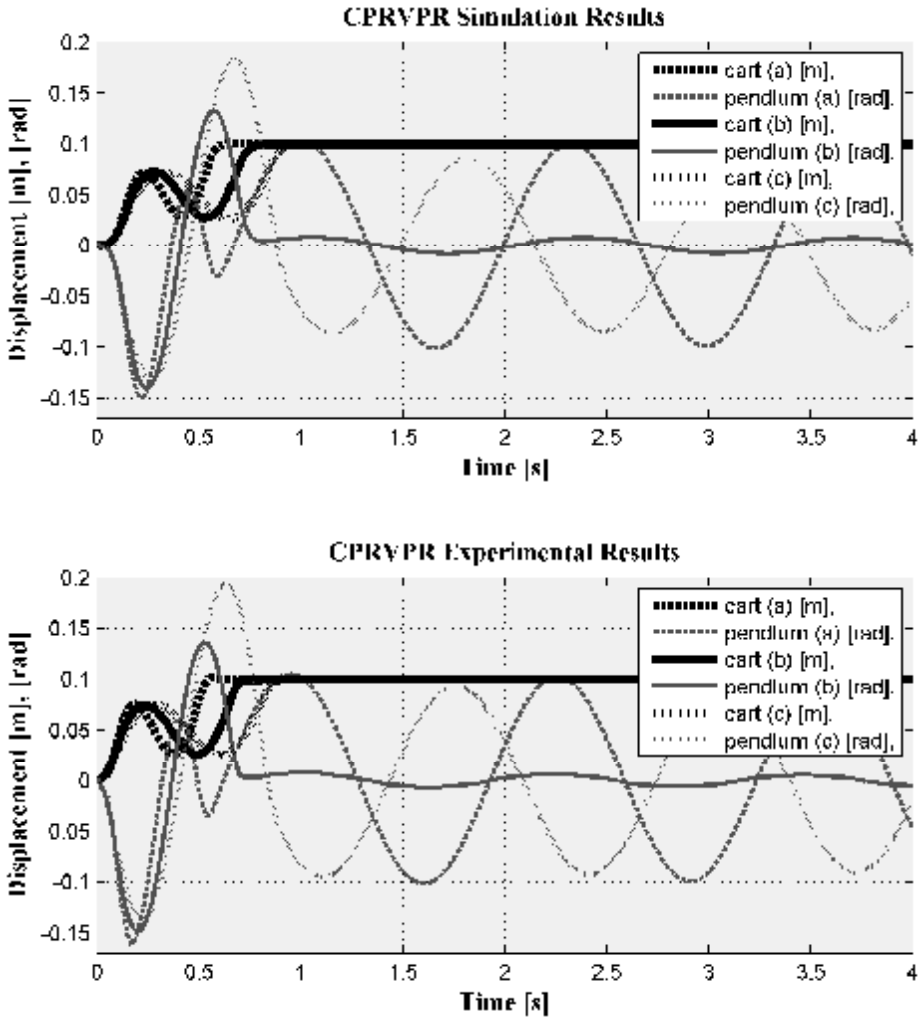

Figure 4.34. CPRVPR reference function with experimental and simulation results for (a) -%25, (b) %0, (c) +%25 estimation error of natural frequency

The theoretical and experimental sensitivity curves for the CPRVPR reference function are shown in Figure 4.36. The experimental results closely match those predicted by the theoretical study. Figure 4.36 shows that the vibration amplitude increases rapidly as the estimated frequency deviates from the actual system frequency. The length of the CPRVPR reference function is the same as that

of the ZV shaper, half damped cycle of vibration. However, the ZV shaper has slightly more robust to modelling errors.

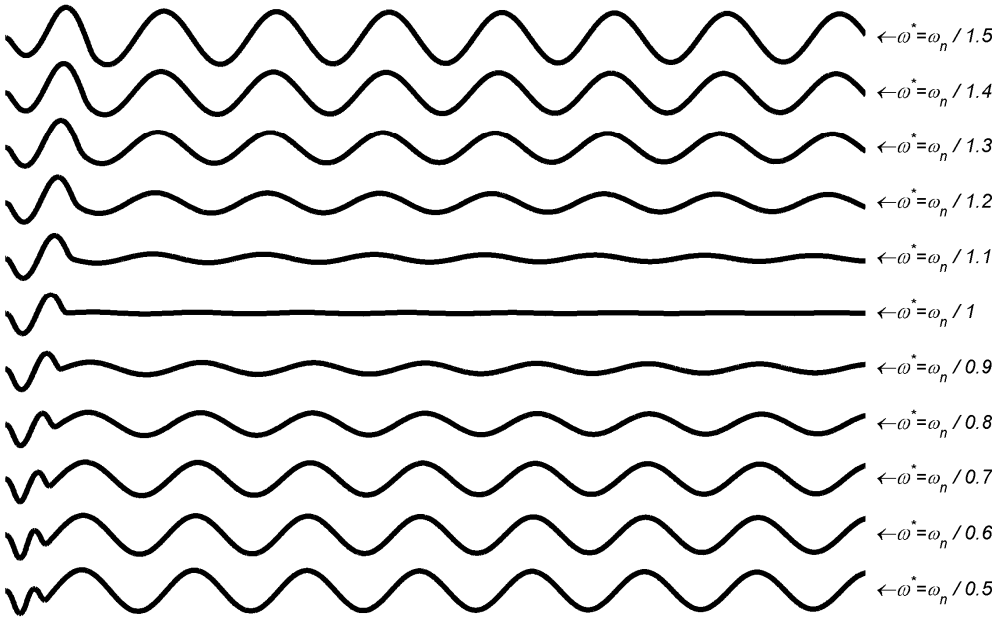

Figure 4.35. Pendulum positions of different predicted natural frequencies for the CPRVPR reference function related experimental results

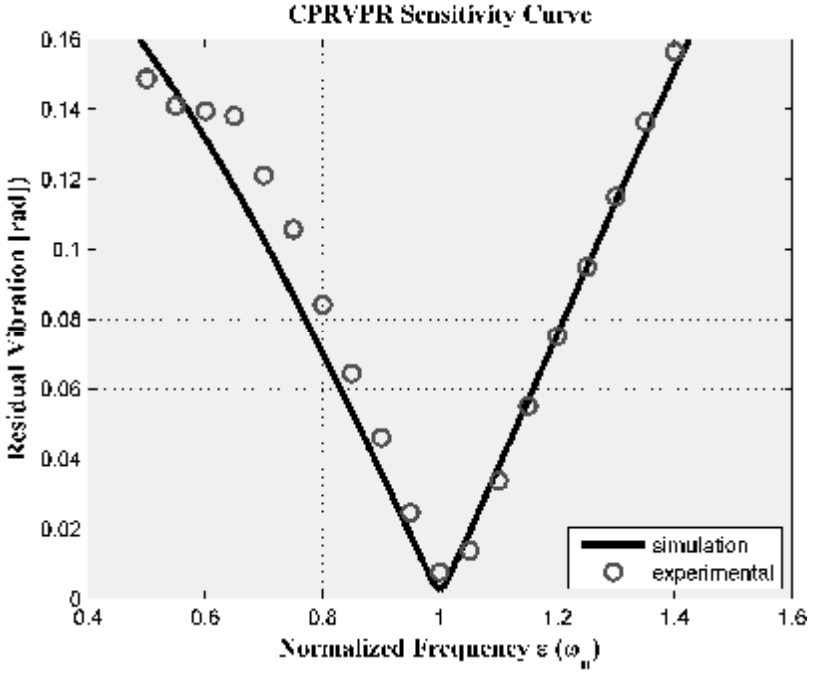

Figure 4.36. Theoretical and experimental sensitivity curves for the CPRVPR reference function

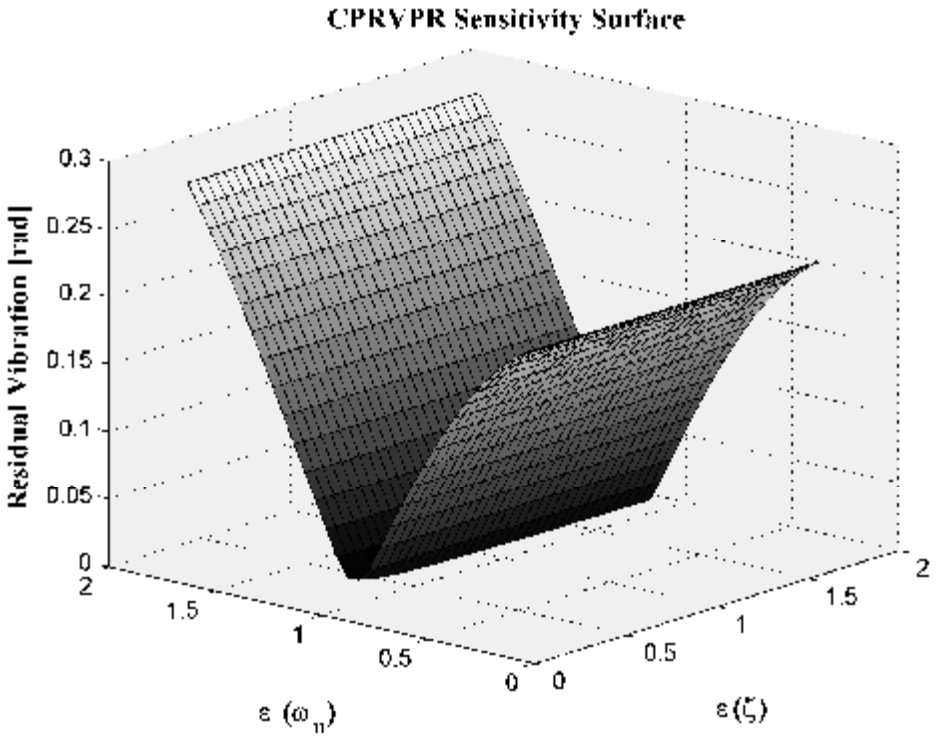

Figure 4.37. Robustness of the system to uncertainties in the mode frequencies and damping ratios for the CPRVPR reference function

In Figure 4.37, the variation of the residual vibration is presented against estimation error in natural frequency and damping ratio of the system. It can clearly be seen that the variation of estimation error (or increasing uncertainty) of damping ratio has relatively reduced the effect on the residual vibration of the system. Therefore, the uncertainties on the damping ratio do not play an important role in affecting the behavior of the system mainly due to its very low value, i.e. ζ =0.004. On the other hand, the estimation error in natural frequency of the system appears to affect the motion of the system and the resulting residual vibration levels.

4.1.1.10. Hybrid Input Shaper (HIS)

In Figures 4.38, the simulation and experimental results of Hybrid Input Shaper (HIS) are illustrated. In the figure, estimation error of ±%25 is introduced to natural frequency of the system used in calculation of the input signals. Figure 4.38 is plotted with estimation errors of (a) -%25, (b) %0, (c) +%25, respectively. The length

of the Hybrid input shaper is the same as that of the ZVD shaper, one damped cycle of vibration. In Figure 4.38, it can be seen that, the estimation error causes increasing residual vibrations of pendulum ranging from 0.0352 to 0. 0398 rad. It can be seen that increasing error in estimation of the natural frequency of the system causes increasing residual vibrations. These results are also validated in Figure 4.39 and 4.40 where pendulum positions of different predicted natural frequencies and related sensitivity curves are presented, respectively.

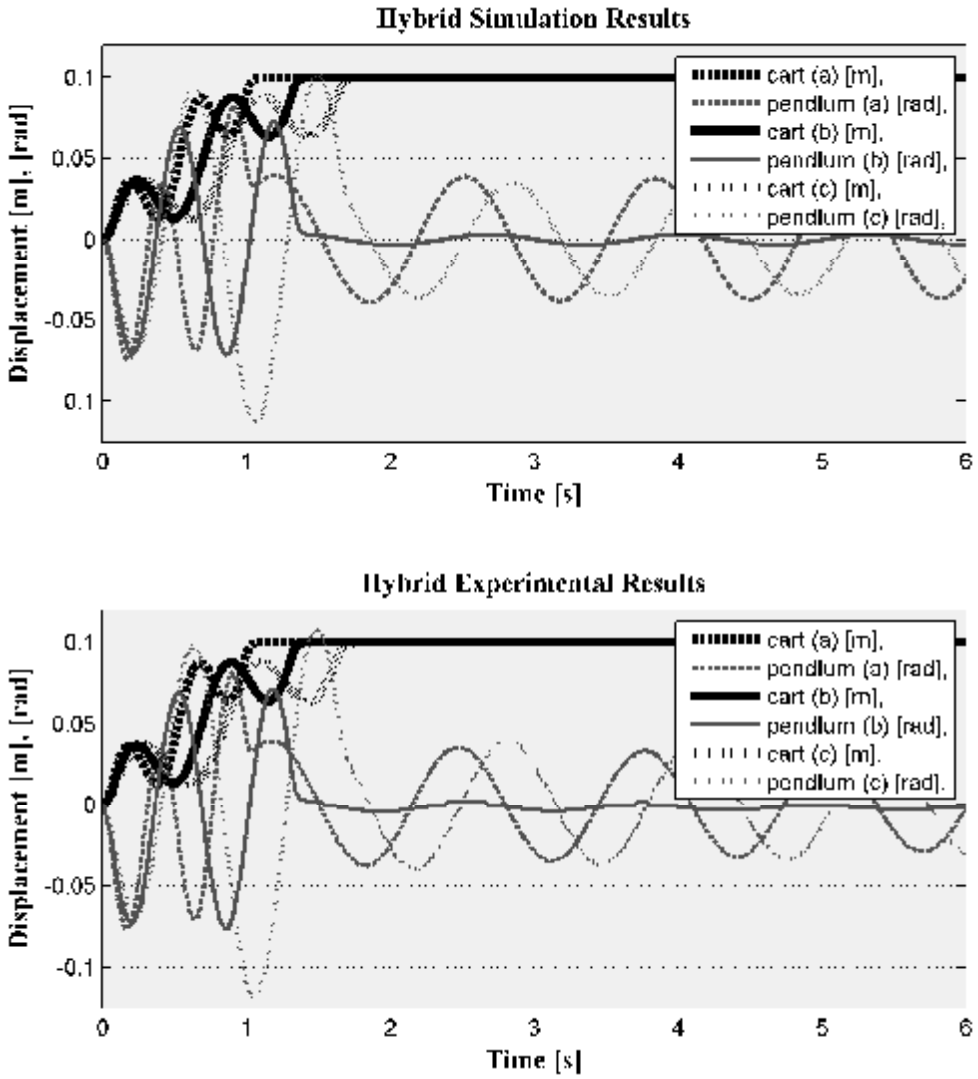

Figure 4.38. Hybrid Input Shaper with experimental and simulation results for (a) -%25, (b) %0, (c) +%25 estimation error of natural frequency

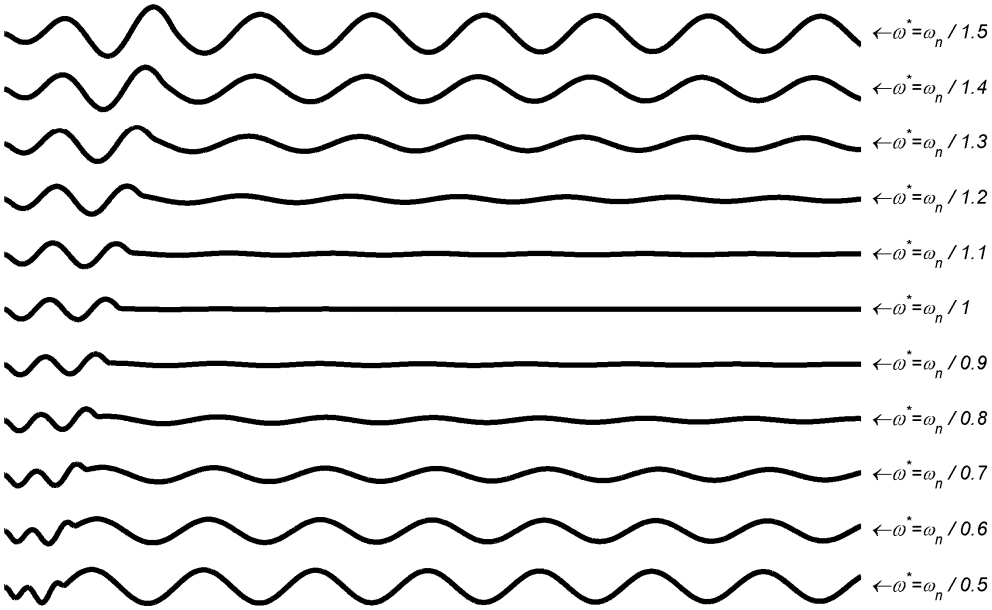

Figure 4.39. Pendulum positions of different predicted natural frequencies for Hybrid Input Shaper related experimental results

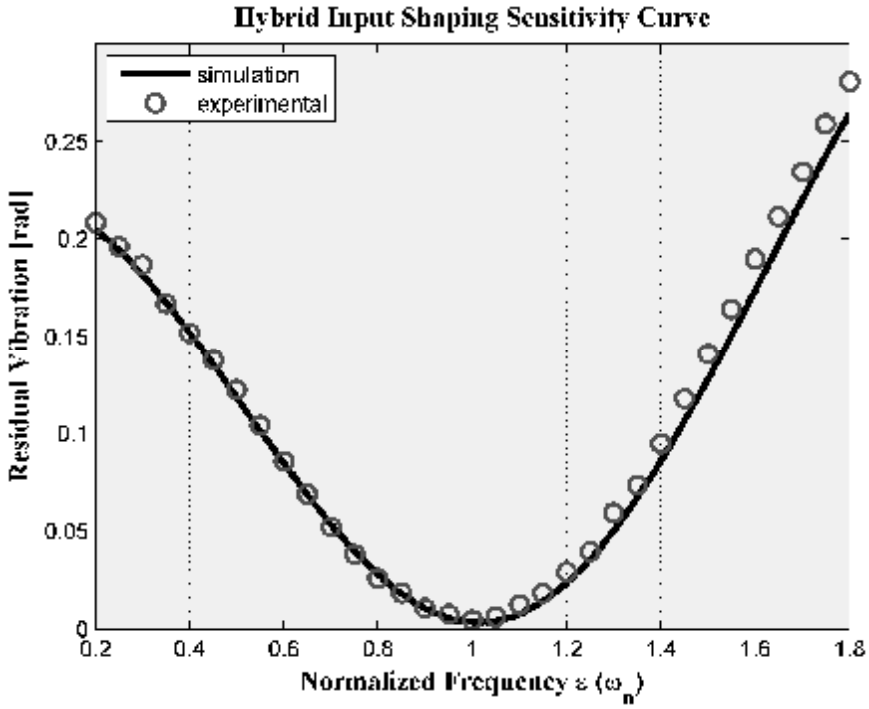

Figure 4.40. Theoretical and experimental sensitivity curves for the Hybrid Input Shaper

The theoretical and experimental sensitivity curves for the Hybrid Input Shaper (HIS) are shown in Figure 4.40. The experimental results closely match those

predicted by the theoretical study. Figure 4.39 and 4.40 shows that the Hybrid Input Shaper is much more insensitive to modelling errors than the ZV shaper. However, the Hybrid Input Shaper has a time duration equal to one period of the vibration frequency, as opposed to the one-half period length of the ZV shaper. The length of the Hybrid input shaper is the same as that of the ZVD shaper, one damped cycle of vibration, but ZVD shaper is slightly more robust to modelling errors.

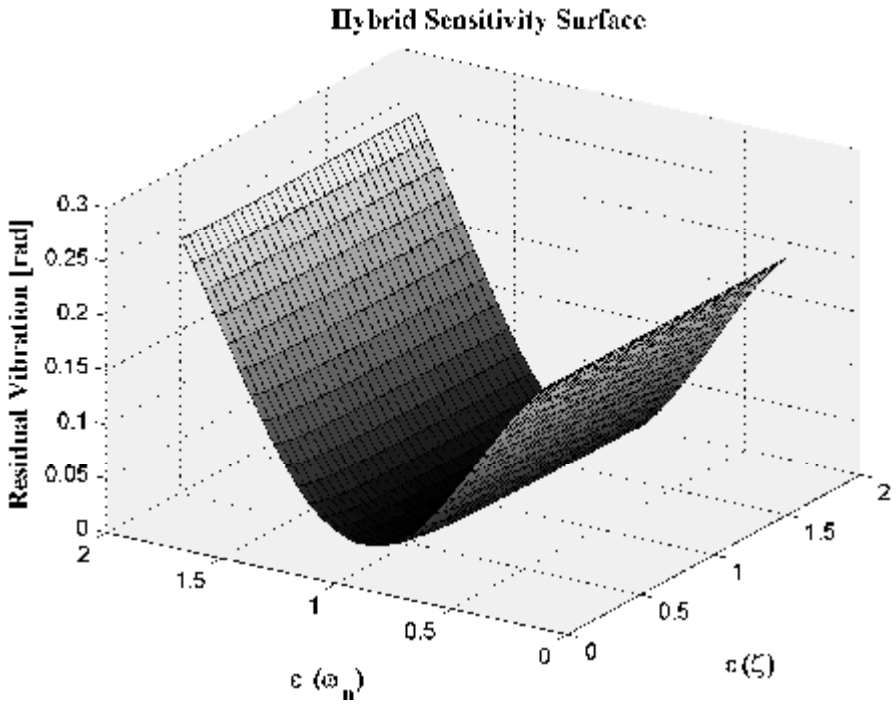

Figure 4.41. Robustness of the system to uncertainties in the mode frequencies and damping ratios for the Hybrid Input Shaper

In Figure 4.41., the variation of the residual vibration is presented against estimation error in natural frequency and damping ratio of the system. It can clearly be seen that the variation of estimation error (or increasing uncertainty) of damping ratio has relatively reduced the effect on the residual vibration of the system. Therefore, the uncertainties on the damping ratio do not play an important role in affecting the behavior of the system mainly due to its very low value, i.e. ζ =0.004. On the other hand, the estimation error in natural frequency of the system appears to affect the motion of the system and the resulting residual vibration levels.

4.1.1.11. Proposed New Input Shaping Technique: Modified Cycloid Plus Ramped Versine Plus Ramp (M-CPRVPR) Reference Function

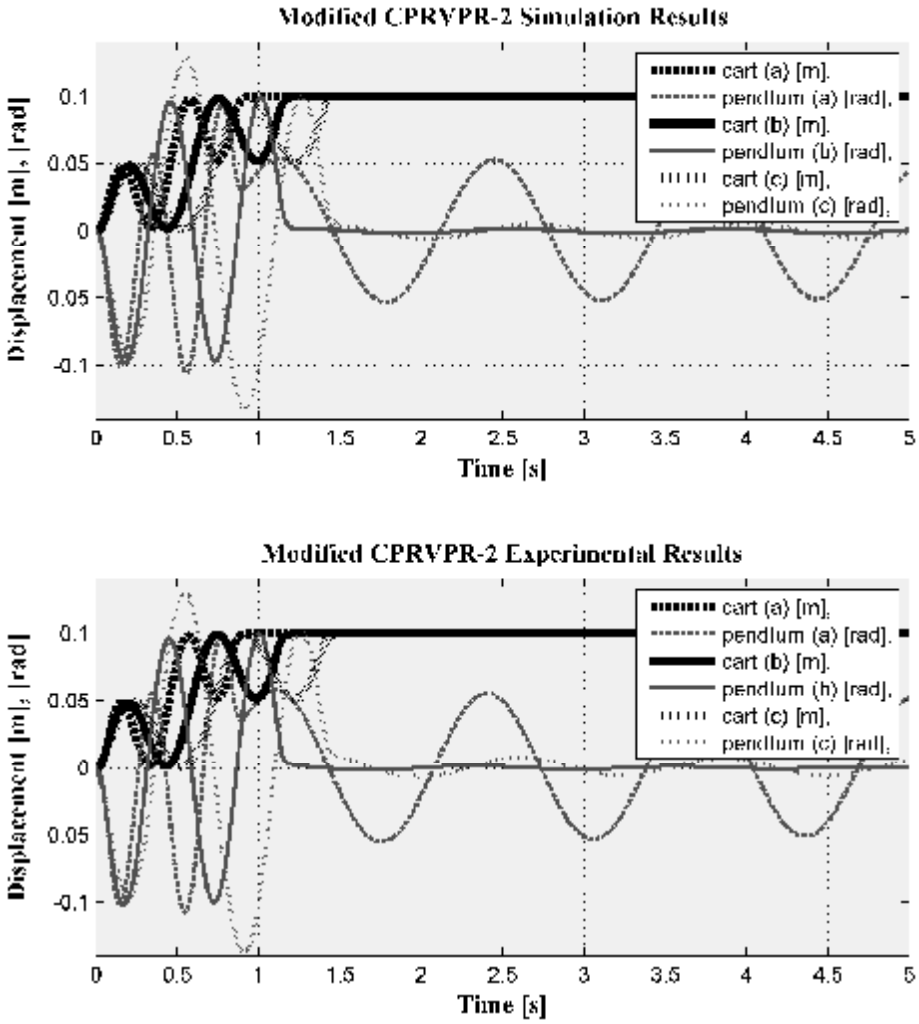

Figure 4.42. Modified CPRVPR2 function for a total travelling distance $L = 0.1$ and travelling time of $t = 0.85T_d$ with experimental and simulation results for (a) -%25, (b) %0, (c) +%25 estimation error of natural frequency

In Figures 4.42 and 4.43, the simulation and experimental results of modified two recursions for cycloid plus ramped versine plus ramp (CPRVPR) reference function are illustrated for different travelling time. In the figures, estimation error of ±%25 is introduced to natural frequency of the system used in calculation of the input signals. Figure 4.42 and 4.43 are plotted with estimation errors of (a) -%25, (b) %0, (c) +%25, respectively. Theoretically, there is no travelling time restriction on the system

and this is the main advantages of this reference command. In Figures 4.42 the travelling time of the M-CPRVPR reference function 0.85 damped cycle of vibration. In Figures 4.43 the travelling time of the M-CPRVPR reference function is the same as that of the ZVD, EI and Hybrid shaper, one damped cycle of vibration.

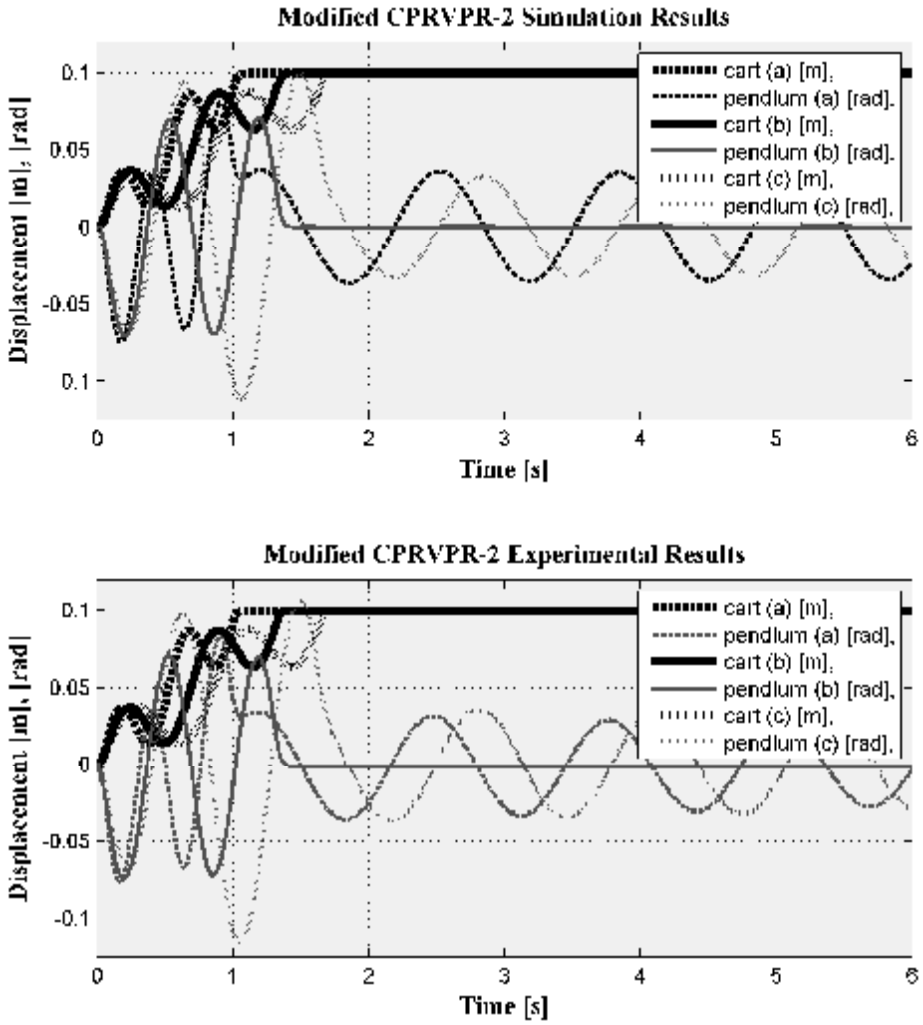

Figure 4.43. Modified CPRVPR2 function for a total travelling distance $L = 0.1$ and travelling time of $t = T_d$ with experimental and simulation results for (a) -%25, (b) %0, (c) +%25 estimation error of natural frequency

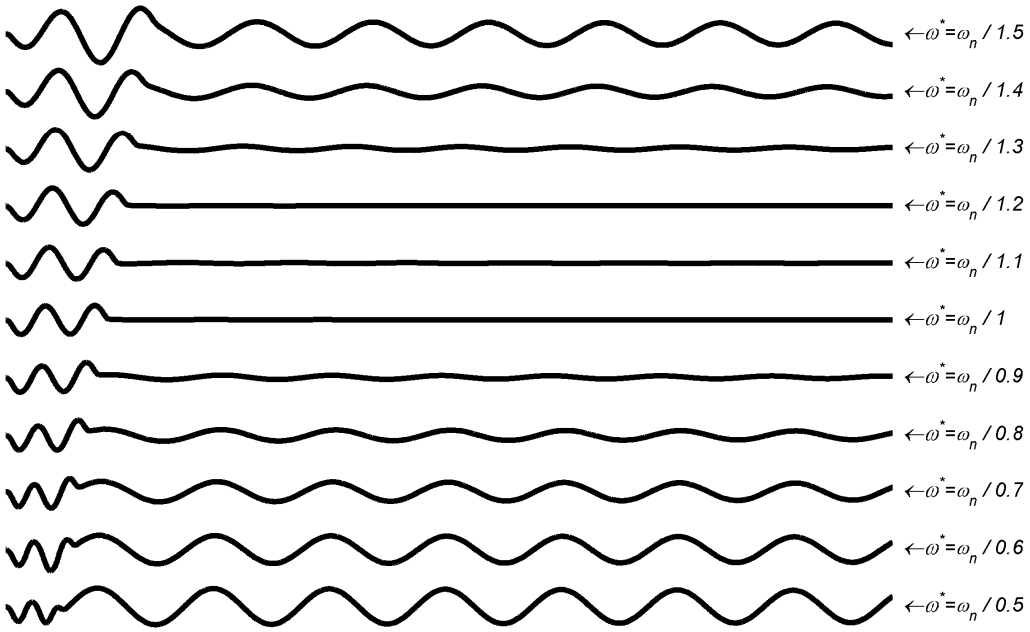

Figure 4.44. Pendulum positions of different predicted natural frequencies for recursion of M-CPRVPR2 for a total travelling distance $L = 0.1$ and travelling time of $t = 0.85T_d$ related experimental results

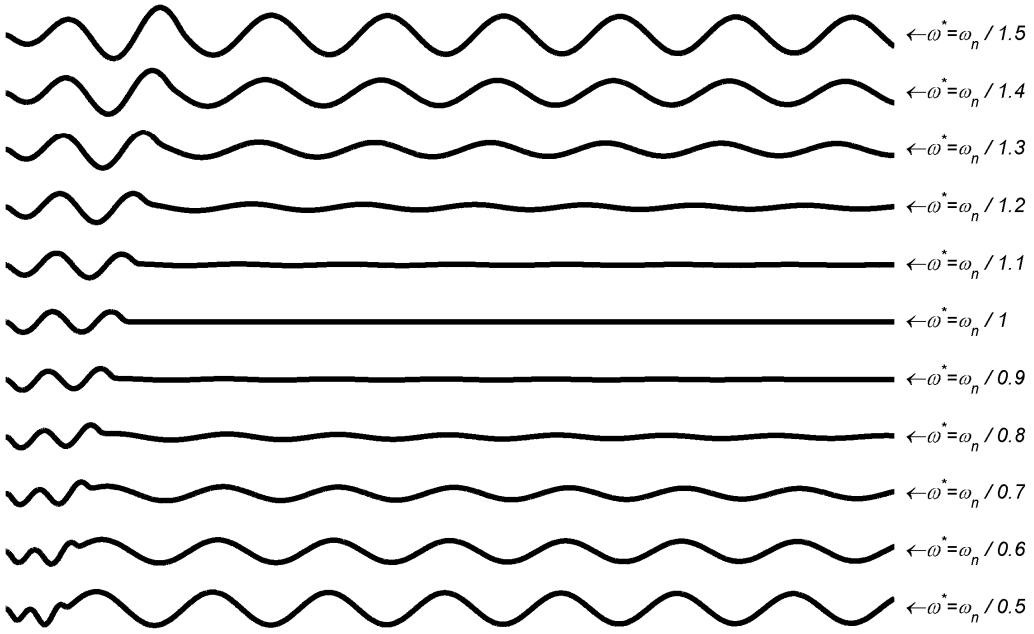

Figure 4.45. Pendulum positions of different predicted natural frequencies for recursion of M-CPRVPR2 for a total travelling distance $L = 0.1$ and travelling time of $t = T_d$ related experimental results

In Figure 4.42, it can be seen that, the estimation error causes increasing residual vibrations of pendulum ranging from 0.0076 to 0. 0552 rad. It can be seen that increasing error in estimation of the natural frequency of the system causes increasing residual vibrations. These results are also validated in Figure 4.44 and 4.46 where pendulum positions of different predicted natural frequencies and related sensitivity curves are presented, respectively.

In Figure 4.43, it can be seen that, the estimation error causes increasing residual vibrations of pendulum ranging from 0.0306 to 0. 0352 rad. It can be seen that increasing error in estimation of the natural frequency of the system causes increasing residual vibrations. These results are also validated in Figure 4.45 and 4.46 where pendulum positions of different predicted natural frequencies and related sensitivity curves are presented, respectively.

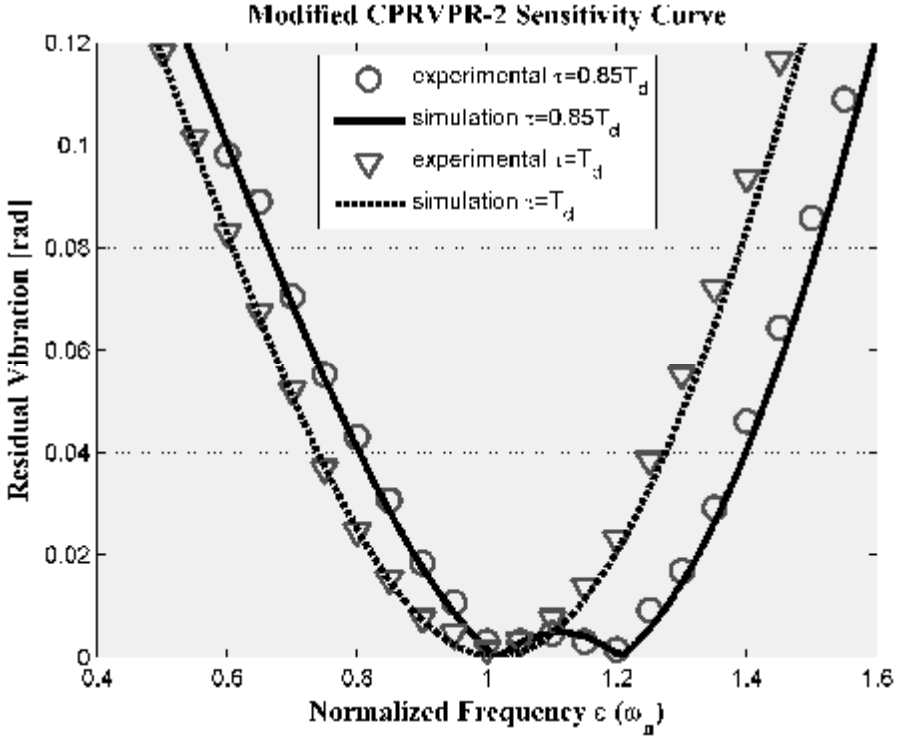

Figure 4.46. Theoretical and experimental sensitivity curves for the Modified CPRVPR2 reference function for different travelling times

The theoretical and experimental sensitivity curves of the Modified CPRVPR2 reference function for different travelling time are shown in Figure 4.46.

The experimental results closely match those predicted by the theoretical study. The Modified CPRVPR2 reference function has a time duration equal to 0.85 period of the vibration frequency, as opposed to the one period length of the ZVD shaper. Theoretically, there is no travelling time restriction on the system and this is the main advantages of this reference command. Figure 4.44 and 4.46 shows that the Modified CPRVPR2 reference function is much more insensitive to modelling errors than the ZVD shaper.

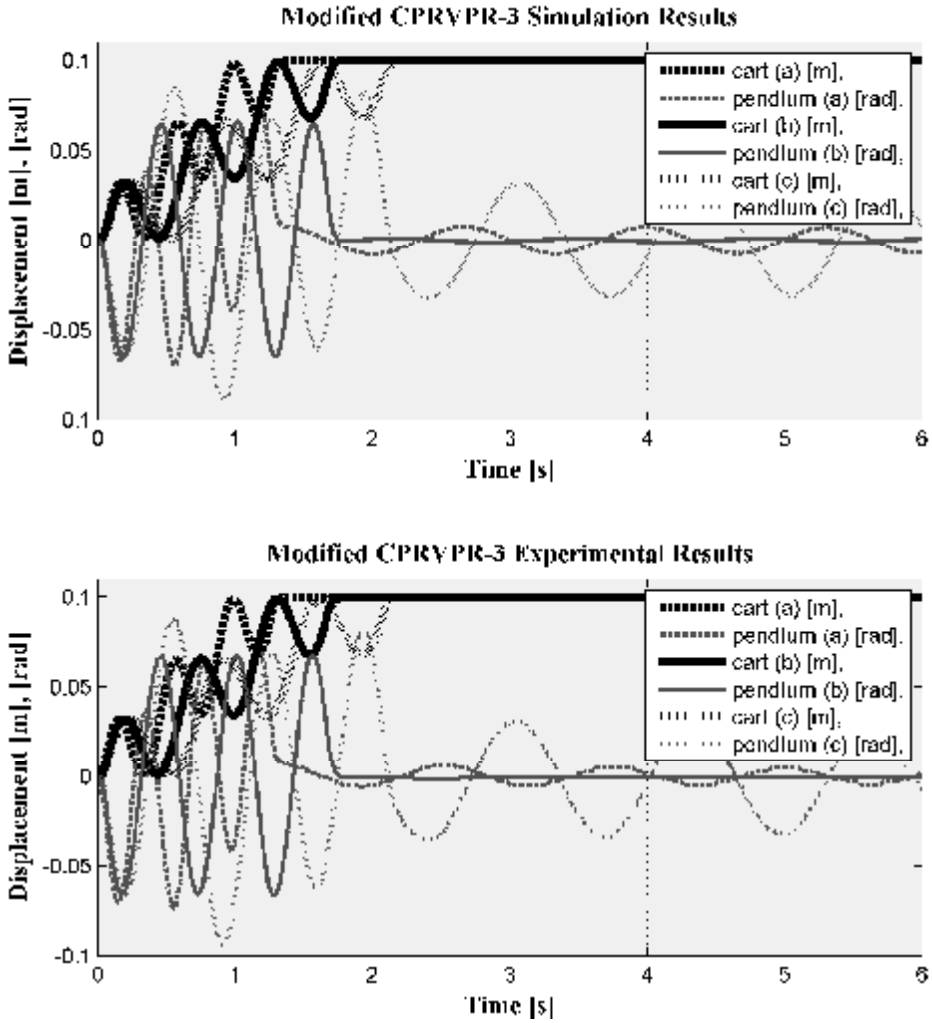

Figure 4.47. Modified CPRVPR3 function for a total travelling distance $L = 0.1$ and travelling time of $t = 1.275T_d$ with experimental and simulation results for (a) -%25, (b) %0, (c) +%25 estimation error of natural frequency

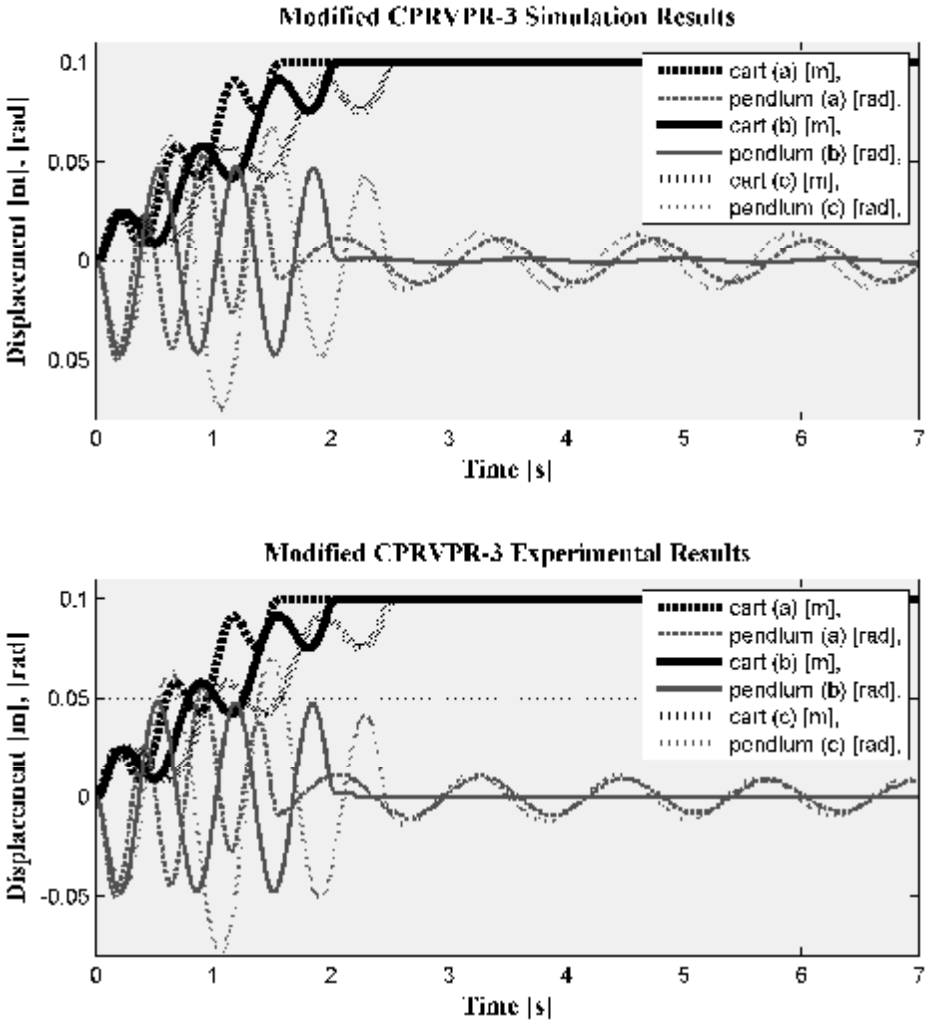

Figure 4.48. Modified CPRVPR3 function for a total travelling distance $L = 0.1$ and travelling time of $t = 1.5T_d$ with experimental and simulation results for (a) -%25, (b) %0, (c) +%25 estimation error of natural frequency

In Figures 4.47 and 4.48, the simulation and experimental results of modified three recursions for cycloid plus ramped versine plus ramp (M-CPRVPR3) reference function are illustrated for different travelling time. In the figures, estimation error of ±%25 is introduced to natural frequency of the system used in calculation of the input signals. Figure 4.47 and 4.48 are plotted with estimation errors of (a) -%25, (b) %0, (c) +%25, respectively. Theoretically, there is no travelling time restriction on the system and this is the main advantages of this reference command. In Figures 4.47 the travelling time of the M-CPRVPR3 reference function 1.275 damped cycle of vibration.

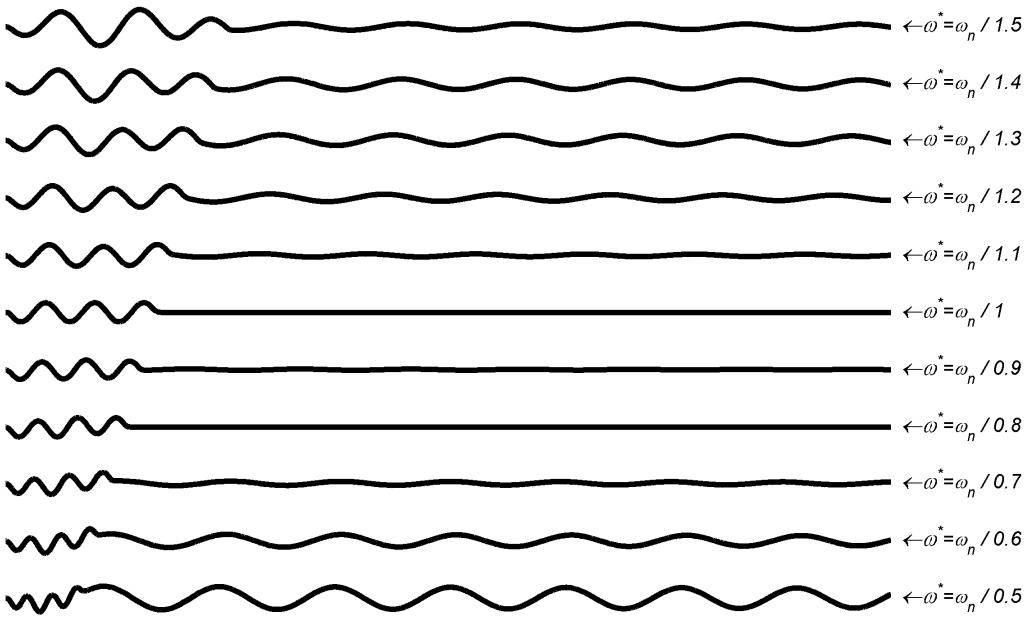

Figure 4.49. Pendulum positions of different predicted natural frequencies for recursion of M-CPRVPR3 for a total travelling distance $L = 0.1$ and travelling time of $t = 1.275T_d$ related experimental results

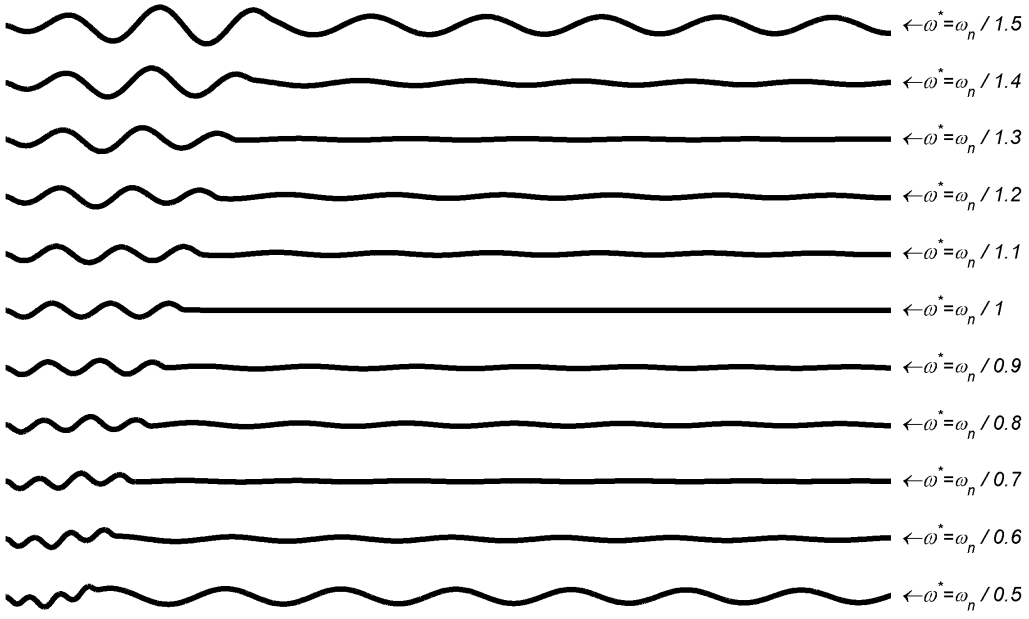

Figure 4.50. Pendulum positions of different predicted natural frequencies for recursion of M-CPRVPR3 for a total travelling distance $L = 0.1$ and travelling time of $t = 1.5T_d$ related experimental results

In Figures 4.48 the travelling time of the M-CPRVPR3 reference function is the same as that of the ZVDD and 2 Hump EI Shaper, one and a half damped cycle of vibration. In Figure 4.47, it can be seen that, the estimation error causes increasing residual vibrations of pendulum ranging from 0.0061 to 0. 0306 rad. It can be seen that increasing error in estimation of the natural frequency of the system causes increasing residual vibrations. These results are also validated in Figure 4.49 and 4.51 where pendulum positions of different predicted natural frequencies and related sensitivity curves are presented, respectively. In Figure 4.48, it can be seen that, the estimation error causes increasing residual vibrations of pendulum ranging from 0.0107 to 0. 0092 rad. It can be seen that increasing error in estimation of the natural frequency of the system causes slightly increasing residual vibrations. These results are also validated in Figure 4.50 and 4.51 where pendulum positions of different predicted natural frequencies and related sensitivity curves are presented, respectively.

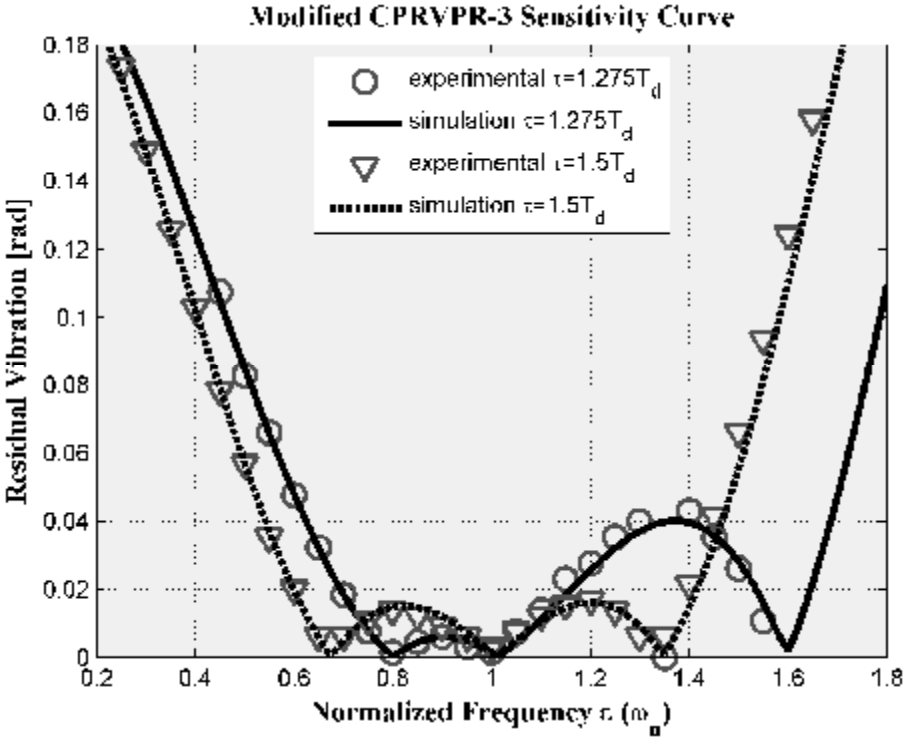

Figure 4.51. Theoretical and experimental sensitivity curves for the Modified CPRVPR3 reference function for different travelling times

The theoretical and experimental sensitivity curves of the Modified CPRVPR3 reference function for different travelling time are shown in Figure 4.56. The experimental results closely match those predicted by the theoretical study. The Modified CPRVPR3 reference function has a time duration equal to 1.275 period of the vibration frequency, as opposed to the one and a half period length of the ZVDD shaper. Theoretically, there is no travelling time restriction on the system and this is the main advantages of this reference command.

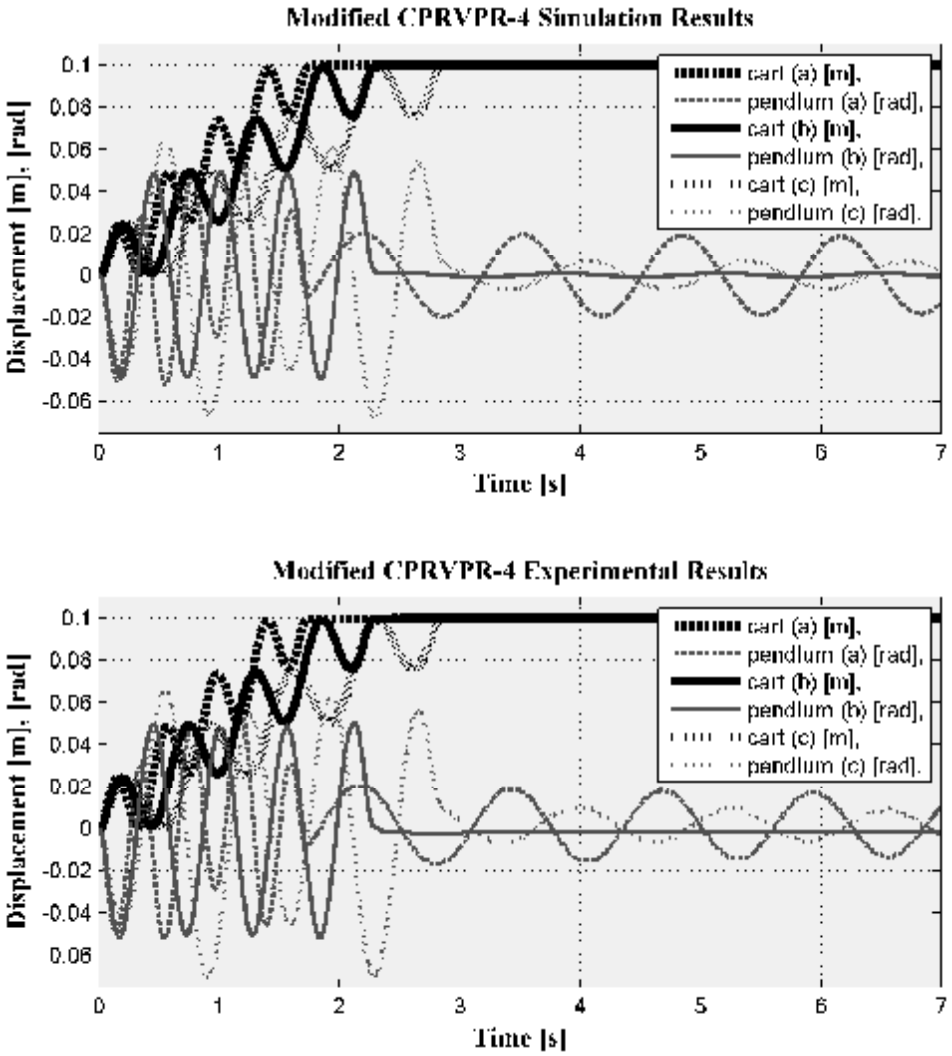

Figure 4.52. Modified CPRVPR4 function for a total travelling distance $L = 0.1$ and travelling time of $t = 1.7T_d$ with experimental and simulation results for (a) -%25, (b) %0, (c) +%25 estimation error of natural frequency

In Figures 4.52 and 4.53, the simulation and experimental results of modified four recursions for cycloid plus ramped versine plus ramp (M-CPRVPR4) reference function are illustrated for different travelling time. In the figures, estimation error of ±%25 is introduced to natural frequency of the system used in calculation of the input signals. Figure 4.52 and 4.53 are plotted with estimation errors of (a) -%25, (b) %0, (c) +%25, respectively. Theoretically, there is no travelling time restriction on the system and this is the main advantages of this reference command. In Figures 4.52 the travelling time of the M-CPRVPR4 reference function 1.7 damped cycle of vibration.

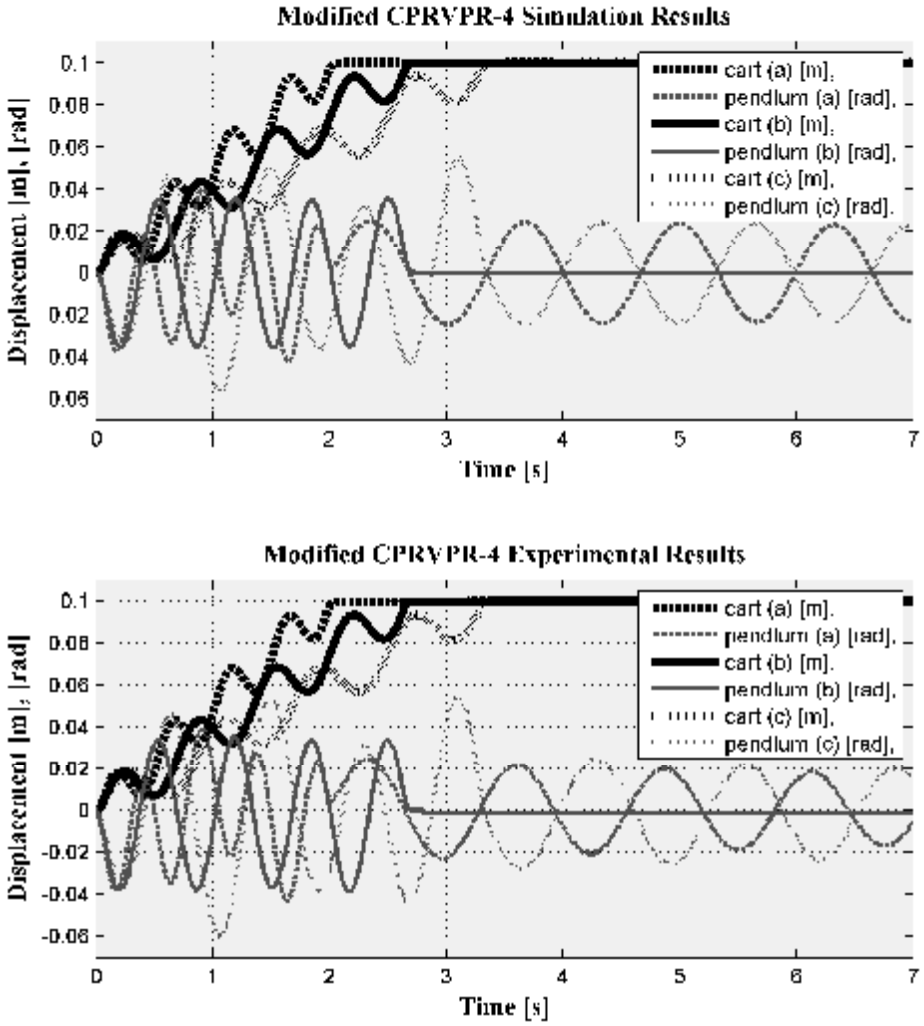

Figure 4.53. Modified CPRVPR4 function for a total travelling distance $L = 0.1$ and travelling time of $t = 2T_d$ with experimental and simulation results for (a) -%25, (b) %0, (c) +%25 estimation error of natural frequency

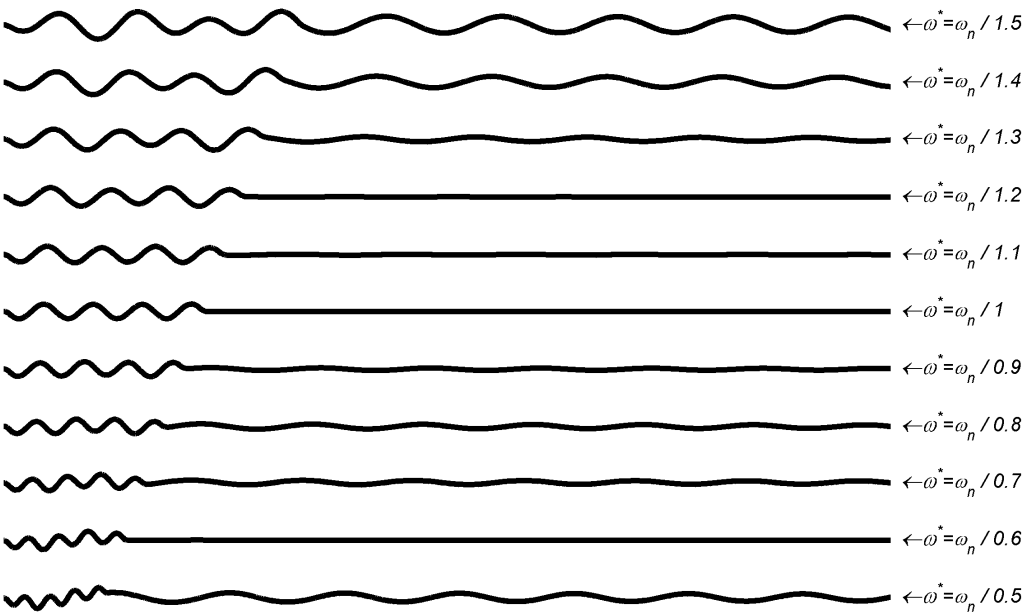

Figure 4.54. Pendulum positions of different predicted natural frequencies for recursion of M-CPRVPR4 for a total travelling distance $L = 0.1$ and travelling time of $t = 1.7T_d$ related experimental results

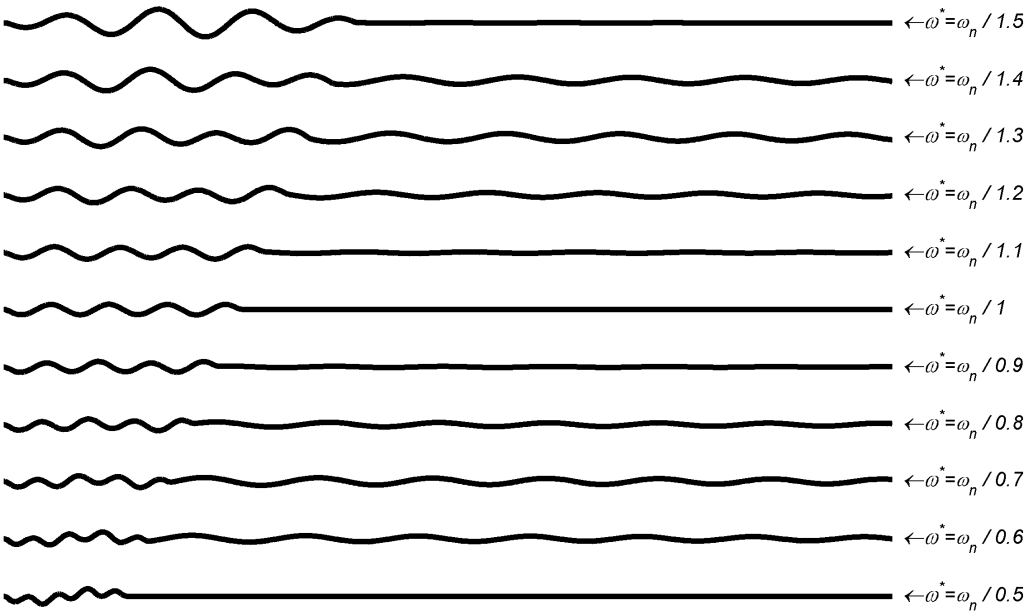

Figure 4.55. Pendulum positions of different predicted natural frequencies for recursion of M-CPRVPR4 for a total travelling distance $L = 0.1$ and travelling time of $t = 2T_d$ related experimental results

In Figures 4.53 the travelling time of the M-CPRVPR4 reference function is the same as that of the ZVDDD and 3 Hump EI Shaper, two damped cycle of vibration.

In Figure 4.52, it can be seen that, the estimation error causes increasing residual vibrations of pendulum ranging from 0.0092 to 0. 0184 rad. It can be seen that increasing error in estimation of the natural frequency of the system causes slightly increasing residual vibrations. These results are also validated in Figure 4.54 and 4.56 where pendulum positions of different predicted natural frequencies and related sensitivity curves are presented, respectively. In Figure 4.53, it can be seen that, the estimation error causes increasing residual vibrations of pendulum ranging from 0.0214 to 0. 0245 rad. It can be seen that increasing error in estimation of the natural frequency of the system causes slightly increasing residual vibrations. These results are also validated in Figure 4.55 and 4.56 where pendulum positions of different predicted natural frequencies and related sensitivity curves are presented, respectively.

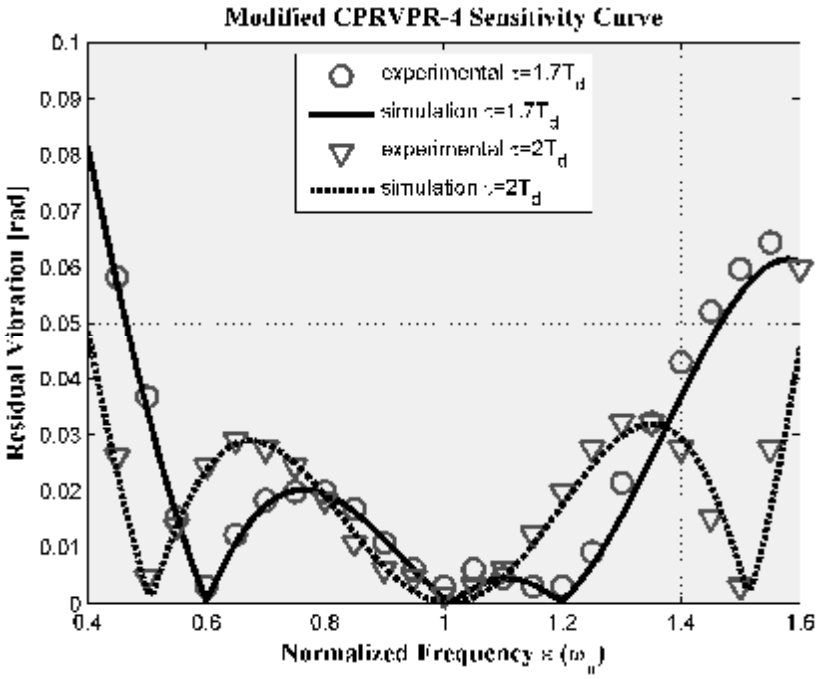

Figure 4.56. Theoretical and experimental sensitivity curves for the Modified CPRVPR4 reference function for different travelling times

The theoretical and experimental sensitivity curves of the Modified CPRVPR4 reference function for different travelling time are shown in Figure 4.56. The experimental results closely match those predicted by the theoretical study. The Modified CPRVPR4 reference function has a time duration equal to 1.7 period of the vibration frequency, as opposed to the two period length of the ZVDDD shaper. Theoretically, there is no travelling time restriction on the system and this is the main advantages of this reference command.

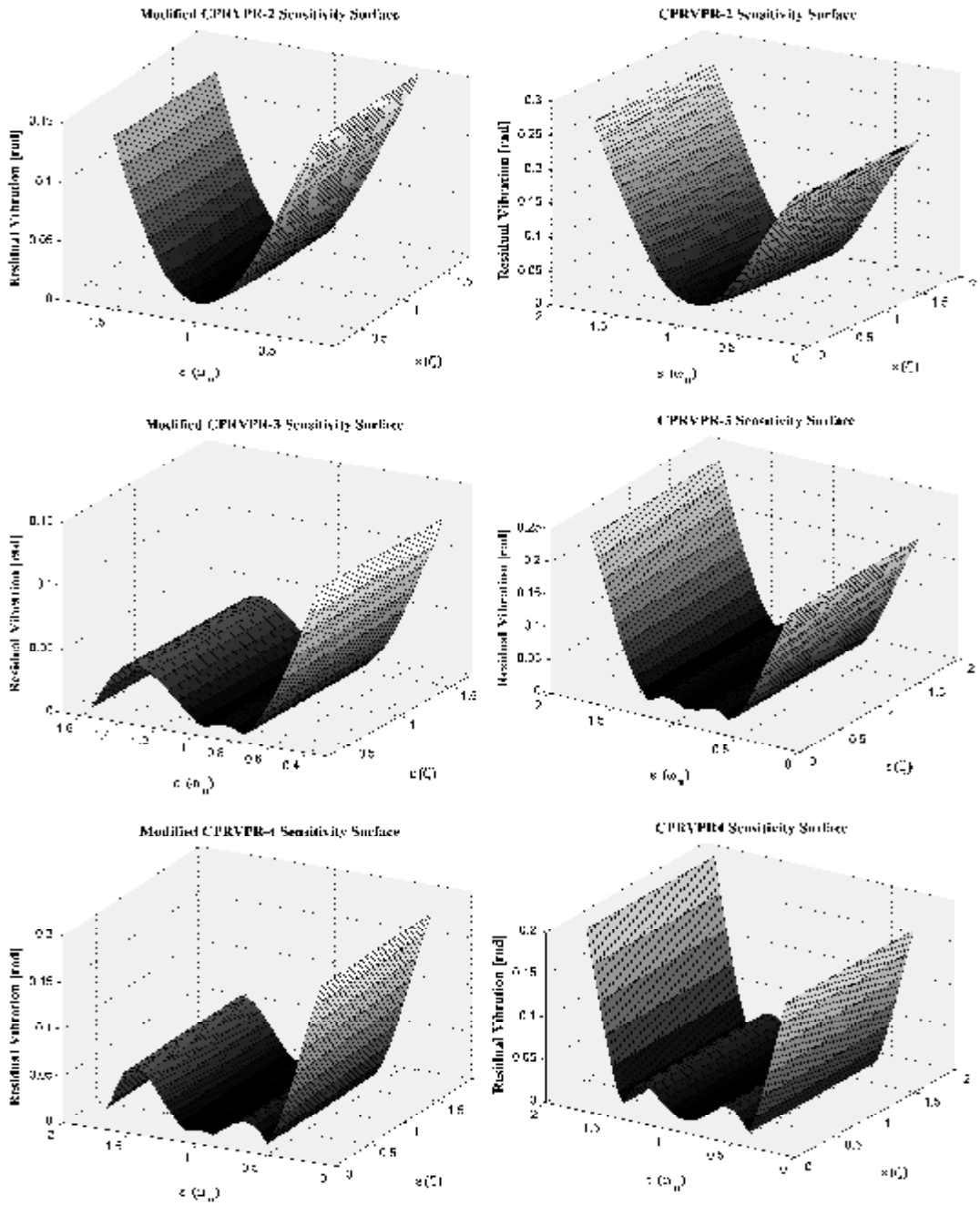

Figure 4.57. Robustness of the system to uncertainties in the mode frequencies and damping ratios for the various M-CPRVPR reference functions

In Figure 4.57., the variation of the residual vibration is presented against estimation error in natural frequency and damping ratio of the system for the various M-CPRVPR reference functions. It can clearly be seen that the variation of estimation error (or increasing uncertainty) of damping ratio has relatively reduced the effect on the residual vibration of the system. Therefore, the uncertainties on the

damping ratio do not play an important role in affecting the behavior of the system mainly due to its very low value, i.e. ζ =0.004. On the other hand, the estimation error in natural frequency of the system appears to affect the motion of the system and the resulting residual vibration levels.

4.1.2. Experiment Set 2: Flexible Link Robotic Manipulator

In this section to validate the proposed techniques and to demonstrate the practical effectiveness of it over the discussed conventional methods, it has been tested in real time experiments using a flexible link robotic manipulator. This manipulator arm is fabricated by Quanser Inc (Quanser Inc., 2012b). The detailed information upon the utilized flexible link manipulator can be found in Section 3.1.2 and from the website of the company (Quanser Inc.).

4.1.2.1. Zero Vibration (ZV) Shaper

In Figures 4.58, the simulation and experimental results of ZV shaper are illustrated. In the figure, estimation error of ±%25 is introduced to natural frequency of the system used in calculation of the input signals. Figure 4.58 is plotted with estimation errors of (a) -%25, (b) %0, (c) +%25, respectively.

In Figure 4.58, it can be seen that, the estimation error causes increasing residual vibrations of tip deflection ranging from 0.112 to 0.1353 rad. The time delay of the Zero Vibration (ZV) shaper is half the period of the system vibration. It can be seen that increasing error in estimation of the natural frequency of the system causes increasing residual vibrations. These results are also validated in Figure 4.59 and 4.60 where tip deflections of different predicted natural frequencies and related sensitivity curves are presented, respectively. The ZV shaper is very sensitive to modelling errors; a small errors in the modelling frequency leads to significant residual vibrations.

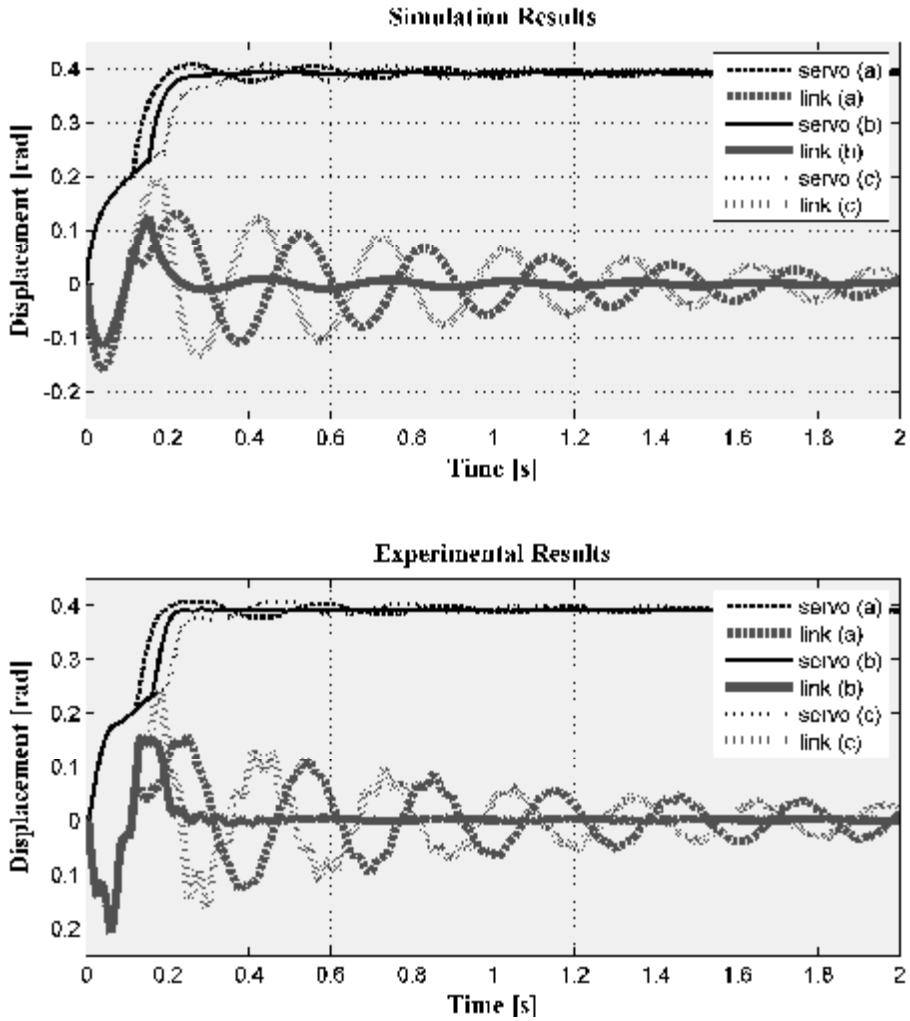

Figure 4.58. ZV shaper with experimental and simulation results for (a) -%25, (b) %0, (c) +%25 estimation error of natural frequency

The theoretical and experimental sensitivity curves for the ZV shaper are shown in Figure 4.60. The experimental results closely match those predicted by the theoretical study. A Zero Vibration, input shaper is the simplest input shaper. The only constraints are minimal time and zero vibration at the modelling frequency. Figure 4.60 shows that the vibration amplitude increases rapidly as the estimated frequency deviates from the actual system frequency. The ZV input shaper is often not very effective on real systems because it is sensitive to modelling errors and system nonlinearities. These results are validated in Figure 4.59 and 4.60.

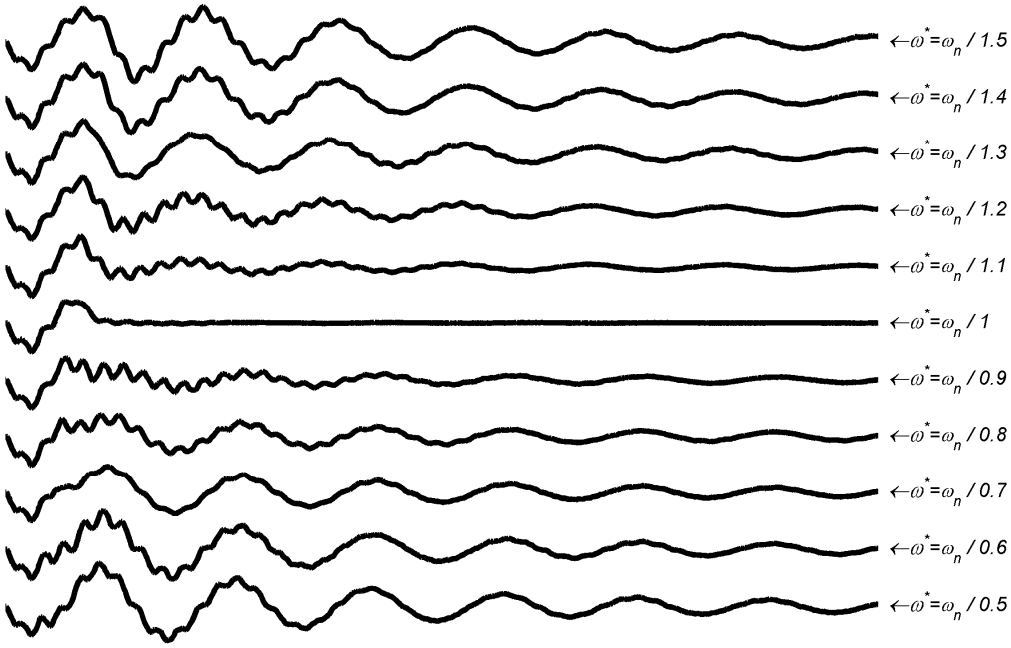

Figure 4.59.Tip deflection of different predicted natural frequencies for ZV shaper related experimental results

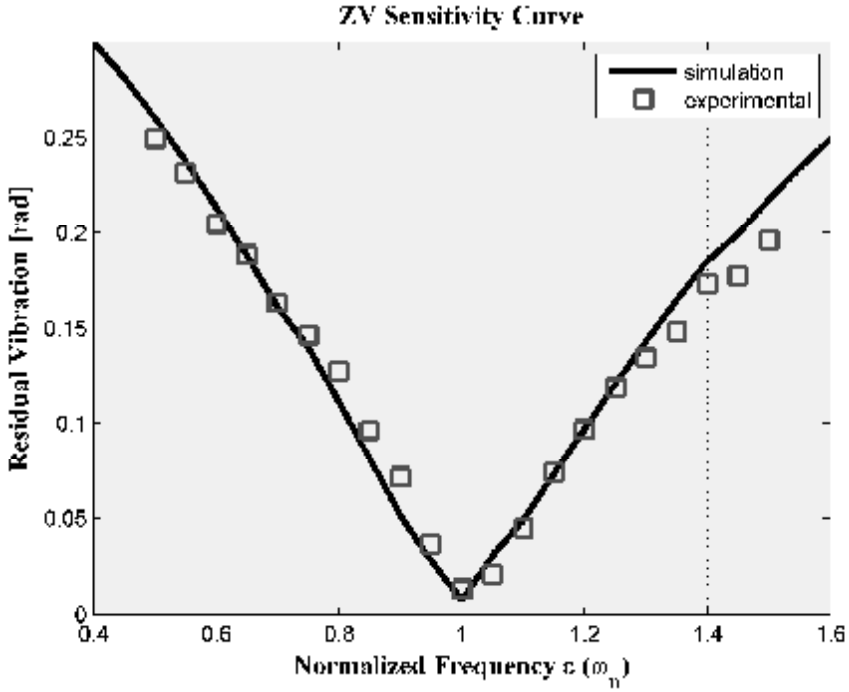

Figure 4.60. Theoretical and experimental sensitivity curves for the ZV shaper

4.1.2.2. Zero Vibration Derivate (ZVD) Shaper

In Figures 4.61, the simulation and experimental results of ZVD shaper are illustrated. In the figure, estimation error of ±%25 is introduced to natural frequency of the system used in calculation of the input signals. Figure 4.63 is plotted with estimation errors of (a) -%25, (b) %0, (c) +%25, respectively.

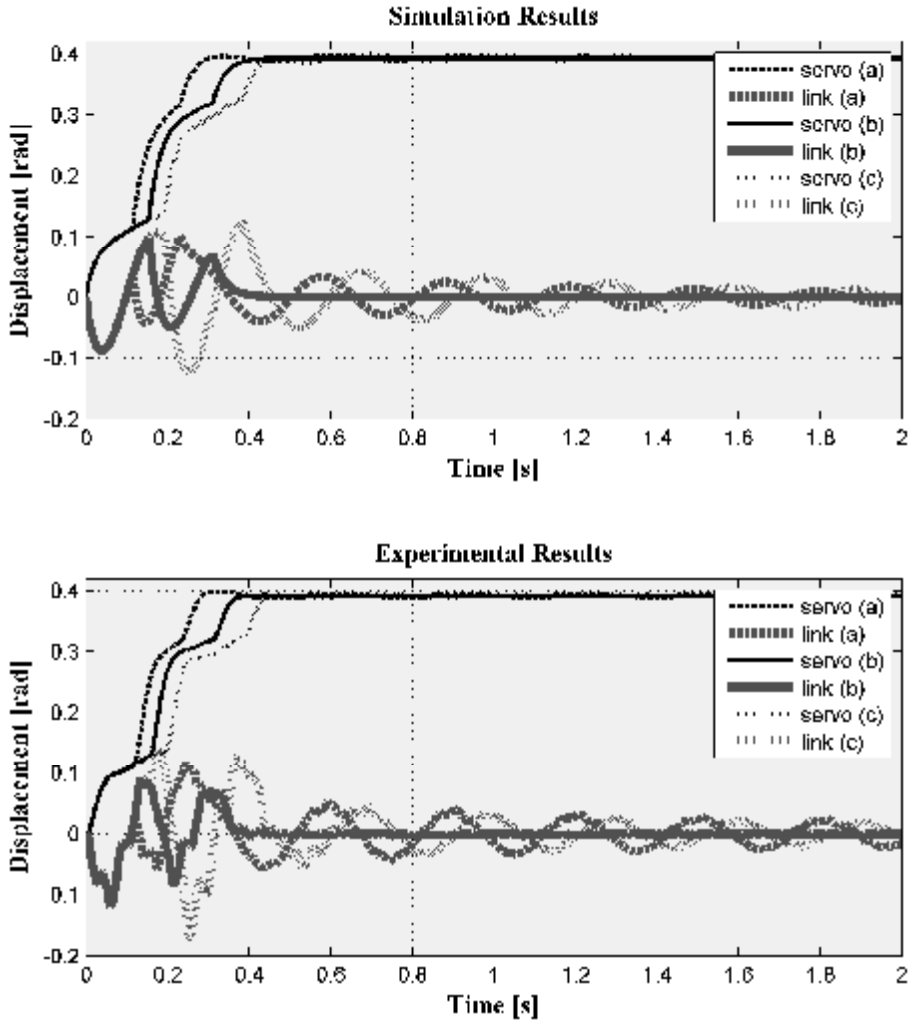

Figure 4.61. ZVD shaper with experimental and simulation results for (a) -%25, (b) %0, (c) +%25 estimation error of natural frequency

In Figure 4.61, it can be seen that, the estimation error causes increasing residual vibrations of tip deflection ranging from 0.0436 to 0.0532 rad. The time delay of the Zero Vibration Derivative (ZVD) shaper is one period of the system vibration. It

can be seen that increasing error in estimation of the natural frequency of the system causes increasing residual vibrations. These results are also validated in Figure 4.62 and 4.63 where tip deflections of different predicted natural frequencies and related sensitivity curves are presented, respectively. The ZVD shaper has considerably more robustness to modelling errors. It is evident by noting that the width of the ZVD curve is much larger than the width of the ZV curve.

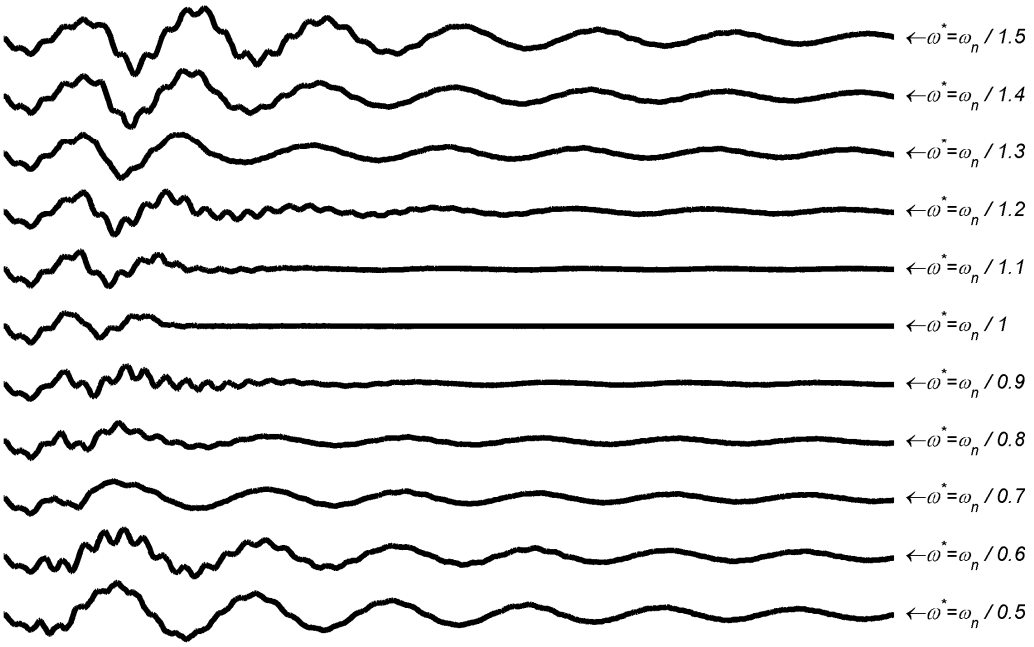

Figure 4.62. Tip deflection of different predicted natural frequencies for ZVD shaper related experimental results

The theoretical and experimental sensitivity curves for the ZVD shaper are shown in Figure 4.63. The experimental results closely match those predicted by the theoretical study. Figure 4.62 and 4.63 shows that the ZVD shaper is much more insensitive to modelling errors than the ZV shaper. However, the ZVD shaper has a time duration equal to one period of the vibration frequency, as opposed to the one-half period length of the ZV shaper. This trade-off is typical of the input shaper design process, increasing insensitivity usually requires increasing the length of travelling time of the input shaper. The additional insensitivity of the ZVD shaper incurs a time penalty; the ZVD shaper is longer than the ZV shaper by one half period of the vibration. This means that a shaped command generated with a ZVD

shaper will be one half period of vibration-longer than a ZV shaped command. In most cases, this is a small price to pay for the large increase in robustness.

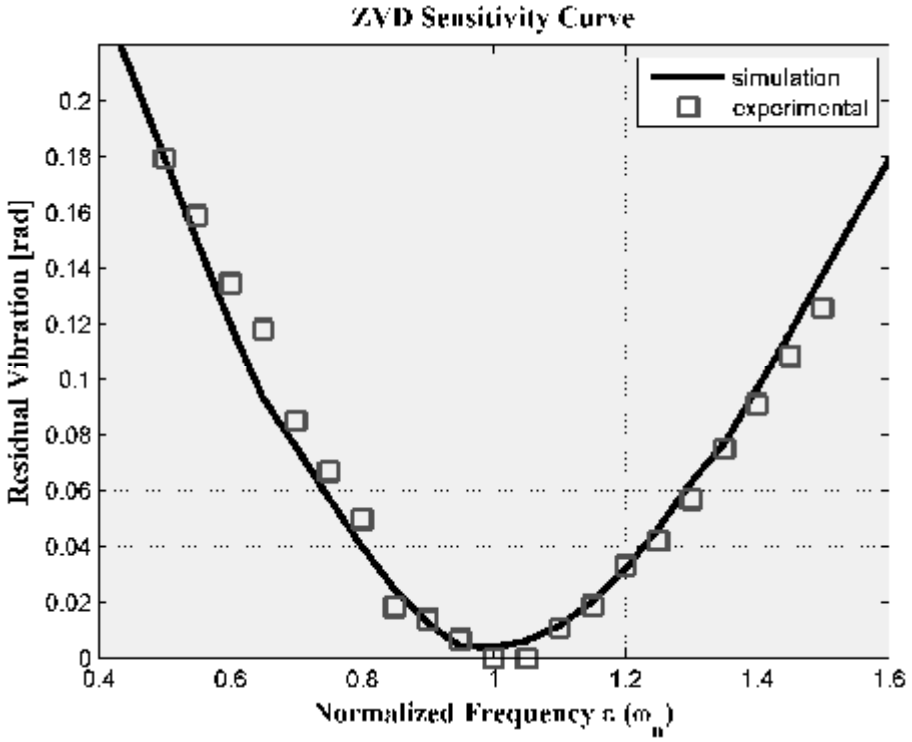

Figure 4.63. Theoretical and experimental sensitivity curves for the ZVD shaper

4.1.2.3. Zero Vibration Derivate Derivative (ZVDD) Shaper

In Figures 4.64, the simulation and experimental results of ZVDD shaper are illustrated. In the figure, estimation error of ±%25 is introduced to natural frequency of the system used in calculation of the input signals. Figure 4.64 is plotted with estimation errors of (a) -%25, (b) %0, (c) +%25, respectively. In Figure 4.64, it can be seen that, the estimation error causes increasing residual vibrations of tip deflection ranging from 0.0088 to 0.0155 rad. It can be seen that increasing error in estimation of the natural frequency of the system causes slightly increasing residual vibrations. These results are also validated in Figure 4.65 and 4.66 where tip deflections of different predicted natural frequencies and related sensitivity curves are presented, respectively.

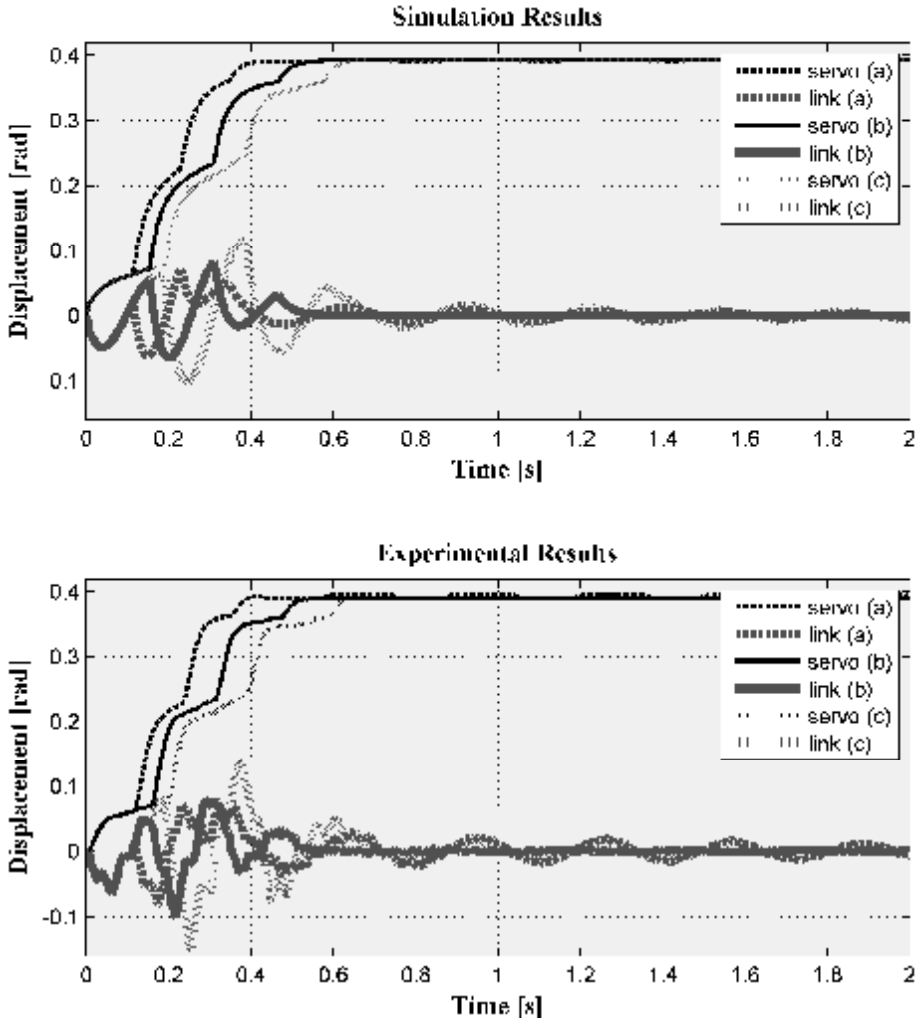

Figure 4.64. ZVDD shaper with experimental and simulation results for (a) -%25, (b) %0, (c) +%25 estimation error of natural frequency

The theoretical and experimental sensitivity curves for the ZVDD shaper are shown in Figure 4.66. The experimental results closely match those predicted by the theoretical study. Figure 4.65 and 4.66 shows that the ZVDD shaper is much more insensitive to modelling errors than the ZVD shaper. However, the ZVDD shaper has a time duration equal to one and a half period of the vibration frequency, as opposed to the one period length of the ZVD shaper. The additional robustness gained from each higher-order derivative is evident in the plot. This trade-off is typical of the input shaper design process, increasing insensitivity usually requires increasing the length of travelling time of the input shaper.

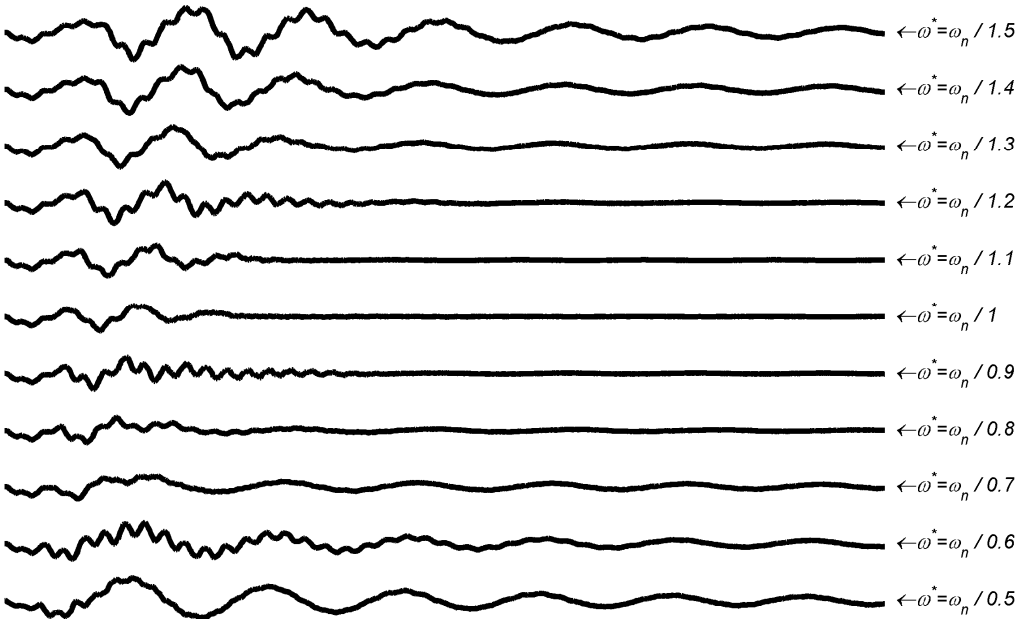

Figure 4.65. Tip deflection of different predicted natural frequencies for ZVDD shaper related experimental results

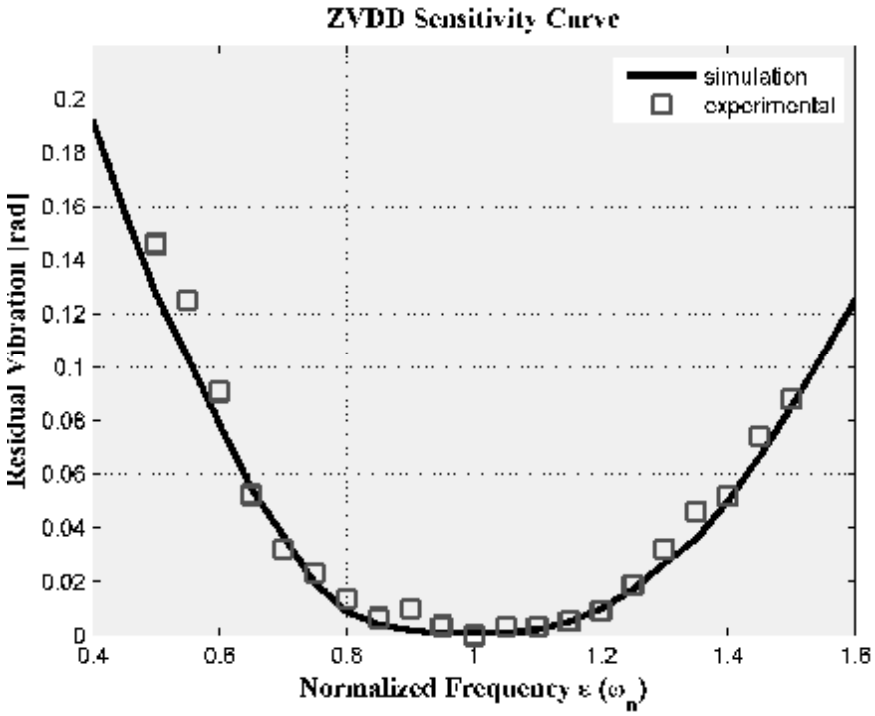

Figure 4.66. Theoretical and experimental sensitivity curves for the ZVDD shaper

4.1.2.4. Zero Vibration Derivate Derivative Derivative (ZVDDD) Shaper

In Figures 4.67, the simulation and experimental results of ZVDDD shaper are illustrated. In the figure, estimation error of ±%25 is introduced to natural frequency of the system used in calculation of the input signals. Figure 4.67 is plotted with estimation errors of (a) -%25, (b) %0, (c) +%25, respectively.

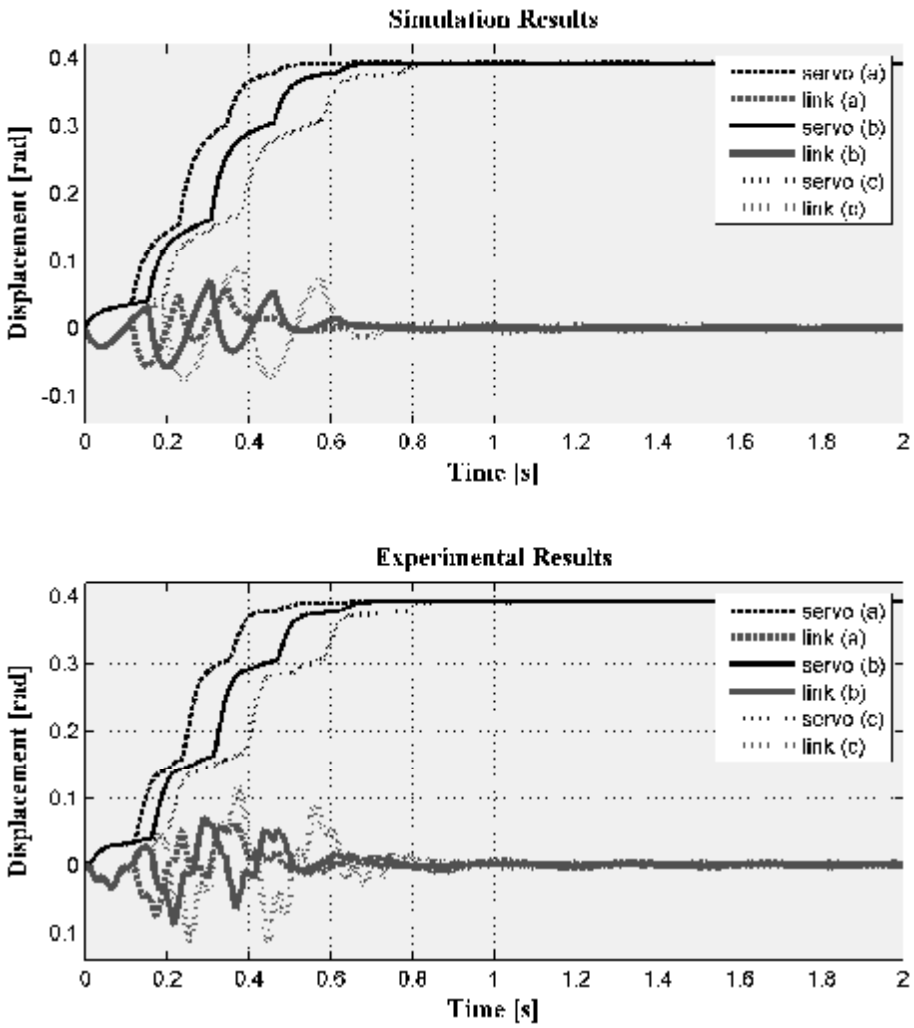

Figure 4.67. ZVDDD shaper with experimental and simulation results for (a) -%25, (b) %0, (c) +%25 estimation error of natural frequency

In Figure 4.67, it can be seen that, the estimation error causes increasing residual vibrations of tip deflection ranging from 0.0032 to 0.005549 rad.

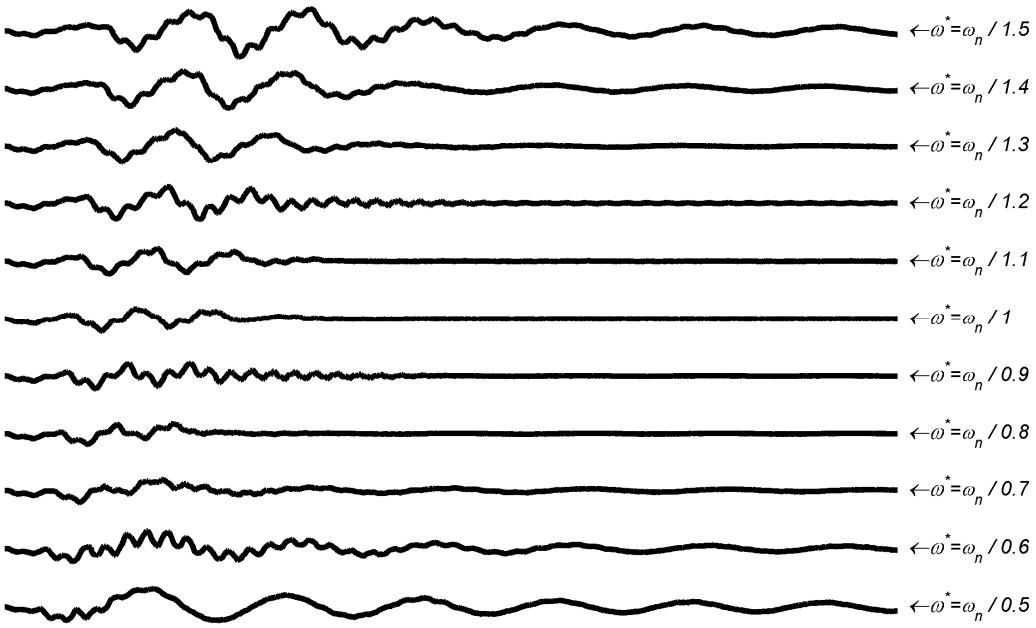

Figure 4.68. Tip deflection of different predicted natural frequencies for ZVDDD shaper related experimental results

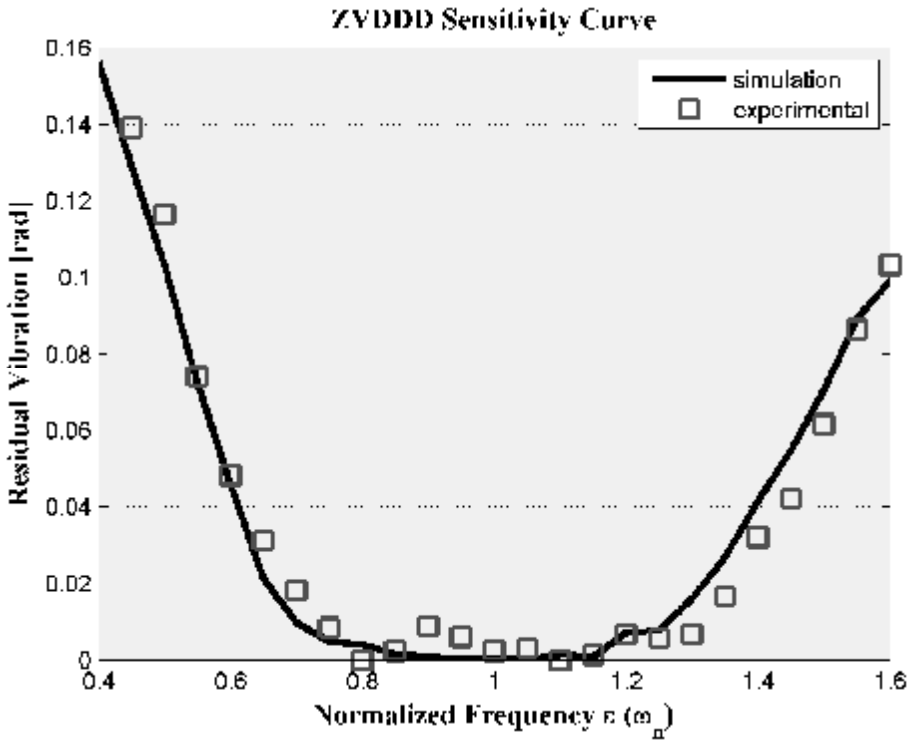

Figure 4.69. Theoretical and experimental sensitivity curves for the ZVDDD shaper

It can be seen that increase error in estimation of the natural frequency of the system does not seem to important affect the residual vibrations. These results are also

validated in Figure 4.68 and 4.69 where tip deflections of different predicted natural frequencies and related sensitivity curves are presented, respectively.

Figure 4.68 and 4.69 shows that the ZVDDD shaper is much more insensitive to modelling errors than the ZVDD shaper. However, the ZVDDD shaper has a time duration equal to two period of the vibration frequency, as opposed to the one and a half period length of the ZVDD shaper. The additional robustness gained from each higher-order derivative is evident in the plot. The algorithm can be extended indefinitely with repeated differentiation of the percentage vibration equation. For each differentiation, an additional impulse is added to the shaper and the shaper is lengthened by one-half period of the frequency.

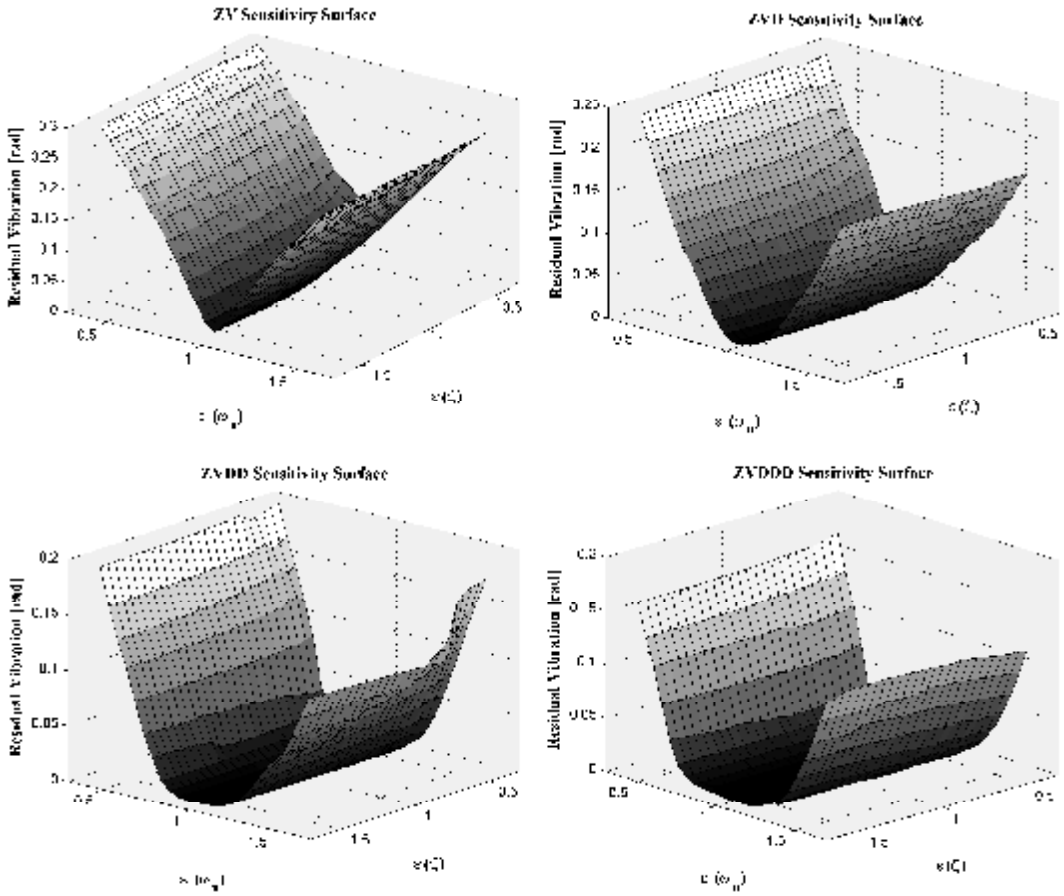

Figure 4.70. Robustness of the system to uncertainties in the mode frequencies and damping ratios for the ZV, ZVD, ZVDD and ZVDDD Input Shapers

In Figure 4.70, the variation of the residual vibration is presented against estimation error in natural frequency and damping ratio of the system for ZV, ZVD, ZVDD and ZVDDD input shapers. It can clearly be seen that the variation of estimation error (or increasing uncertainty) of damping ratio has relatively reduced the effect on the residual vibration of the system. Therefore, the uncertainties of the damping ratio do not play an important role in affecting the behavior of the system mainly due to its very low value, i.e. ζ =0.07. On the other hand, the estimation error in natural frequency of the system appears to affect the motion of the system and the resulting residual vibration levels.

4.1.2.5. Extra Insensitive (EI) Input Shaper

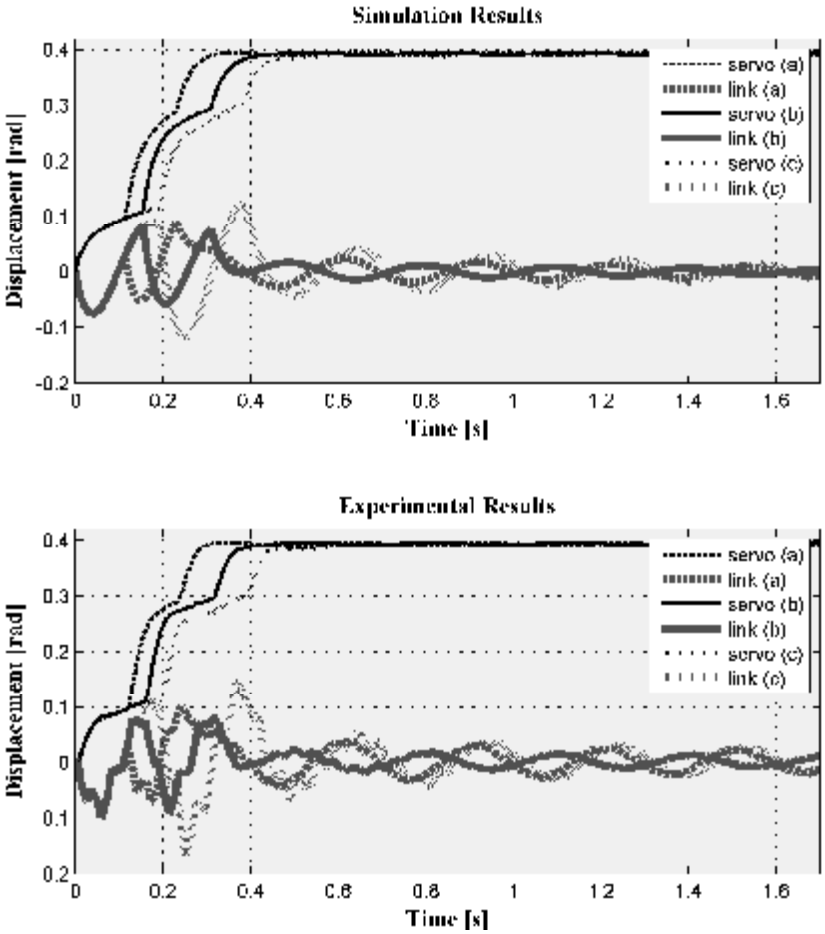

Figure 4.71. EI shaper with experimental and simulation results for (a) -%25, (b) %0, (c) +%25 estimation error of natural frequency

In Figures 4.71, the simulation and experimental results of EI shaper are illustrated. In the figure, estimation error of ±%25 is introduced to natural frequency of the system used in calculation of the input signals. Figure 4.71 is plotted with estimation errors of (a) -%25, (b) %0, (c) +%25, respectively. In Figure 4.71, it can be seen that, the estimation error causes increasing residual vibrations of tip deflection from 0.0233 to 0.0391 rad. It can be seen that increasing error in estimation of the natural frequency of the system causes increasing residual vibrations. These results are also validated in Figure 4.72 and 4.73 where tip deflections of different predicted natural frequencies and related sensitivity curves are presented, respectively.

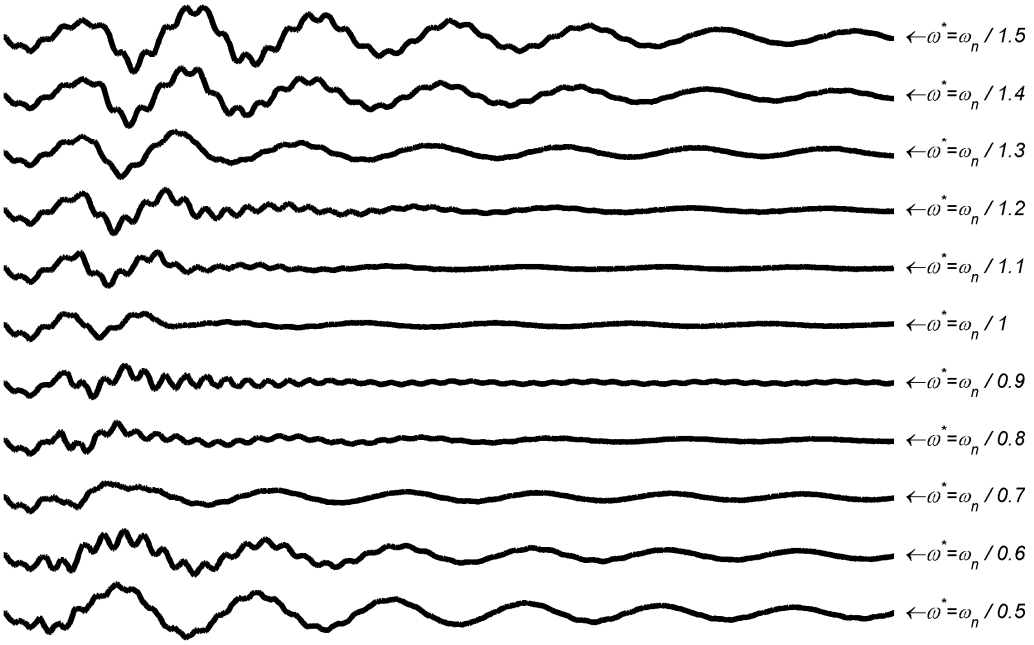

Figure 4.72. Tip deflection of different predicted natural frequencies for EI shaper related experimental results

Unlike the ZV, ZVD, ZVDD and ZVDDD shapers, the EI shaper does not attempt to force the vibration to zero at the modelling frequency. Rather, the vibration is limited to some low, but acceptable level of residual vibration. The sensitivity curve for an EI shaper designed to limit vibration below 5% and 10% is shown in Figure 4.73. The travelling time of the EI shaper is the same as that of the ZVD shaper, one damped cycle of vibration, but it is considerably more robust. Thus,

the application of EI shapers is for systems where some small vibration is allowable, and the systems parameters are expected to change considerably.

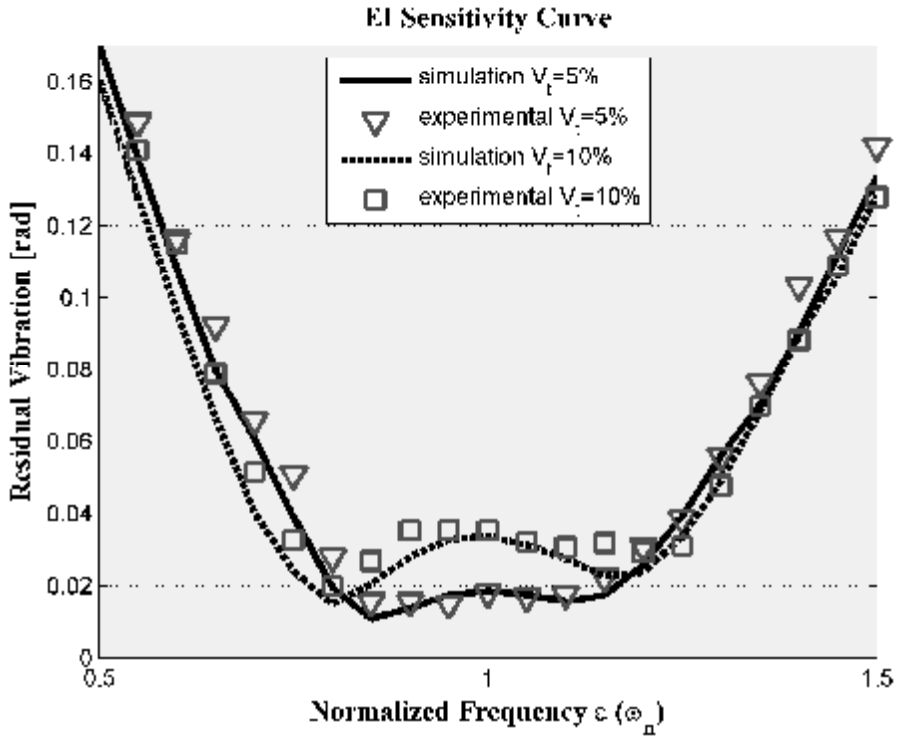

Figure 4.73. Theoretical and experimental sensitivity curves for the EI shaper

4.1.2.6. Two Hump Extra Insensitive (2H-EI) Input Shaper

In Figures 4.74, the simulation and experimental results of Two Hump EI shaper are illustrated. In the figure, estimation error of ±%25 is introduced to natural frequency of the system used in calculation of the input signals. Figure 4.74 is plotted with estimation errors of (a) -%25, (b) %0, (c) +%25, respectively. In Figure 4.74, it can be seen that, the estimation error causes increasing residual vibrations of tip deflection from 0.0101 to 0.0121 rad. It can be seen that increase error in estimation of the natural frequency of the system does not seem to important affect the residual vibrations. These results are also validated in Figure 4.75 and 4.76 where tip deflections of different predicted natural frequencies and related sensitivity curves are presented, respectively.

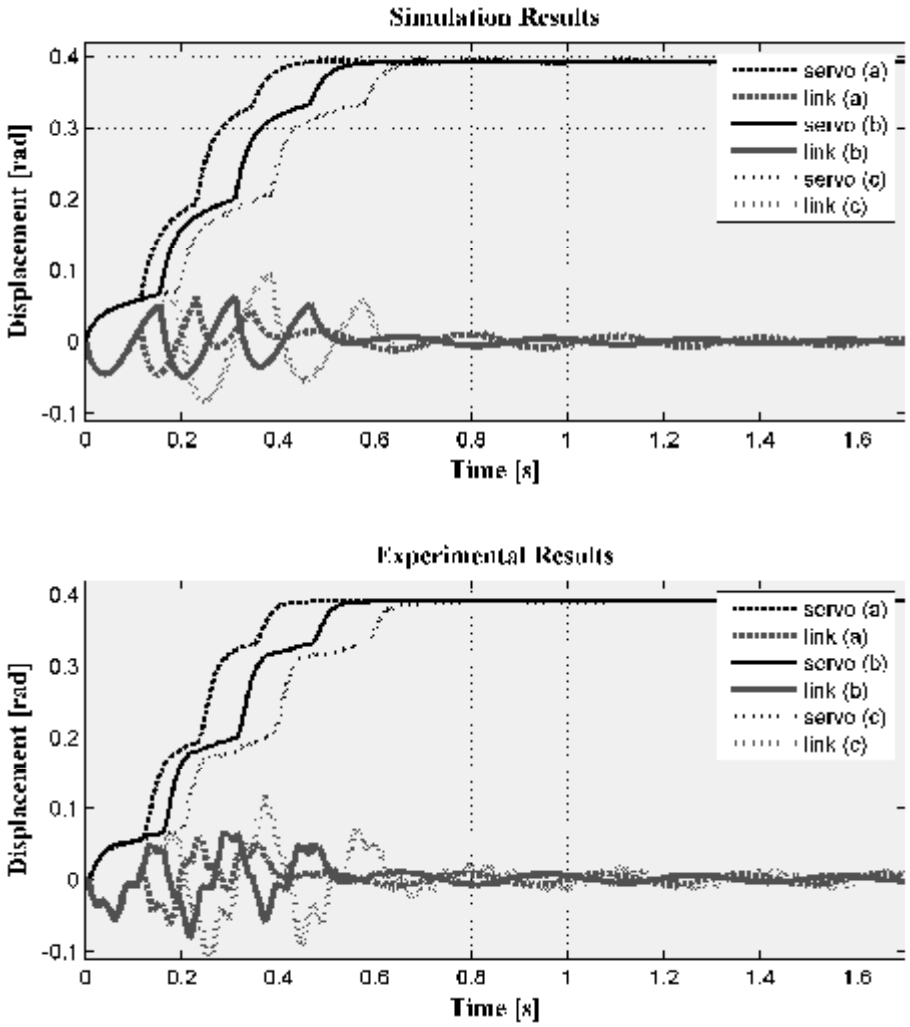

Figure 4.74. Two Hump EI shaper with experimental and simulation results for (a) -%25, (b) %0, (c) +%25 estimation error of natural frequency

The sensitivity curves for two-hump EI shapers designed to limit vibration below 5% and 10% are shown in Figure 4.76. As with the derivative-method (ZVD, ZVDD and ZVDDD) input shapers, the price for increased robustness is a corresponding increase in shaper duration. Note, however, that the penalty is not uniform across all shapers. The Two-Hump EI shaper has the same duration as the ZVDD shaper. However, the Two-Hump EI shapers have much more robustness, as can be seen in Figure 4.75 and 4.76.

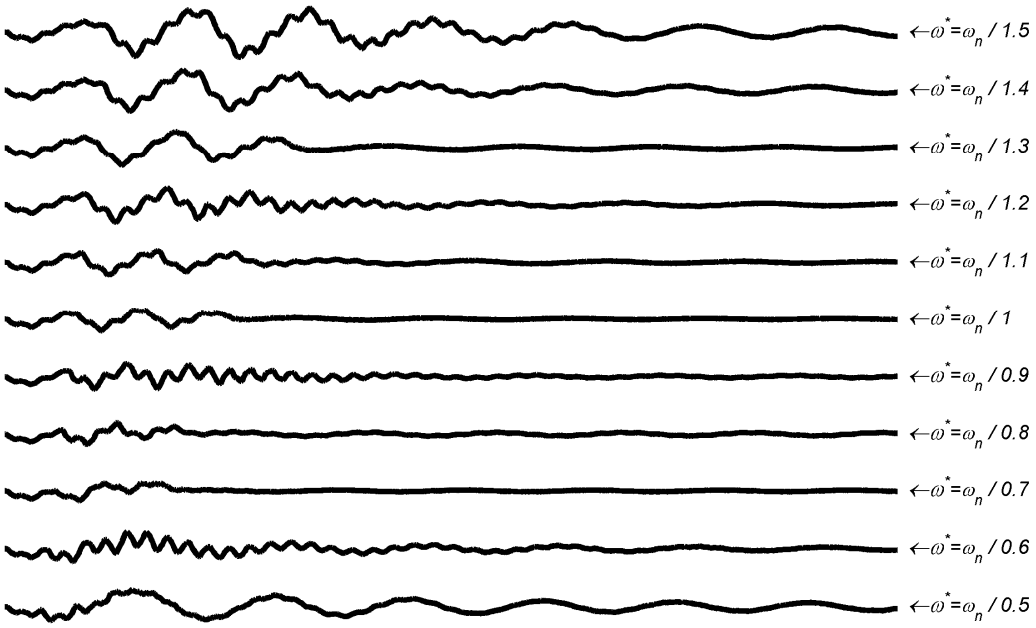

Figure 4.75. Tip deflection of different predicted natural frequencies for Two Hump EI shaper related experimental results

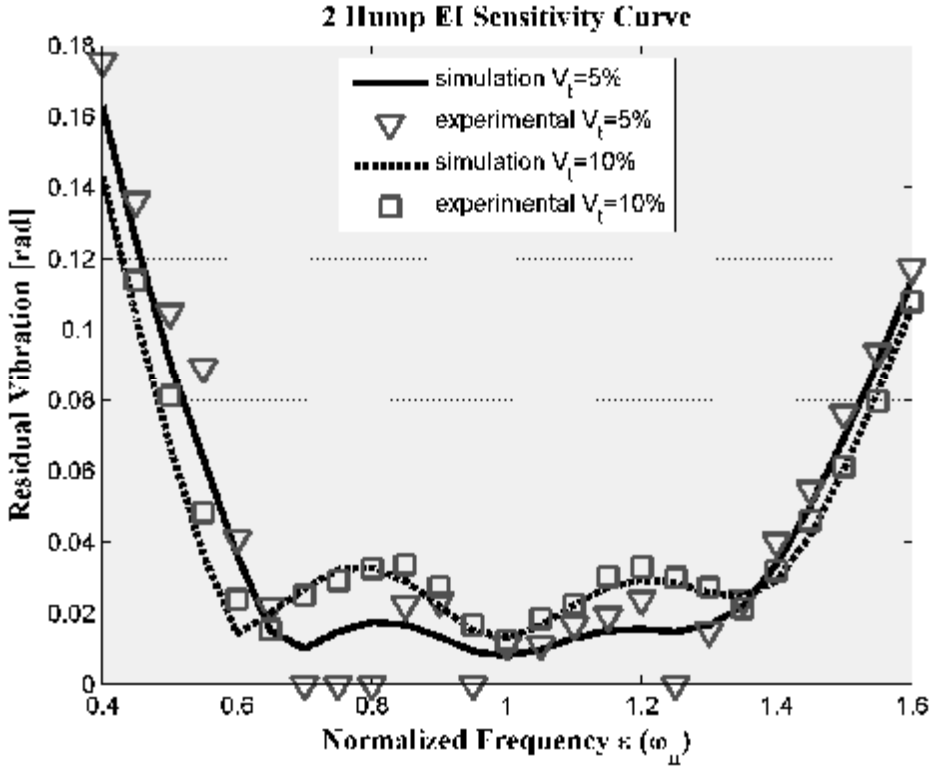

Figure 4.76. Theoretical and experimental sensitivity curves for the Two Hump EI shaper

4.1.2.7. Three Hump Extra Insensitive (3H-EI) Input Shaper

In Figures 4.77, the simulation and experimental results of Three Hump EI shaper are illustrated. In the figure, estimation error of ±%25 is introduced to natural frequency of the system used in calculation of the input signals. Figure 4.77 is plotted with estimation errors of (a) -%25, (b) %0, (c) +%25, respectively. In Figure 4.77, it can be seen that, the estimation error causes increasing residual vibrations of tip deflection from 0.0076 to 0.0121 rad.

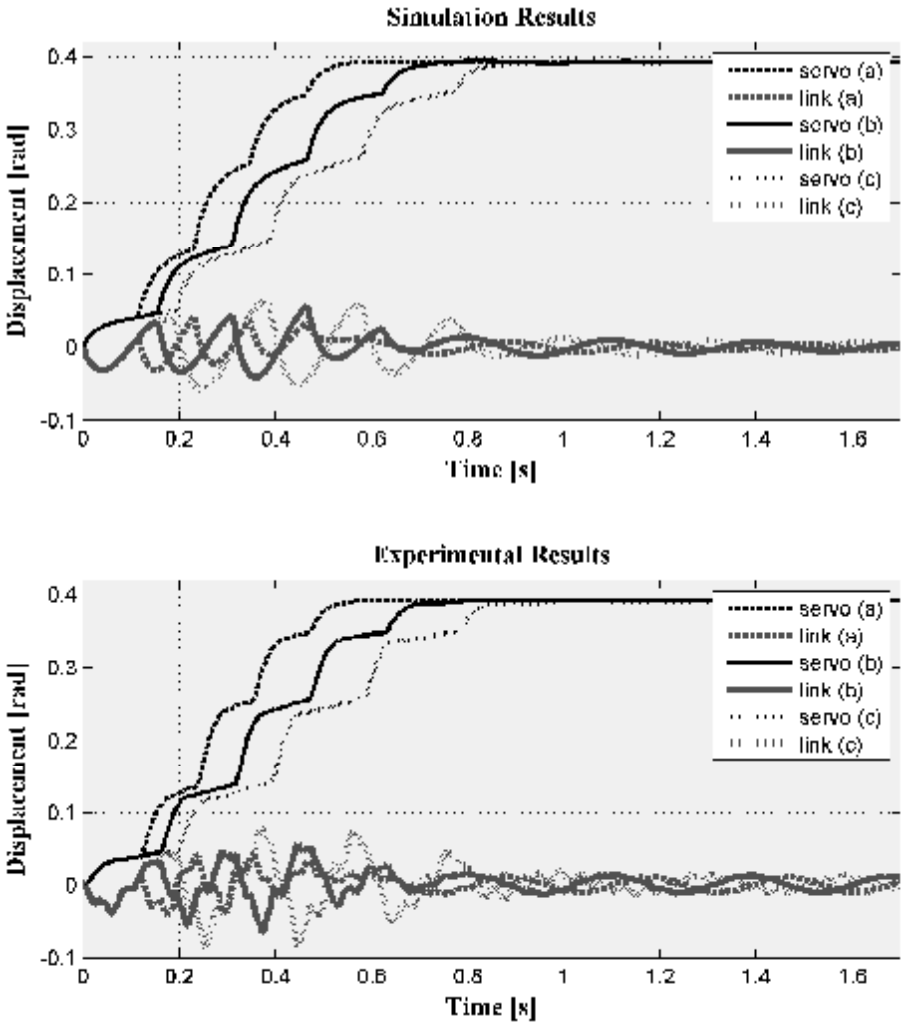

Figure 4.77. Three Hump EI shaper with experimental and simulation results for (a) -%25, (b) %0, (c) +%25 estimation error of natural frequency

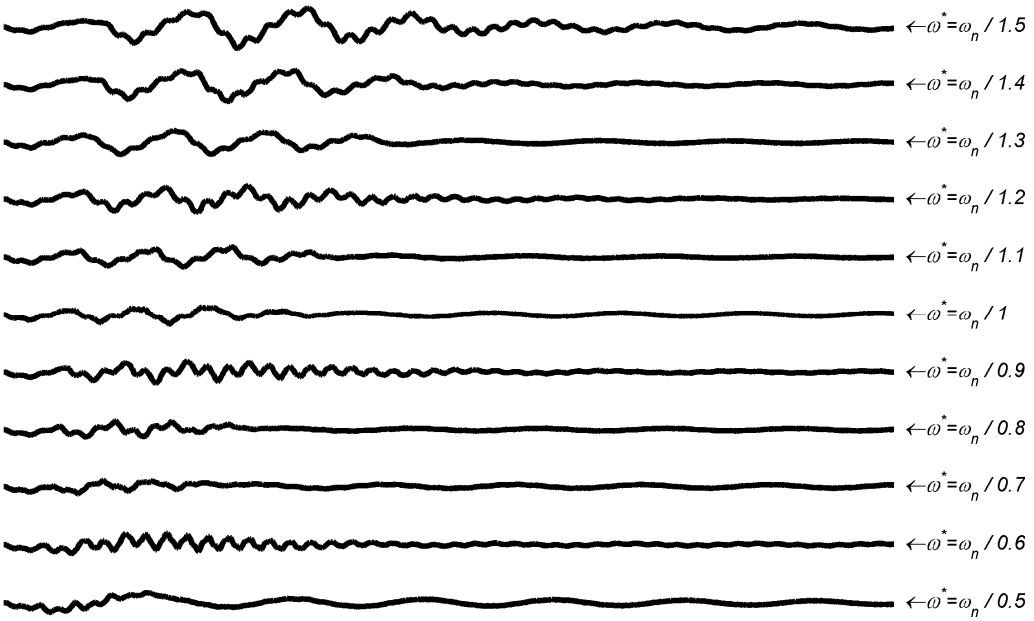

Figure 4.78. Tip deflection of different predicted natural frequencies for Three Hump EI shaper related experimental results

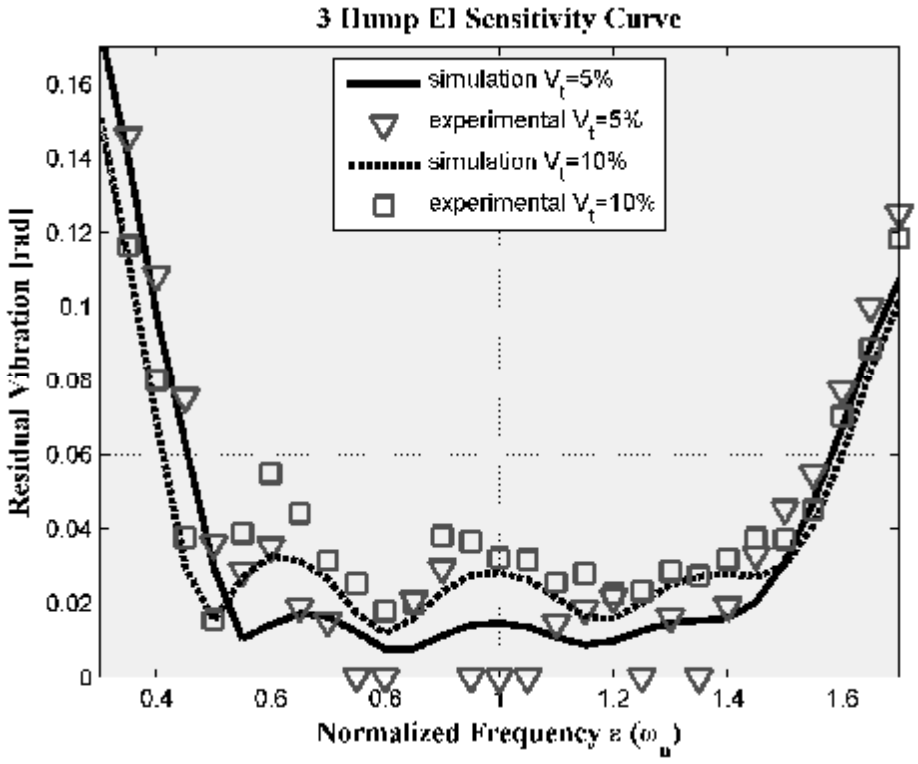

Figure 4.79. Theoretical and experimental sensitivity curves for the Three Hump EI shaper

It can be seen that increase error in estimation of the natural frequency of the system does not seem to important affect the residual vibrations. These results are also validated in Figure 4.78 and 4.79 where tip deflections of different predicted natural frequencies and related sensitivity curves are presented, respectively.

The sensitivity curves for three-hump EI shapers designed to limit vibration below 5% and 10% are shown in Figure 4.79. Note that the three-hump EI shaper suppresses vibration over the entire range shown. As with the derivative-method (ZVD, ZVDD and ZVDDD) input shapers, the price for increased robustness is a corresponding increase in shaper duration. Note, however, that the penalty is not uniform across all shapers. The Three-Hump EI shaper has the same duration as the ZVDDD shaper. However, the Three-Hump EI shapers have much more robustness, as can be seen in Figure 4.78 and 4.79.

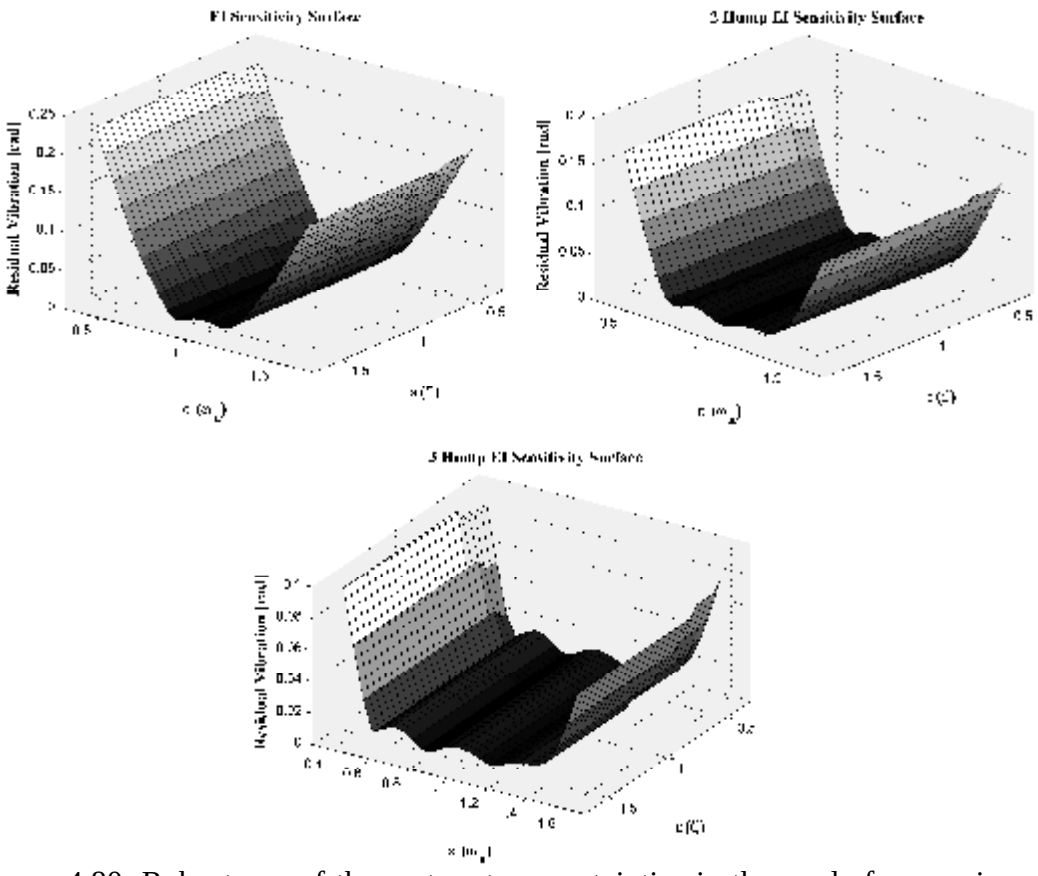

Figure 4.80. Robustness of the system to uncertainties in the mode frequencies and damping ratios for the EI, Two Hump EI and Three Hump EI Input Shapers

In Figure 4.80, the variation of the residual vibration is presented against estimation error in natural frequency and damping ratio of the system for EI, Two Hump EI and Three Hump EI input shapers. It can clearly be seen that the variation of estimation error (or increasing uncertainty) of damping ratio has relatively reduced the effect on the residual vibration of the system. Therefore, the uncertainties on the damping ratio do not play an important role in affecting the behaviour of the system mainly due to its very low value, i.e. ζ =0.07. On the other hand, estimation error in natural frequency of the system appears to affect the motion of the system and the resulting residual vibration levels.

4.1.2.8. Modified Input Shaper (MIS)

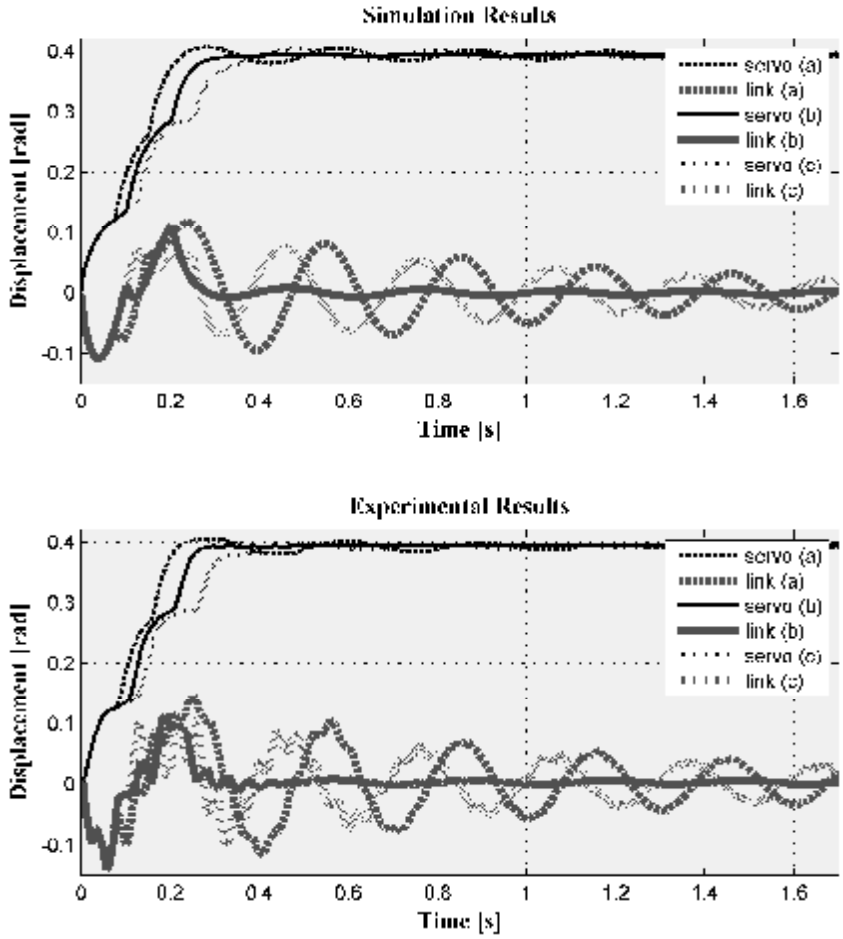

Figure 4.81. MIS-ZV-3 Impulse shaper with experimental and simulation results for (a) -%25, (b) %0, (c) +%25 estimation error of natural frequency

In Figures 4.81, the simulation and experimental results of MIS ZV 3 impulse shaper are illustrated. In the figure, estimation error of ±%25 is introduced to natural frequency of the system used in calculation of the input signals. Figure 4.81 is plotted with estimation errors of (a) -%25, (b) %0, (c) +%25, respectively. In Figure 4.81, it can be seen that, the estimation error causes increasing residual vibrations of tip deflection from 0.0899 to 0.1033 rad. It can be seen that increasing error in estimation of the natural frequency of the system causes increasing residual vibrations. These results are also validated in Figure 4.82 and 4.89 where tip deflections of different predicted natural frequencies and related sensitivity curves are presented, respectively.

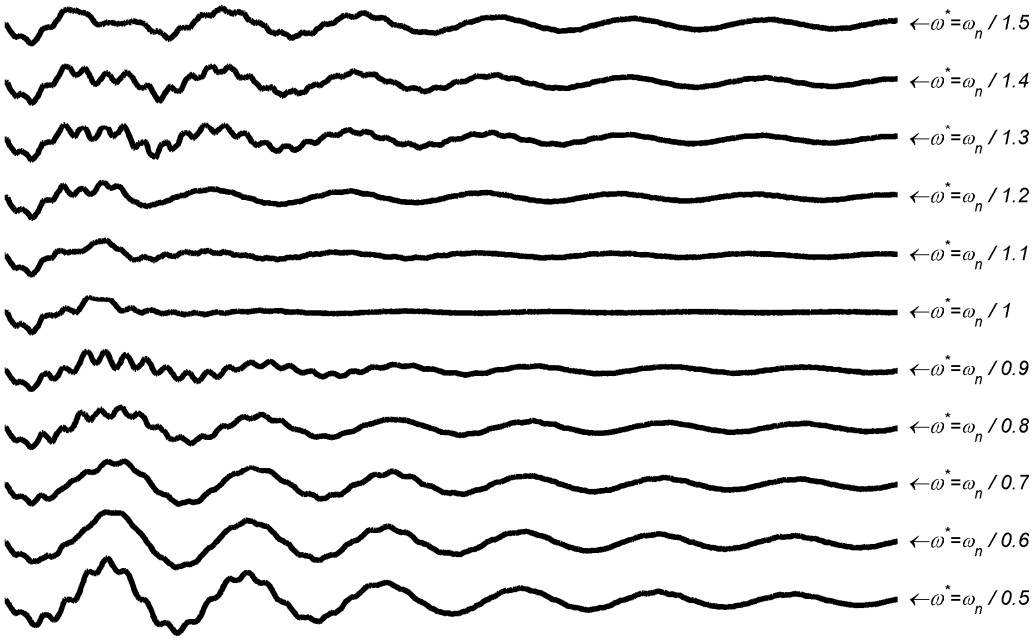

Figure 4.82. Tip deflection of different predicted natural frequencies for the MIS-ZV-3 shaper related experimental results

In Figures 4.83, the simulation and experimental results of MIS ZV 4 impulse shaper are illustrated. In the figure, estimation error of ±%25 is introduced to natural frequency of the system used in calculation of the input signals. Figure 4.83 is plotted with estimation errors of (a) -%25, (b) %0, (c) +%25, respectively. In Figure 4.83, it can be seen that, the estimation error causes increasing residual vibrations of tip deflection ranging from 0.0886 to 0.0969 rad. It can be seen that increasing error in

estimation of the natural frequency of the system causes increasing residual vibrations. These results are also validated in Figure 4.84 and 4.89 where tip deflections of different predicted natural frequencies and related sensitivity curves are presented, respectively.

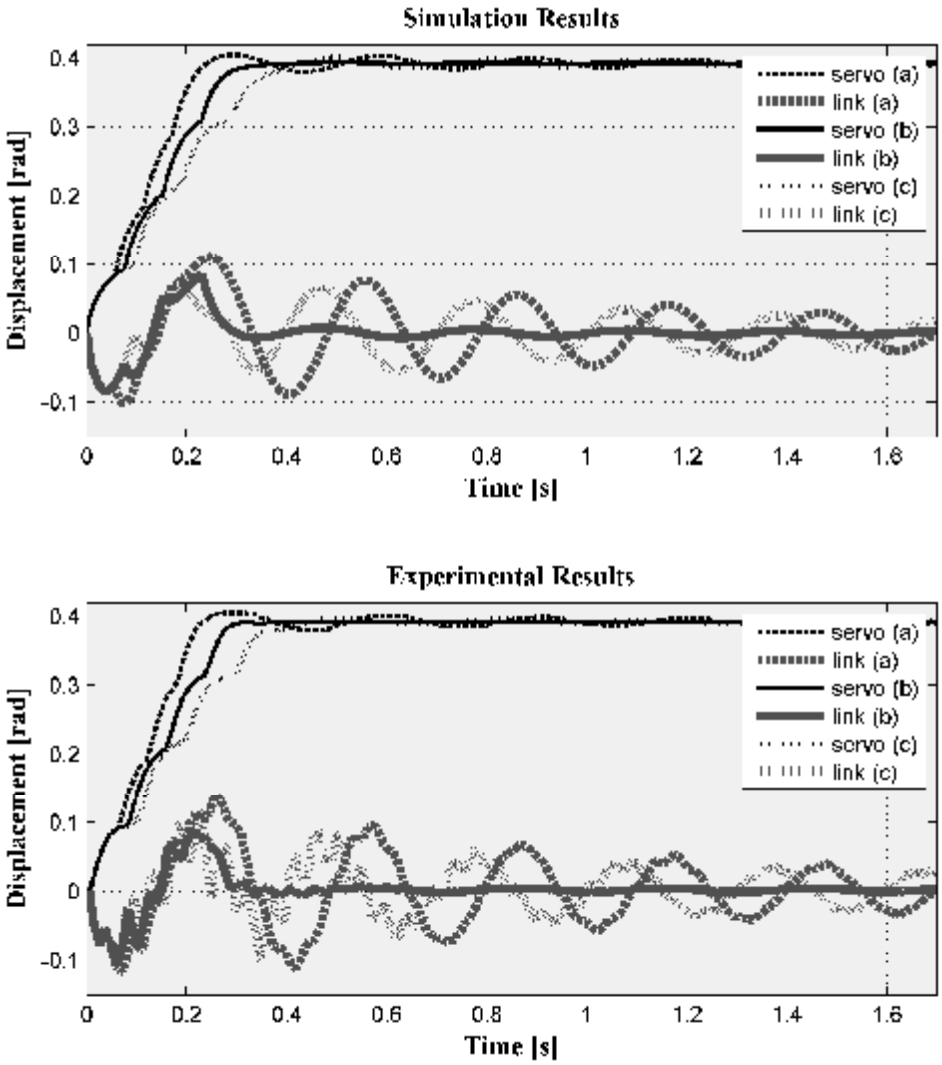

Figure 4.83. MIS-ZV-4 Impulse shaper with experimental and simulation results for (a) -%25, (b) %0, (c) +%25 estimation error of natural frequency

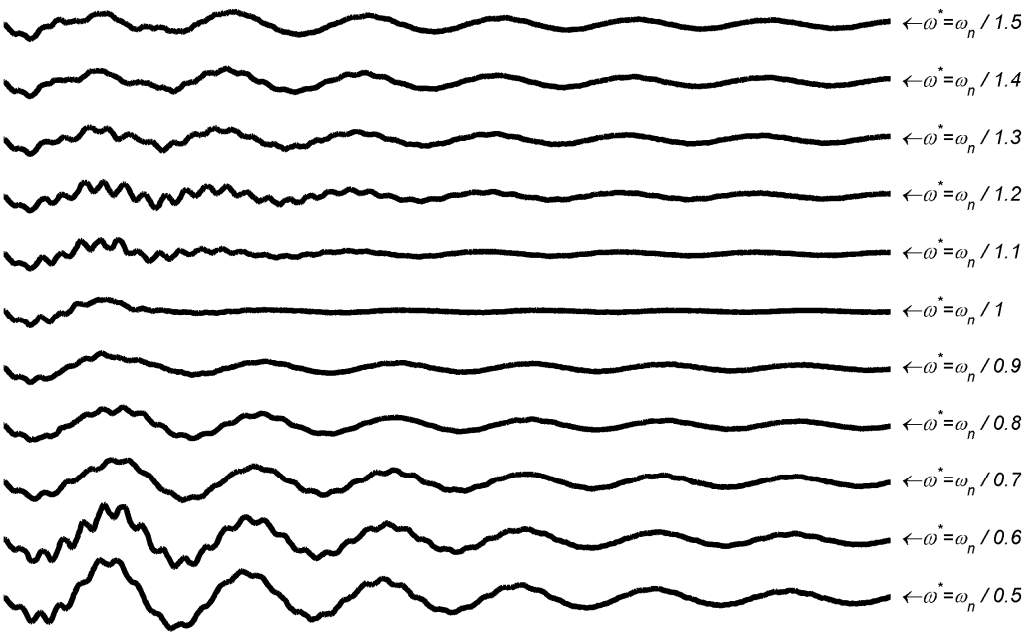

Figure 4.84. Tip deflection of different predicted natural frequencies for the MIS-ZV-4 shaper related experimental results

In Figures 4.85, the simulation and experimental results of MIS ZV 5 Impulse shaper are illustrated. In the figure, estimation error of ±%25 is introduced to natural frequency of the system used in calculation of the input signals. Figure 4.85 is plotted with estimation errors of (a) -%25, (b) %0, (c) +%25, respectively. In Figure 4.85, it can be seen that, the estimation error causes increasing residual vibrations of tip deflection ranging from 0.0606 to 0.0742 rad. It can be seen that increasing error in estimation of the natural frequency of the system causes increasing residual vibrations. These results are also validated in Figure 4.86 and 4.89 where tip deflections of different predicted natural frequencies and related sensitivity curves are presented, respectively.

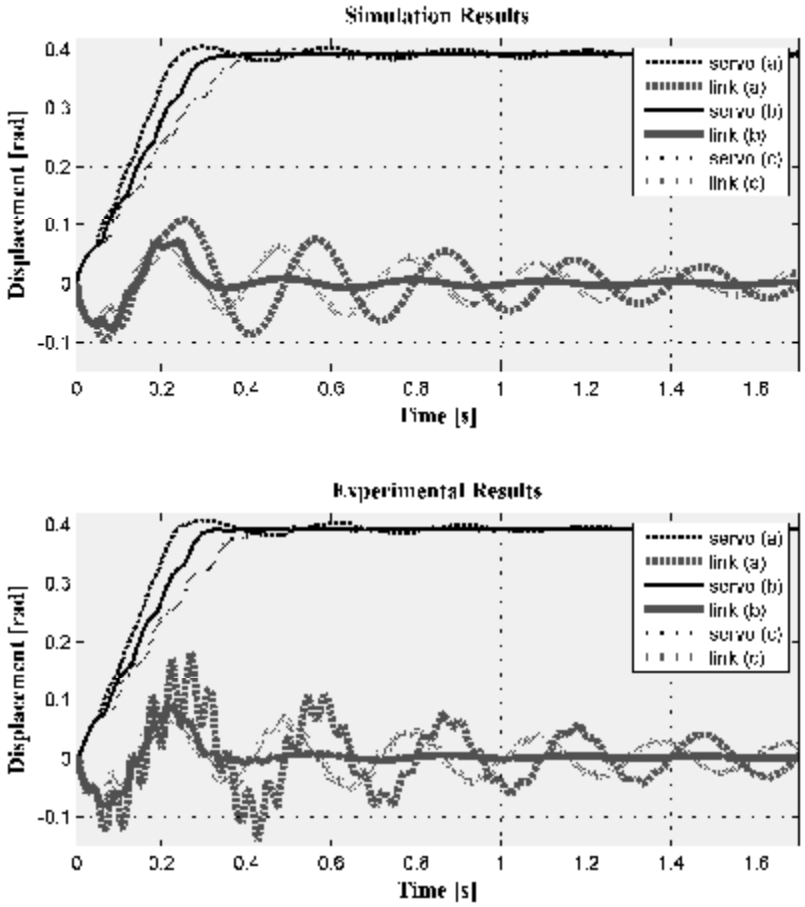

Figure 4.85. MIS-ZV-5 Impulse shaper with experimental and simulation results for (a) -%25, (b) %0, (c) +%25 estimation error of natural frequency

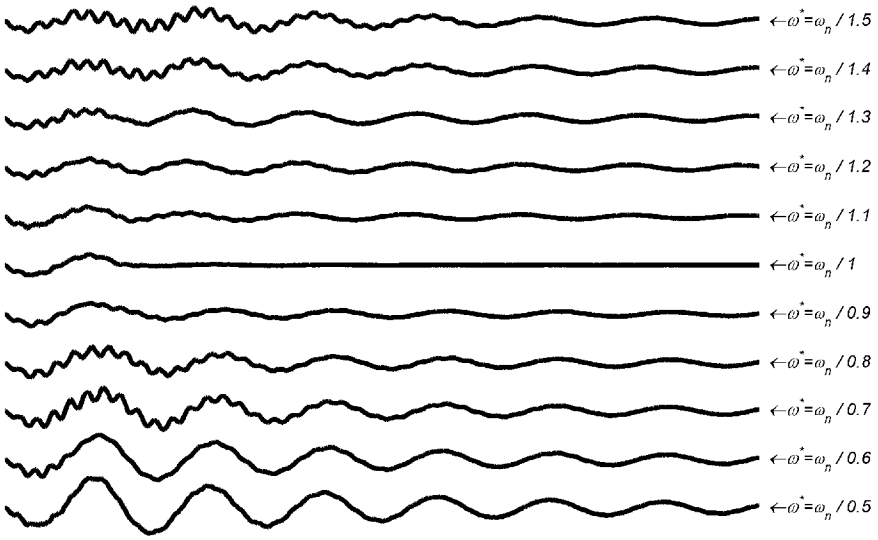

Figure 4.86. Tip deflection of different predicted natural frequencies for the MIS-ZV-5 shaper related experimental results

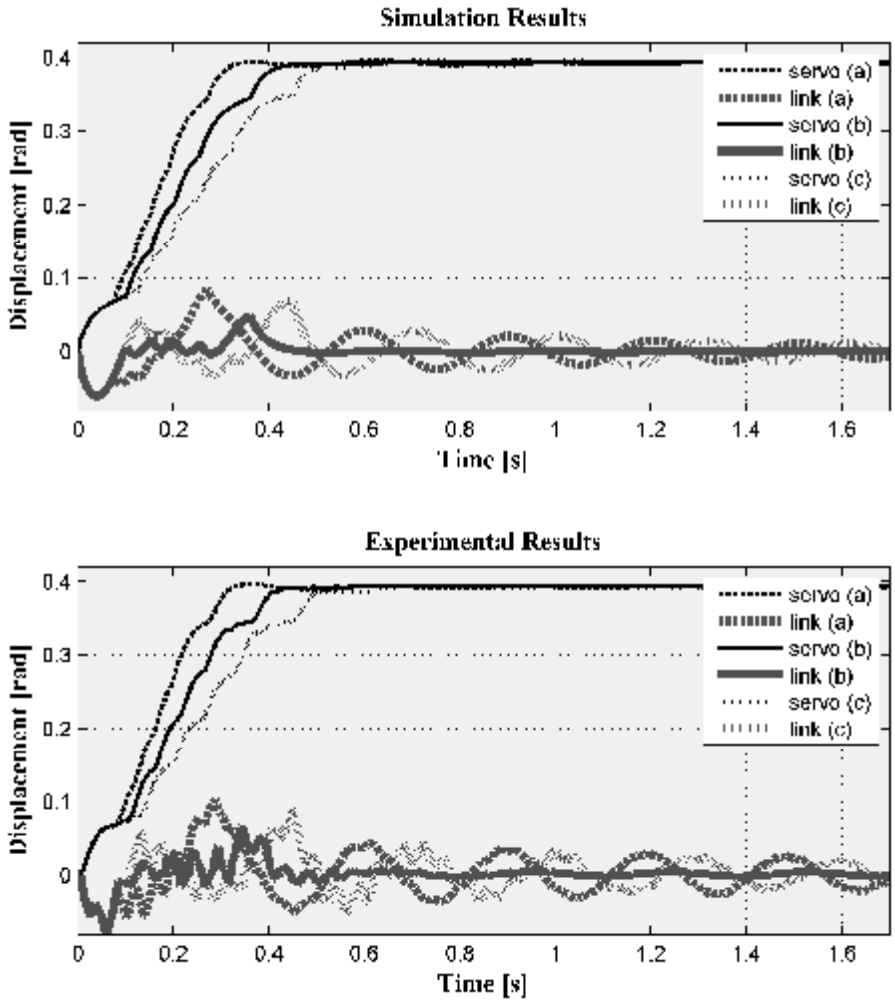

Figure 4.87. MIS-ZVD-6 Impulse shaper with experimental and simulation results for (a) -%25, (b) %0, (c) +%25 estimation error of natural frequency

In Figures 4.87, the simulation and experimental results of MIS ZVD 6 Impulse shaper are illustrated. In the figure, estimation error of ±%25 is introduced to natural frequency of the system used in calculation of the input signals. Figure 4.87 is plotted with estimation errors of (a) -%25, (b) %0, (c) +%25, respectively. In Figure 4.87, it can be seen that, the estimation error causes increasing residual vibrations of tip deflection ranging from 0.0280 to 0.0285 rad. It can be seen that increasing error in estimation of the natural frequency of the system causes increasing residual vibrations. These results are also validated in Figure 4.88 and 4.89 where tip deflections of different predicted natural frequencies and related sensitivity curves are presented, respectively.

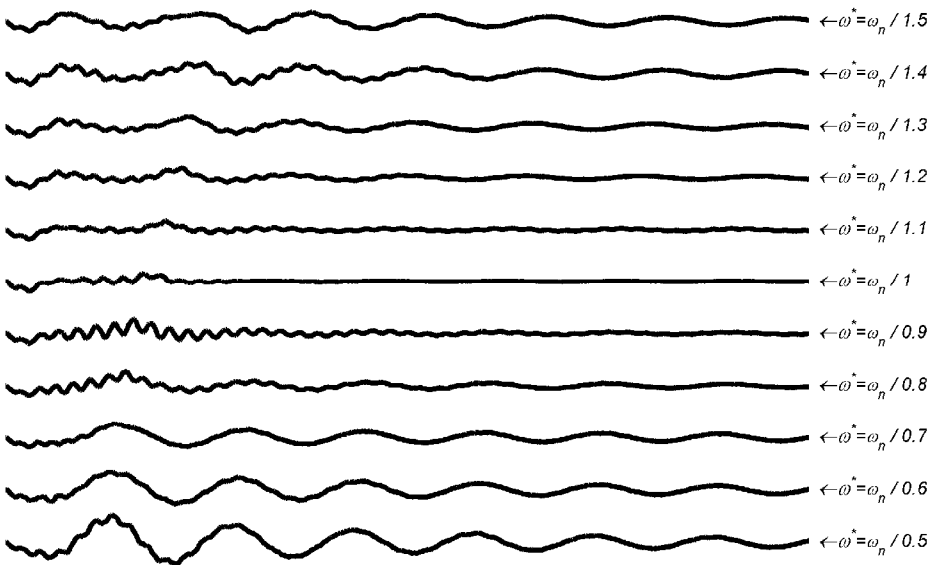

Figure 4.88. Tip deflection of different predicted natural frequencies for the MIS-ZVD-6 shaper related experimental results

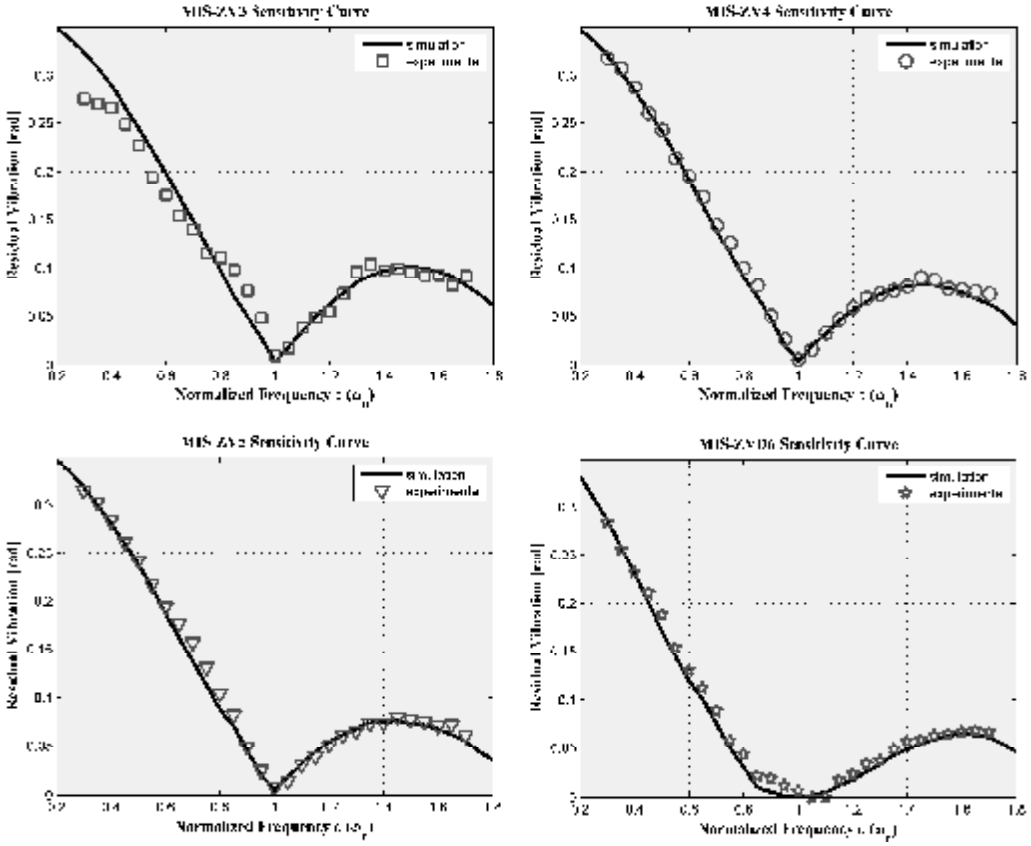

Figure 4.89. Theoretical and experimental sensitivity curves for the Modified Input Shapers

Theoretical and experimental sensitivity plots for three to five-impulse MIS-ZV shapers and six impulse MIS-ZVD shaper are shown in Figure 4.89. For each shaper, the experimental results closely follow the theoretical results. One can see that the additional impulses only provide a minimal increase in shaper insensitivity for MIS-ZV shapers. The 6-Impulse MISZVD shaper, however, exhibits good robustness to modelling errors in natural frequency. It should be noted that a 4-impulse MISZVD shaper is the traditional ZVD shaper. The performance of MISZV stands between ZV and ZVD input shapers. The travelling time and robustness properties of the MISZV methods stand in between ZV and ZVD methods. Each additional impulse to the reference command improves the robustness performance while extending the travelling time.

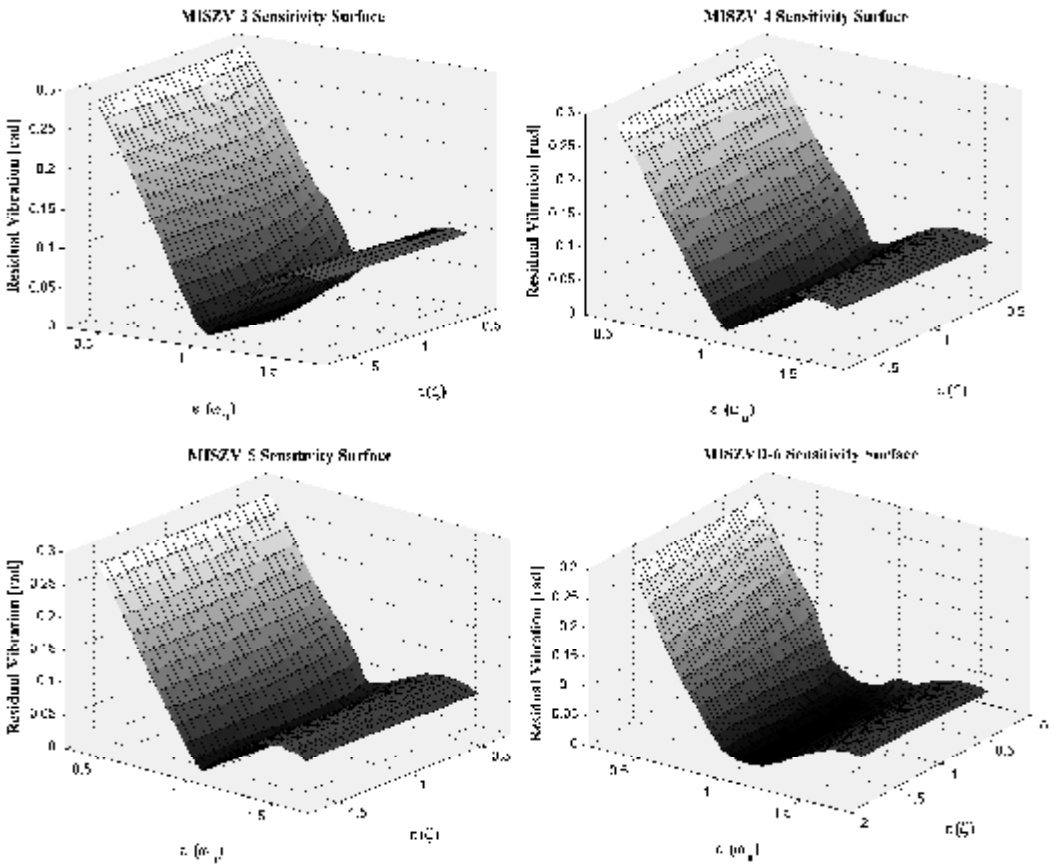

Figure 4.90. Robustness of the system to uncertainties in the mode frequencies and damping ratios for the MIS-ZV3, MIS-ZV4, MIS-ZV5 and MIS-ZVD6 Shapers

In Figure 4.90, the variation of the residual vibration is presented against estimation error in natural frequency and damping ratio of the system for various MIS techniques. It can clearly be seen that the variation of estimation error (or increasing uncertainty) of damping ratio has relatively reduced the effect on the residual vibration of the system. Therefore, the uncertainties of the damping ratio do not play an important role in affecting the behaviour of the system mainly due to its very low value, i.e. ζ =0.07. On the other hand, the estimation error in natural frequency of the system appears to affect the motion of the system and the resulting residual vibration levels.

4.1.2.9. Cycloid Plus Ramped Versine Plus Ramp (CPRVPR) Function

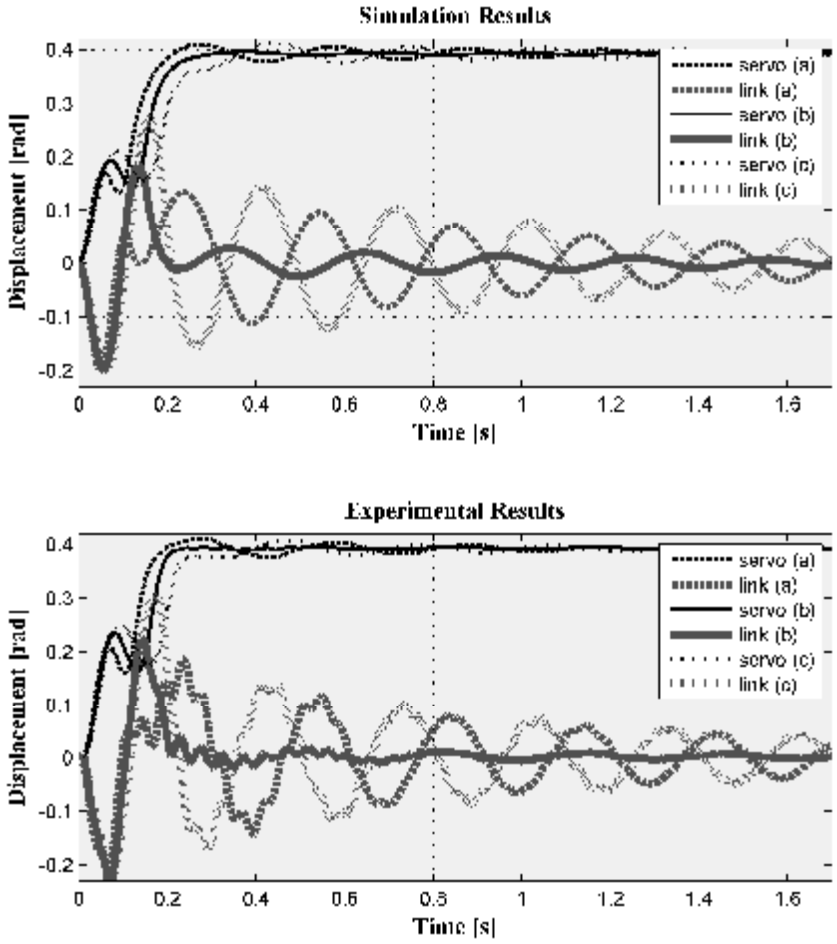

Figure 4.91. CPRVPR reference function with experimental and simulation results for (a) -%25, (b) %0, (c) +%25 estimation error of natural frequency

In Figures 4.91, the simulation and experimental results of CPRVPR reference function are illustrated. In the figure, estimation error of ±%25 is introduced to natural frequency of the system used in calculation of the input signals. Figure 4.91 is plotted with estimation errors of (a) -%25, (b) %0, (c) +%25, respectively. The length of the CPRVPR reference function is the same as that of the ZV shaper, half damped cycle of vibration. In Figure 4.91, it can be seen that, the estimation error causes increasing residual vibrations of tip deflection ranging from 0.0961 to 0.1432 rad. It can be seen that increasing error in estimation of the natural frequency of the system causes increasing residual vibrations. These results are also validated in Figure 4.92 and 4.93 where tip deflection of different predicted natural frequencies and related sensitivity curves are presented, respectively.

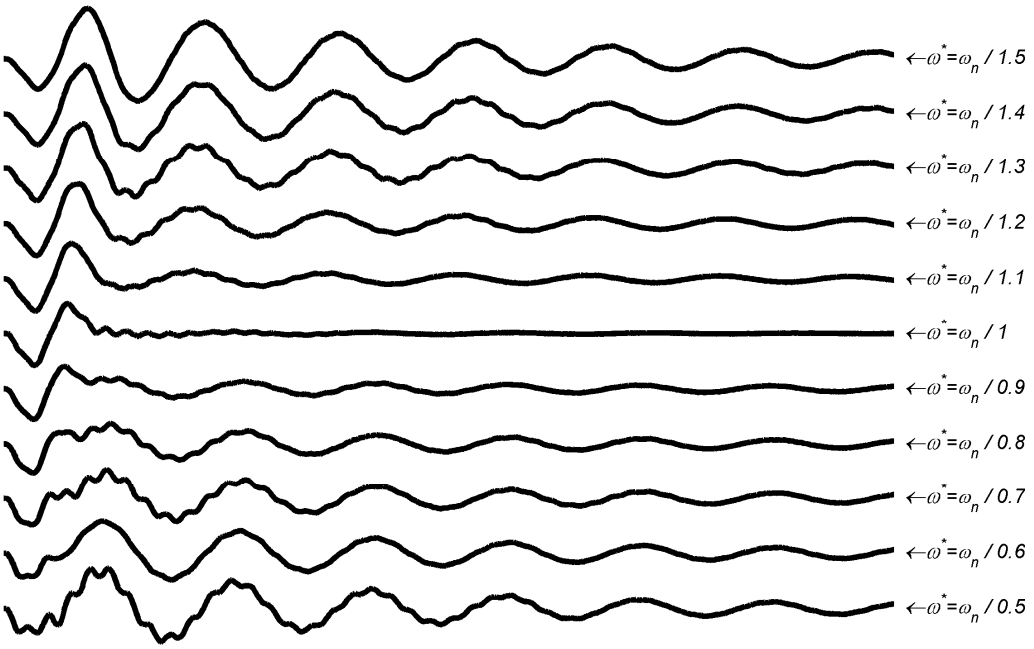

Figure 4.92. Tip deflection of different predicted natural frequencies for CPRVPR reference function related experimental results

The theoretical and experimental sensitivity curves for the CPRVPR reference function are shown in Figure 4.93. The experimental results closely match those predicted by the theoretical study. Figure 4.93 shows that the vibration amplitude increases rapidly as the estimated frequency deviates from the actual system frequency. The length of the CPRVPR reference function is the same as that

of the ZV shaper, half damped cycle of vibration. However, the ZV shaper has slightly more robust to modelling errors.

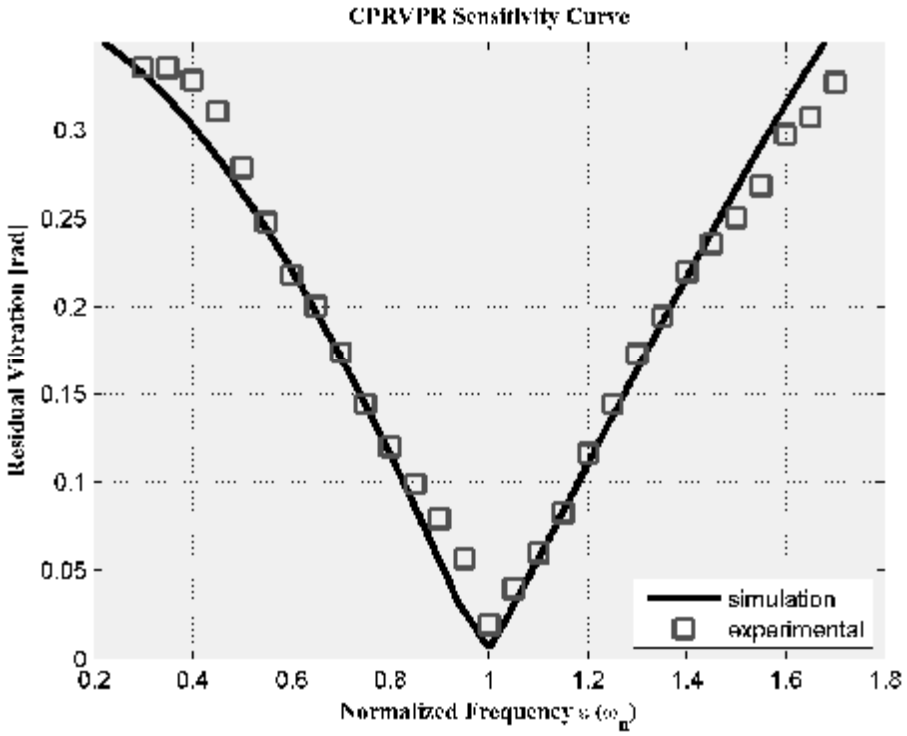

Figure 4.93. Theoretical and experimental sensitivity curves for the CPRVPR reference function

In Figure 4.94, the variation of the residual vibration is presented against estimation error in natural frequency and damping ratio of the system. It can clearly be seen that the variation of estimation error (or increasing uncertainty) of damping ratio has relatively reduced the effect on the residual vibration of the system. Therefore, the uncertainties on the damping ratio do not play an important role in affecting the behaviour of the system mainly due to its very low value, *i.e.* ζ =0.07. On the other hand, the estimation error in natural frequency of the system appears to affect the motion of the system and the resulting residual vibration levels. The cycloid plus ramped versine plus ramp (CPRVPR) reference function is very sensitive to modelling errors; a small errors in the modelling frequency leads to significant residual vibrations.

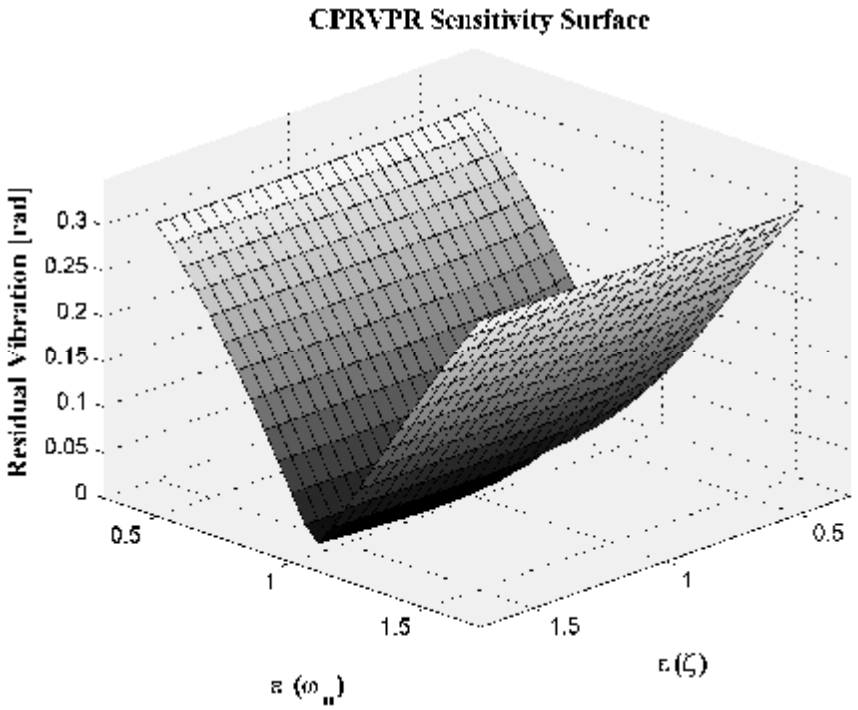

Figure 4.94. Robustness of the system to uncertainties in the mode frequencies and damping ratios for the CPRVPR reference function

4.1.2.10. Hybrid Input Shaper (HIS)

In Figures 4.95, the simulation and experimental results of Hybrid Input Shaper (HIS) are illustrated. In the figure, estimation error of ±%25 is introduced to natural frequency of the system used in calculation of the input signals. Figure 4.95 is plotted with estimation errors of (a) -%25, (b) %0, (c) +%25, respectively. The length of the Hybrid input shaper is the same as that of the ZVD shaper, one damped cycle of vibration. In Figure 4.95, it can be seen that, the estimation error causes increasing residual vibrations of tip deflection ranging from 0.038 to 0. 055 rad. It can be seen that increasing error in estimation of the natural frequency of the system causes increasing residual vibrations. These results are also validated in Figure 4.96 and 4.97 where tip deflections of different predicted natural frequencies and related sensitivity curves are presented, respectively.

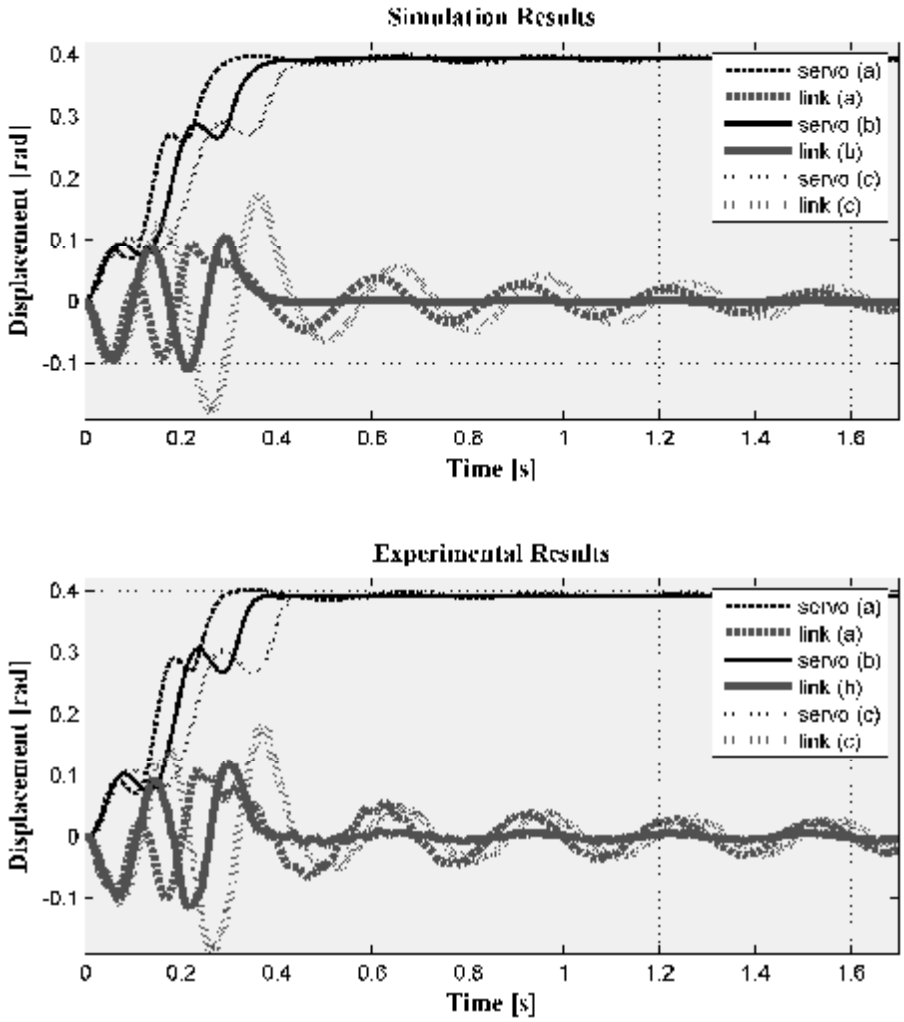

Figure 4.95. Hybrid Input Shaper with experimental and simulation results for (a) -%25, (b) %0, (c) +%25 estimation error of natural frequency

The theoretical and experimental sensitivity curves for the Hybrid Input Shaper are shown in Figure 4.97. The experimental results closely match those predicted by the theoretical study. Figure 4.96 and 4.97 shows that the Hybrid Input Shaper is much more insensitive to modelling errors than the ZV input shaper. However, the Hybrid Input Shaper has a time duration equal to one period of the vibration frequency, as opposed to the one-half period length of the ZV shaper. The length of the Hybrid input shaper is the same as that of the ZVD shaper, one damped cycle of vibration, but ZVD shaper is slightly more robust to modelling errors.

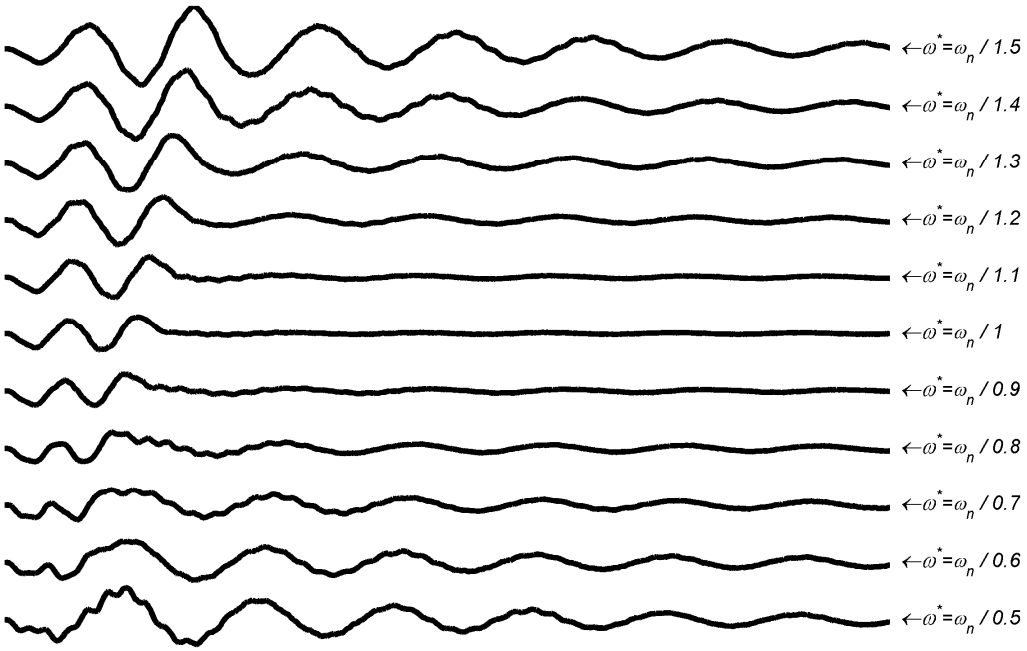

Figure 4.96. Tip deflection of different predicted natural frequencies for the Hybrid Input Shaper related experimental results

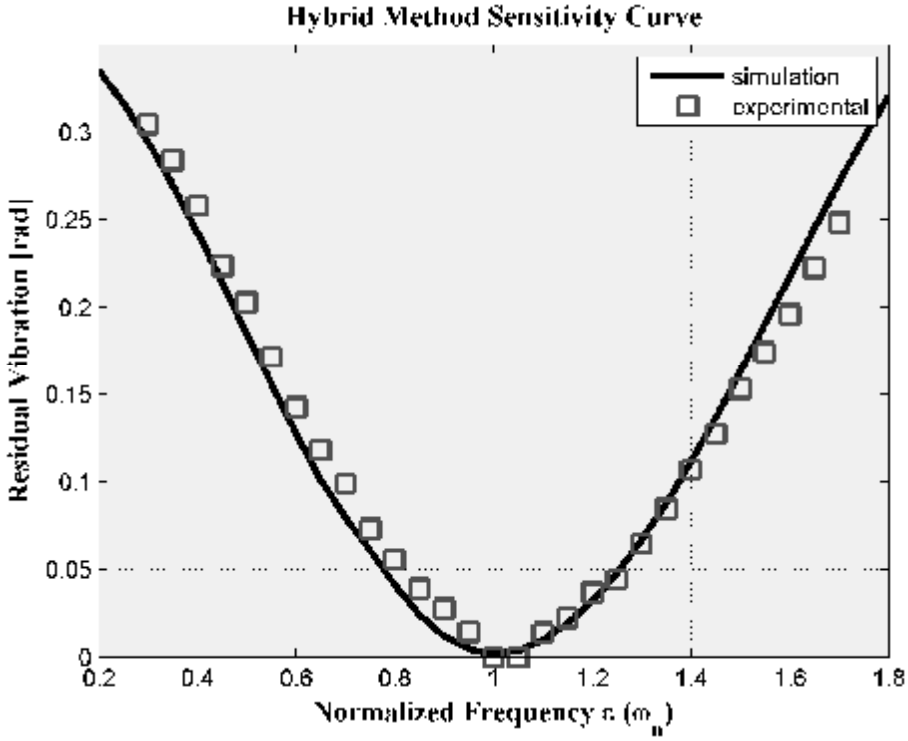

Figure 4.97. Theoretical and experimental sensitivity curves for the Hybrid Input Shaper

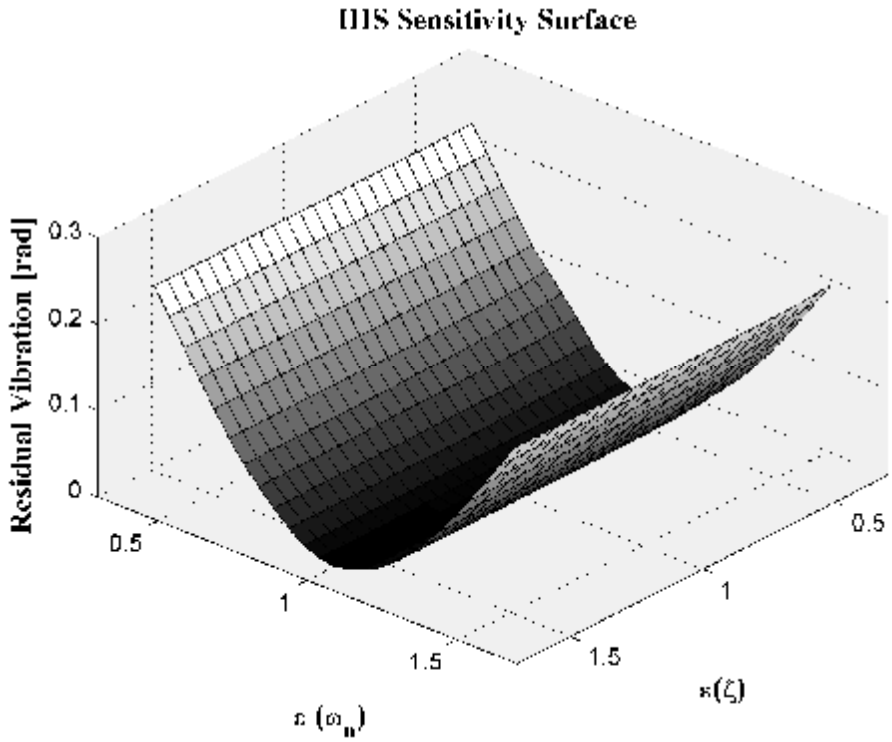

Figure 4.98. Robustness of the system to uncertainties in the mode frequencies and damping ratios for the Hybrid Input Shaper

In Figure 4.98, the variation of the residual vibration is presented against estimation error in natural frequency and damping ratio of the system. It can clearly be seen that the variation of estimation error (or increasing uncertainty) of damping ratio has relatively reduced the effect on the residual vibration of the system. Therefore, the uncertainties on the damping ratio do not play an important role in affecting the behaviour of the system due to its very low value, *i.e.* ζ =0.07. On the other hand, the estimation error in natural frequency of the system appears to affect the motion of the system and the resulting residual vibration levels.

4.1.2.11. Proposed New Input Shaping Technique: Modified Cycloid Plus Ramped Versine Plus Ramp (M-CPRVPR) Reference Function

In Figures 4.99 and 4.100, the simulation and experimental results of modified two recursions for cycloid plus ramped versine plus ramp (CPRVPR) reference function are illustrated for different travelling time. In the figures, estimation error of

±%25 is introduced to natural frequency of the system used in calculation of the input signals.

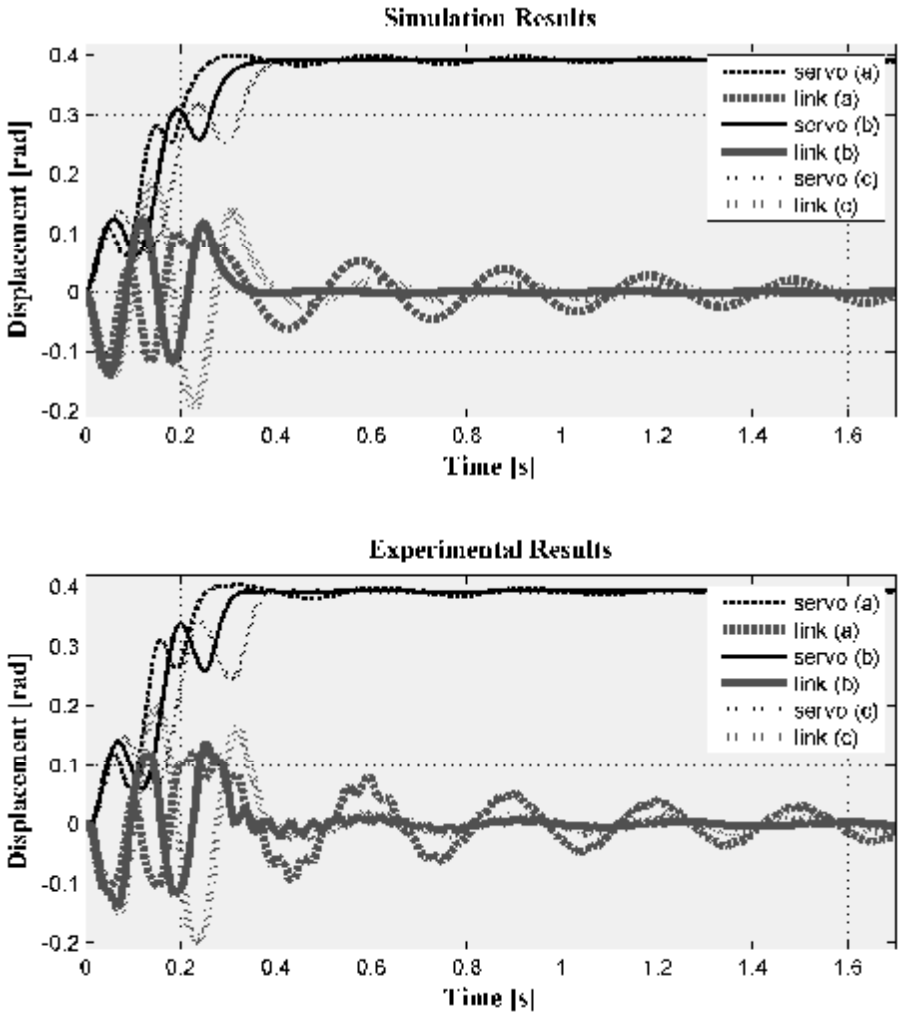

Figure 4.99. Modified CPRVPR2 function for a total travelling distance $L = \pi/8$ and travelling time of $t = 0.85T_d$ with experimental and simulation results for (a) -%25, (b) %0, (c) +%25 estimation error of natural frequency

Figure 4.99 and 4.100 are plotted with estimation errors of (a) -%25, (b) %0, (c) +%25, respectively. Theoretically, there is no travelling time restriction on the system and this is the main advantages of this reference command. In Figures 4.99 the travelling time of the M-CPRVPR2 reference function 0.85 damped cycle of vibration. In Figures 4.100 the travelling time of the M-CPRVPR reference function is the same as that of the ZVD, EI and Hybrid shaper, one damped cycle of vibration.

In Figure 4.99, it can be seen that, the estimation error causes increasing residual vibrations of tip deflection ranging from 0.0182 to 0. 0527 rad. It can be seen that increasing error in estimation of the natural frequency of the system causes increasing residual vibrations. These results are also validated in Figure 4.101 and 4.103 where tip deflections of different predicted natural frequencies and related sensitivity curves are presented, respectively.

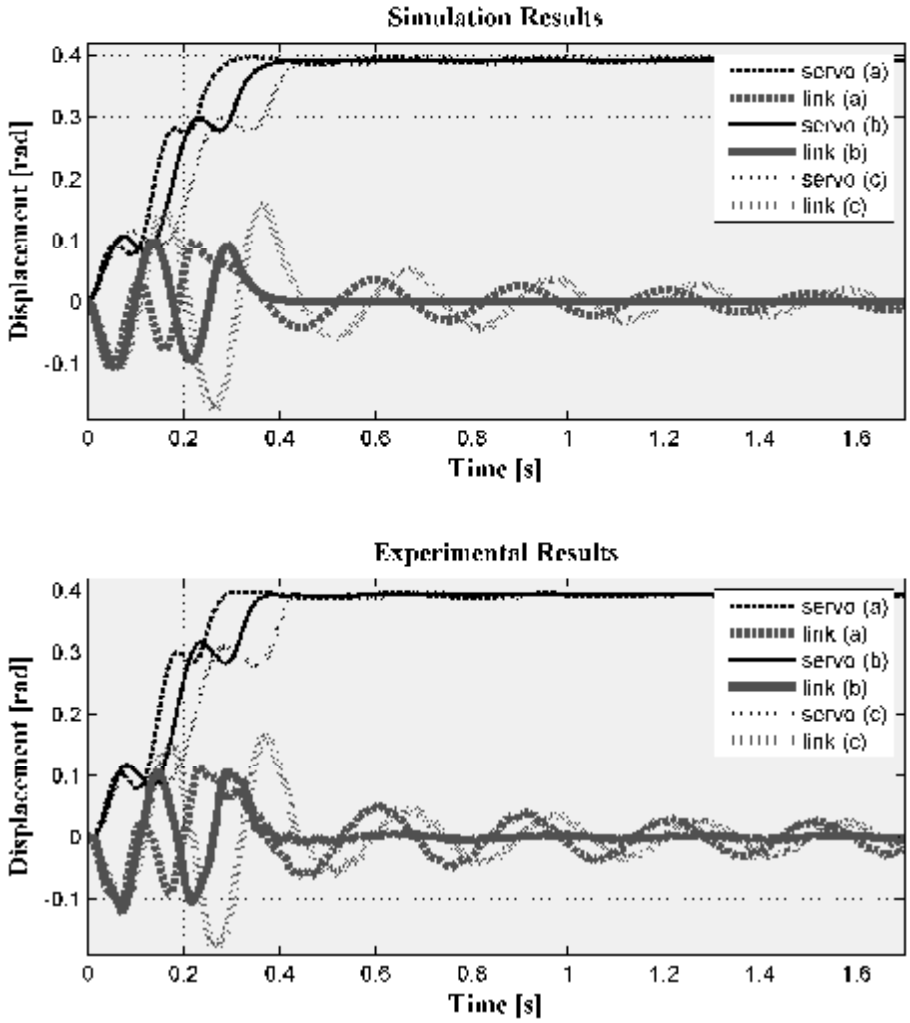

Figure 4.100. Modified CPRVPR2 function for a total travelling distance $L = \pi/8$ and travelling time of $t = T_d$ with experimental and simulation results for (a) -%25, (b) %0, (c) +%25 estimation error of natural frequency

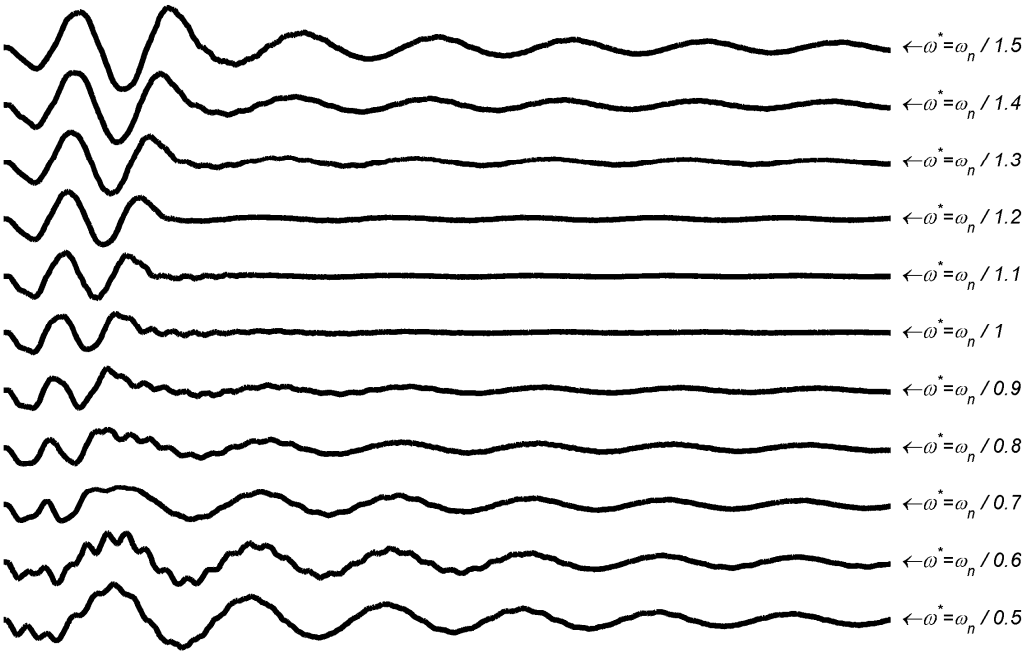

Figure 4.101. Tip deflection of different predicted natural frequencies for recursion of M-CPRVPR2 for a total travelling distance $L=\pi/8$ and travelling time of $t=0.85T_d$ related experimental results

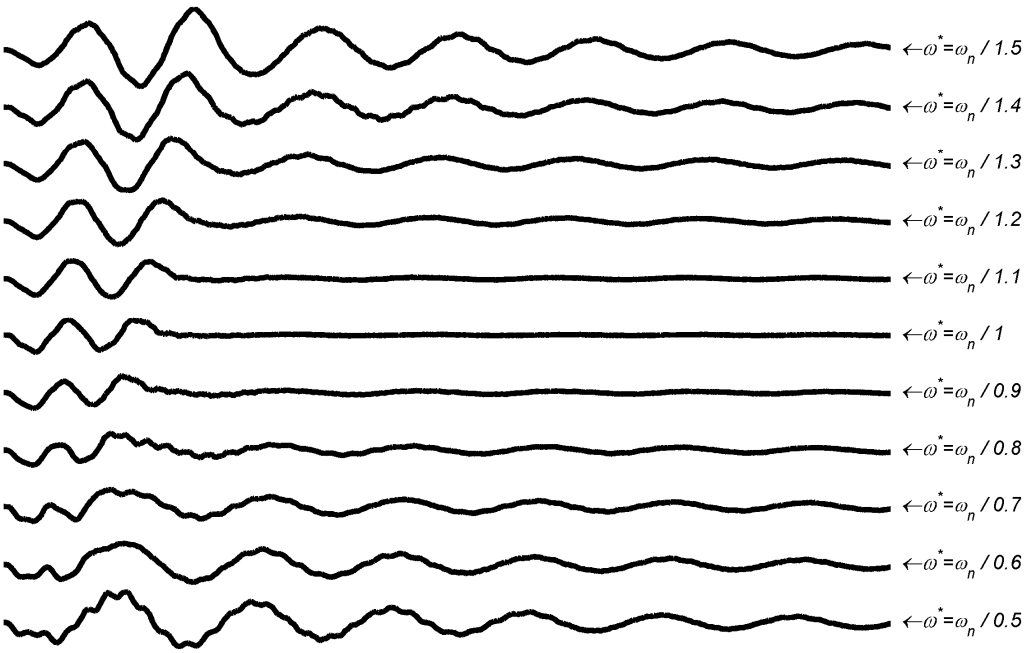

Figure 4.102. Tip deflection of different predicted natural frequencies for recursion of M-CPRVPR2 for a total travelling distance $L=\pi/8$ and travelling time of $t=T_d$ related experimental results

In Figure 4.100, it can be seen that, the estimation error causes increasing residual vibrations of tip deflection ranging from 0.0354 to 0. 0501 rad. It can be seen that increasing error in estimation of the natural frequency of the system causes increasing residual vibrations. These results are also validated in Figure 4.102 and 4.103 where tip deflections of different predicted natural frequencies and related sensitivity curves are presented, respectively.

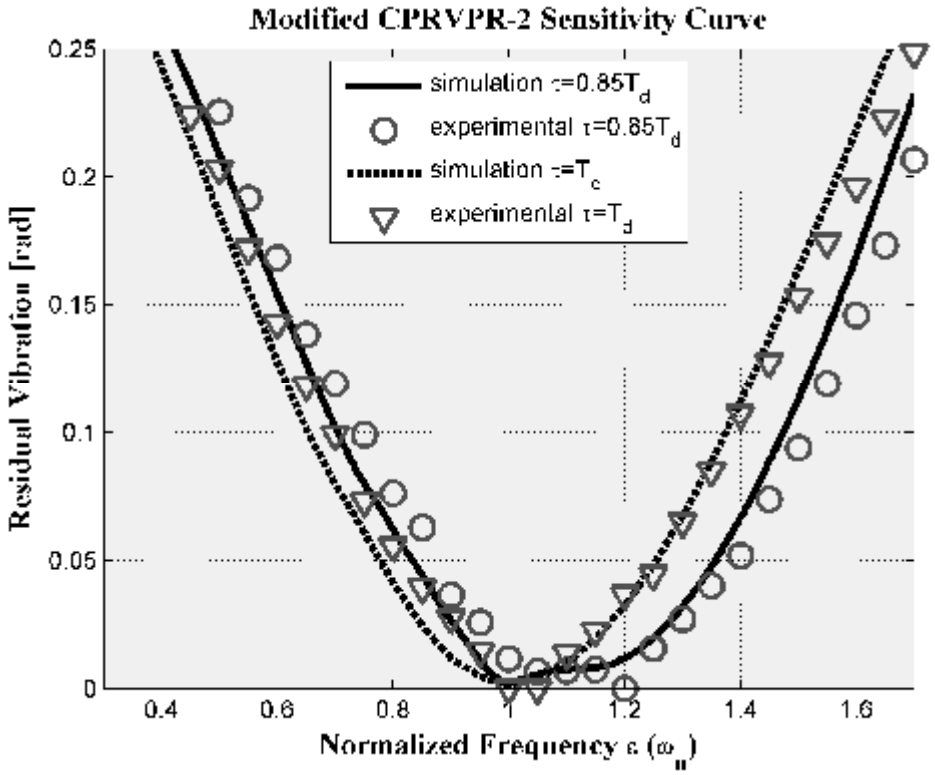

Figure 4.103. Theoretical and experimental sensitivity curves for the Modified CPRVPR2 reference function for different travelling times

The theoretical and experimental sensitivity curves of the Modified CPRVPR2 reference function for different travelling time are shown in Figure 4.103. The experimental results closely match those predicted by the theoretical study. The Modified CPRVPR2 reference function has a time duration equal to 0.85 period of the vibration frequency, as opposed to the one period length of the ZVD shaper. Theoretically, there is no travelling time restriction on the system and this is the main advantages of this reference command. Figure 4.103 shows that the Modified

CPRVPR2 reference function is more insensitive to modelling errors than the ZVD shaper.

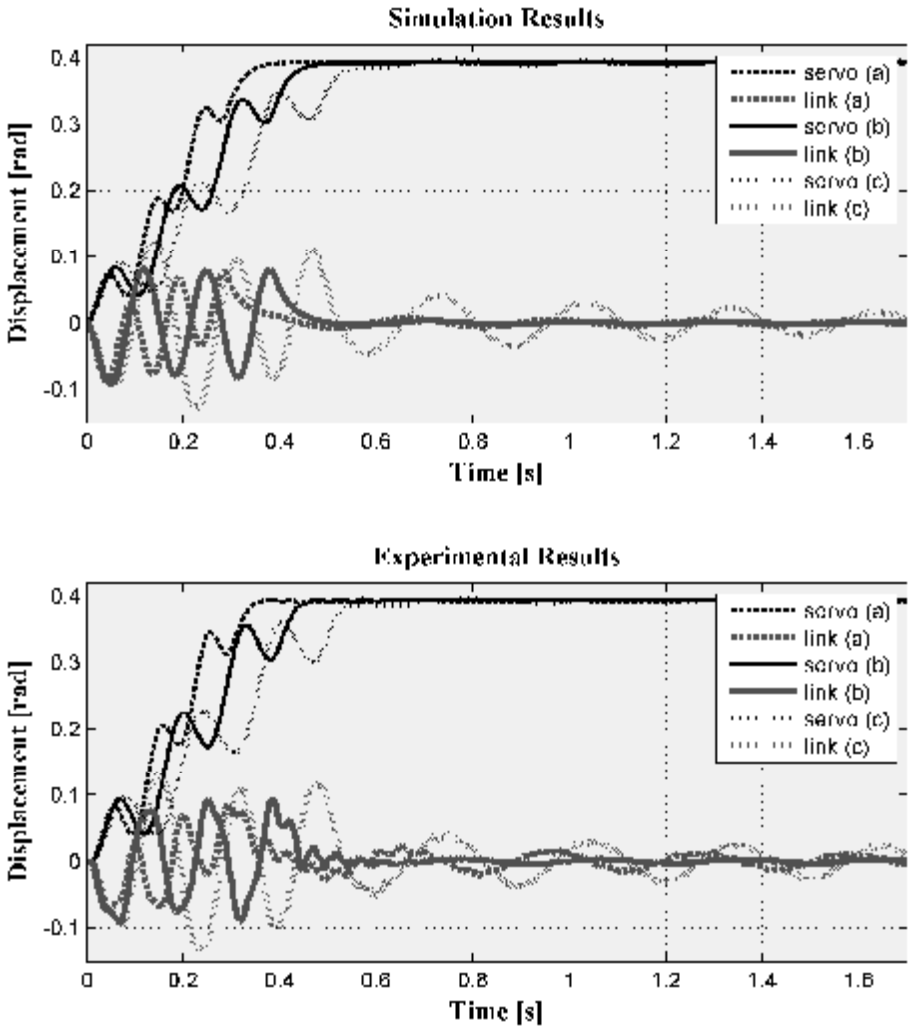

Figure 4.104. Modified CPRVPR3 function for a total travelling distance $L = \pi/8$ and travelling time of $t = 1.275T_d$ with experimental and simulation results for (a) -%25, (b) %0, (c) +%25 estimation error of natural frequency

In Figures 4.104 and 4.105, the simulation and experimental results of modified three recursions for cycloid plus ramped versine plus ramp (M-CPRVPR3) reference function are illustrated for different travelling time. In the figures, estimation error of ±%25 is introduced to natural frequency of the system used in calculation of the input signals. Figure 4.104 and 4.105 are plotted with estimation errors of (a) -%25,

(b) %0, (c) +%25, respectively. Theoretically, there is no travelling time restriction on the system and this is the main advantages of this reference command. In Figures 4.104 the travelling time of the M-CPRVPR3 reference function 1.275 damped cycle of vibration.

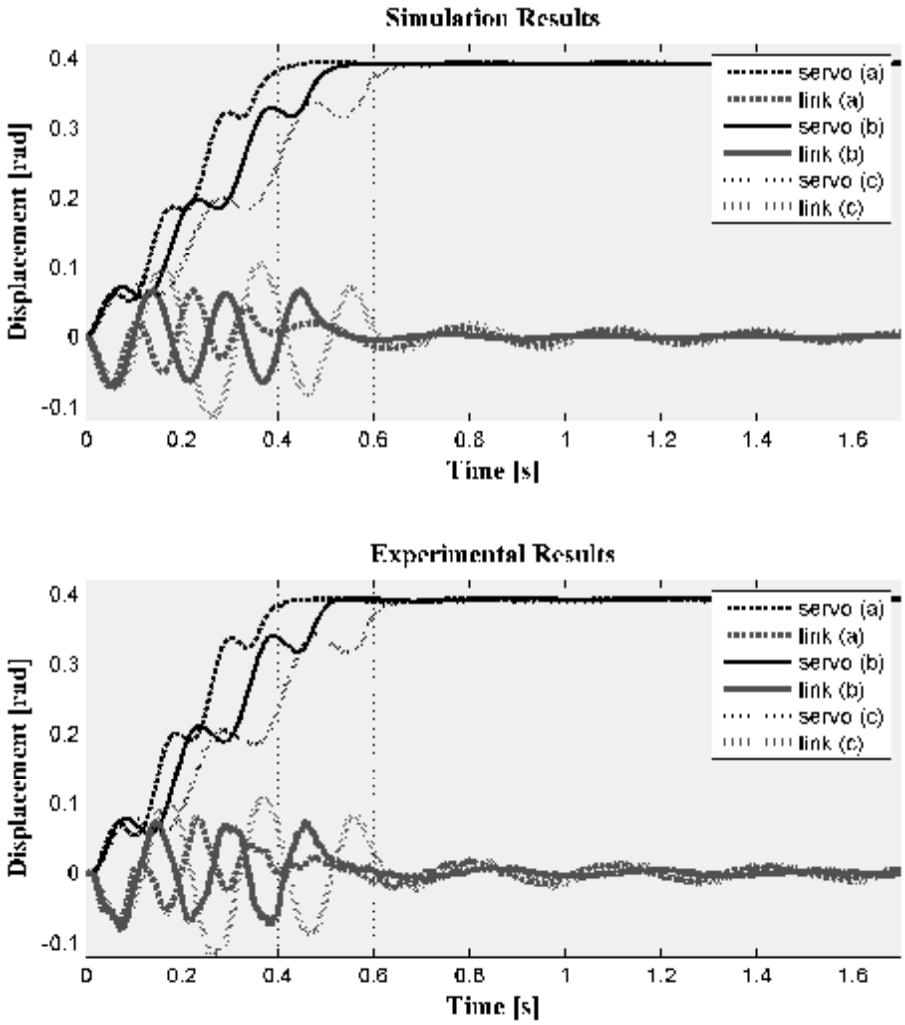

Figure 4.105. Modified CPRVPR3 function for a total travelling distance $L = \pi/8$ and travelling time of $t = 1.5T_d$ with experimental and simulation results for (a) -%25, (b) %0, (c) +%25 estimation error of natural frequency

In Figure 4.105 the travelling time of the M-CPRVPR3 reference function is the same as that of the ZVDD and 2 Hump EI Shaper, one and a half damped cycle of vibration.

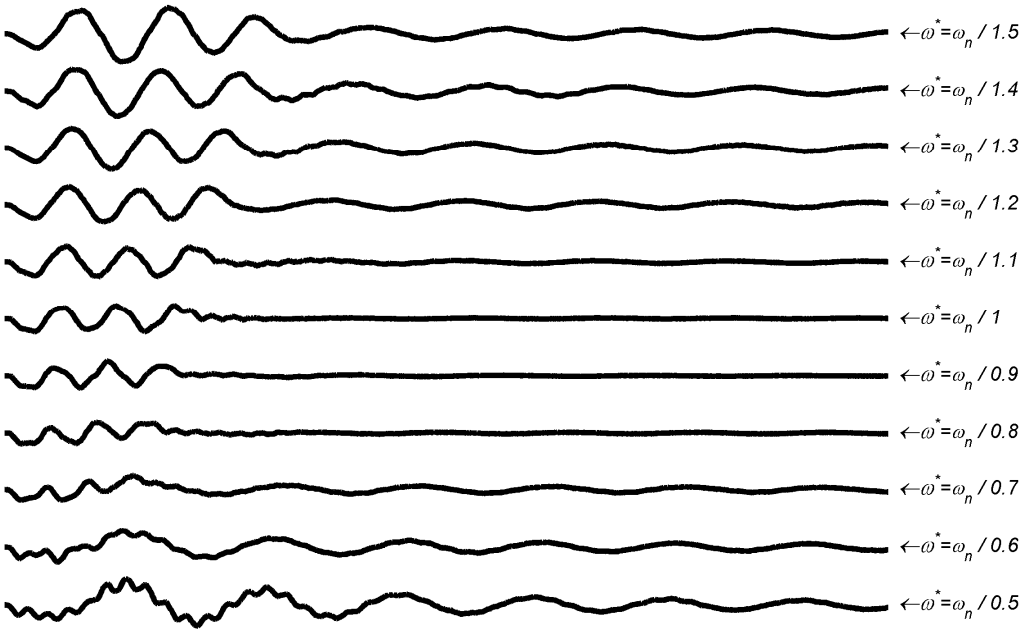

Figure 4.106. Tip deflection of different predicted natural frequencies for recursion of M-CPRVPR3 for a total travelling distance $L = \pi / 8$ and travelling time of $t = 1.275 T_d$ related experimental results

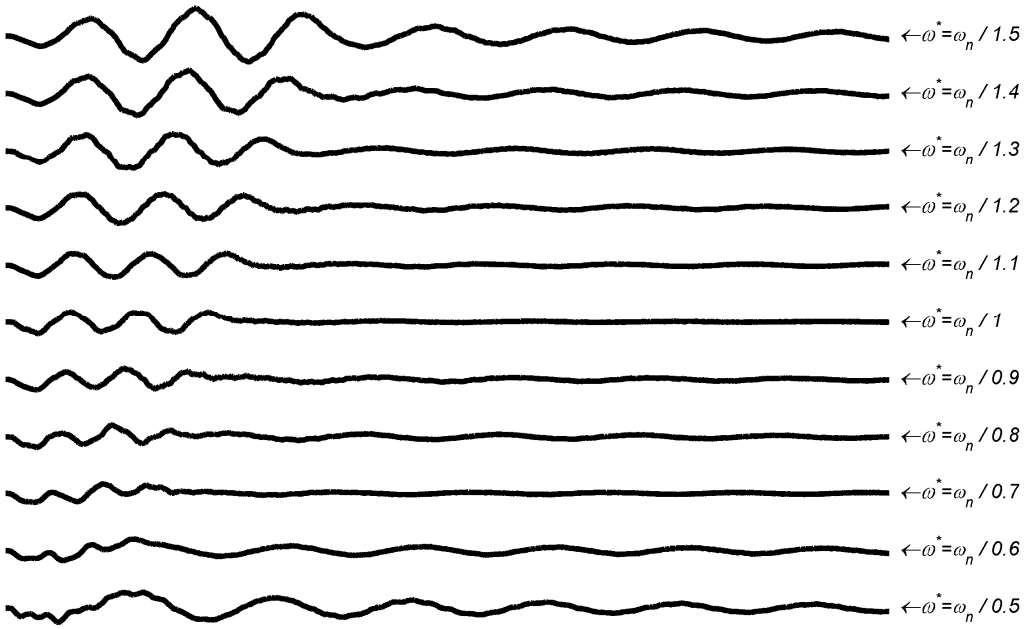

Figure 4.107. Tip deflection of different predicted natural frequencies for recursion of M-CPRVPR3 for a total travelling distance $L = \pi / 8$ and travelling time of $t = 1.5 T_d$ related experimental results

In Figure 4.104, it can be seen that, the estimation error causes increasing residual vibrations of tip deflection ranging from 0.0067 to 0. 041 rad. It can be seen

that increasing error in estimation of the natural frequency of the system causes increasing residual vibrations. These results are also validated in Figure 4.106 and 4.108 where tip deflections of different predicted natural frequencies and related sensitivity curves are presented, respectively. In Figure 4.105, it can be seen that, the estimation error causes increasing residual vibrations of tip deflection ranging from 0.0147 to 0. 0172 rad. It can be seen that increasing error in estimation of the natural frequency of the system causes slightly increasing residual vibrations. These results are also validated in Figure 4.107 and 4.108 where tip deflections of different predicted natural frequencies and related sensitivity curves are presented, respectively.

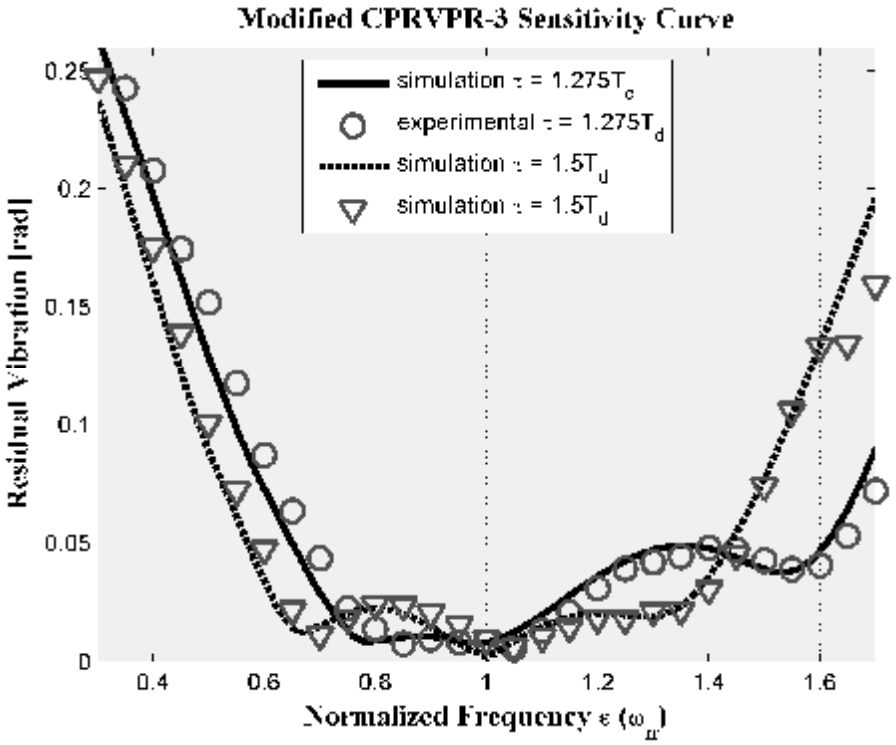

Figure 4.108. Theoretical and experimental sensitivity curves for the Modified CPRVPR3 reference function for different travelling times

The theoretical and experimental sensitivity curves of the Modified CPRVPR3 reference function for different travelling time are shown in Figure 4.108. The experimental results closely match those predicted by the theoretical study. The Modified CPRVPR3 reference function has a time duration equal to 1.275 period of the vibration frequency, as opposed to the one and a half period length of the ZVDD

shaper. Theoretically, there is no travelling time restriction on the system and this is the main advantages of this reference command.

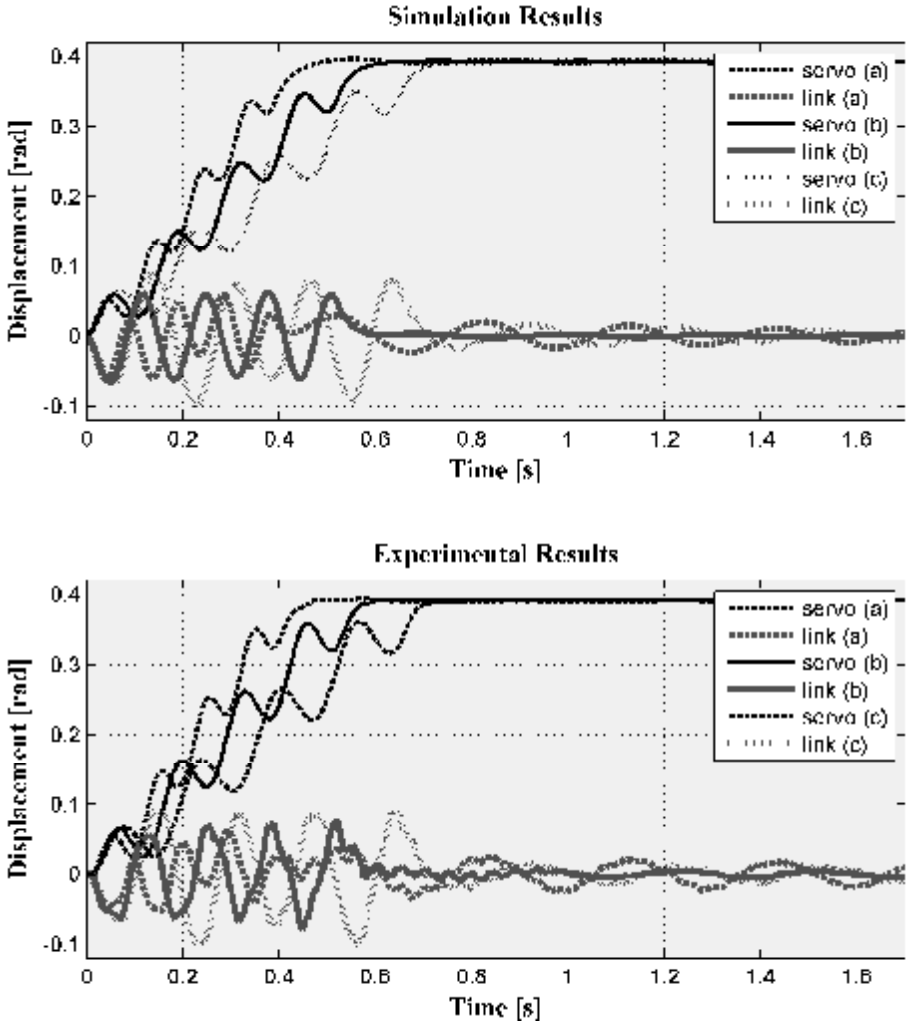

Figure 4.109. Modified CPRVPR4 function for a total travelling distance $L = \pi/8$ and travelling time of $t = 1.7T_d$ with experimental and simulation results for (a) -%25, (b) %0, (c) +%25 estimation error of natural frequency

In Figures 4.109 and 4.110, the simulation and experimental results of modified four recursions for cycloid plus ramped versine plus ramp (M-CPRVPR4) reference function are illustrated for different travelling time. In the figure, estimation error of ±%25 is introduced to natural frequency of the system used in calculation of the input signals. Figure 4.109 and 4.110 are plotted with estimation errors of (a) -%25,

(b) %0, (c) +%25, respectively. Theoretically, there is no travelling time restriction on the system and this is the main advantages of this reference command. In Figures 4.109 the travelling time of the M-CPRVPR4 reference function 1.7 damped cycle of vibration. In Figures 4.110 the travelling time of the M-CPRVPR4 reference function is the same as that of the ZVDDD and 3 Hump EI Shaper, two damped cycle of vibration.

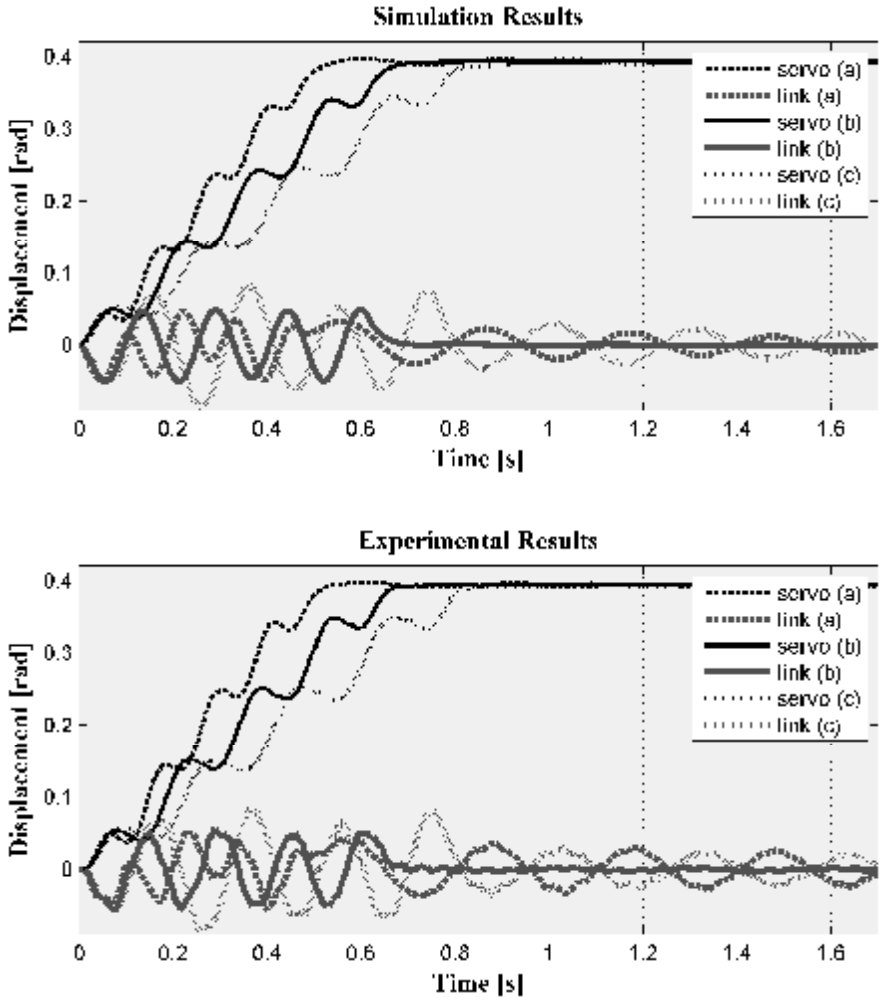

Figure 4.110. Modified CPRVPR4 function for a total travelling distance $L = \pi / 8$ and travelling time of $t = 2T_d$ with experimental and simulation results for (a) -%25, (b) %0, (c) +%25 estimation error of natural frequency

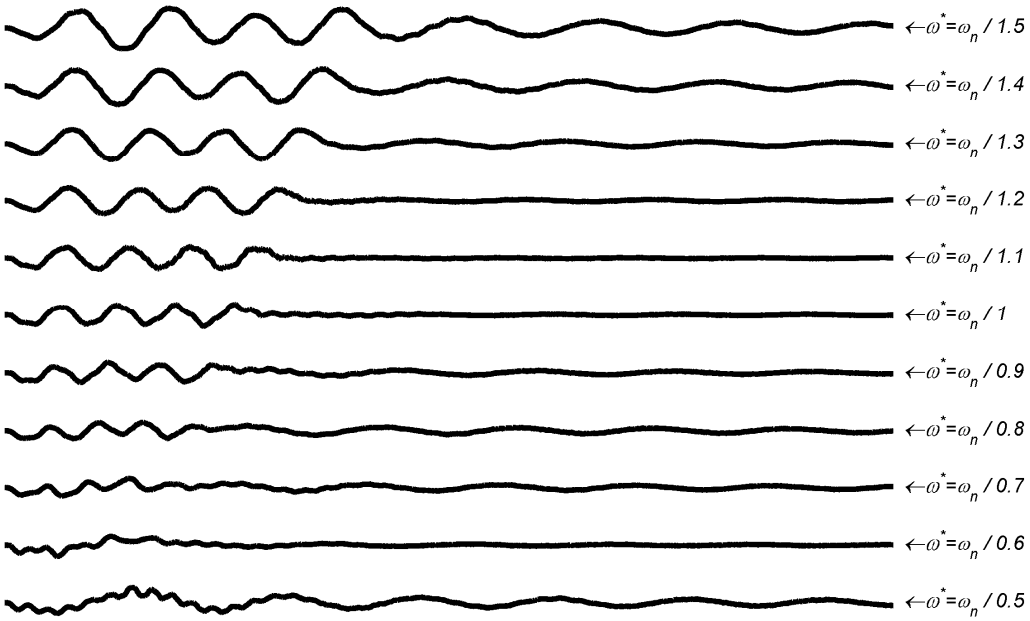

Figure 4.111. Tip deflection of different predicted natural frequencies for recursion of M-CPRVPR4 for a total travelling distance $L = \pi / 8$ and travelling time of $t = 1.7T_d$ related experimental results

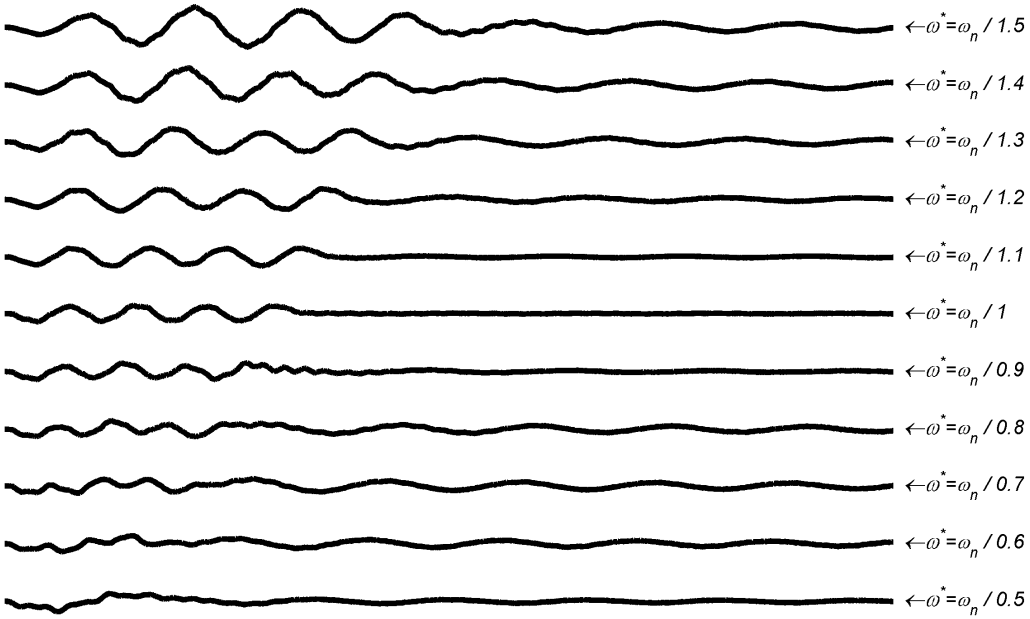

Figure 4.112. Tip deflection of different predicted natural frequencies for recursion of M-CPRVPR4 for a total travelling distance $L = \pi / 8$ and travelling time of $t = 2T_d$ related experimental results

In Figure 4.109, it can be seen that, the estimation error causes increasing residual vibrations of tip deflection ranging from 0.0159 to 0. 0203 rad. It can be seen

that increasing error in estimation of the natural frequency of the system causes slightly increasing residual vibrations. These results are also validated in Figure 4.111 and 4.113 where tip deflections of different predicted natural frequencies and related sensitivity curves are presented, respectively. In Figure 4.110, it can be seen that, the estimation error causes increasing residual vibrations of tip deflection ranging from 0.0225 to 0. 0297 rad. It can be seen that increasing error in estimation of the natural frequency of the system causes slightly increasing residual vibrations. These results are also validated in Figure 4.112 and 4.113 where tip deflections of different predicted natural frequencies and related sensitivity curves are presented, respectively.

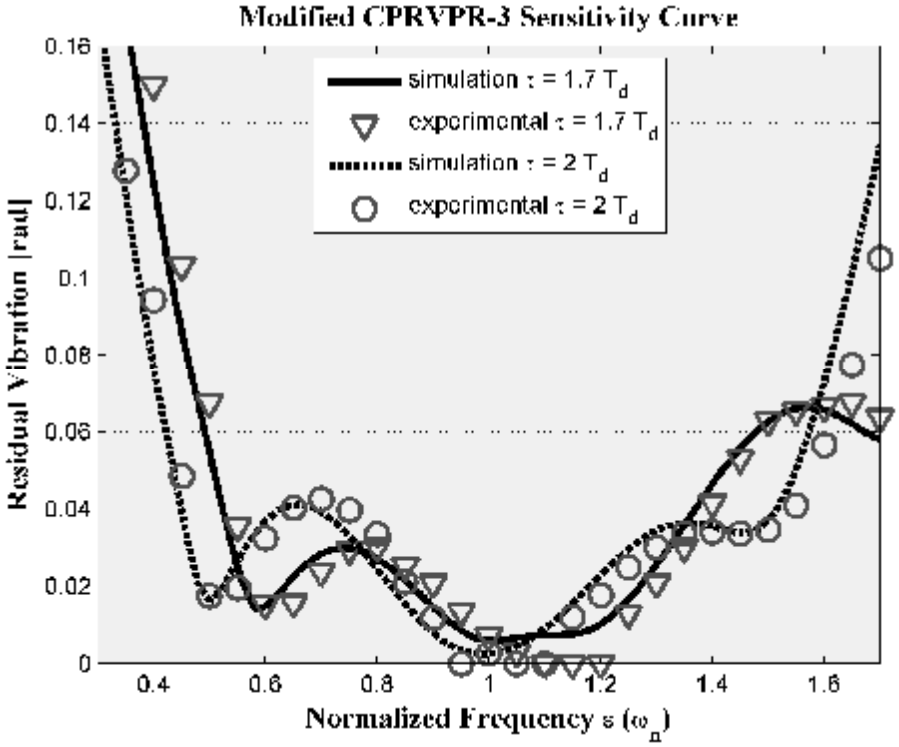

Figure 4.113. Theoretical and experimental sensitivity curves for the Modified CPRVPR4 reference function for different travelling times

The theoretical and experimental sensitivity curves of the Modified CPRVPR4 reference function for different travelling time are shown in Figure 4.113. The experimental results closely match those predicted by the theoretical study. The Modified CPRVPR4 reference function has a time duration equal to 1.7 period of the vibration frequency, as opposed to the two period length of the ZVDDD shaper.

Theoretically, there is no travelling time restriction on the system and this is the main advantages of this reference command.

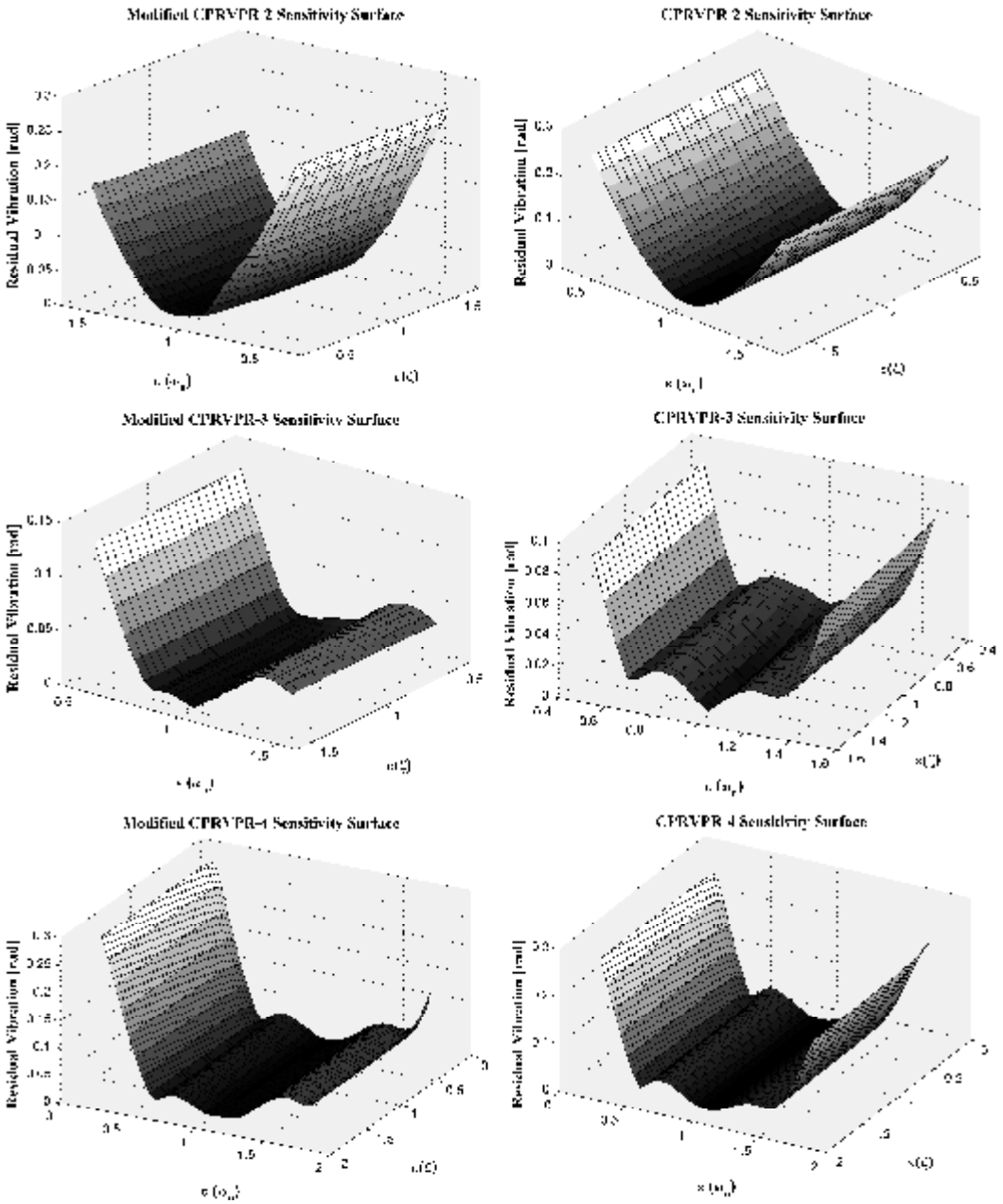

Figure 4.114. Robustness of the system to uncertainties in the mode frequencies and damping ratios for the various M-CPRVPR reference functions

In Figure 4.114., the variation of the residual vibration is presented against estimation error in natural frequency and damping ratio of the system for the various

M-CPRVPR reference functions. It can clearly be seen that the variation of estimation error (or increasing uncertainty) of damping ratio has relatively reduced the effect on the residual vibration of the system. Therefore, the uncertainties on the damping ratio do not play an important role in affecting the behaviour of the system mainly due to its very low value, *i.e.* ζ =0.07. On the other hand, the estimation error in natural frequency of the system appears to affect the motion of the system and the resulting residual vibration levels.

4.2. Discussions

In the previous sections the simulation and the experimental results of some selected positive and smoothly shaped reference commands and novel robust command shaping techniques are presented. Further details on the presented methods are available by referring to the Chapter 2 where some additional information as well relevant references are provided. The successful implementation of the presented input shaping methods requires accurate estimation or determination of the natural frequency and the damping ratio of the system in concern. However, the mathematical models of any flexible system cannot be modelled perfectly. The variations or change of the system parameters influences the shaped signal and also the system response. Therefore, the robustness of shaped signal to modelling uncertainty is an important performance comparison tool for command shaping methods. For almost all the robust shaping methods, the shaper duration (and as a result, command rise time) increases with the increasing robustness performance. However, this compromise is not consistent for all shaping methods. Some robust shaping methods provide robustness more efficiently, in terms of shaper duration.

In this section, the presented methods are compared for length of travelling time, their robustness for system parameter estimation errors and efficiency of insensitivity (Vaughan et al., 2007).

Table 4.1. Performance criteria for comparison of positive input shaper

Method	**Duration T_d (cycle)**	**Robustness 5%**	**Efficiency of insensitivity 5%**	**Robustness 10%**	**Efficiency of insensitivity 10%**
ZV	0.5	0.063	0.126	0.1278	0.2556
ZVD	1	0.2876	0.287	0.4098	0.4098
ZVDD	1.5	0.480	0.32	0.6143	0.4095
ZVDDD	2	0.627	0.3135	0.7602	0.3801
EI	1	0.40	0.4	0.5604	0.5604
2HEI	1.5	0,732	**0.488**	0.9097	**0.6064**
3HEI	2	0.97	0.485	1.1337	0,5668
MISZV-3	0.665	0.082	0.124	0.1673	0,251
MISZV-4	0.749	0.090	0.121	0.1828	0.244
MISZV-5	0,799	0.094	0.1176	0.1914	0.2395
MISZVD4	1	0.287	0.287	0.4098	0.4098
MISZVD6	1.16	0.332	0.286	0.4824	0.4158

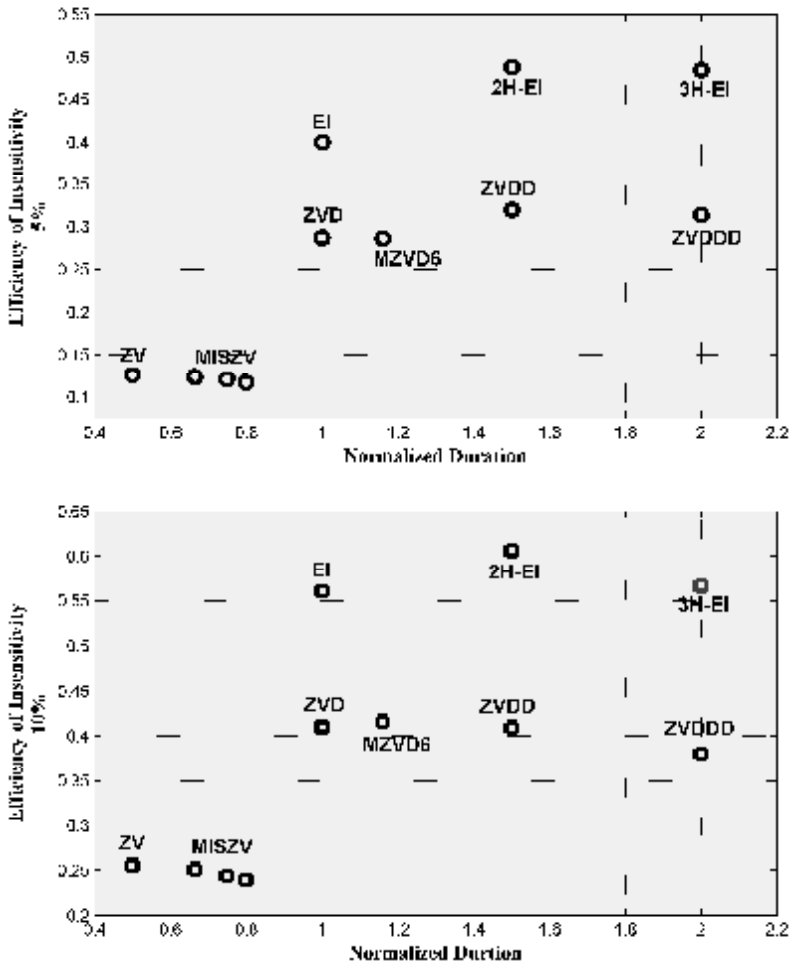

Figure 4.115. Efficiency of insensitivity comparison for positive input shapers

In Table 4.1 and Figure 4.115, the performance evaluation criteria for positive input shapers are provided. From the details provided in Table 4.1, it can be concluded that;

- The robust shapers typically have longer travelling times that leads to slower system response. This creates a compromise between shaper robustness and the rise/travelling time.
- The increasing travelling time appears to cause an increasing robustness that is mostly input shaping method dependent. Hence, the compromise on increasing travelling time gains increasing robustness that varies for each method. In other words, the efficiency of insensitivity varies from one method to another.
- The ZV shaper is very sensitive to modelling errors; a small errors in the modelling frequency leads to significant residual vibrations.
- The ZVD shaper has considerably more robustness to modelling errors than ZV input shaping method. It is evident by noting that the width of the ZVD robustness curve is much larger than the width of the ZV robustness curve.
- The additional insensitivity of the ZVD shaper incurs a time penalty; the ZVD shaper is longer than the ZV shaper by one half period of the vibration. This means that a shaped command generated with a ZVD shaper will be one half period of vibration longer than a ZV shaped command. In most cases, this is a small price to pay for the large increase in the robustness.
- The performance of MISZV stands between ZV and ZVD. The travelling time and robustness properties of the MISZV method stand in between ZV and ZVD methods. Each additional impulse to the reference command improves the robustness performance while extending the travelling time.
- The EI shaper is essentially the same length as the ZVD shaper, but it is considerably more robust. The two-hump EI has the same duration as the ZVDD, while the three-hump EI and ZVDDD have the same durations.

However, the multi hump EI shapers have much more robustness compared to derivative methods (ZVD, ZVDD, ZVDDD).

- Performances of the techniques are compared for efficiency of insensitivity for which it is shown that two hump extra insensitive (2HEI) seems to be the best of all.

Table 4.2. Performance criteria for comparison of negative input shapers

Method	**Duration T_d (cycle)**	**Robustness 5%**	**Efficiency of insensitivity 5%**
PS-ZV	0.29	0.054	0.186
UM-ZV	0.33	0.0548	0.166
PS-ZVD	0.67	0.2535	0.3783
UM-ZVD	0.73	0.2585	0.3541
PS-EI	0.67	0.3481	0.5119
UM-EI	0.73	0.3559	0.4875
PS-2HEI	1.12	0.6437	**0.5747**
UM-2HEI	1.18	0.659	0.5584

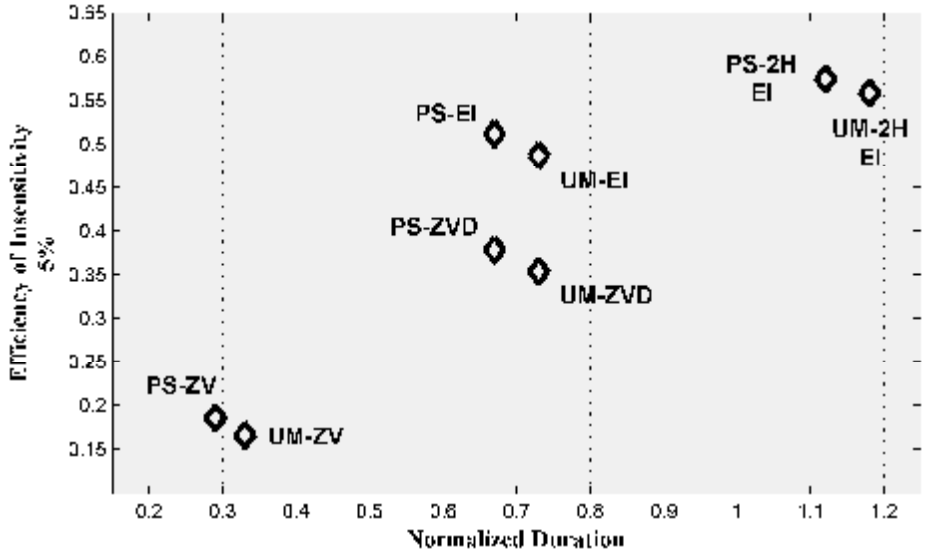

Figure 4.116. Efficiency of insensitivity comparison for negative input shapers

In Table 4.2 and Figure 4.116, the performance evaluation criteria for negative input shapers are provided. From the details provided in Table 4.2, it can be concluded that;

- A negative shaper will have slightly poorer performance than a positive shaper in the presence of modelling errors, even though they satisfy the same robustness constraints.
- It can be seen from Table 4.2 and Figure 4.116 that the time delay for the input shapers increases with increasing insensitivity. This indicates that there is a conflict between the shaper robustness and the shaper time delay.
- Performances of the techniques are compared for efficiency of insensitivity (Vaughan et al., 2007) for which it is shown that partial sum two hump extra insensitive (PS-2HEI) seems to be the best of all.

Table 4.3. Performance criteria for comparison of smoothly shaped reference commands

Method	**Duration T_d (cycle)**	**Robustness 5%**	**Efficiency of insensitivity 5%**	**Robustness 10%**	**Efficiency of insensitivity 10%**
CPRVPR	0.5	0.0585	0.117	0.1175	0.235
HIS	1	0.2754	0.2754	0.3927	0.3927
M-CPRVPR2	0.85	0.3392	**0.399**	0.4491	0.5283
M-CPRVPR2	1	0.2755	0.2755	0.3927	0.3927
M-CPRVPR3	1.275	0.3713	0.2912	0.494	0.3874
M-CPRVPR3	1.5	0.4162	0.2774	0.8233	**0.5488**
M-CPRVPR4	1.7	0.4521	0.2659	0.7939	0.467
M-CPRVPR4	2	0.4086	0,2043	0.7057	0.3528

In Table 4.3 and Figure 4.117, the performance evaluation criteria for smoothly shaped reference commands are provided. From the details provided in Table 4.3, it can be concluded that;

- The time delay for the input shapers increases with increasing insensitivity. This indicates that there is a conflict between shaper robustness and the shaper time delay just as in the case of other input shaping methods.
- The CPRVPR reference function is very sensitive to modelling errors; a small errors in the modelling frequency leads to significant residual vibrations.

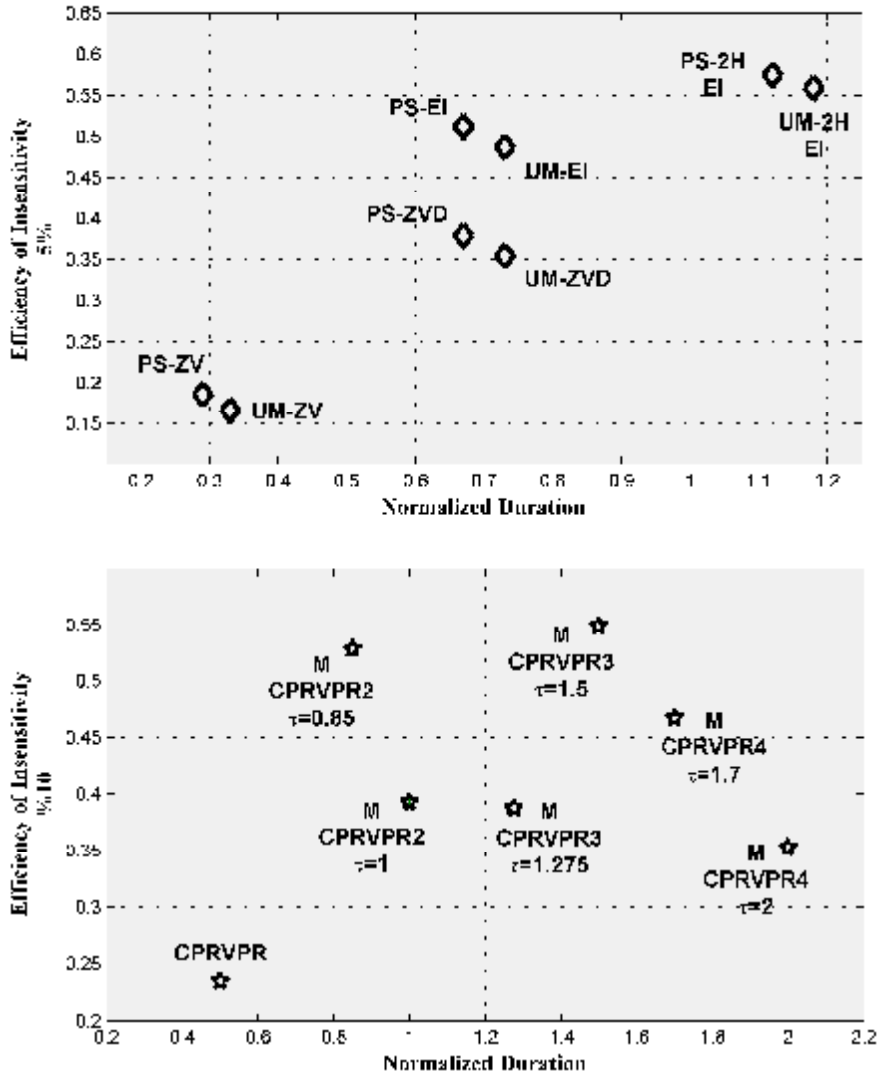

Figure 4.117. Efficiency of insensitivity comparison for smoothly shaped reference commands

- Hybrid input shaper is much more insensitive to modelling errors than the CPRVPR reference function. However, the Hybrid input shaper has a time duration equal to one period of the vibration frequency, as opposed to the one-half period length of the CPRVPR reference function.
- Performances of the techniques are compared for %5 efficiency of insensitivity for which it is shown that Modified CPRVPR2 ($\tau=0.85T_d$) reference function seems to be the best of smoothly shaped reference commands.

- The M-CPRVPR2 ($\tau=0.85T_d$) reference function almost the same efficiency of insensitivity value as the EI input shaper. The EI shaper has a time duration equal to one period of the vibration frequency, as opposed to the 0.85 period length of the M-CPRVPR2 reference function.
- Performances of the techniques are compared for %10 efficiency of insensitivity for which it is shown that Modified CPRVPR3 ($\tau =1.5T_d$) reference function seems to be the best of smoothly shaped reference commands.
- Performances of the techniques are compared for %10 efficiency of insensitivity for which it is shown that performance of Modified CPRVPR4 ($\tau=1.7T_d$) reference function stands between ZVDDD and 3HEI. The ZVDDD and 3HEI shaper has a time duration equal to 2 times the period of the vibration frequency, as opposed to the 1.7 period length of the M-CPRVPR4 reference function.
- The advantage of the proposed technique (M-CPRVPR) is that it neither limits nor increases the move time, i.e. no time limitation or time penalty. Most conventional input shaping methods, however, tend to increase the travelling time by at least a half damped period or more.
- It is shown that proposed the new technique is simple and easy to implement, and can be considered as a versatile and effective way to determine a trajectory resulting in reduced or eliminated residual vibrations of flexible systems with high robustness.

5. CONCLUSIONS AND RECOMMENDATIONS

The motion control and related studies have become one of the main subjects of robotics and other automation related research areas in recent years. In modern manufacturing industry, high speed and sensitive motion control is necessary for the high speed and high quality production. However, the high speed requirement makes the sensitive motion control difficult due to residual vibrations. Therefore, finding a balance between the speed of motion and the elimination or at least reduction of residual vibration becomes an important part of a motion control study and related practical applications.

One of the methods used to reduce or eliminate residual vibrations is to modify the input signal by using the system parameters that are known beforehand. In order to eliminate the residual vibration completely, these system parameter must be known very accurately. In real systems, achieving such accuracy may not always be possible. To address the problem and to provide a solution, in this thesis, a new residual vibration elimination method is introduced. This new method proves to be very useful especially in the case of estimated system parameters with uncertainty. s. The simulation and the experimental results show that the presented new technique is capable of handling high levels of uncertainty and able to successfully eliminate or reduce residual vibrations in flexible systems. The advantage of the proposed technique is that it neither limits nor increases the move time, i.e. no time limitation or time penalty. Most conventional input shaping methods, however, tend to increase the travelling time by at least a half of the damped system period or more. The proposed new command shaping method divides the travelling time into two or more sections and calculates the command input as two or more separate inputs, and then joins them to form the new input. In generation of each of the input signal, cycloid-plus-ramped and versine-plus-ramp functions are used. This reference input is composed of three functions. Considering the total distance to be covered within a specified time, it is divided into three parts. Each part is travelled by each of the three functions within the same travel time. Provided that the specified move time and the total distance are unchanged, the residual vibrations can be eliminated by adjusting

excursion distance of each function. Each component of input creates such oscillations that they cancel each other out. The new method allows virtually division of the motion of the system into two or more steps. Because the first step completes with almost steady motion with relatively reduced vibration levels, the other parts of the motions starts with the advantage of very little or almost no residual vibrations. Consequently, the result of the additional each part of the motion yields better performance in reducing the residual vibrations.

This study presents a review of command pre-shaping methods and investigates the compromise between rapidity of motion and shaper robustness. The reviewed methods cover almost all types of positive and negative input shapers, and smoothly shaped reference commands reported in literature. Therefore, the presented study provides almost a complete picture of the research topic for the researchers working in the area. The study is structured in a way that it provides all the necessary theoretical background and the implementation related details for each of the method presented.

The study presents theoretical and experimental results of the techniques applied to the flexible mechanical systems where the comparative study of robustness performance is also provided. In order to perform a comparison amongst the input shaping methods and the experimental results of the techniques, the previously described experimental setups and the mathematical models of the systems are used. The experimental setups are driven using each input and the resulting residual vibrations as well as the cart and the servo position are measured. The Matlab (2009a) models of the systems are also provided with the same input commands to demonstrate the correlation between the theoretical and the experimental results obtained. The simulation and the experimental results show that the proposed new technique is simple and easy to implement, and can be considered as a versatile and an effective way to determine a trajectory resulting in reduced or eliminated residual vibrations of flexible robotic systems with high robustness in the presence of system parameters uncertainty.

Many possible areas for future work lie in the development of new types of practical constraints that can be appended to this approach. For example, constraint

equations to regulate power consumption or system deflection may yield a new class of practical command profiles.

Considering that controlling of flexible link robotic systems using input shaping methods reveal that especially robotic manipulators could be made of flexible links and still very high positioning accuracy and very high repeatability could be achieved. Therefore, in the future, it is expected to see new generation of robotic manipulators using input shaping methods that will be more flexible and probably under actuated.

The further developments expected in the area would be use of Artificial Intelligence in input shaping. This development would allow generation and application of input shaping for robust and vibration free operation of robotic and other similar industrial systems. It would then be possible to make these systems at high performance, lower cost and ease of application.

REFERENCES

ALICI, G., KAPUCU, S., and BAYSEÇ, S., 1999. Swing-free transportation of suspended objects with robot manipulators, Robotica, 17:513-521.

ALICI, G., KAPUCU, S., and BAYSEÇ, S., 2000. On preshaped reference inputs to reduce swing of suspended objects transported with robot manipulators. Mechatronics, 10:609–626.

ALICI, G., KAPUCU, S., and BAYSEÇ, S., 2006. A robust motion design technique for flexible-jointed manipulation systems. Robotica, 24:95-103.

ASPINWALL, D. M., 1980. Acceleration profiles for minimizing residual response. ASME Journal of Dynamic Systems Measurement and Control, 102(3): 3–6.

BANERJEE, A. K. and SINGHOSE, W. E., 1998. Command shaping in tracking control of a two-link flexible robot. Journal of Guidance, Control, and Dynamics, 21:1012-1015.

BANERJEE, A. K., 1993. Dynamics and control of the wisp shuttle antennae system. Journal of Astronautical Sciences, 41:73-90.

BANERJEE, A. K., PEDREIRO, N. and SINGHOSE, W., 2001. Vibration reduction for flexible spacecraft following momentum dumping with/without slewing. Journal of Guidance, Control, and Dynamics, 24:417-428.

BIEDIGER, E., SINGHOSE, W., OKADA, H. and MATUNAGA, S., 2003. Trajectory planning for coordinating satellites using command generation. 10th International Space Conference of Pacific-basin Societies.

BLACKBURN, D., SINGHOSE, W., KITCHEN, J., PATRANGENARU, V., LAWRENCE, J., KAMOI, T., and TAURA, A., 2010. Command shaping for nonlinear crane dynamics. Journal of Vibration and Control, 16(4):477–501.

BOOK, W. and MAJETTE M., 1983. Controller design for flexible distributed parameter mechanical arms via combined state space and frequency domain techniques. Journal of Dynamic Systems Measurement and Control, 105(4):245-249.

BOUCETTA, R., and ABDELKRIM, M. N., 2012. Neural network modeling of a flexible manipulator robot. 11th IFIP TC 8 International Conference on Computer Information Systems and Industrial Management. September, 395-404, Venice, Italy.

CHAN, T., GODBOLE, K., and HOU, E., 2003. Optimal input shaper design for high-speed robotic workcells. Journal of Vibration and Control, 9(12):1359–1376.

CONKER, C., BILGIC, H. H., YAVUZ, H., 2015. Esnek sistemlerin artık titreşim kontrolünde konvansiyonel negatif girdi şekillendirme teknikleri ve gürbüzlüklerinin kıyaslanması. Uluslararası Katılımlı 17. Makina Teorisi Sempozyumu. June, İzmir, TURKEY.

CONKER, C., KILIC, A., MISTIKOĞLU, S., KAPUCU, S., YAVUZ, H., 2014a. An enhanced control technique for elimination of residual vibrations in flexible-joint manipulator. Strojniškivestnik – Journal of Mechanical Engineering, 60(9):592-599.

CONKER, C., YAVUZ, H., KAPUCU, S., BALTACIOĞLU, M. K., ARAT, H. T., BURGAC, A., 2014b. Comparison of robust input shapers for elimination of residual vibrations. Applied Mechanics and Materials, 490:997-1002.

DANIELSON, J., VAUGHAN, J., SINGHOSE, W., WIDLER, L. and GLAUSER, U., 2008. Design of a mobile boom crane for research and educational applications, International Conference on Motion and Vibration Control.

DAQAQ, M. F. and MASOUD, Z. N., 2006. Nonlinear input-shaping controller for quay-side container cranes. Nonlinear Dynamics, 45:149-170.

DHARNE, A. G., and JAYASURIYA, S., 2007. Robust adaptive control of residual vibration in point-to-point motion of flexible bodies. Journal of Vibration and Control, 13(7):951–968.

DIMO, H.O., JIN, D., and ZHANG, R., 2001. Vibration control of a redundant robot for grinding. 2001 IEEE International Conference on Systems, Man, and Cybernetics. October, 389-394, Tucson, USA.

DWIVEDY, S. K. and EBERHAD, P., 2006. Dynamic analysis of flexible manipulators, a literature review. Mechanism and Machine Theory, 41:749-777.

FEDDEMA, J. T., 1993. Digital filter control of remotely operated flexible robotic structures. American Control Conference. 2710-2715, San Francisco, USA.

FORTGANG, J., SINGHOSE, W., and MÁRQUEZ, J., 2005. Command shaping for micro-mills and CNC controllers. American Control Conference, June, 4531-4536, Portland, USA.

FREESE, M., FUKUSHIMA, E., HIROSE, S. and SINGHOSE, W., 2007. Endpoint vibration control of a mobile mine-detecting robotic manipulator. American Control Conference. July, 7-12, New York, USA.

GORINEVSKY, D. and VUKOVICH, G., 1998. Nonlinear input shaping control of flexible spacecraft reorientation maneuver. Journal of Guidance, Control, and Dynamics, 21:264-270.

GROSSER, K. and SINGHOSE, W., 2000. Command generation for reducing perceived lag in flexible telerobotic arms. JSME International Journal, 43:755-761.

GURLEYUK, S. S., 2007. Optimal unity-magnitude input shaper duration analysis. Archive of Applied Mechanics, 77:63-71.

GURLEYUK, S. S., and CINAL, S., 2007. Robust three-impulse sequence input shaper design. Journal of Vibration and Control, 13:1807–1818.

GURLEYUK, S. S., BAHADIR, O., TURKKAN, Y., and ÜSENTI, H., 2008. Improved three-step input shaping control of crane system. WSEAS Transactions on Systems 7(6):652-661.

HILLSLEY, K. L. and YURKOVICH, S., 1991. Vibration control of a two-link flexible robot arm. Proceedings of the IEEE International Conferences on Robotics and Automation. April, 2121-2126, Sacramento, USA.

HILLSLEY, K. L. and YURKOVICH, S., 1993. Vibration control of a two-link flexible robot arm. Journal of Dynamics and Control, 3:261-280.

HONG, K. T. and HONG, K. S., 2004. Input shaping and VSC of container cranes. Proceedings of the 2004 IEEE International Conference on Control Applications, 1570-1575.

HU, Q., 2008. Input shaping and variable structure control for simultaneous precision positioning and vibration reduction of flexible spacecraft with saturation compensation. Journal of Sound and Vibration, 318:18-35.

HUEY, J. R., SORENSEN, K. L., and SINGHOSE, W., 2008. Useful applications of closed-loop signal shaping controllers. Control Engineering Practice, 16:836-846.

JABBOUR, E. S., MAHGOUB, H. M., MEKHAIL, N. G., and ELRAOUF, A. M. A., 2009. Dynamic modelling for robotics for various regions of speed. 13th Aerospace Sciences and Aviation Technology. May, 1-11, Cairo, Egypt.

JONES, S. D., and ULUSOY, A. G., 1994. Control input shaping for coordinate measuring machines. Proceedings of the American Control Conference. June, 2899-2903, Baltimore, USA.

JUNG, J. K., YOUM, W. S., and PARK, K. H., 2009. Vibration reductioncontrol of a voice coil motor (vcm) nano scanner. International Journal of Precision Engineering and Manufacturing, 10(3):167-170.

KAPUCU, S. KAPLAN, M., and BAYSEC, S., 2005. Vibration reduction of a lightly damped system using a hybrid input shaping method. Proceedings of the Institution of Mechanical Engineersi Part I, Journal of System and Control Engineering, 219(5):335-342.

KAPUCU, S., ALICI, G., and BAYSEC, S., 2001. Residual swing/vibration reduction using a hybrid input shaping method. Mechanism and Machine Theory, 36:311–326.

KAPUCU, S., and BAYSEC, S., 1997. On the identification of linear mechanical systems. Mechatronics, 7(3):297-313.

KAPUCU, S., BAYSEC, S., and ALICI, G., 2006. Residual vibration suppression of a flexible joint system using a systematic command shaping technique. The Arabian Journal for Science and Engineering, 31(2):139-152.

KAPUCU, S., YILDIRIM, N., YAVUZ, H., BAYSEC, S., 2008. Suppression of residual vibrations of a translating-swinging load by a flexible manipulator. Mechatronics, 18:121-128.

KHOIY, K. A., DAVATGARZADEH, F., and TAHERI, M., 2013. Application of assumed mode method in nonlinear dynamic analysis of elastic robot arms. The International Journal of Engineering and Science, 2(10):2319-1805.

KIM, D. and SINGHOSE, W., 2007. Studies of human operators manipulating double-pendulum cranes. European Control Conference. July, 3471-3478, Kos, GREECE.

KIM, D. and SINGHOSE, W., 2010. Performance studies of human operators driving double-pendulum bridge cranes. Control Engineering Practice, 18(6):567–576.

KOZAK, K., EBERTUPHOFF, I., and SINGHOSE, W., 2004. Locally linearized dynamic analysis of parallel manipulators and application of input shaping to reduce vibrations. ASME Journal of Mechanical Design, 126:156–168.

KWON, D., HWANG, D., BABCOCK, S. M., and BURKS, B. L., 1994. Input shaping filter methods for the control of structurally flexible, long-reach manipulators. Proceedings of the IEEE International Conferences on Robotics and Automation. May, 3259-3264, San Diego, USA.

LIU, Q. and WIE, B., 1992. Robust time-optimal control of uncertain flexible spacecraft. Journal of Guidance, Control, and Dynamics, 15:597-604.

MAGEE, D. and BOOK, W. J., 1992. The application of input shaping to a system with varying parameters. Japan/USA Symposium on Flexible Automation, 1:519–526.

MAGEE, D. and BOOK, W. J., 1993. Eliminating multiple modes of vibration in a flexible manipulator. Proceedings of the IEEE International Conference on Robotics and Automation. May, 474-479, Atlanta, USA.

MAGEE, D. and BOOK, W. J., 1994. Filtering schilling manipulator commands to prevent flexible structure vibration. American Control Conference. June, 2538-2542, USA.

MAGEE, D. and BOOK, W. J., 1995. Filtering micro manipulator wrist commands to prevent flexible base motion. American Control Conference. June, 924-928, Seattle, Washington, USA.

MANNING, R., KIM, D. and SINGHOSE, W., 2008. Reduction of distributed payload bridge crane oscillations. Proceedings of the 10th WSEAS International Conference on Automatic Control, Modelling and Simulation. 133-139, Wisconsin, USA.

MASOUD, Z. N. and DAQAQ, M. F., 2006. A graphical approach to input-shaping control design for container cranes with hoist. IEEE Transactions on Control Systems Technology, 14(6):1070-1077.

MECKL, P. H., and SEERING, W., 1990. Experimental evaluation of shaped inputs to reduce vibration for a cartesian robot. ASME Journal of Dynamic Systems, Measurement and Control, 112:159–165.

MOHAMED, Z. and TOKHI, M. O., 2004. Command shaping techniques for vibration control of a flexible robot manipulator. Mechatronics, 14(1):69-90.

MOHAMED, Z., MARTINS, J. M., TOKHI, M. O., COSTA, J. S., and BOTTO, M. A., 2005. Vibration control of a very flexible manipulator system. Control Engineering Practice, 13:267-277.

OGATHA, K., 2003. System Dynamics, Prentice Hall, New Jersey, 768.

PAO, L. Y. and LAU, M. A., 2000. Robust input shaper control design for parameter variations in flexible structures. Journal of Dynamic Systems, Measurement, and Control, 122:63–70.

PAO, L., and SINGHOSE, W., 1995. On the equivalence of minimum time input shaping with traditional time-optimal control. IEEE Conference on Control Applications. September, 1120-1125, Albany, USA.

PAO, L., and SINGHOSE, W., 1996. Unity magnitude input shapers and their relation to time-optimal control. IFAC World Congress, San Francisco, USA.

PARK, B. J., HONG, K. S. and HUH, C. D., 2000. Time-efficient input shaping control of container cranes. Proceedings of the 2000 IEEE International Conference on Control Applications, September, 80-85, Anchorage, USA.

PARK, J. and RHIM, S., 2008. Extraction of optimal time-delay in adaptive command shaping filter for flexible manipulator control. Journal of Institute of Control, Robotics and Systems, 14(6):564-572.

PARK, S., HONG, S., CHOI, H., and SINGHOSE, W., 2007. Discretization effects of real-time input shaping in residual vibration reduction for precise XY stage. Trans. of the Korean Society of Machine Tool Engineers, 16:71-78.

PARKER, G. G., GROOM, K., HURTADO, J. E., FEDDEMA, J., ROBINETT, R. D. and LEBAN, F., 1999. Experimental verification of a command shaping boom crane control system. American Control Conference. Jun, 86-90, San Diego, USA.

PARMAN, S. and KOGUCHI, H., 1999. Controlling the attitude maneuvers of flexible spacecraft by using time-optimal/fuel efficient shaped inputs. Journal of Sound and Vibration, 221:545-565.

PIAZZI, A., and VISIOLI, A., 2000. Minimum-time system-inversion-based motion planning for residual vibration reduction. IEEE/ASME Transactions on Mechatronics, 5(1):12–22.

QUANSER INC., 2012a, Linear pendulum gantry experiment for MATLAB/Simulink Users, www.quanser.com.

QUANSER INC., 2012b, Flexible link experiment for MATLAB/Simulink Users, www.quanser.com.

RANA, D. S., and DEEPIKA, 2014. Modelling, stability and control of flexible single link robotic manipulator. International Journal of Advanced Research in Electrical, Electronics, and Instrumentation Engineering, 3(2):7390-7401.

RAPPOLE, B. W., SINGER, N. C., and SEERING, W. P., 1993. Input shaping with negative sequences for reducing vibrations in flexible structures. American Control Conference. June, 2695-2699, San Francisco, USA.

ROBERTSON, M., TIMM, A. and SINGHOSE, W., 2005. Evaluation of command generation techniques for tethered satellite retrieval, AIAA Space Flight Mechanics Conference.

SAHINKAYA, M. N., 2001. Input shaping for vibration-free positioning of flexible systems. Proceedings of the Institution of Mechanical Engineers, Part I 215:467–481.

SAHINKAYA, M. N., 2004. Exponential input shaping for vibration free positioning of lightly damped multi-mode systems. 7th International Conference on Motion and Vibration Control, St. Louise, USA.

SETH, N., RATTAN, K. S., and BRANDSTETTER, R. W., 1992. Vibration control of a coordinate measuring machine. IEEE Conference on Control Applications. September, 368-373, Dayton, Ohio, USA.

SHAN, J., LIU, H., and SUN, D., 2005. Modified input shaping for a rotating single-link flexible manipulator. Journal of Sound and Vibration, 285:187–207.

SINGER, N. C., 1989. Residual vibration reduction in computer controlled machines. Massachusetts Institute of Technology, PhD thesis.

SINGER, N. C., and SEERING, W. P., 1988. Using acausal shaping techniques to reduce robot vibration. IEEE International Conference on Robotics and Automation. April, 1434-1439, Philadelphia, USA.

SINGER, N. C., and SEERING, W. P., 1990. Preshaping command inputs to reduce systems vibration. Journal of Dynamic Systems Measurement and Control, 112:76-82.

SINGER, N., SINGHOSE, W., and KRIIKKU, E., 1997. An input shaping controller enabling cranes to move without sway. American Nuclear Society 7th Topical Meeting on Robotics and Remote Systems. April, Washington, USA.

SINGH, P. K. and KRISHNA, M., 2014. Continuum arm robotic manipulator: a review. Universal Journal of Mechanical Engineering, 2(6):193-198.

SINGH, T. and VADALI, S. R., 1993. Input shaped control of three dimensional maneuvers of flexible spacecraft. Journal of Guidance, Control, and Dynamics, 16:1061-1068.

SINGH, T., 2010. Optimal Reference Shaping for Dynamical Systems: Theory and Applications. CRC Press, Boca Raton, 416 p.

SINGHOSE, W., 1995. Minimizing Structural Vibrations with Input Shaping; CR-189439, Final Report for Contract, Convolve, Inc., NAS5-32034, 169 p.

SINGHOSE, W., 1997. Command Generation for Flexible Systems. Massachusetts Institute of Technology, PhD thesis.

SINGHOSE, W., 2009. Command shaping for flexible systems: a review of the first 50 years, International Journal of Precision Engineering and Manufacturing, 10:153-168.

SINGHOSE, W., and KIM, D., 2008. Input shaping control of double pendulum bridge crane oscillations. Journal of Dynamic Systems Measurement and Control, 130:1-7.

SINGHOSE, W., and PAO, L., 1997. A comparison of input shaping and time optimal flexible body control. Control Engineering Practice, 5(4):459-467.

SINGHOSE, W., and SINGER, N., 1996. Effects of input shaping on two-dimensional trajectory following. IEEE Trans. On Robotics and Automation, 12:881-887.

SINGHOSE, W., DEREZINSKI, S. and SINGER, N., 1996. Extra insensitive input shapers for controlling flexible spacecraft. Journal of Guidance, Control, and Dynamics, 19:385-391.

SINGHOSE, W., PORTER, L., and SINGER, N. C., 1995. Vibration reduction using multi-hump extra insensitive input shapers. American Control Conference. June, 3835-3839, Seattle, USA.

SINGHOSE, W., PORTER, L., KENISON, M., and KRIIKKU, E., 2000. Effects of hoisting on the input shaping control of gantry cranes. Control Engineering Practice 8(10): 1159–1165.

SINGHOSE, W., SEERING, W. P., and SINGER, N. C., 1990. Shaping inputs to reduce vibration: a vector diagram approach. IEEE International Conference on Robotics and Automation. May, 922-927, Newyork, USA.

SINGHOSE, W., SEERING, W. P., and SINGER, N. C., 1994. Residual vibration reduction using vector diagrams to generate shaped inputs. ASME Journal of Mechanical Design, 116:654-659.

SINGHOSE, W., SEERING, W. P., and SINGER, N. C., 1996. Input shaping for vibration reduction with specified insensitivity to modeling errors. Proceedings of the Japan–USA Symposium on Flexible Automation. June, 307-313, Boston, USA.

SINGHOSE, W., SEERING, W. P., and SINGER, N. C., 1997. Time-optimal negative input shapers. Journal of Dynamic Systems Measurement and Control, 119(2):198-205.

SINGHOSE, W., SINGER, N., and SEERING, W., 1994. Design and implementation of time-optimal negative input shapers. Mechanical Engineering Congress and Exposition. 151-158, Chicago, USA.

SMITH, J., KOZAK, K., and SINGHOSE, W., 2002. Input shaping for a simple non-linear system. American Control Conference, 821-826, Anchorage, USA.

SMITH, O. J. M., 1957. Posicast control of damped oscillatory systems. Proceedings of the Institute of Radio Engineers, 45:1249-1255.

SONG, G., BUCK, N. and AGRAWAL, B., 1999. Spacecraft vibration reduction using pulse-width pulse-frequency modulated input shaper. Journal of Guidance, Control & Dynamics, 22:433-440.

STARR, G. P., 1985, Swing-free transport of suspended objects with a path controlled robot manipulator. ASME Journal of Dynamic Systems Measurement and Control, 107:97-100.

STRIP, D. R., 1989. Swing-free transport of suspended objects: a general treatment. IEEE Transactions on Robotics and Automation, 5(2):234-236.

SUNG, Y. G. and WANDER, J. P., 1993. Applications of vibration reduction of flexible space structure using input shaping technique. Proceedings of the 26th Southeastern Symposium on System Theory. March, 333-336, Athens, USA.

SUNG, Y. G., and LEE, K. T., 2006. An adaptive tracking controller for vibration reduction of flexible manipulator. International Journal of Precision Engineering and Manufacturing, 7(3):51-55.

SWIGERT, C. J., 1980. Shaped torque techniques. Journal of Guidance and Control, 3(5):460-467.

TUTTLE, T. D., and SEERING, W. P., 1994. A zero-placement technique for designing shaped inputs to suppress multiple-mode vibration. Proceedings of the American Control Conference, June, 2533-2537, Baltimore, USA.

TUTTLE, T. D., and SEERING, W. P., 1995. Vibration reduction in 0-g using input shaping on the mit middeck active control experiment. American Control Conference. June, 919-923, Seattle, USA.

TZES, A. P., ENGLEHART, M. J., and YURKOVICH, S., 1989. Input preshaping with frequency domain information for flexible-link manipulator control. AIAA Guidance, Navigation and Control Conference. 1167-1175, Boston, USA.

VAUGHAN, J., YANO, A., and SINGHOSE, W., 2007. Performance comparison of robust input shapers. IEEE International Conference on Control and Automation. May, 2111-2116, Guangzhou, China.

VAUGHAN, J., YANO, A., and SINGHOSE, W., 2008. Comparison of robust input shapers. Journal of Sound and Vibration, 315:797-815.

VAUGHAN, J., YANO, A., and SINGHOSE, W., 2009. Robust negative input shapers for vibration suppression. ASME Journal of Dynamic Systems, Measurement, and Control, 131(3): 031014-1-9.

WIE, B., SINHA, R. and LIU, Q., 1993. Robust time-optimal control of uncertain structural dynamic systems. Journal of Guidance, Control, and Dynamics, 15:980-983.

WILSON, D. G., STOKES, D., STARR, G., and ROBINETT, R. D., 1996. Optimized input shaping for a single flexible robot link, 5th International Conf. and Expo. on Engineering, Construction, and Operations in Space, 1225-1229.

YANO, K., and TERASHIMA, K., 2005. Sloshing suppression control of liquid transfer systems considering a 3-D transfer path. IEEE-ASME Transactions on Mechatronics, 10:8-16.

YAVUZ, H., MISTIKOGLU, S., and KAPUCU, S., 2011. Hybrid input shaping to suppress residual vibration of flexible systems. Journal of Vibration and Control, 18(1):132–140.

YURKOVICH, S., TZES, A. P. and HILLSLEY, K. L., 1990. Controlling coupled flexible links rotating in the horizontal plane. American Control Conference. May, 362-368, San Diego, USA.

ZOU, K., DRAPEAU, V., and WANG, D., 1995. Closed loop shaped-input strategies for flexible robots. International Journal of Robotics Research, 14:510-529.

ZRNIĆ, N., PETKOVIĆ, Z. and BOŠNJAK, S., 2005. Automation of ship-to-shore container cranes: a review of state-of-the-art. FME Transactions, 33:111-121.

CURRICULUM VITAE

Çağlar CONKER was born on October 18, 1986 in Ankara. After completing his education in Danişment Gazi Anatolian High School, he enrolled in Mustafa Kemal University Mechanical Engineering Department in 2004. He had graduated from the Mechanical Engineering Department of Mustafa Kemal University with a Bachelor of Science degree in 2008 and Master of Science degree in 2010. He had started to Doctor of Philosophy education in Çukurova University Mechanical Engineering Department. He has been working as a research assistant in İskenderun Technical University since 2011. His current research interests include input shaping, command shaping, robotics, modelling and simulation of electromechanical systems.

APPENDIX

Appendix 1

Paper I- An Enhanced Control Technique for the Elimination of Residual Vibrations in Flexible-Joint Manipulators

This paper was published in Strojniški vestnik - Journal of Mechanical Engineering, Vol. 60(2014), pp. 592-599, DOI:10.5545/sv-jme.2014.1698

Strojniški vestnik - Journal of Mechanical Engineering 60(2014)9, 592-599

DOI:10.5545/sv-jme.2014.1698

Original Scientific Paper

Received for review: 2014-01-23
Received revised form: 2014-05-01
Accepted for publication: 2014-05-23

An Enhanced Control Technique for the Elimination of Residual Vibrations in Flexible-Joint Manipulators

Caglar Conker[1,*] – Ali Kilic[2] – Selcuk Mistikoglu[1] – Sadettin Kapucu[2] – Hakan Yavuz[3]

[1] Mustafa Kemal University, Faculty of Engineering, Turkey
[2] Gaziantep University, Faculty of Engineering, Turkey
[3] Cukurova University, Faculty of Engineering, Turkey

One method used to reduce or eliminate residual vibrations is to modify the input signal by using previously determined system parameters. In order to eliminate the residual vibration completely, these system parameters must be very accurately determined. In real systems, achieving such accuracy may not always be possible. To address this problem and to provide a solution, a new residual vibration elimination method is introduced in this study, which has proven to be useful especially in cases of uncertain parameters of estimated or predicted systems. It is shown that the technique is capable of handling high levels of uncertainty and is able to successfully eliminate or reduce residual vibrations in flexible systems. In this approach, the desired position of the system is primarily divided into two equal parts, and the generated input signal is used to eliminate vibration. This study presents theoretical and experimental results of the techniques applied to a flexible mechanical system; a comparative study of robustness performance is also provided. Simulation and experimental results show that the oscillations are considerably decreased with a high degree of robustness in the presence of uncertainty regarding system parameters.

Keywords: residual vibration, input shaping, flexible-joint manipulator, command shaping

0 INTRODUCTION

Motion control studies have become a key subject of robotics and other automation-related research areas. In the manufacturing industry, high-speed and sensitive motion control are necessary for high-speed and high quality production [1]. However, the requirement for high speed makes sensitive motion control difficult to accomplish due to residual vibrations. Therefore, finding a balance between the speed of motion and the elimination, or at least the reduction of, residual vibration has become an important part of the study of motion control and related practical applications [2] to [4].

When a force applied to a flexible mechanical system causes motion, it results in vibrations. Controlling the behaviour of such mechanical systems is generally difficult. In particular, the situation worsens if light and flexible components are used for a fast response. There are some studies relating to the control of the vibration of mechanical systems with flexible elements [5] to [7]. Command pre-shaping or input-shaping based methods have attracted the attention of some researchers [8] to [10]. A feed-forward control is suggested as another input-shaping method, in which the shape of the command signal is altered to reduce system oscillations [11]. The initial works were conducted by Smith [12], whose technique is based on dividing a step input into two smaller steps, one of which is delayed in time. Next, the super-positioning of the step responses results in the cancellation of vibration on the system and provides a reduction in the settling time. However, there are some problems related to the robustness of the method due to uncertainties in the natural frequency and damping ratio.

Aspinwall [13] also suggested a different command-shaping approach. This method is based on shaping a rectangular or a 'bang-bang' forcing function. Another suggestion came from Meckl and Seering [14], who advised the construction of the input signal from either ramped sinusoids or versine functions. Due to the advantage of the rectangular function used in this method, the motion of the system is completed in a shortened period owing to the shape of the signal. Piazzi and Visioli [15] recently suggested a new technique based on shaping the input signal via inverse dynamic analysis. They proposed a polynomial function as a desired output to produce the input signal. Sahinkaya [16] and [17] suggested using a third order exponential function for the output motion to shape input signals using inverse dynamics.

Another approach to the problem is the use of an input-shaping technique that is based on convolving the reference command with a sequence of impulses [18] and [19]. This approach is reported in [20] to [22]. The increasing number of impulses used in the shaped signal leads to improvements in robustness to uncertainty in the system parameters. However, it also causes longer delays in system responses [23] and [24]. Magee and Book [25] suggested using an adaptive approach to implement a two-mode shaper.

In this study, a new residual vibration elimination method is presented. The benefit of the new technique is that it has a wider frequency range for which the results are insensitive to estimation errors of natural

*Corr. Author's Address: Mustafa Kemal University, Dept. of Mechanical Engineering, Hatay, Turkey, cconker@mku.edu.tr

frequency. The input-shaping technique proposed in this study neither limits nor increases/decreases travelling time, i.e. without time limitation or time penalty. Due to their definition, most input-shaping methods, however, increase the travelling time by at least a half damped period or more [24], [26] and [27]. Further details on the comparison of methods of residual vibration elimination, such as zero vibration, zero vibration derivative, zero vibration double derivative and extra insensitive are provided by Singhose [7], Singhose et al. [27] and Vaughan et al. [28].

In the proposed approach, the distance to be travelled by the system is primarily divided into two equal parts. In the generation of each of the input signals, cycloid-plus-ramped and versine-plus-ramp functions are used [29]; then these two signals are joined to form the input signal applied to the system used in the elimination of residual vibration. Hence, a more robust method is obtained in reducing the residual vibrations. The proposed method has been applied in a flexible mechanical system. In the further sections of the presented work, the simulation and the experimental results of the new methods have been presented. In order to demonstrate the effectiveness of the proposed technique, the simulation and experimental results are compared with the results reported by Kapucu et al. [29]. The simulation and the experimental results show that the residual vibrations are considerably decreased with a high degree of robustness in the presence of uncertainty regarding the system parameters.

The outline of the paper is as follows: the first section presents the details of the experimental setup, which is followed by a section in which detail of the model of the system is provided. In the third section, the input-shaping methods are presented. In fourth section, the results related to computer simulation and experiments are presented. In the last section, concluding comments are made.

1 EXPERIMENTAL SETUP

The experimental setup used for performance analysis of the techniques is shown in Fig. 1. The experimental setup consists of a compound pendulum bonded to the sliding member (cart) fixed on the horizontal position of the hydraulically driven Stanford type manipulator, details of which are presented by Kapucu [29].

2 MODELLING OF THE SYSTEM

The mathematical model of the test setup is developed by using the Lagrange method. The model neglects the Coulomb friction of the joint and assumes that the manipulator is working in the horizontal plane and the pendulum in a vertical plane. Then, the equations of motion of the flexible system are [29]:

$$\left(M_c + m_p\right)\ddot{x} + m_p l\ddot{\theta}\cos\theta + c_c\dot{x} - m_p l\dot{\theta}^2\sin\theta = \\ = P_1 A_1 - P_2 A_2, \quad (1)$$

$$m_p l\cos\theta\ddot{x} + m_p l\ddot{\theta} + c_p\dot{\theta} + m_p lg\sin\theta = 0, \quad (2)$$

where; m_p is the mass of the pendulum (including the equivalent mass of the slender aluminium bar), M_c the mass of sliding member (cart and translating link), c_c the damping coefficient of the hydraulic cylinder, c_p the damping coefficient of the pendulum, A_1 the piston area, A_2 the area of piston rod side, P_1 the pressure having impact on piston area, P_2 the pressure having impact on the area of the piston rod side.

The control system of the hydraulic cylinder and the servo valve is shown in Fig. 1. The generated force on the hydraulic piston is controlled by an electro-hydraulic servo-valve. The control variable is the position of the spool of the servo valve that is defined by equations that are provided by Baysec and Jones [30].

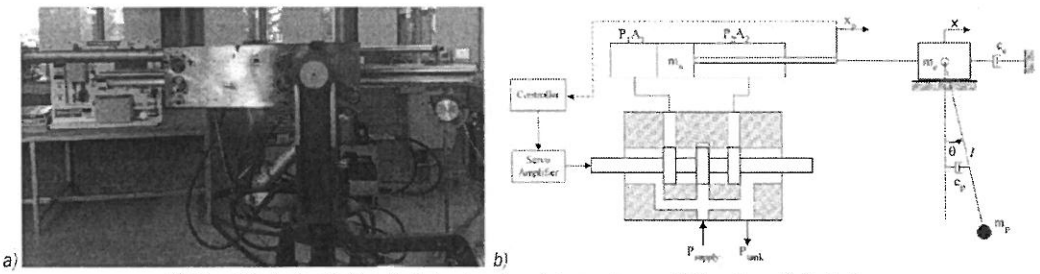

Fig. 1. *a) The hydraulically activated cart and pendulum system; and b) its schematic illustration*

3 INPUT-SHAPING METHODS

The presented study deals with two different approaches used in the elimination of residual vibration. The first method (Method A) is proposed by Kapucu et al. [29], details of which are presented in Section 3.1. The second method (Method B) is the proposed new method, details of which are presented in Section 3.2.

3.1 Method A: A Ramp-Plus-Ramped Cycloid-Plus-Ramped Versine-Based Reference Input Pre-Shaping Technique

In this approach, the reference input is composed of three functions. The total distance to be covered within a specified time is divided into three parts. Each part is travelled by each of the three functions within the same travel time. Provided that the specified move time and the total distance are unchanged, vibration can be eliminated by adjusting the excursion distance of each function. Each component of the input creates such oscillations that they cancel each other out. This results in a reduction of residual vibration. Most elastic mechanical systems can be modelled with a second order differential equation.

The motion equation of such a system with damping ratio ζ and natural frequency ω_n can be defined as:

$$\ddot{x}(t)+2\zeta\omega_n\dot{x}(t)+\omega_n^2 x(t)=2\zeta\omega_n\dot{y}(t)+\omega_n^2 y(t), \quad (3)$$

where $\omega_n=\sqrt{k/m}$.

A motion profile of a cycloid-plus-ramped versine-plus-ramp function is expressed as:

$$Y=\frac{L_1 Rt}{2\pi}+\frac{L_2}{2\pi}\left[Rt-\sin(Rt)\right]+\frac{L_3 Rt}{2\pi}+ +\frac{L_3}{2\pi}\left[1-\cos(Rt)\right], \quad (4)$$

where L_1 is the maximum excursion distance to be travelled by ramp motion profile, L_2 the maximum excursion distance to be travelled by cycloid motion profile, L_3 the maximum excursion distance to be travelled by ramped versine motion profile, t time into motion, τ the travelling time, and $R=2\pi/\tau$. Furthermore, the total distance can be written as $L=L_1+L_2+L_3$, then arranging the equation above becomes:

$$Y(t)=\frac{LRt}{2\pi}-\frac{L_2}{2\pi}\sin(Rt)+\frac{L_3}{2\pi}\left(1-\cos(Rt)\right). \quad (5)$$

The corresponding velocity profile is:

$$\dot{Y}(t)=\frac{LR}{2\pi}-\frac{L_2 R}{2\pi}\cos(Rt)-\frac{L_3 R}{2\pi}\sin(Rt). \quad (6)$$

The solution of the equation of motion, Eq. (3), under the effect of the positional input Eq. (5) and the corresponding velocity Eq. (6) yields the following excursion distance values (L_1, L_2 and L_3) for zero residual vibration with zero initial conditions:

$$L_1=\frac{LR\left(R-2\zeta\omega_n\right)}{\omega_n^2}=\frac{LT_n\left(T_n-2\zeta\tau\right)}{\tau^2},$$
$$L_2=L\left(1-\frac{R^2}{\omega_n^2}\right)=L\left(1-\frac{T_n^2}{\tau^2}\right),$$
$$L_3=\frac{2L\zeta R}{\omega_n}=\frac{2L\zeta T_n}{\tau}, \quad L=L_1+L_2+L_3. \quad (7)$$

where ω_n is the natural frequency, and T_n the natural frequency period. Variations of L_1, L_2 and L_3 are possible with traveling time τ to result in an oscillation-free displacement of the system. Theoretically, there is no traveling time restriction on the system, and this is the main advantage of this reference input-shaping technique [29].

3.2 Method B: Proposed Input-Shaping Technique

The proposed input-shaping method (Method B) utilises the first technique (Method A) presented in Section 3.1. With Method A, the Eqs. (4) to (7) are used to generate the command input required for the system. The proposed method, in contrast, divides the travelling time into two sections and calculates the command input as two separate inputs and then joins them to form the new input.

The calculations for the new method are as follows, where the input is divided into two sections, and each one is calculated independently to form the first and the second parts of the input signal.

$$L=L_a+L_b, \quad L_a=L_b=L/2, \quad (8)$$

$$\tau=\tau_a+\tau_b, \quad \tau_a=\tau_b=\tau/2, \quad (9)$$

$$R_{a,b}=2\pi/\tau_{a,b}, \quad (10)$$

$$L_{1_{(a,b)}}=\frac{LR_{a,b}\left(R_{a,b}-2\zeta\omega_n\right)}{\omega_n^2},$$
$$L_{2_{(a,b)}}=\frac{L\left(1-R_{a,b}\right)}{\omega_n^2}, \quad L_{3_{(a,b)}}=\frac{2L\zeta R_{a,b}}{\omega_n}. \quad (11)$$

$$Y=\begin{cases} 0\le t\le \dfrac{\tau}{2}\rightarrow Y=\dfrac{L_{1a}R_a t}{2\pi}+\dfrac{L_{2a}}{2\pi}\left(R_a t-\sin(R_a t)\right)+ \\ \qquad +\dfrac{L_{3a}R_a t}{2\pi}+\dfrac{L_{4a}}{2\pi}\left(1-\cos(R_a t)\right) \\ \dfrac{\tau}{2}\le t\le \tau\rightarrow Y=\dfrac{L_{1b}R_b t}{2\pi}+\dfrac{L_{2b}}{2\pi}\left(R_b t-\sin(R_b t)\right)+ \\ \qquad +\dfrac{L_{3b}R_b t}{2\pi}+\dfrac{L_{4b}}{2\pi}\left(1-\cos(R_b t)\right) \end{cases}. \quad (12)$$

As defined in Eqs. (8) to (12), the new method allows a virtual division of the motion of the system into two steps. Because the first step is completed with almost steady motion and with relatively reduced vibration levels, the second part of the motions starts with the advantage of very little or almost no residual vibrations. Consequently, the result of the second part of the motion yields better performance relative to the previously mentioned method.

The details provided in Fig. 2 illustrate the command inputs generated using two different methods considered for analysis. The details on the generation of input-shaping functions for Methods A and B can be found in Sections 3.1 and 3.2, respectively.

As illustrated in Fig. 2, Method A consists of two components with which the resulting residual vibration cancels out due to reverse act. However, Method B consists of four parts resulting in eliminated residual vibration at half way to the destination position. These features of the input signals can be seen clearly in Fig. 2.

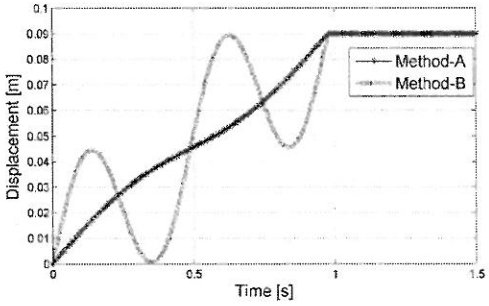

Fig. 2. The input-shaping methods and generated input commands for total travelling distance of L = 0.09 m and travelling time τ = 0.9703 s ($R_{a,b}$ = 12.8503, $L_{1a,b}$ = 2.7508, $L_{2a,b}$ = -2.2680, $L_{3a,b}$ = 0.0172)

4 SIMULATION AND EXPERIMENTS

In order to perform a comparison amongst the input-shaping methods and the experimental results of the techniques, the previously described experimental setup and the mathematical model of the system is used. The experimental setup is driven using each input and the resulting residual vibrations as well as the cart position are measured. The Matlab model of the system is also provided with the same input commands to demonstrate the correlation between the theoretical and experimental results obtained.

For the randomly selected motion time τ = 0.9703 s and the travel distance of the hydraulic cylinder L = 0.09 m, the generated input commands are applied to the Matlab model of the system and the experimental setup. The results of the study are presented in Figs. 3 to 5 for Methods A, B. In Figs. 3 to 5, ω_n^* represents the estimated values the natural frequencies of the system.

In Figs. 3 to 5, the reference input and displacement of the hydraulic cylinder are given in meters. In contrast, the pendulum oscillation is given in the unit of radians. It can be seen that the simulation and test results match up very closely. This simply indicates that the behaviour of the developed Matlab model and the experimental setup are very much the same. This is mainly due to the accurate mathematical model of the mechanical [29] and the hydraulic systems [30]. In Figs. 3 to 5, simulation and experimental results of Methods A and B are illustrated. In these figures, an estimation error of ±25% is introduced to the natural frequency of the system used in the calculation of the input signals. Figs. 3 to 5 are plotted with estimation errors of −25, 0, +25%, respectively. In Figs. 3 to 5, it can be seen that Method A, the estimation error causes increasing residual vibrations of the pendulum ranging from 4.68×10^{-4} to 1.92×10^{-2} rad. It can be seen that increase error in estimation of the natural frequency of the system causes increasing residual vibrations. These results are also validated in Fig. 6 (Method A) and Fig. 7 (Method A) where different predicted natural frequencies and sensitivity curves are presented, respectively.

In Figs. 3 to 5, however, the results differ, ranging from 3.195×10^{-3} to 1.23×10^{-2} rad. As can be seen from Figs. 3 to 5, the increase in estimation of the natural frequency of the system causes much less increase in residual vibrations. Therefore, it can be concluded that the proposed new method is better in comparison to the old method. This conclusion is much clearer from the Fig. 7 (Method B) where the sensitivity curve for the new method is provided. The proposed new method has a wider insensitivity to variation of natural frequency resulting in a wider spectra compared to the old method.

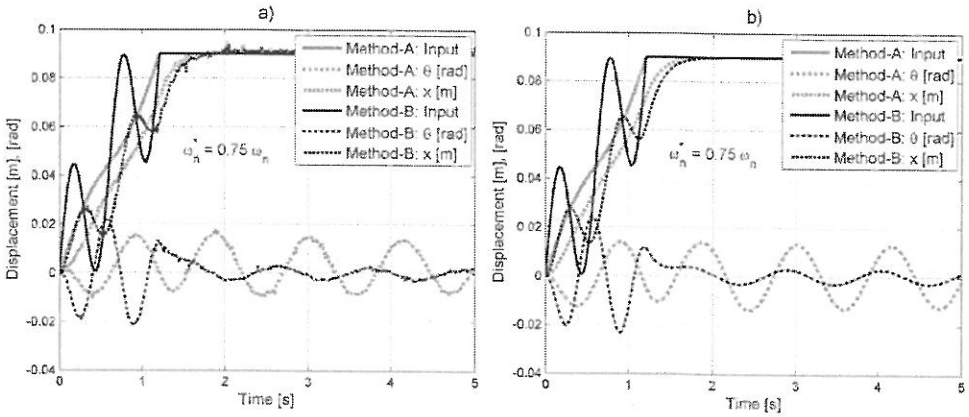

Fig. 3. *Method A and Method B with a) experimental and b) simulation results for total travelling distance of L = 0.09 m and travelling time τ = 1.293 s for -25% estimation error of natural frequency*

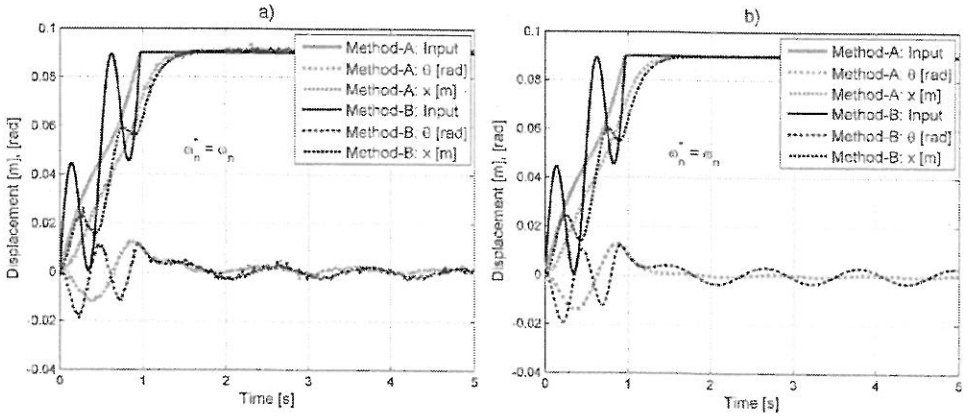

Fig. 4. *Method A and Method B with a) experimental and b) simulation results for total travelling distance of L = 0.09 m and travelling time τ = 0.9703 s for accurate estimation of natural frequency*

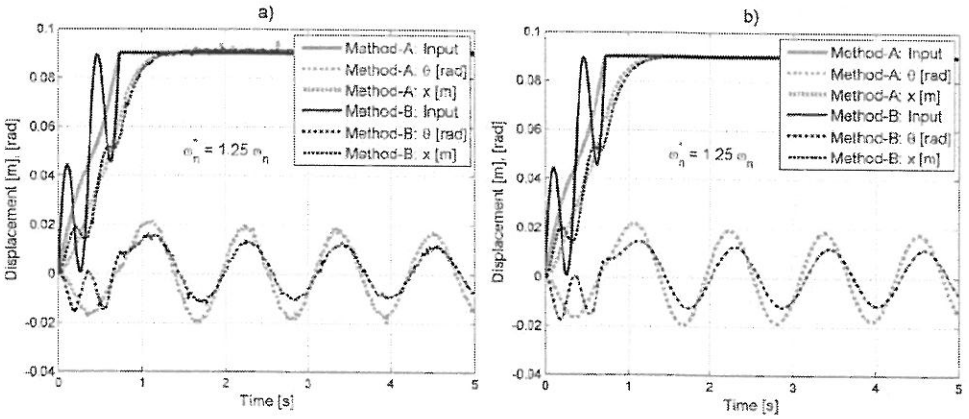

Fig. 5. *Method A and Method B with a) experimental and b) simulation results for total travelling distance of L = 0.09 m and travelling time τ = 0.776 s for +25% estimation error of natural frequency*

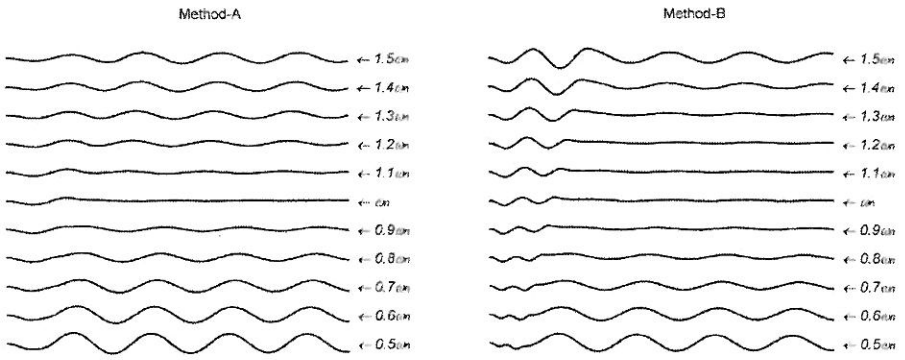

Fig. 6. *Pendulum positions of different predicted natural frequencies for input-shaping Methods A and B-related experimental results for total travelling distance of L = 0.09 m, travelling time τ = 0.9703 s*

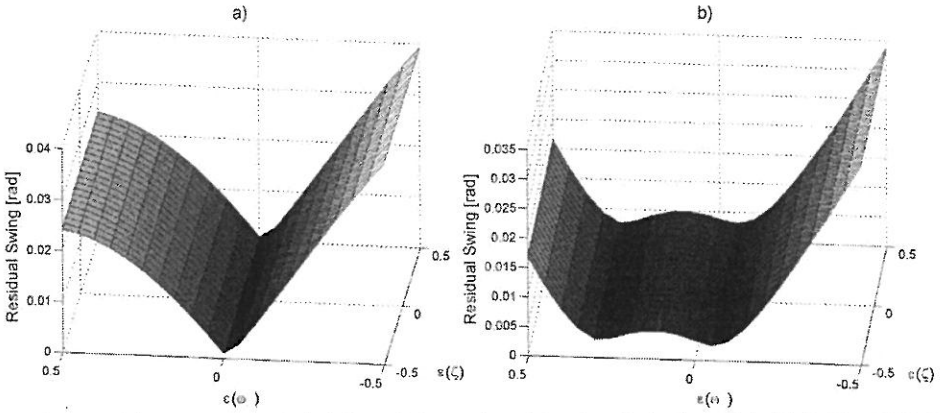

Fig. 7. Robustness of the system to uncertainties in the mode frequencies and damping ratios for the studied; a) Method A and b) Method B

In order to estimate the robustness of the proposed methods against estimation error of the natural frequency of the model parameters, an error function has been defined as:

$$\varepsilon\left(\omega_n\right)=\frac{\omega_n}{\omega_n^*}-1, \tag{13}$$

where, ω_n, ω_n^* shows actual and predicted values the natural frequencies of system, respectively.

Due to the very low level of the damping ratio of the system ($\zeta=0.08$), its variation due to estimation error does not seem to affect the results as shown in Fig. 7. Therefore, the robustness analysis is performed only for the natural frequency estimation error-related variations.

In Fig. 7, the variation of the residual vibration is presented against estimation error in the natural frequency and damping ratio. It can clearly be seen that the variation of error or uncertainty of damping ratio has a relatively reduced effect on the residual vibration of the system. Therefore, the uncertainties of the damping ratio do not play an important role in affecting the behaviour of the system due to its very low value, $\zeta = 0.08$. In contrast, the estimation error in the natural frequency appears to affect the motion of the system and the resulting residual vibration levels.

The figure also shows that the proposed method provides a more robust response relative to Method A. It is noteworthy that the lowest level of residual vibration is achieved using the proposed new technique.

5 CONCLUSION

In this study, a new residual vibration elimination method is introduced, and a comparative study of two input-shaping techniques is performed. Both the theoretical and practical results have shown that the new technique seems to perform better relative to the other method mentioned.

- From the simulation and experimental results, it is possible to conclude the following:
- It is shown that the proposed method (Method B) is far more robust than the old method (Method A). In other words, the proposed new method has a relatively wider insensitive natural frequency spectra in comparison to the old one.
- The advantage of the proposed technique is that it neither limits nor increases the move time, i.e. no time limitation or time penalty. Most conventional input-shaping methods, however, tend to increase the travelling time by at least a half damped period or more.

It is shown that proposed new technique is simple and easy to implement, and can be considered to be a versatile and effective way to determine a trajectory resulting in reduced or eliminated residual vibrations of flexible systems with high robustness.

Therefore, it can be concluded that the proposed new method (Method B) is better relative to the old one (Method A) and to other conventional methods.

6 REFERENCES

[1] Radoičić, G., Jovanović, M. (2013). Experimental identification of overall structural damping of system. *Strojniški vestnik – Journal of Mechanical Engineering*, vol. 58, no. 4, p. 260-268, DOI:10.5545/sv-jme.2012.569.

[2] Changa, P.H., Park, H.S. (2005). Time-varying input shaping technique applied to vibration reduction of an industrial robot. *Control Engineering Practice*, vol. 13, no. 1 p. 121-130, DOI:10.1016/j.conengprac.2004.02.009.

[3] Jokić, M., Stegić, M., Kranjčević, N. (2012). Structural stiffness optimization with respect to vibration response. *Transactions of FAMENA*, vol. 36, no. 2, p. 1-8.

[4] Golubović, Z., Lekić, Z., Jović, S. (2012). Influence of bucket wheel vertical vibration on bucket wheel excavator (BWE) digging force. *Tehnički vjesnik – Technical Gazette*, vol. 19, no. 4, p. 807-812.

[5] Singhose, W., Pao, L. (1997). A comparison of input shaping and time-optimal flexible-body control. *Control Engineering Practice*, vol. 5, no. 4, p. 459-467, DOI:10.1016/S0967-0661(97)00025-7.

[6] Shan, J., Liu, H., Sun, D. (2005). Modified input shaping for a rotating single-link flexible manipulator. *Journal of Sound and Vibration*, vol. 285, p. 187-207, DOI:10.1016/j.jsv.2004.08.035.

[7] Singhose, W. (2009). Command shaping for flexible systems: A review of the first 50 years. *International Journal of Precision Engineering and Manufacturing*, vol. 10, no. 4, p. 153-168, DOI:10.1007/s12541-009-0084-2.

[8] Raubar, E., Vrančić, D. (2012). Anti-sway system for ship-to-shore cranes. *Strojniški vestnik – Journal of Mechanical Engineering*, vol. 58, no. 5, p. 338-344, DOI:10.5545/sv-jme.2010.127.

[9] Singhose, W., Porter, L., Kenison, M., Kriikku, E. (2000). Effects of hoisting on the input shaping control of gantry cranes. *Control Engineering Practice*, vol. 8, no. 10, p. 1159-1165, DOI:10.1016/S0967-0661(00)00054-X.

[10] Changa, P.H., Park, J. (2001). A concurrent design of input shaping technique and a robust control for high-speed/high-precision control of a chip mounter. *Control Engineering Practice*, vol. 9, no. 12, p. 1279-1285, DOI:10.1016/S0967-0661(01)00092-2.

[11] Kim, D., Singhose, W. (2010). Performance studies of human operators driving double-pendulum bridge cranes. *Control Engineering Practice*, vol. 18, no. 6, p. 567-576, DOI:10.1016/j.conengprac.2010.01.011.

[12] Smith, O.J.M. (1958). *Feedback Control Systems*, McGraw-Hill, New York.

[13] Aspinwall, D.M. (1980). Acceleration profiles for minimizing residual response. *ASME Journal of Dynamic Systems, Measurement and Control*, vol. 102, no. 1, p. 3-6, DOI:10.1115/1.3140620.

[14] Meckl, P.H., Seering, W. (1990). Experimental evaluation of shaped inputs to reduce vibration for a Cartesian robot. *ASME Journal of Dynamic Systems, Measurement and Control*, vol. 112, no. 2, p. 159-165, DOI:10.1115/1.2896122.

[15] Piazzi, A., Visioli, A. (2000). Minimum-time system-inversion- based motion planning for residual vibration reduction. *IEEE/ASME Transactions on Mechatronics*, vol. 5, no. 1, p. 12-22, DOI:10.1109/3516.828585.

[16] Sahinkaya, M.N. (2001). Input shaping for vibration-free positioning of flexible systems. *Proceedings of the Institution of Mechanical Engineers*, Part I, p. 467-481.

[17] Sahinkaya, M.N. (2004). Exponential input shaping for vibration free positioning of lightly damped multi-mode systems. *7th International Conference on Motion and Vibration Control*, p. 8-11.

[18] Mimmi, G., Pennacchi, P. (2001). Pre-shaping motion input for a rotating flexible link. *International Journal of Solids and Structures*, vol. 38, no. 10-13, p. 2009-2023, DOI:10.1016/S0020-7683(00)00149-9.

[19] Cutforth, C.F., Pao, L.Y. (2004). Adaptive input shaping for maneuvering flexible structures. *Automatica*, vol. 40, no. 4, p. 685-693, DOI:10.1016/j.automatica.2003.11.013.

[20] Park, J.Y., Chang, P.H. (2004). Vibration control of a telescopic handler using time delay control and commandless input shaping technique. *Control Engineering Practice*, vol. 12, no. 6, p. 769-780, DOI:10.1016/j.conengprac.2003.09.005.

[21] Gurleyuk, S.S., Cinal, S. (2007). Robust three-impulse sequence input shaper design. *Journal of Vibration and Control*, vol. 13, no. 12, p. 1807-1818, DOI:10.1177/1077546307080012.

[22] Gurleyuk, S.S., Hacioglu, R., Cinal, S. (2007). Three-step input shaper for damping tubular step motor vibrations. *Journal of Mechanical Engineering Science*, vol. 221, no. 1, p. 1-9, DOI:10.1243/0954406JMES381.

[23] Singer, N.C. (1989). *Residual Vibration Reduction in Computer Controlled Machines*. PhD thesis, MIT Artificial Intelligence Laboratory, Massachusetts.

[24] Singer, N.C., Seering, W.P. (1990). Preshaping command inputs to reduce system vibration. *ASME Journal of Dynamic Systems, Measurement and Control*, vol. 112, p. 76-82, DOI:10.1115/1.2894142.

[25] Magee, D.P., Book W.J. (1993). Implementing modified command filtering to eliminate multiple modes of vibration. *Proceedings of the American Control Conference*, p. 2700-2704.

[26] Singhose, W., Seering, W., Singer, N. (1994). Residual vibration reduction using vector diagrams to generate shaped inputs. *Journal of Mechanical Design*, vol. 116, no. 2, p. 654-659, DOI:10.1115/1.2919428.

[27] Singhose, W., Porter, L., Singer, N. (1995). Vibration reduction using multi-hump extra-insensitive input shapers. *American Control Conference*, p. 3830-3834.

[28] Vaughan, J., Yano, A., Singhose, W. (2008). Comparison of robust input shapers. *Journal of Sound and Vibration*, vol. 315, no. 4-5, p. 797-815, DOI:10.1016/j.jsv.2008.02.032.

[29] Kapucu, S., Yildirim, N., Yavuz, H., Baysec, S. (2008). Suppression of residual vibration of a translating–swinging load by a flexible manipulator. *Mechatronics*, vol. 18, no. 3, p. 121-128, DOI:10.1016/j.mechatronics.2007.10.007.

[30] Baysec, S., Jones, J.R. (1987). An improved model of an electro hydraulic servo valve. *Proceedings of 7th IFToMM Congress*, p. 1489-1494.

Appendix 2

Paper II- Comparison of Robust Input Shapers for Elimination of Residual Vibrations

This paper was published in Applied Mechanics and Materials, Vol. 490-491(2014), pp. 997-1002, DOI:10.4028/www.scientific.net/AMM.490-491.997

Applied Mechanics and Materials Vols. 490-491 (2014) pp 997-1002
© (2014) Trans Tech Publications, Switzerland
doi:10.4028/www.scientific.net/AMM.490-491.997

Comparison of Robust Input Shapers for Elimination of Residual Vibrations

ÇAĞLAR CONKER[1,a], HAKAN YAVUZ[2,b], SADETTİN KAPUCU[3,c], MUSTAFA KAAN BALTACIOĞLU[4,d], HÜSEYİN TURAN ARAT[4,e], ALPER BURGAÇ[5,f]

[1]Department of Mechanical Engineering, Faculty of Engineering, Mustafa Kemal University, Hatay, TURKEY

[2]Department of Mechanical Engineering, Faculty of Engineering and Architecture, Çukurova University, Adana, TURKEY

[3]Department of Mechanical Engineering, Faculty of Engineering, Gaziantep University, Gaziantep, TURKEY

[4]Department of Petroleum and Natural Gas Engineering, Faculty of Engineering, Mustafa Kemal University, Hatay, TURKEY

[5]Department of Energy System Engineering, Faculty of Technology, Mustafa Kemal University, Hatay, TURKEY

[a]cconker@mku.edu.tr, [b]dr.hakanyavuz@gmail.com, [c]kapucu@gantep.edu.tr, [d]kaanbalta@mku.edu.tr, [e]htarat@mku.edu.tr, [f]aburgac@mku.edu.tr

Keywords: Flexible Mechanical System, Residual Vibration, Input Shaping, Command Pre-shaping, Vibration Reduction

Abstract. Input shaping is a feedforward control technique for improving the settling time and positioning accuracy, while minimizing residual vibrations. Shaped command profiles are generated by convolving a sequence of impulses. To design an input shaping controller, estimates of the system natural frequency and damping ratio are required. However, real systems cannot be modeled exactly, making the robustness to modeling errors an important consideration. Many robust input shapers have been developed, but robust shapers typically have longer durations that slow the system response. This creates a compromise between shaper robustness and rise time. This paper analyses the compromise between shaper duration and robustness for several robust input shapers

Introduction

When a flexible mechanical system is moved, it has a tendency to vibrate. Controlling the behaviour of such systems are generally difficult especially if they consist of light and flexible components used for a fast response. There is a great deal of literature relating to control vibration of flexible systems. Among these methods, command pre-shaping or input shaping based methods have attracted the attention of many researchers [1-8]. One of the solutions suggested in the literature is a feed-forward control method which alters the shape of command signal to reduce system oscillations. The earliest form of command pre-shaping was the use of posicast control by Smith [1]. This technique involves breaking a step input into two smaller steps, one of which is delayed in time. Superposition of the step responses results in cancellation of vibration. It also allows reduction in the settling time. However, this method is not generally favoured due to problems related to robustness in natural frequency and damping ratio uncertainties. In order to solve this problem, Singer and Seering [2] proposed an acausal shaping technique for robot vibration suppression. Their work significantly extended the application range of input shaping method, in which the robustness was taken into account. In the following research, they had performed lots of works to design input shaper [3, 4]. Singer and Seering proposed an approach to improve the robustness of input shaping, in which the derivative of residual vibration amplitude ratio with respect to the frequency was set to zero, i.e. a three-pulse Zero

Vibration and Derivative (ZVD) shaper was obtained. The ZVD shaper was much more robust, however the cost of the shaping time delay was also extended. The delay time of the ZV shaper is half period of system vibration, while the ZVD shaper extends to one complete vibration period, which means one more vibration period will be added during the system rise time if the shaper is employed. It is obviously difficult to suppress the residual vibration amplitude to zero, and in fact such a strict requirement is seldom implemented in actual applications. If the condition of residual vibration amplitude is relaxed to non-zero, the robustness of the system can be increased notably. Based on that idea, Singhose et al [5] proposed Extra Insensitive (EI) input shaping approach. The EI shaper's robustness has been significantly improved compared with ZVD shaper, although they provide the same time delay. Further details on residual vibration elimination performance comparison of methods such as ZV, ZVD, ZVDD and EI are provided by Singhose et al. [6, 7] and Vaughan et al. [8].

Many robust input shapers have been developed, but robust shapers typically have longer durations that slow the system response [8]. This creates a compromise between shaper robustness and rise time. This paper analyses the compromise between rapidity of motion and shaper robustness for several input shaping techniques.

Overview of Input Shaping

Input shaping is a technique that reduces vibration in a flexible system. Input shaping works by convolving a reference signal with a series of impulses called an input shaper. The timing and amplitude of these impulses are chosen such that when applied to an oscillatory system, the vibration caused by the sequence impulses cancels out.

To understand how input shaping works, first consider a single impulse, A1, applied to a flexible system. Then, another impulse, A2, of the same amplitude is applied one half of the period of oscillation later. The response from both impulses is shown in Fig. 1. If a system is sufficiently linear, superposition may be used to find the total response to both impulses. This total superimposed response is also shown in Fig. 1 as a solid line. Because the amplitudes of the impulses are equal and they are separated by one half of the oscillation period, the vibration caused by A1 is cancelled by A2 [7, 8].

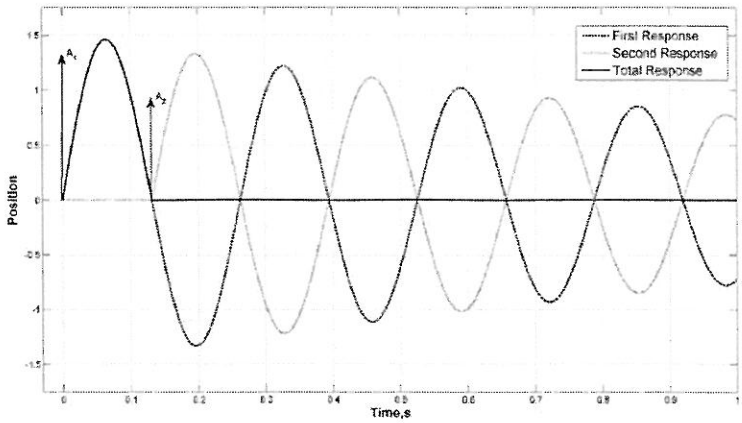

Fig. 1 Zero vibration response to two impulses

Constraint Equations

The constraint on vibration amplitude can be expressed as the ratio of residual vibration amplitude with shaping to that without shaping. This percentage vibration can be determined by using the expression for residual vibration of a second order harmonic oscillator of frequency ω radians/sec and damping ratio ζ, which is given in Bolz and Tuve [9]. The vibration from a series of impulses is divided by the vibration from a single impulse with unity magnitude to get the vibration percentage as follows:

$$V(\omega,\zeta)=e^{-\zeta\omega_n}\sqrt{(C(\omega,\zeta))^2+(S(\omega,\zeta))^2} \tag{1}$$

where

$$C(\omega,\zeta)=\sum_{i=1}^{n}A_i e^{\zeta\omega_n t_i}\cos\left(\omega_n\sqrt{1-\zeta^2}t_i\right) \text{ and } S(\omega,\zeta)=\sum_{i=1}^{n}A_i e^{\zeta\omega_n t_i}\sin\left(\omega_n\sqrt{1-\zeta^2}t_i\right) \tag{2}$$

where A_i and t_i are the amplitudes and time locations of the impulses, n is the number of impulses in the input shaper, and t_n is the time of the last impulse.

Zero Vibration (ZV) Input Shaper

A Zero Vibration, ZV, input shaper is the simplest input shaper. The only constraints are minimal time and zero vibration at the modeling frequency. If these constraints are satisfied, the ZV shaper has the form of impulse amplitudes Ai and times ti

$$ZV=\begin{bmatrix}A_j\\t_j\end{bmatrix}=\begin{bmatrix}\frac{1}{1+K} & \frac{K}{1+K}\\0 & 0.5T_d\end{bmatrix} \tag{3}$$

where $K=e^{-\frac{\zeta\pi}{\sqrt{1-\zeta^2}}}$ and $t_d=2\pi/\omega_n\sqrt{1-\zeta^2}$

While the ZV shaper provides the shortest impulse trains, it requires very good knowledge of the plant. Singer and Seering [3] reported that the ZV shaper is robust for only small variations (±5%) in modal frequency.

As indicated in Fig. 2, a major problem with the ZV shaper is the robustness to parameter variations. If the original system parameters change or the system modelled incorrectly, then the system suffers from residual vibrations.

Derivative Methods (ZVD and ZVDD)

A Zero Vibration and Derivative, ZVD, shaper is a command generation scheme designed to make the input-shaping process more robust to modeling errors. To achieve this, another constraint is added to the definition. Then, the formulation of the shaper is set by the derivative of the vibration with respect to frequency which is equal to zero [3, 4]:

$$\frac{d}{d\omega}\left[e^{-\zeta\omega_n}\sqrt{\left(C(\omega,\zeta)\right)^2+\left(S(\omega,\zeta)\right)^2}\right]=0 \tag{4}$$

The resulting shaper is called a zero vibration and derivative (ZVD) shaper. The times and magnitudes for this shaper are:

$$ZVD = \begin{bmatrix} A_j \\ t_j \end{bmatrix} = \begin{bmatrix} \frac{1}{1+2K+K^2} & \frac{2K}{1+2K+K^2} & \frac{K^2}{1+2K+K^2} \\ 0 & 0.5T_d & T_d \end{bmatrix} \tag{5}$$

where K and T_d are defined by equations (3)

As shown in Fig. 3, ZVD shaper is much more insensitive to modeling errors than the ZV shaper. However, the ZVD shaper has a time duration equal to one period of the vibration frequency, as opposed to the one-half period length of the ZV shaper. This trade-off is typical of the input shaper design process increasing insensitivity usually increases time penalty [8].

The addition of derivative based algorithm can be extended indefinitely with repeated differentiation of the percentage vibration equation. For each differentiation, an additional impulse is added to the shaper and the shaper's time penalty is increased by one-half period of the natural frequency.

$$ZVDD = \begin{bmatrix} A_j \\ t_j \end{bmatrix} = \begin{bmatrix} \frac{1}{1+3K+3K^2+K^3} & \frac{3K}{1+3K+3K^2+K^3} & \frac{3K^2}{1+3K+3K^2+K^3} & \frac{K^3}{1+3K+3K^2+K^3} \\ 0 & 0.5T_d & T_d & 1.5T_d \end{bmatrix} \tag{6}$$

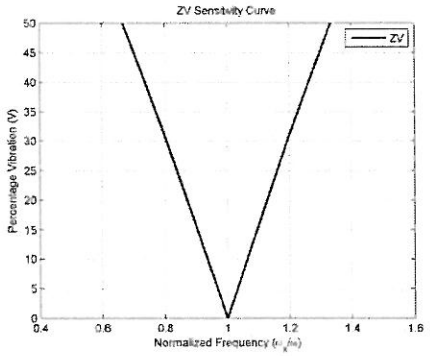

Fig 2. ZV input shaper sensitivity curve

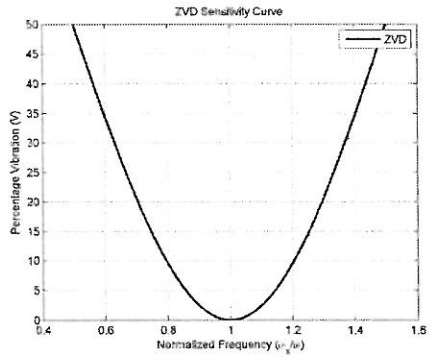

Fig 3. ZVD input shaper sensitivity curve

Extra Insensitive (EI) Input Shapers

Unlike the ZV, ZVD and ZVDD shapers, the extra insensitive (EI) shaper does not attempt to force the vibration to zero at the modeling frequency. Rather, the vibration is limited to some low, but

acceptable level of residual vibration. The sensitivity curve for an EI shaper designed to limit the vibration below 5% is shown in Fig. 5. For this purpose, the following definitions are made [6];

$$V = e^{-\zeta w_n t_N}\sqrt{\left(C(\omega,\zeta)\right)^2+\left(S(\omega,\zeta)\right)^2} \tag{7}$$

$$\frac{\partial}{\partial w}\left[e^{-\zeta w_n t_N}\sqrt{\left(C(\omega,\zeta)\right)^2+\left(S(\omega,\zeta)\right)^2}\right]=0 \tag{8}$$

$$\sum A = 1 \tag{9}$$

The times and magnitudes for this shaper are:

$$EI=\begin{bmatrix}A_j\\t_j\end{bmatrix}=\begin{bmatrix}\frac{1+V_{tol}}{4} & \frac{1-V_{tol}}{4} & \frac{1+V_{tol}}{4}\\ 0 & 0.5T_d & T_d\end{bmatrix} \tag{10}$$

Fig. 5 shows the sensitivity for the single mode EI shaper. The insensitivity of the EI shaper is 0.4 which is larger than either the ZV or ZVD shapers. Notice that the slope of the residual vibration is equal to zero when the normalized frequency equals one, and that the residual vibration equals the tolerable limit of 5% rather than zero.

Table 1. The input shaping techniques and related information

	Technique	Time Penalty	Robustness (%5)	Time Restrictions	Is travelling time could be below time constant of the system
1	ZV	π/w_d	0.06	Yes	Yes but not robust to uncertainty
2	ZVD	$2\pi/w_d$	0.28	Yes	No
3	ZVDD	$3\pi/w_d$	0.48	Yes	No
4	EI	$2\pi/w_d$	0.40	Yes	No

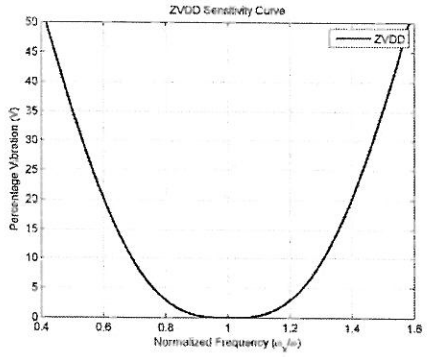

Fig 4. ZVDD input shaper sensitivity curve

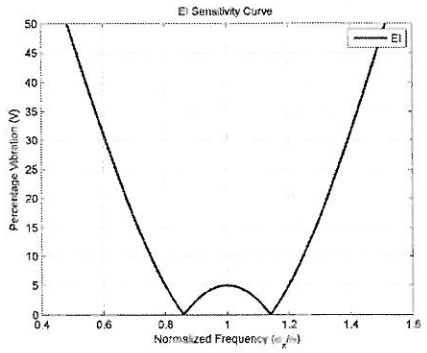

Fig 5. EI input shaper sensitivity curve

Conclusions

This paper presented an overview of various conventional input shapers, with emphasis on the compromise between shaper duration and robustness. The theoretical results have shown that Extra Insensitive (EI) input shaping technique seems to perform better relative to the other mentioned methods.

References

[1] O.J.M. Smith: Posicast control of damped oscillatory systems, Proceedings of the Institute of Radio Engineers, Vol. 45 (1957), p. 1249-1255.

[2] N.C. Singer, W.P. Seering: Using acausal shaping techniques to reduce robot vibration (IEEE International Conference on Robotics and Automation, USA, 1988).

[3] N.C. Singer, W.P. Seering: Preshaping command inputs to reduce systems vibration, Journal of Dynamic Systems, Measurement, and Control Vol. 112 (1990), p. 76-82.

[4] N.C. Singer: Residual vibration reduction in computer controlled machines. PhD thesis, Massachusetts Institute of Technology. (1989).

[5] W. Singhose, W. Seering, N.C. Singer: Residual vibration reduction using vector diagrams to generate shaped inputs, ASME Journal of Mechanical Design, Vol. 116 (1994), p. 654-659.

[6] W. Singhose, L. Porter, N.C. Singer: Vibration Reduction Using Multi-Hump Extra Insensitive Input Shapers (American Control Conference, USA, 1995).

[7] W. Singhose: Command Shaping for Flexible Systems: A Review of the First 50 Years, International Journal of Precision Engineering and Manufacturing, Vol. 10 (2009), p. 153–168.

[8] J. Vaughan, A. Yano, W. Singhose: Comparison of robust input shapers, Journal of Sound and Vibration, Vol. 315 (2008), p. 797-815.

[9] R.E. Bolz, G.L. Tuve: CRC Handbook of Tables for Applied Engineering Science (CRC Press, Inc., Boca Raton, FL. 1973).

Appendix 3

PAPER III- Esnek Sistemlerin Artık Titreşim Kontrolünde Konvansiyonel Negatif Girdi Şekillendirme Teknikleri ve Gürbüzlüklerinin Kıyaslanması

This paper was presented at the TrC-IFToMM Symposium on Theory of Machines and Mechanisms/ UMTS2015, İzmir, Turkey (2015)

Uluslararası Katılımlı 17. Makina Teorisi Sempozyumu, İzmir, 14-17 Haziran 2015

Esnek Sistemlerin Artık Titreşim Kontrolünde Konvansiyonel Negatif Girdi Şekillendirme Teknikleri ve Gürbüzlüklerinin Kıyaslanması

Ç. Conker*
Mustafa Kemal Üniversitesi
Hatay

H. H. Bilgiç†
Mustafa Kemal Üniversitesi
Hatay

H. Yavuz‡
Çukurova Üniversitesi
Adana

Özet—*Artık titreşimlerin yok edilmesi veya azaltılması için kullanılan yöntemlerden bir tanesi girdi sinyalinin, tabi frekans ve sönüm oranı gibi önceden bilinen sistem parametreleri kullanılarak düzenlenmesidir. Ancak artık titreşimi tamamen yok etmek için bu parametrelerin tam olarak bilinmesi gereklidir. Gerçekte ise bu mümkün olmamaktadır. Bu çalışmada, konvensiyonel negatif girdi şekillendirme teknikleri için hatalı belirlenen ya da tahmin edilen sistem parametrelerine rağmen esnek sistemlerin artık titreşimlerinin yok edilmesi veya oldukça azaltılmasının yöntemlerinden bahsedilmektedir. Ayrıca çalışmada şekillendiricilerin seyahat süreleri ve gürbüzlükleri arasındaki ilişkinin analizi sunulmaktadır.*

Anahtar kelimeler: artık titreşim, girdi şekillendirme, esnek mekanik sistem

Abstract—*One of the methods used to reduce or eliminate residual vibrations is modifying input signal using the system parameters such as natural frequency and damping ratio are known beforehand. However, in order to eliminate residual vibration completely, these parameters must be known exactly. In reality, it is not possible. In this study, conventional negative input shapers mentioned about in spite of the wrong estimated or predicted system parameters the elimination or reducing fairly of residual vibrations in flexible systems. This paper analyses the compromise between shaper duration and robustness for several negative input shapers.*

Keywords: residual vibration, input shaping, flexible mechanical system

I. Giriş

Esnek mekanik sistemler için hareket kontrol teknikleri ileri besleme (açık çevrim) ve geri besleme (kapalı çevrim) kontrol sistemleri olarak sınıflandırılabilir.

Geri beslemeli kontrol sistemleri, hassas hareket kontrolü için fizksel sistemin durum tahminlerini ve ölçüm sonuçlarını kullanır. Bu kontrol tekniğinde ölçüm sonuçlarının alınabilmesi için sensörler kullanılması gerekebileceğinden dolayı uygulanmaları zor ve pahalı olabilir. Dahası, geri beslemeli kontrol sistemleri önemli ölçüde işlem gücü gerektirebilir ve kararsız sistem davranışı olasılığını yükseltebilir [1]. İleri besleme kontrol teknikleri, artık titreşimleri önlemek için sistemin fiziksel parametrelerini dikkate alarak kontrol sinyali üretir. Bu yöntemde herhangi bir ek sensöre ihtiyaç duyulmaz ve bir kez girdi geliştirildikten sonra sistemdeki değişiklikler hesaba katılmaz [2].

Esnek sistemlerin titreşimlerini kontrol etmek için literatürde çok fazla çahşma vardır. Bu yöntemler arasında; komut ön şekillendirme veya girdi şekillendirme temelli yöntemler birçok araştırmacının ilgisini çekmiştir [3, 4, 5, 6, 7, 8]. Komut ön şekillendirme, pozitif yönlendirme kontrolü olarak ilk kez Smith tarafından önerilmiştir [9].

Bu yöntem bir adım girdisini iki parçalı merdiven girişine dönüştürür. Adım yanıtlarının süper pozisyonu, titreşimlerin birbirlerini sönümlemesini sağlar. Ancak bu yöntem sistemin doğal frekans ve sönüm oranının tam olarak tahmin edilmesine dayanmaktadır. Sistem parametrelerinin tam olarak tahmin edilmesinde karşılaşılan zorluklardan dolayı bu metot tercih edilmez. Bu problemi çözmek için, Singer ve Seering artık titreşimleri bastırmaya yönelik yeni bir girdi yöntemi önermişlerdir [10]. Çalışmaları gürbüzlüğü dikkate alan girdi şekillendirme uygulamalarının yelpazesini önemli ölçüde genişletmiştir. İlerleyen yıllarda girdi şekillendirici tasarımında yeni yaklaşımlar önerilmiştir [11, 12]. Çalışmalarda artık titreşim genliği oranının türevi sıfıra ayarlanmıştır, yani bir üç-darbe Türevsel Sıfır Titreşim (TST) şekillendirici elde edilmiştir. TST şekillendirici daha gürbüzdür, ancak şekillendirme girdi zaman gecikmesine neden olmuştur. TST şekillendirici hareket süresi tam bir titreşim periyodundayken, Sıfır Titreşim (ST) şekillendirici hareket süresi titreşiminin yarı periyodudur.

Artık titreşim genliğini mutlak sıfıra indirmek çok zordur ve böyle bir durum gerçek uygulamalarda nadiren istenmektedir. Eğer artık titreşim genliği şartı sıfırın dışına genişletilebilirse, sistemin gürbüzlüğü önemli ölçüde artırılabilir. Bu fikre dayanarak, Singhose ve arkadaşları Ekstra Duyarsız (ED) girdi şekillendirme yaklaşımını önermiştir [13]. TST şekillendirici ile karşılaştırıldığında ED şekillendiriciler aynı seyahat süresine sahip olmakla birlikte gürbüzlükleri önemli

* cconker@mku.edu.tr
† hhbilgic@mku.edu.tr
‡ hyavuz@cu.edu.tr

ölçüde geliştirilmiştir. Pozitif Girdi şekillendirme teknikleri için detaylı performans karşılaştırmaları Singhose ve arkadaşları [14], Vaughan ve arkadaşları [15]. Singhose [16] tarafından sunulmuştur.

Şekillendirici gürbüzlüğünün artması ile seyahat süresi de genellikle artar bu durum sistem cevabını önemli ölçüde etkiler. Şekillendirici gürbüzlüğü ve gecikme zamanı arasında bir ilişki olduğu açıktır. Mükemmele yakın bir yaklaşım elde etmek için, şekillendirici parametreleri dikkatli bir şekilde seçilmelidir. Pozitif darbe genliklerinin değerini belirlemek için sıklıkla kısıtlama denklemleri kullanılmıştır. Ancak hareket süresi, şekillendiricinin negatif darbeler içermesiyle önemli ölçüde azaltılabilir. Negatif şekillendiricilerin bazı tipleri esnek sistemlerin optimal zaman kontrolünü sağlamak için Pao ve Singhose tarafından sunulmuştur [17].

Pozitif girdi şekillendiricilerin aksine, negatif şekillendiriciler zamanın küçük periyotları için şekillenmemiş komut büyüklüğünü aşan komut profillerine sebep olabilir. Bu genlik aşmaları, çoğu uygulama için sorun değildir, çünkü yükselticiler ve motorlar müsaade edilen sabit durum seviyesinden daha fazla tepe akımına sahiptirler [18].

Bu çalışmada, konvensiyonel negatif girdi şekillendirme teknikleri için hatalı belirlenen ya da tahmin edilen sistem parametrelerine rağmen esnek sistemlerin artık titreşimlerinin yok edilmesi veya oldukça azaltılmasının yöntemlerinden bahsedilmekte, seyahat süreleri (travelling time) ve gürbüzlükleri (robustness) arasındaki ilişkinin karşılaştırılması sunulmaktadır. Çalışmada kütle yay sönümleyi sistemi için matematiksel model oluşturularak benzetim ortamında test sonuçları üretilmiştir. Benzetim ortamında incelenen sistem için tabi frekans (ω) 27.45 ve sönüm oranı (ξ) 0 olarak kabul edilmiştir.

II. Negatif Girdi Şekillendirme Teknikleri

Artık titreşimlerin yok edilmesi veya azaltılması için kullanılan yöntemlerden bir tanesi girdi sinyalinin, önceden bilinen sistem parametreleri kullanılarak düzenlenmesidir. Düzenlenecek girdi profilinin hesaplanmasında negatif darbelere izin verildiğinde seyahat süresi önemli ölçüde azaltılabilir. Negatif genliklerin kullanılması durumunda Parçalı Toplam (PT) ve Birim Genlik (BG) olmak üzere iki temel yaklaşım geliştirilmiştir. Örnek olarak negatif Sıfır Titreşim (ST) kısıtlamalarını karşılamak için, negatif şekillendiriciler üç darbeye sahip olmalıdır. BG-ST ve PT-ST için şekillendirici genlikleri;

$$PT-ST = A_i = [1 \quad -2 \quad 2] \tag{1}$$

$$BG-ST = A_i = [1 \quad -1 \quad 1] \tag{2}$$

olarak gösterilmektedir. Her bir darbenin zaman konumu sönüm oranı ζ'nın karmaşık bir fonksiyonudur. Çözümler Singhose tarafından BG ve PT genlik kısıtlamalarının her biri için ζ'nın geniş bir aralığı üzerinden elde edilebilmektedir [1, 19, 20].

Literatürde adı geçen negatif girdi şekillendiricilerin bir çoğu için kapalı form çözümlerinin kolayca elde edilemeyeceği bildirilmiştir [1, 19, 20]. Negatif girdi şekillendirme için analitik çözümler Tablo 1-3'de listelenmiş, sonuçlar da Şekil 1-3'de sunulmaktadır. Analitik çözümler hakkında daha fazla bilgi için, Singhose tarafından yapılan çalışmalara bakılabilir [20].

A. Negatif Sıfır Titreşim (ST) Şekillendiriciler

ST şekillendiriciler sistem parametrelerinin doğru tahminine dayandıkları için gerçek sistemlerin çoğunda iyi çalışmazlar fakat sistem frekansları kesin bir şekilde bilindiği zaman şekillendirici performansı en kısa ve en hızlısıdır [19]. Ayrıntılı kapalı form tanımı Singhose ve Pao, Singhose ve arkadaşları, Pao ve Singhose tarafından yapılmıştır[3, 18, 19].

Parçalı Toplam-Sıfır Titreşim (PT-ST) ve Birim Genlik-Sıfır Titreşim (BG-ST) şekillendiriciler için genlikler ve genliklerin zaman değerleri, sönüm oranının bir fonksiyonu olarak Tablo 1'de görülmektedir [19, 20]. PT-ST ve BG-ST şekillendiricilere uyan eğriler için ζ; $0 \le \zeta \le 0,3$ aralığındadır.

	$t_i = \left(M_0 + M_1\zeta + M_2\zeta^2 + M_3\zeta^3\right)T_d,\ T_d = 2\pi/\omega$					
Şekillendirici	A_i	t_i	M_0	M_1	M_2	M_3
PT-ST	1	t_1	0	0	0	0
	-2	t_2	0.2097	0.2244	0.0802	0.2312
	2	t_3	0.2901	0.0955	0.1034	0.2462
BG-ST	1	t_1	0	0	0	0
	-1	t_2	0.1665	0.2927	0.0754	0.2133
	1	t_3	0.3332	0.0053	0.1791	0.2012

TABLO 1. Sayısal Olarak Hesaplanmış Negatif ST Girdi Şekillendiriciler

Parçalı toplam ST ve birim genlik ST girdi şekillendiriciler ve hassasiyet eğrileri Şekil 1'de gösterilmiştir. Genlik 1 iken, PT-ST şekillendiricilerin seyahat süresi 0.29 T_d'dir. Burada T_d titreşim periyodunu göstermektedir. Pozitif ST şekillendiricinin seyahat süresi $0.5T_d$ iken, BG-ST şekillendiricinin seyahat süresi 0.33 T_d'dir. Negatif ST şekillendiriciler model hatalarının varlığında gürbüzlük kısıtlamasını sağlasa bile pozitif ST şekillendiriciye göre biraz daha düşük bir performans göstermek ile birlikte daha kısa seyahat sürelerine sahiplerdir [19].

B. Negatif Türevsel Sıfır Titreşim (TST) Şekillendiriciler

TST şekillendiriciler sistem parametrelerinin belirli ölçüde hatalı tahmin edilmesine olanak sağladıkları için gerçek sistemlerin çoğuna uygulanabilirler. Gürbülüğü arttırabilmek için girdi beş darbeyi içermekte ve seyahat süresi ST girdi şekillendiriciye göre daha uzun olmaktadır [19].

Genlik 1 İken, PT-TST şekillendiricinin seyahat süresi $0.67T_d$'dir. Pozitif TST şekillendiricinin seyahat süresi T_d iken, BG-TST şekillendiricinin seyahat süresi 0.73 T_d'dir. Negatif bir şekillendirici model hataları varlığında pozitif bir şekillendiriciye göre gürbüzlük kısıtlamasını sağlasa bile daha kötü bir performans gösterecektir. PT-TST şekillendirici ve BG-TST şekillendirici için girdi profilleri, sistem yanıtları ve hassaslık eğrileri Şekil 2 'de gösterilmiştir. Daha detaylı bilgiler Tablo 4'de sunulmuştur.

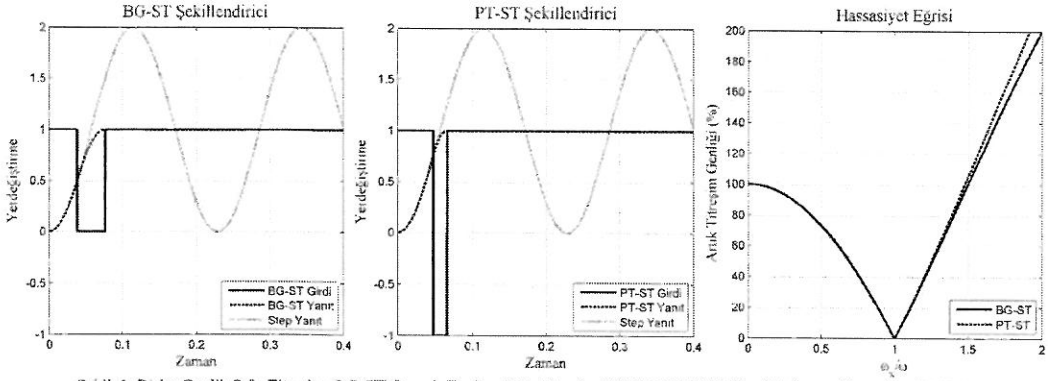

Şekil. 1. Birim Genlik Sıfır Titreşim (BG-ST) Parçalı Toplam Sıfır Titreşim (PT-ST) Girdi Şekillendiriciler ve Hassasiyet Eğrileri

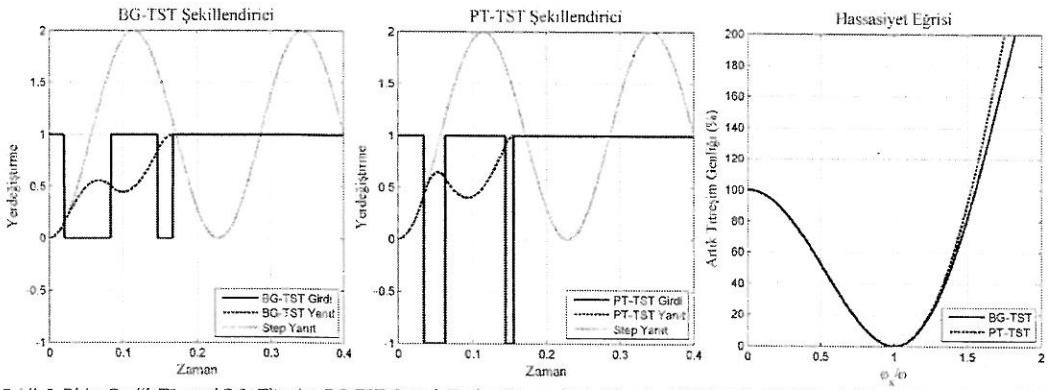

Şekil. 2. Birim Genlik Türevsel Sıfır Titreşim (BG-TST) Parçalı Toplam Türevsel Sıfır Titreşim (PT-TST) Girdi Şekillendiriciler ve Hassasiyet Eğrileri

	$t_j = \left(M_0 + M_1\zeta + M_2\zeta^2 + M_3\zeta^3\right)T_d,\ T_d = 2\pi/\omega$					
Şekillendirici	A_j	t_j	M_0	M_1	M_2	M_3
PT-TST	1	t_1	0	0	0	0
	-2	t_2	0.1523	0.2339	0.1516	0.2131
	2	t_3	0.2773	0.1114	0.0461	0.2878
	-2	t_4	0.6311	0.3493	0.1184	0.5255
	2	t_5	0.6787	0.1941	0.2743	0.4850
BG-TST	1	t_1	0	0	0	0
	-1	t_2	0.0894	0.2841	0.2301	0.1640
	1	t_3	0.3661	-0.0883	0.2404	0.1700
	-1	t_4	0.6427	0.2910	0.2326	0.4378
	1	t_5	0.7322	0.0099	0.4938	0.3863

TABLO 2. Sayısal Olarak Hesaplanmış Negatif TST Girdi Şekillendiriciler

C. *Negatif Ekstra Duyarsız (ED) Şekillendiriciler*

Singhose ve arkadaşları titreşim kısıtlaması için sönüm oranı ve genlik kısıtlamasına uygun bir denklem dizisi üzerinden BG ve PT ED genlik kısıtlamalarını çözmüştür [19].Tablo 3 artık titreşimler %5 iken negatif ED şekillendiricilerin zaman konumlarına uyan eğrileri içermektedir. Tablo 3 incelendiğinde, ED şekillendiricilerin ζ değerinden bağımsız olarak TST şekillendiricilerle aynı seyahat süresine sahip olduğu

görülmektedir. Ancak ED şekillendiriciler modelleme hatalarına göre TST girdi şekillendiricilerden daha gürbüzdür.

Parçalı toplam ED ve birim genlik ED girdi şekillendiriciler ve hassasiyet eğrileri Şekil 3'de gösterilmiştir. PT-ED girdi şekillendiricinin seyahat süresi pozitif ED girdi şekillendiricinin % 68'i iken BG-ED şekillendiricinin seyahat süresi pozitif ED girdi şekillendiricinin % 73'üdür.

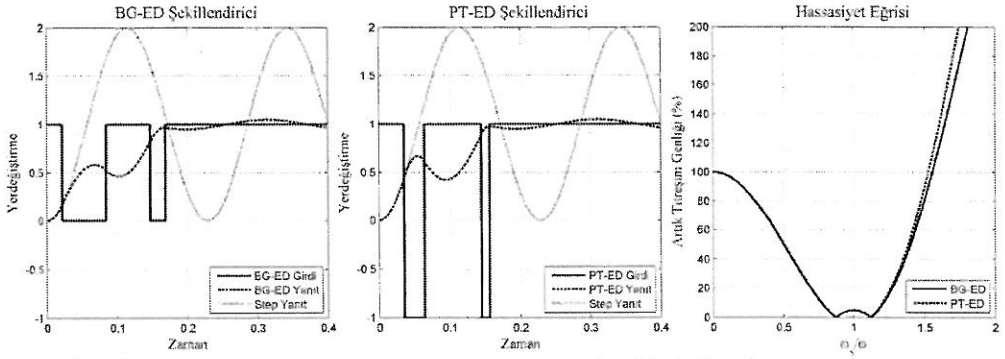

Şekil. 3. Birim Genlik Ekstra Duyarsız (BG-ED) Parçalı Toplam Ekstra Duyarsız (PT-ED) Girdi Şekillendiriciler ve Hassasiyet Eğrileri

	$t_j=\left(M_0+M_1\zeta+M_2\zeta^2+M_3\zeta^3\right)T_d,\ T_d=2\pi/\omega$					
Şekillendirici	A_j	t_j	M_0	M_1	M_2	M_3
PT-ED V=5%	1	t_1	0	0	0	0
	-2	t_2	0.1563	0.2655	0.0532	0.6945
	2	t_3	0.2808	0.1393	-0.0562	0.7542
	-2	t_4	0.6342	0.3414	0.1537	0.3290
	2	t_5	0.6841	0.1849	0.3105	0.2856
BG-ED V=5%	1	t_1	0	0	0	0
	-1	t_2	0.0937	0.3190	0.1358	0.6527
	1	t_3	0.3679	-0.0589	0.1364	0.6326
	-1	t_4	0.6425	0.2859	0.2633	0.2499
	1	t_5	0.7366	0.0016	0.5274	0.1920

TABLO 3. Sayısal Olarak Hesaplanmış Negatif ED Girdi Şekillendiriciler

III. Konvensiyonel Negatif Girdi Şekillendiricilerin Karşılaştırılması

Önceki bölümde seçilmiş bazı negatif komut şekillendirme teknikleri sunulmuştur. Sunulan girdi şekillendirme yöntemlerine ilişkin ayrıntılı bilgilere ilgili referanslardan ulaşılabilir. Sunulan girdi şekillendirme yöntemlerinin başarıyla uygulanması için ilgili sistem parametrelerinin (sönüm oranı ve doğal frekans) doğru tahmin edilmesi veya belirlenmesi gerekir. Ancak, herhangi bir esnek sistemin matematiksel modeli mükemmel olarak elde edilemez. Sistem parametrelerinin varyasyonları veya değişiklikleri şekillendirilmiş sinyali ve aynı zamanda sistem cevabını etkiler. Bu nedenle, matematiksel modelden kaynaklanan hatalara karşı sinyal gürbüzlüğü komut şekillendirme yöntemleri için önemli bir performans karşılaştırma aracıdır. Bu bölüm tartışılan negatif girdi şekillendirme tekniklerinin seyahat süreleri ve sistem parametrelerinin hatalı tahminleri için gürbüzlüklerinin karşılaştırılmasını sunmaktadır. Karşılaştırmada dikkate alınan gürbüzlük hassasiyet eğrisinden türetilmektedir. Çalışmada % 5 artık titreşim genliğinin altında kalan bölge ölçülerek gürbüzlük hesaplanmıştır. Duyarsızlık oranı ise gürbüzlüğün seyahat süresine oranıdır [15].

	PT-ST	BG-ST	PT-TST	BG-TST	PT-ED	BG-ED
Seyahat Süresi T_d	0.29	0.33	0.67	0.73	0.68	0.73
Gürbüzlük 5%	0.054	0.0548	0.2535	0.2585	0.3481	0.3559
Duyarsızlık Oranı [15]	0.186	0.166	0.3783	0.3541	0.5119	0.4875

TABLO 4. Negatif Girdi Şekillendiricilerin Karşılaştırması İçin Performans Kriterleri

Tablo 4'de negatif girdi şekillendiriciler için performans ölçütleri verilmektedir. Tablo 4'de verilen bilgilerden şu sonuçlara ulaşılabilir.

- Aynı gürbüzlük kısıtlamalarını karşılasalar bile, modelleme hataları olduğu zaman negatif şekillendiricilerin pozitif şekillendiricilerden kötü bir performansı olacaktır.
- Tablo 4'de girdi şekillendiriciler için seyahat süresinin artmasıyla gürbüzlüklerin arttığı görülmektedir.
- Negatif ST girdi şekillendiriciler modelleme hatalarına karşı oldukça duyarlıdır, hesaplamada

yapılan hatalar artık titreşim oluşmasına neden olmaktadır.

- Negatif TST girdi şekillendiriciler modelleme hatalarına karşı negatif ST şekillendiricilerden daha duyarsız olmakla birlikte seyahat süreleri daha fazladır.
- Gürbüzlüğün seyahat süresi oranına bakıldığında performans olarak en iyi şekillendiricinin PT-ED şekillendirici olduğu görülmektedir.

IV. Sonuçlar

Bu çalışma konvansiyonel negatif girdi şekillendirme tekniklerinin seyahat süreleri ve sistem parametrelerinin hatalı tahminleri için gürbüzlüklerinin karşılaştırılmasını sunmaktadır. Çalışmada, toplamda altı farklı negatif girdi şekillendirme yöntemi incelenmiştir.

Çalışmada sunulan her bir yöntemle ilgi teorik arka plan ve uygulamalar sunulmuştur. Benzetim sonuçlarının ayrıntılarından, şu sonuca varılabilir;

Gürbüz şekillendiriciler daha uzun seyahat süresine sahiptirler bu da daha yavaş sistem cevabına neden olur. Bu durum da şekillendirici gürbüzlüğü ve seyahat süresi arasında bir ilişki olduğunu açıkça ortaya koymaktadır.

Kaynakça

[1] Vaughan J. Dynamics and control of mobile cranes. PhD thesis, Georgia Institute of Technology, 2008.

[2] Shan J., Liu H. ve Sun D. Modified input shaping for a rotating single-link flexible manipulator. Journal of Sound and Vibration, 285: 187–207, 2005.

[3] Singhose W. ve Pao L. A comparison of input shaping and time optimal flexible body control. Control Engineering Practice, 5(4): 459–467, 1997.

[4] Singhose W., Porter L., Kenison M. ve Kriikku E. Effects of hoisting on the input shaping control of gantry cranes. Control Engineering Practice, 8(10): 1159–1165, 2000.

[5] Dharne A. G. ve Jayasuriya S. Robust adaptive control of residual vibration in point-to-point motion of flexible bodies. Journal of Vibration and Control, 13(7): 951–968, 2007.

[6] Gürleyük S.S. ve Cinal S. Robust three-impulse sequence input shaper design. Journal of Vibration and Control, 13: 1807–1818, 2007.

[7] Blackburn D., Singhose W., Kitchen J., Patrangenaru V., Lawrence J., Kamoi T. ve Taura A. Command shaping for nonlinear crane dynamics. Journal of Vibration and Control, 16(4): 477–501, 2010.

[8] Kim D. ve Singhose W. Performance studies of human operators driving double-pendulum bridge cranes. Control Engineering Practice, 18(6): 567–576, 2010.

[9] Smith O.J.M. Posicast control of damped oscillatory systems. Proceedings of the Institute of Radio Engineers, 45: 1249–1255, 1957.

[10] Singer N.C. ve Seering W.P. Using acausal shaping techniques to reduce robot vibration. In: IEEE International Conference on Robotics and Automation, USA, 1988.

[11] Singer N.C. Residual Vibration Reduction in Computer Controlled Machines, MIT Artificial Intelligence Laboratory Technical Report Number AITR-1030, MIT Artificial Intelligence Laboratory, 1989.

[12] Singer N.C. ve *Seering* W.P. Preshaping command inputs to reduce systems vibration. Journal of Dynamic Systems Measurement and Control: 112, 76–82, 1990.

[13] Singhose W. Seering W. ve Singer N.C. Residual vibration reduction using vector diagrams to generate shaped inputs. ASME Journal of Mechanical Design, 116: 654-659, 1994.

[14] Singhose W., Porter L. ve Singer N.C. Vibration reduction using multi-hump extra insensitive input shapers. American Control Conference, USA, 1995.

[15] Vaughan J., Yano A. ve Singhose W. Comparison of robust input shapers. Journal of Sound and Vibration, 315: 797-815, 2008.

[16] Singhose W. Command shaping for flexible systems: a review of the first 50 years. International Journal of Precision Engineering and Manufacturing, 10: 153–168, 2009.

[17] Pao L. ve Singhose W. On the equivalence of minimum time input shaping with traditional time-optimal control. IEEE Conference on Control Applications, Albany, USA, 1995.

[18] Pao L. ve Singhose W. Unity magnitude input shapers and their relation to time-optimal control. IFAC World Congress, San Francisco, USA, 1996.

[19] Singhose W., Singer W. ve Seering W. Time optimal negative input shapers. Journal of Dynamical systems Measurement and Control, 119: 198-205, 1997.

[20] Singhose W. Command Generation for Flexible Systems. PhD thesis, Massachusetts Institute of Technology, 1997.